MICROFLUIDIC DEVICES FOR NEMATODE-BASED BEHAVIOURAL ASSAYS USING ELECTROTAXIS

By
POUYA REZAI
B.Sc., M.Sc.

A Thesis
Submitted to the School of Graduate Studies
in Partial Fulfilment of the Requirements for the Degree of
Doctor of Philosophy in Mechanical Engineering

McMaster University

MICROFLUIDIC DEVICES FOR NEMATODE-BASED BEHAVIOURAL ASSAYS USING ELECTROTAXIS

McMaster University DOCTOR OF PHILOSOPHY (2012)
Hamilton, Ontario, Canada

TITLE: Microfluidic Devices for Nematode-based Behavioural Assays Using Electrotaxis

AUTHOR: Pouya Rezai
B.Sc. (Isfahan University of Technology)
M.Sc. (Chalmers University of Technology)

SUPERVISOR: Professor P. Ravi Selvaganapathy

NUMBER OF PAGES: xx, 193

ABSTRACT

Small nematode model organisms such as *Caenorhabditis elegans* are widely used in the fields of neurobiology, toxicology, drug discovery, etc. They are advantageous due to their fully characterized genomic and cellular system. Traditional screening methods involve the exposure of animals to chemicals/drugs inside multiwell-plates while its effects on growth, movement and other cellular/sub-cellular processes are monitored by visual inspection. Yet, these methods are time-consuming, low-throughput, expensive, tedious, difficult to control, hard to modulate instantaneously, prone to subjectivity and not suitable for movement-based behavioural assays. Hence, a method to induce and to quantify movement on-demand in a rapid, sensitive, precise and reversible manner would greatly facilitate biological studies. In this thesis, microfluidic engineering approaches have been utilized in nematode-based assays due to their potential to obtain high precision measurements in a low-cost, rapid and automated manner. Movement response of worms to a diverse range of electric signals has been quantitatively characterized. DC and pulse-DC electric fields have been shown to stimulate worms' swimming towards the negative electrode inside a microchannel (electrotaxis). AC electric fields were used to inhibit movement on-demand. Animals' movement has been characterized in terms of speed and range of motion, body-bend frequency and turning time. Electrotaxis was shown to be mediated by neuronal activities and correlations between animal's behaviour and neuronal signalling has also been demonstrated. Using this basic understanding, multiple microfluidic components such as position sensors and electric immobilizers have been developed. Electrotaxis has then been applied as a technique to sort worms in accordance to their size/age and phenotype as well as to perform drug screening at a single-animal level. Integration of the techniques and components developed during this research is expected to have a significant impact on the development of an integrated microfluidic platform for high throughput automated behavioural screening of nematodes with applications in drug discovery, toxicology, neurobiology and genetics.

ACKNOWLEDGEMENT

I would like to take this opportunity to express my sincere appreciation to all individuals and organisations for their extended support towards the completion of this dissertation. This research would have never been made possible without the encouragement and devotion of my family and colleagues.

First, I am very grateful to my advisor, Professor Ponnambalam Ravi Selvaganapathy, for supervising this research and his unconditional support during the past four years. His vast knowledge and extensive level of expertise in mechanical, electrical, electrochemical and even biological field was indeed one of the main forces allowing this research to go forward.

Second, I am very thankful to Professor Bhagwati P Gupta for allowing me to access his laboratory's facilities and the expertise of his students. He was always there for me and truly supported the biological aspects of the research. Being a scientist, he always fascinated me with his engineering insights and skills.

I am also grateful to Professors Chan Ching and Qiyin Fang, for their advice in the fields of fluid mechanics and photonics as well as giving me access to the resources in their laboratories. Professor Ching always challenged me positively and made me more and more enthusiastic in advancing my research.

The work done in this research would have not been made possible without the help that I received from my colleagues Sangeena Salam, Asad Siddiqui, Justin Tong, Allison Yeh and Reza Ghaemi. I would also like to acknowledge the support of the Center of Emerging Device Technology (Dr Z. Peng and Mrs. Doris V. Stevanovic) and the Mechanical Engineering Department Machine Shop Facilities (R. Lodewykes, Joe Verhaeghe and all other technicians) for their assistance for the fabrication and development of the devices and setups.

I also thank all CAMEF group members, Dr. W. Wu, Dr. G. Mahadevan, S. Shinwary, M. Hasnain, S. Safari, A. Noori, L. Hsu, B. Dang, S. Islam, A. Shahid, P. Lee, C. Zhu and M. Reza for their endless friendship, productive discussions and fabulous group lunches which were all full of joy and energy.

Finally and most importantly, I would like to deeply appreciate the everlasting love and support received from my wife, Shabnam Nikfar; my parents, Dr A. Rezai and Mrs. A. Rahmani; and my siblings, Pejhman, Pegah and Parva Rezai. Shabnam's enduring love, encouragement, support, patience and gifted sense of humor made this journey so much easier for me. Her sacrifices, which were realized by our loss of precious time together, were for me the most painful and humbling of all. But, all these encouraged me to pursue this dream more seriously. This thesis is after all dedicated to her and our lovely daughter, Adrina.

TABLE OF CONTENT

LIST OF FIGURES

LIST OF TABLES

LIST OF ABREVIATIONS

6-OHDA	6-Hydroxydopamine
α-syn	α-Synuclein
Aβ	β−Amyloid
AC	Alternating current
ACMF	Alternating current magnetic field
AD	Alzheimer's disease
Caenorhabditis briggsae	C. briggsae
Caenorhabditis elegans	C. elegans
CD	Compact disc
CFP	Cyan fluorescent protein
CMOS	Complementary metal oxide semiconductor
CO2	Carbon dioxide
COPAS	Complex object parametric analyser and sorter
DA	Dopaminergic neurons
DC	Direct current
DIC	Differential interference contrast
DMD	Duchenne's muscular dystrophy
E. coli	Escherichia coli
FRET	Föster Resonance Energy Transfer
GABA	γ-Aminobutyric acid
GFP	Green fluorescent protein
HD	Huntinton's disease
htn	Huntingtin
HTS	High-throughput screening
LB	Lewy body
MPP+	1-Methyl-4-phenylpyridinium
MPTP	1-Methyl-4-phenyl-1,2,3,6-tetrahydropyridine
MTR	Mithramycin

NG	Nematode Growth
NMDA	*N*-methyl-d-aspartic acid
OFM	Optofluidic microscopy
PC	olycarbonate
PCR	Polymerase Chain Reaction
PD	Parkinson's disease
PDMS	Polydimethylsiloxane
PKC	Protein kinase c
Poly-Q	Poly-glutamine
RNAi	RNA interference
SMF	Static magnetic field
TSA	Trichostatin A
YFP	Yellow fluorescent protein

CHAPTER 1

1. Introduction

1.1 Thesis Goals

This thesis aims to control, quantitatively characterize and understand the movement behaviour of nematodes (e.g. *Caenorhabditis elegans* (*C. elegans*)) through the use of various electrical signal waveforms integrated with the microfluidic technology in order to apply it for quantitative worm-screening assays that have applications in drug discovery, toxicology and neurobiology. It develops various electro-fluidic techniques, methods and devices to automate and perform drug discovery and toxicology assays on *C. elegans,* including animal sorting; selection and compartmentalization; drug exposure; movement analysis; position sensing; immobilization and imaging. While these microchips are developed as stand-alone units, they are designed to be integrated into a single microfluidic platform potentially used for automated behavioural chemical screening on nematodes.

1.2 Worm-Based Drug Screening Using Microfluidics

The objective of a significant portion of biological researches today is to understand human diseases and to develop new and effective treatments for

them. Multidisciplinary research approaches serve to identify the genetic basis of these pathologies in order to better understand their mechanism of action and treat them. Due to the enormous complexity associated with cellular and molecular processes in humans, as well as the inherent ethical issues, researchers have focused on a number of eukaryotic systems that are simpler and easier to manipulate, yet complex enough to address many of the questions relevant to human biology. Animal models offer an ideal system to observe the implications of complex interaction of disease mechanism in the whole organism. Nematode *C. elegans* is one such model organism that has greatly facilitated the study of conserved biological processes. It offers a number of useful features such as small size (~1,000 somatic cells), well-mapped neuronal connectivity and cellular system, body transparency, short life-cycle (~2.5 days), and the ability to generate many progeny in a relatively short time. The analysis of the *C. elegans* genome sequence has revealed the presence of a large number (~65%) of human disease orthologs that are very useful in investigating the underlying mechanism of gene function [1]. Worms have been used successfully as models for a variety of human disorders, such as obesity [2], hypertension [3], Duchenne's Muscular Dystrophy (DMD) and neurodegeneration (e.g. Huntington's disease, HD; Parkinson's disease, PD) [2-9]. For instance, one of the major causes of PD in humans is the marked loss of dopaminergic (DA) neurons in substantia nigra, a region of the brain that controls the balance and body movement. Its major symptoms are tremor, bradykinesis (slow movement), stiffness of the limbs and trunks or akinesia (inability to move), and postural instability (impaired balance and coordination). *C. elegans* possesses four pairs of these DA neurons. *C. elegans* PD models have been generated that show degeneration of DA neurons and movement defects [10]. Neurotoxins have also been identified that can cause degeneration of DA neurons and subsequent PD symptoms. Accordingly, these worms serve as effective PD models to study the basis of neuro-degeneration and facilitate screening of genes and chemical compounds that protect neurons from toxin-induced damage.

Conventional methods of chemical screening involve exposure of worms to thousands of chemical compounds individually and inside multi-well plate dishes, while monitoring the subsequent effects on biological processes by immobilization and visual inspection. These experiments are typically carried out manually and are consequently time-consuming and prone to human errors. Robotics can automate many steps but it is expensive and inaccessible to the majority of researchers. In addition, most conventional plate-based methods are currently focused on the cellular level analysis and tend to ignore the movement behaviour of worms which is one of the most important parameters particularly for movement disorder diseases.

In the recent past, a diverse range of microfluidic devices have been developed to facilitate sub-cellular, cellular, neuronal and even behavioural studies on *C. elegans* [11-14]. Most of these devices are fabricated from polydimethylsiloxane (PDMS, a transparent flexible polymer) and provide excellent scalable environments for manipulation, immobilization and live imaging of these animals for sorting, phenotypic analysis and laser-assisted neuronal ablation and regeneration studies. Despite being very informative and useful in cellular and sub-cellular studies, they are again not as beneficial for nematode-based behavioural assays such as the study of its movement. Although researchers have used microfluidics to explore animals' behaviour inside environments mimicking their natural habitat soil or in response to attractive or repulsive chemicals, these methods are also not suitable for studying worms' movement. They are mostly difficult to control, do not produce movement on-demand and instantaneously in a repeatable and robust manner and are not suitable for High Throughput Screening (HTS) assays.

In contrast, electric fields can be easily and controllably applied inside microfluidic environments, be turned on or off instantaneously, be generated less expensively and most importantly, are amenable to multiplexing and parallel fabrication for the aim of developing HTS microfluidic devices. It is shown in this thesis that *C. elegans* movement can be fully controlled and characterized by a diverse range of electric field signals (electrotaxis) inside microfluidic platforms. The electrotactic response of *C. elegans* in a microchannel is instantaneous, highly sensitive, and robust; and, therefore, can be used to perform movement-based behavioural studies. Electrotaxis is also highly-suited for other screening-based applications, such as genetic analysis, drug screening and toxicology. Results from this thesis demonstrate that the electrotaxis can be used as a reliable and faithful indicator of neuronal and muscular activities that modulate movement in worms. Multiple electric field-based microfluidic chips and techniques have also been developed for localizing, sorting, immobilizing and sensing of nematodes inside microchannels. Additionally, it will be demonstrated that the electric-based microdevices designed throughout this thesis are well-suited for automated chemical screening on worms with potential of being scaled up for high throughput behavioural screening assays.

1.3 Contributions

Thesis contributions to the general body of knowledge can be divided into the fundamental and the applied categories. At the fundamental level, an innovative technique has been developed to accurately control and quantitatively analyze the movement behaviour (initiation [15-17] and inhibition [18, 19]) of nematodes

at a precise, repeatable, sensitive and robust manner. This has been achieved through the integration of electric signals inside microfluidic environments and the fascinating observation of electric field-induced movement response of worms towards the cathode (electrotaxis) inside microfluidic channels. This phenomenon has been thoroughly investigated in regards to various electric field waveforms, age of the animal, role of the neuronal and muscular systems of the worm in electrotaxis, sensitivity to electric field and also subsequent effects of exposure to electric signal in lifespan, reproduction and chemotaxis behaviour. Finally, neuronal correlation with behavioural electrotactic movement has also been demonstrated using real-time neuronal activity monitoring by the Föster Resonance Energy Transfer method (FRET) [20].

At an applied level, the fundamental electro-fluidic and electrotactic movement control techniques, achieved through the first stage of the thesis, have been utilized to develop a variety of microfluidic components and devices for localization [18], sorting [21-23], chemical screening, position detection, immobilization and imaging [24] of *C. elegans*. All these components have been developed with a common purpose of being integrated into an automated high throughput microfluidic behavioural assay chip at a later stage. Electric field-based microfluidic techniques are most amenable to parallelization and development of high-throughput screening devices. The utilization of the outcomes of this research, in on-demand movement analysis of nematodes, drug screening, toxicology, genetic analysis of electrotaxis and many more application areas is proposed.

The following describes my contributions to the articles constituting Chapters 2-6. Majority of Chapter 2 was published as a book chapter [11] with contents on drug discovery and animal model sections mostly written by Dr B. P. Gupta and rest of the chapter by myself with revisions by the co-authors. Chapters 3-6 experiments were performed in collaboration with Mr. Asad Siddiqui (undergraduate) and Ms. Sangeena Salam (graduate), both working in Gupta lab. They are co-authors on papers that resulted from these studies. They helped in growing and staging worms for various assays and wrote parts of the experimental procedures for papers. In addition, Sangeena also carried out life span and chemotaxis assays. Mrs. Shu-Chi Allison Yeh assisted in acquiring the FRET images on the microscope and in analyzing them for Section 4.3.3. Mr. Reza Ghaemi assisted with the design and experiments of the Wheatstone bridge used for electrical sensing described in Chapter 5, Section 5.3. For all the research and studies, I designed and performed all phases of projects from literature survey through data analysis. I wrote the first drafts of manuscripts and the initial responses to the comments of the journal reviewers. Dr. Selvaganapathy provided guidance with the research focus, idea development,

analysis of the results and manuscript revisions. Dr. Gupta provided guidance with biological aspects of the project, analysis of the results and manuscript revisions. Dr. Ching provided advice on the fluid mechanisms and device designs during the CAMEF (Centre for Advanced Micro Electro Fluidics) group meetings. Dr. Fang provided advice on the photonic aspects of the project especially for real-time neuronal imaging of worms using the FRET method in Section 4.3.3.

1.4 Thesis Outline

This thesis contains 7 chapters presented in a “standard” style. The contents of Chapters 2-5 have been mainly extracted from a number of published articles. The following chapters of this thesis are summarized as:

Chapter 2: Animal Models in Drug Discovery and Screening Methods

In this chapter, fundamental description of the drug discovery process and various biological organisms and substances used in it are provided with a focus on the nematode *C. elegans* as one of the most widely-studied bio-organisms in drug discovery, toxicology and neurobiology. Some human diseases, that *C. elegans* has been modeled for, are reviewed to emphasize on the importance of this model organism and to better understand the bottlenecks and requirements of the research works performed on this animal, including the low-speed handling and the qualitative screening techniques. The conventional and high-throughput screening and animal-handling methods are then discussed. Afterwards, microfluidic techniques for performing biological unit operations on *C. elegans*, which are among the most cost-efficient and accurate methods, are comprehensively reviewed. This approach is adapted in this thesis to develop novel techniques for controlling and screening the *C. elegans* movement behaviour and for applying it in a set of unit operations, such as sorting, immobilizing, imaging and chemical/drug screening.

Chapter 3: Device Design, Methods and Experimental Procedures

In this chapter, a brief theory behind the design of the presented microfluidic devices, introduced throughout the thesis, is provided. These devices are developed using a common set of fabrication techniques, which are discussed for the single- and multi-layer devices. Animal preparation techniques, experimental procedures and data analysis methods which are similar and commonly used for most of the experiments are also described. These techniques and experimental setups have been used to develop devices for animal movement control and analysis (Chapter 4), as well as localization, detection, sorting, immobilization and chemical screening (Chapters 5-6).

Chapter 4: Electrotaxis of Nematodes in Microchannels - Behavioural and Neuronal Analysis

This chapter mainly focuses on the techniques developed to stimulate, control and quantitatively analyze the movement of *C. elegans* and *C. briggsae* inside microfluidic environments by using electric fields inside the embedded microchannels. This behaviour is termed “electrotaxis” and is quantitatively analyzed in terms of the worms’ swimming speed, body bend frequency and rotation time inside the microchannel. Electrotaxis of worms is studied very comprehensively in this chapter with regards to various animal stages/ages and diverse ranges of electric field wave-shapes such as direct current (DC) and pulse-DC signals. Cellular basis of the elctrotaxis response and its sensitivity correlations with the age and size of the animal is investigated. Finally, the correlation between neuronal activity and electrotactic behaviour is experimentally determined by using a neuronal FRET imaging technique. While the majority of microfluidic-based worm chips in the literature have been developed for cellular and sub-cellular level studies (reviewed in Section 2.5), contributions from this chapter are fundamentally applicable in nematodes movement behavioural studies in a highly precise, repeatable, robust and quantitative manner. The techniques developed in this chapter are well-suited for more applied-level movement-based assays, as described in Chapters 5 and 6.

Chapter 5: Micro-Electro-Fluidic Devices to Perform Unit Operations on *C. elegans*

One of the main focuses of this thesis is to develop the fundamental operational units required to perform automated movement-based chemical/drug screening (in addition to the cellular- and neuronal-based assays) on worms. In order to be able to develop such a system, various subcomponents are required to be separately designed and tested as categorized into (1) manipulation and loading; (2) exposure and culturing; and (3) characterization units. Most of these operations on worms are currently performed manually or by robotic tools which are respectively time-consuming, labour-intensive and prone to user flaws or highly expensive and inaccessible to researchers. In Chapter 5, microfluidic-based techniques and methods, which are mostly based on worms’ electrotaxis movement behaviour, are developed to perform these biological unit operations on nematodes in a more automated and low-cost manner with amenability to parallelization and high throughput. Microfluidic passive sorters, remote localizers, touch-less immobilizers and on-chip position detectors have been developed all with electrical-operation principles. Therefore, contributions from this chapter are all at an applied level and as opposed to conventional assays (mostly analyzing cellular processes), are focused on animals behavioural assessments.

Chapter 6: Integrated Microfluidic Device for Nematode Chemical Screening by Electrotactic Movement Assay

An integrated microfluidic chemical screening device must have the capability of sorting a group of animals and compartmentalizing them individually in separate units; exposing them to chemicals, drugs or odorants; and finally screening the worms both for behavioural and cellular/neuronal effects. This thesis has aimed to develop all the components of such a system as stand-alone units while keeping the designs amenable to integration and an eventual development of such a system. After developing these sub-units, mostly in Chapters 4 and 5, a proof of principle device is developed in this chapter that can screen chemicals on a single worm with a fine spatiotemporal exposure precision and a quantitative post-exposure electrotactic movement-based assay. Some of the challenges are the integration of electrotactic screening channel with the drug exposure unit, viably isolating individual animals from a suspension and loading them into the screening section, isolating the non-loaded animals while preventing them from being exposed to the chemicals, maintaining the loaded animal inside the exposure chamber and preventing its escape, controlling the exposure dosage and time, and finally studying the movement of the worm quantitatively afterwards. This proof of principle device should have also been amenable to parallelization and multiplexing for the aim of HTS.

Chapter 7: Summary and Recommendations for the Future Work

In this chapter, an overview of the conclusions and discussions presented in the previous chapters of this thesis is provided, which is followed by the research contributions and recommendations for the future work.

Appendices

This chapter presents the detailed information and standard operating procedures for conducting the experiments and fabricating the devices described in the thesis. It also provides more in-depth theoretical and experimental facts relevant to the thesis.

CHAPTER 2

2. Animal Models in Drug Discovery and Screening Methods *

Drug discovery is the process of identifying potential therapeutic drugs for human diseases. It involves multiple stages through which the effect of a large number of chemical compounds is screened against a diverse range of bio-organisms from cells to animal models at the preclinical stage to human subjects

* Parts of this chapter has been gathered from the introduction sections of the published book chapter and journal articles (permissions acquired and presented in the following):

1. Rezai, P., et al., Electrotaxis of Caenorhabditis elegans in a microfluidic environment. *Lab Chip*, 2010. **10**(2): p. 220-6.
2. Rezai, P., et al., Behavior of Caenorhabditis elegans in alternating electric field and its application to their localization and control. *Appl Phys Lett*, 2010. **96**(15): p. 153702.
3. Rezai, P., et al., Effect of pulse direct current signals on electrotactic movement of nematodes Caenorhabditis elegans and Caenorhabditis briggsae. *Biomicrofluidics*, 2011. **5**(044116): p. 1-9.
4. Rezai, P., et al., Electrical sorting of Caenorhabditis elegans. *Lab Chip*, 2012. **12**: p. 1831-1840
5. Rezai, P., et al., Microfluidic systems to study the biology of human diseases and identify potential therapeutic targets in C. elegans, in Integrated Microsystems, K. Iniewski, Editor. 2011, CRC Press. p. 581-608.
6. Rezai, P., et al., In vivo Detection of Electric Field-induced Neuronal Activity in C. elegans Under Preparation, 2012.

at the clinical stages. Due to the complexity and ethical issues associated with experimentation on human subjects, researchers have developed alternative models of human diseases in animals such as mice, rat, *Drosophila* and *C. elegans*. Since a large number of chemical compounds should be assayed against these models, various screening methods such as robotic- and microfluidic-based ones have been developed for this purpose. This chapter provides a comprehensive review of HTS and drug discovery-related research in *C. elegans*. It begins with a brief description of leading animal models with an emphasis on *C. elegans*. This is followed by a survey of currently available microfluidic and other robotic systems for various worm applications. The chapter ends with a discussion of tools and approaches needed to facilitate high-throughput microfluidic screens in *C. elegans* for the study of movement behaviour and related disorders.

2.1 Drug Discovery

Drug discovery is the process of identifying drugs for human diseases, partially involving the use of *in vitro* and *in vivo* disease models for screening various chemical compounds against certain targets in cells [25]. In general, the process includes five stages: target identification and validation; lead screening; optimization; preclinical development; and clinical trials. A protein or biochemical pathway that plays a key role in the origin or progression of the disease is identified in the target identification and validation stage. The lead screening stage involves screening a large number of chemical compounds against the bio-molecular target protein or gene in order to identify candidates with potential therapeutic effect. This is followed by an optimization stage in which small chemical modifications of the initial lead compounds are made and screened to produce an optimal chemical species. The preclinical stage involves testing the candidates in various animal models for efficacy as well as toxicity, and finally, in the clinical stage, testing is carried out in humans on a smaller scale. If successful, the drug is made commercially available in the market.

The lead screening and optimization in the drug discovery process is frequently carried out by HTS of chemical compounds using *in vitro* assays (e.g., against a protein target present either in solution or in cultured cells). As these approaches ignore the complexity of biological processes in the context of multi-cellular organisms that involve interactions between different types of cells and tissues, they often fail to produce desired results in subsequent animal and human trials. This results in poor efficacy, nonspecific effects, delay in clinical trials, and a significant increase in the cost of developing new drugs. A better approach would be to use a whole animal model that also allows monitoring the

various other aspects of drug screening, such as administration, distribution, metabolism, and toxicity. Although human subjects are ideal, they cannot be easily tested due to the enormous complexity of their cellular and molecular processes, as well as the ethical issues associated with subjecting them to experimentation. Therefore, alternative eukaryotic systems (e.g., *C. elegans*) are desired that are simpler and easier to manipulate yet complex enough to address many of the questions relevant to human biology.

Traditional methods of drug screening and studies of its mode of action in animal models have involved feeding the subjects with chemicals present in food (i.e. on a Petri dish or in a 96-well microtiter plate) while monitoring the effects on various biological processes, and parameters such as growth and fertility, by visual inspection [2]. These methods are time-consuming, expensive, tedious, prone to human flaws, and therefore subjected to a high degree of failure. It is a significant bottleneck that has forced the use of animal model approaches to later stages of lead optimization step. Using them at earlier stages of screening will increase the physiological relevance of drug candidates during the lead identification process as well as reveal potential toxic effects, thereby helping to accelerate the process of drug discovery. This could be achieved by automation and parallelization of screening that will enable low-cost high-throughput analysis in a rapid, sensitive, and accurate manner.

2.2 Model Organisms to Study Human Diseases

Researchers have established various alternative models to study disease mechanisms and search for potential drug targets [4, 5, 26-28]. This includes cultured cells (the *in vitro* approach) as well as unicellular and multi-cellular animals (the *in vivo* approach). In addition, computer software is also used to study biological processes by developing mathematical models (the *in silico* approach) and to analyze large experimental datasets.

The *in vivo* approach, involving animals, has traditionally focused on a relatively small set of living entities known as model organisms. Much of our understanding of human biology and diseases has come from studies carried out in these systems. Such models have been immensely useful for the understanding of fundamental biological processes such as cell division and differentiation that occur in all eukaryotes. They provide powerful tools to accelerate studies on diseases without dealing with actual human subjects and free from ethical considerations. By reducing the time needed to study diseases and find cures, they help improve our lives.

2.2.1 Cultured Cells and Eukaryotes

In vitro cultures of animal cells offer several advantages in biological studies over whole organisms. These cultures mimic many of the cellular and molecular processes observed in live animals, increase the throughput of the experiment, and do not require the space and infrastructure compared to that needed to house animals. A large number of cell cultures, derived from humans and other animals, are currently available for investigation. Many of these are well characterized in terms of growth and differentiation properties. This, together with the relative ease in culturing and obtaining large quantities of pure cell populations, has been valuable for investigating processes in normal and disease conditions [29, 30].

Two eukaryotic model organisms that resemble cultured cells in many ways are the baker's yeast *Saccharomyces cerevisiae* (*S. cerevisiae*) and the fission yeast *S. pombe*. Both are rapidly growing micron-size organisms that can be cultured fairly easily and inexpensively in the laboratory. Normally they reproduce asexually (*S. cerevisiae* by budding and *S. pombe* by fission); however, in certain conditions they can also mate and reproduce sexually. The ability to switch between asexual and sexual lifestyles provides many advantages in genetic experiments. Both organisms have been at the forefront of many biological discoveries for decades. They offer a number of powerful genetic, biochemical, and molecular biological tools to accelerate the study of conserved processes (e.g., cell cycle control) [31, 32] and human diseases [33, 34]. While the cell cultures and unicellular organisms are useful in biological studies, they poorly mimic the three-dimensional environment and complexity observed in multi-cellular animals. Since live cells communicate with their neighbors as well as the environment, diseases affecting one tissue or cell population often indirectly impact other parts of the body. In this respect, whole animal models provide advantages to study the broad range of phenotypes, disease mechanisms, and complex cellular interactions.

A number of animal models are available today for experimentation that include vertebrates such as mouse (*Mus musculus*) and zebrafish (*Danio rerio*), and invertebrates such as worm (*C. elegans*) and fruitfly (*Drosophila melanogaster*). The main advantages of vertebrates are their higher degree of genetic and physiological similarities to humans. Due to their large size, these animals can be surgically operated to isolate tissues and cells for various experiments. They also offer rich morphological and behavioural features that make them suitable models for many human diseases. However, vertebrates also have several drawbacks that limit their use in the laboratory. These include slow growth, long life span, and high cost of maintenance. Additionally, the large size and slow growth of vertebrates are not suitable for HTS-based studies. In

these respects the invertebrate models, *C. elegans* and *D. melanogaster*, possess many features that are particularly appealing. For example, they have a short generation time (few days) and are relatively cheap to maintain and perform experiments on. A number of pioneering discoveries on these organisms have helped improve our understanding of human biology and diseases. Both of these boast a rich history, powerful cellular, molecular, and genomic tools, and extensive literature to undertake detailed investigations of biological problems. However, due to their small size (1-4 mm), one needs special tools and microscopes for handling them. This poses difficulties in studies requiring the examination of a large number of such animals.

2.2.2 The Nematode *Caenorhabditis elegans*

C. elegans is an established model organism to investigate the molecular mechanisms of conserved biological phenomena that occur in all organisms including humans [35]. It is one of the most thoroughly studied multi-cellular organisms in terms of genetics, development, behaviour, and physiology. It offers many experimental advantages including small size (~1 mm at adulthood), ease of culture conditions, rapid life cycle (2.5 days through 4 larval stages, Figure 2-1), high rate of progeny, well-mapped neuronal connectivity [36] and transparency. The adult worm has roughly 1000 somatic cells and a transparent body that allows visualization of cellular and molecular events in live animals using fluorescent proteins, such as green fluorescent protein (GFP), without the need for sacrificing the animal. Accordingly, the identity and lineage of every cell in the worm is known, which enables researchers to address biological questions at single cell resolution. The worm genome is compact (~20 times smaller than the human genome) and is fully sequenced, which greatly facilitates experimental manipulations and the study of gene function. The amenability of the organism to genetic analysis has led to isolation of a large pool of mutant strains (see http://www.wormbase.org) that can be effectively used to study gene function in regulating various developmental, behavioural, and physiological processes. Such studies have established the roles of many genes (e.g., HOX family members) and signaling pathways (e.g., Ras) in normal and disease processes [37, 38]; thereby facilitating the study of their homologues in other organisms including humans.

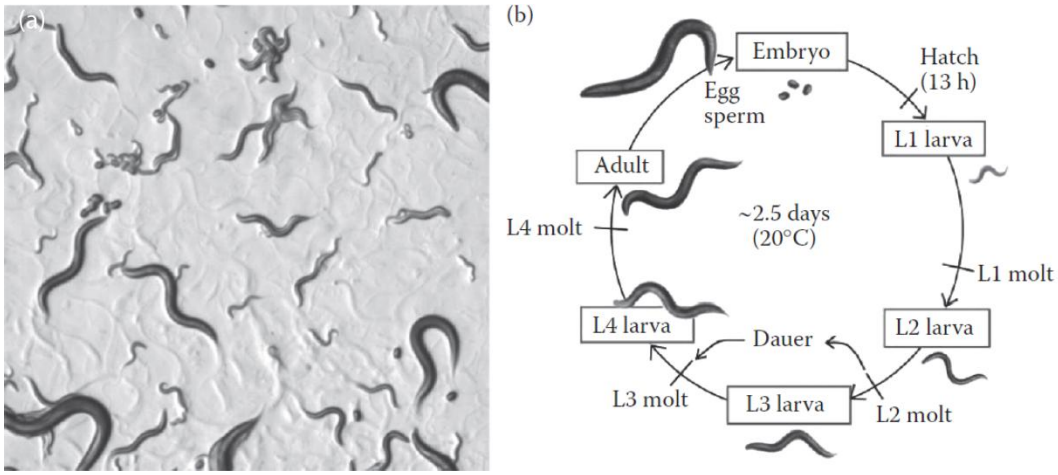

Figure 2-1 C. elegans and its life cycle. (a) A typical culture on an agar plate. Different stages of animals are visible. (b) Life cycle of C. elegans at 20°C. A fertilized embryo goes through four larval stages to give rise to an adult in roughly two-and-a-half days. Dauer is a reversible alternative developmental program that is induced by unfavorable growth conditions.[11]

2.2.2.1 Conservation of Biological Processes

The amenability of *C. elegans* to genetic manipulations has led researchers to study biological processes by means of isolating mutations and characterizing phenotypes. This “forward genetics” approach has been very successful in understanding the development and behaviour of the worm and the extent to which molecular mechanisms are conserved in eukaryotes. The availability of the genome sequence of *C. elegans* has further strengthened its utility by enabling large-scale functional genomic approaches to identify genes and understand their *in vivo* function. The findings have revealed that *C. elegans* shares more than half of its genes with humans and utilizes many of the same processes [1]. For example, genetic and molecular studies have identified conserved cellular machinery that control processes such as cell proliferation, cell differentiation, and cell death. It has been demonstrated that these processes utilize similar mechanisms in almost all eukaryotes, supporting the conclusion that results obtained in worms can be successfully translated to other organisms including humans. In addition to its value in addressing basic questions about animal development and behaviour, *C. elegans* has also proven to be an excellent system for studying the biology of human diseases. The worm genome contains many human disease gene orthologs [1, 39] that makes it possible to establish worm disease models, study cellular and molecular changes, and develop potential drug targets. This is evident through research on diseases such as cancers [40], bacterial and fungal infections [41], obesity [2], hypertension [3] and neuronal disorders [2-9]. Researchers have established mutant strains for these diseases that serve as models to study the underlying mechanism as well as to

search for chemical compounds/drugs to inhibit the defects. Some of these models have also been used for screening chemical compounds to identify gene targets and cellular processes, using conventional plate-based approaches. For example, in the case of the *C. elegans* HD model, chemical screening has identified two compounds, mithramycin (MTR) and trichostatin A (TSA) with demonstrated significant effect on promoting neuronal survival [42].

2.2.2.2 Development and Behaviour

The worm contains two sexes, self-fertilizing hermaphrodites and rare males. The hermaphrodites are essentially females except that they initially produce sperm for a few hours before switching to make oocytes. While males are not necessary for reproduction, mating provides opportunities for new genetic material to be introduced. The fertilized embryo goes through four larval stages (L1–L4) to generate an adult animal (Figure 2-1). An adult hermaphrodite contains 959 somatic nuclei that are organized into specialized cell types such as neurons, muscles, and intestine. Due to its small size and transparent body, *C. elegans* allows the study of biological processes at a single-cell resolution. Through a laser-assisted cell ablation technique, researchers have determined the lineage history and function of every cell in the animal. The electron microscopy technique was used in ultra-structural studies, which among other things has revealed interconnections of all neurons (302 in total). This serves as an invaluable resource in the study of the development and function of the nervous system.

The abovementioned cells constitute worm's sensory and motor systems that enable them to perceive and to move appropriately in response to a wide range of mechanical [43, 44], thermal [45], chemical [46], optical [47], magnetic [48] and electrical [49, 50] stimuli. One of the major sets of neurons in the worm that senses external stimuli is the amphid neurons which are extended from the head to tail (see Figure 2-2). For instance, a well-developed chemosensory system allows *C. elegans* to detect a wide variety of volatile and water-soluble chemicals in the environment. This allows the animal to find food, avoid harmful substances, and modulate physiological conditions such as diapause. Additionally, *C. elegans* contains thermosensory and mechanosensory neurons to sense temperature and external environment (e.g., soil particles) that make physical contacts with the animal in its habitat. Various standard assays and protocols have been developed to study these behavioural responses in worms on open surfaces through the analysis of speed of motion (0.2-0.6 $cm.s^{-1}$), omega turn, reversal frequency, stops and body bend frequencies. While these studies have provided us with significant details [51] to identify genes and mechanisms, few others such

as responses to light (phototaxis) and electric field (electrotaxis) are poorly characterized.

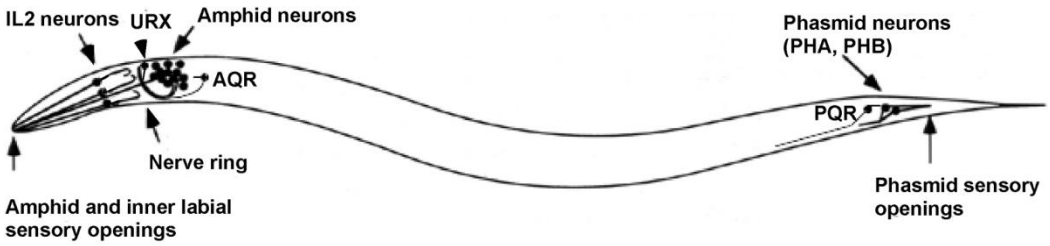

Figure 2-2 Schematic of chemosensory neurons' location in C. elegans [46].

Observation of the movement provides valuable information about the functionality of the neuronal and muscular system of the worm and allows functional dissection of molecular mechanisms by means of mutations, chemicals and drugs. Alternatively, changes in the movement behaviour can be used to deduce the impact of drugs and other environmental factors on the neuronal and muscular system.

2.2.2.3 Generation of Movement Behaviour through External Stimuli

During all stimulus-based responses, one of the assessable phenotypes of C. elegans, frequently used in behavioural studies, is its sinusoidal pattern of movement. When a worm moves on an agar gel surface, it leaves behind prints of its sinusoidal locomotion pattern and this has been used conventionally by biologists to study the worm's locomotion behaviour [52]. Locomotion movement of *C. elegans* has been generally classified into four distinct state modes: (i) forward motion, (ii) backward motion, (iii) omega turns (locomotion direction change by forming a body bend by bringing the head closer to the tail and forming an omega shape) and (iv) resting [53]. Speed as well as stroke and turn frequencies have been considered as the most important phenotypes of interest that provide quantitative information for movement behaviour.

At the cellular level, neuronal cells sense the stimuli and respond to them by changing their electrophysiological and biochemical properties inside the cell, resulting in the motor output. Yet, very little is known about the physiology of *C. elegans* neurons. Laser ablation studies have assisted in revealing the functionality and circuit connectivity of the 12 amphid sensory neurons. Goodman *et al.* [54] have shown that the neurons transmit signals through two voltage-dependent membrane currents, (potassium, K^{+1}, and calcium, Ca^{+2}, currents). These signaling pathways have been investigated through physical probing of neurons [54] as well as calcium transient imaging of intact animals *in vivo* [55-59] by using the FRET technique.

In particular, the FRET-based calcium sensors (i.e. macromolecules expressing the cyan and yellow fluorescent protein at both ends), tagged to individual neurons in worms, became good candidates for probing neuronal signaling. FRET-based studies have revealed insights regarding neuronal signaling actions during chemosensory, thermosensory and mechanosensory processes in *C. elegans.* In this technique, the animal is irreversibly immobilized during neuronal imaging and hence, correlations between neuronal activities and the overall movement behaviour of the animal cannot be determined. In order to achieve this goal, the animal should be allowed to freely move in response to stimulation. For instance, *C. elegans* behaviour under exposure to repellent chemicals has been investigated simultaneously with correlation to neuronal Ca^{+2} transient levels [59]. To achieve this, a dual imaging system has been used for recording the behaviour of the worm by a low magnification optical imaging apparatus from one side and the neuronal Ca^{+2} transient activities by a high magnification fluorescent imager from the other side of the worm.

Through the use of conventional electrophysiological probing and the abovementioned techniques, it has been reported that *C. elegans* senses and responds to electric signal within 60ms (16 Hz) [60], to light touch within 5 ms [61], and to isoamyl alcohol odour within 15-20 ms [62]. *C. elegans* shows negative phototaxis in exposure to light with a response time of 1s [47] or avoidance locomotion in exposure to $CuCl_2$ chemical with a latency of <10 s [59]. Clark *et al*. [63], in their study of thermosensory neurons using the Ca^{+2} binding protein, showed that the intracellular Ca^{+2} is maximized within 10 s and decreases to baseline within 40 s. Among the sensory behaviours mentioned above, the electrotactic behaviour of *C. elegans*, which was first reported in 1978 [49], has not been investigated as much as others. Although some of the neurons mediating this behaviour (such as ASJ and ASH) are known [60], the molecular mechanism of electrotaxis still remains unidentified. Whether the stimulation is sourced electrically, chemically (food, odor), mechanically (touch) or optically, a distinct attractive or repulsive response in *C. elegans* locomotion is observed. Locomotion behaviour has therefore been exclusively studied on *C. elegans* laboratory habitant agar gel plates. However, studying the worms' motion on an open surface is challenging mainly due to the voluntary nature of worm's movement, its randomness, and lack of control over the stimulation as well as environmental conditions on such surfaces.

2.3 *C. elegans* as a Model for Studying Neuro-Degenerative and Movement Disorders

Because of its simpler anatomy and comparatively fewer neuronal and muscle cells, *C. elegans* is an ideal system for studying disorders affecting these cell types. The worm contains just 302 neurons, as compared to over 100 billion in the human brain, thus conferring unparalleled precision and control in the identification and manipulation of neuronal cells. In the case of muscles, the most abundant class (somatic, striated type) consists of 95 body wall muscles that are used for locomotion. They are arranged in a stereotypic manner and can be readily visualized under a microscope. Studies on *C. elegans* have revealed that neuronal and muscle cells share many similarities with humans in terms of structure, composition and function. Furthermore, mutations in human disease gene orthologs that affect these cells can be readily analyzed in worms due to its amenability to genetic analysis and the power to probe gene function at a single-cell level. These and other features described earlier make *C. elegans* a valuable model for gaining insights into movement-related disorders, such as Duchenne's muscular dystrophy (DMD), Alzheimer's disease (AD), Huntington's disease (HD) and Parkinson's disease (PD) [4, 8, 9]. In addition to learning the basis of these diseases, *C. elegans* is also promising in accelerating the process of drug discovery by helping us to perform high-throughput genetic and chemical screens (Table 2-1) [64, 65].

Table 2-1 Disease models, candidate targets, and potential drugs that confer protection [11]

Disease Model	Mode of Induction	Genetic and Cellular Target(s)	Protecting Chemicals/Drugs
DMD	*dys-1/dystrophin; hlh-1/MyoD* mutants		Serotonin Prednisone
AD	Ectopic Aβ (1–42) expression	Insulin signaling pathway αB-cystallin Tumor necrosis factor-induced protein 1 Arsenite-inducibel protein (AIP-1)	*Ginkgo biloba* extract EGb 761
HD	Ectopic Poly-Q expression		Lithium chloride Mitramycin Trichostatin A
PD	6-OHDA exposure	*dat-1/dat1* Mitochondrial enzyme complex I and IV *egl-1/puma* *cep-1/p53*	GABA NMDA Bromocriptine Quinpirol Acetaminophen
	MPTP exposure	Mitochondrial enzyme complex I	Rofecoxib Modafinil
	Rotenone exposure	Mitochondrial enzyme complex I	D-α-Hydroxybutyrate in combination with Tauroursodeoxycholic acid
	Ectopic α-syn expression	ER-to-Golgi trafficking, mitochondria Aging-associated genes, such as *sir-2.1/SIRT1* and *lagr-1/LASS2* Endocytic pathway genes Cellular trafficking genes	1,2,3,4-Tetra-hydroquinolinones
	TH over-expression		Acetaminophen

2.3.1 Muscle Disorders

C. elegans possesses many conserved genes that are involved in muscular dystrophy. One of these, *dystrophin*, is linked to DMD [66]. DMD is a X-linked recessive disorder that is characterized by progressive degeneration of skeletal and cardiac muscles [67]. The presence of dystrophin-like gene *dys-1* in *C. elegans* has been useful for studying the mechanism of muscle degeneration [68-70]. In addition, researchers have carried out pilot screens for candidate drugs that suppress the disease phenotype [71, 72] (Table 2-1). These studies illustrate the use of the worm DMD model in understanding the disease mechanism and identifying potential treatments.

2.3.2 Neurodegenerative Diseases

C. elegans neurodegenerative disease models include three major disorders (AD, HD, and PD), all of which cause age-dependent progressive loss of neurons

or neural activity. A common feature of these disorders is the accumulation of misfolded protein aggregates. Because of its short lifespan and other experimental advantages (see Section 2.2.2), *C. elegans* can be used to facilitate and speed up the research on disease mechanisms. Researchers have created transgenic worm strains that are valuable in understanding the basis of protein aggregation and neuronal defects and search for therapeutic targets.

2.3.2.1 Alzheimer's Disease

AD symptoms include memory loss and cognitive decline that become severe with age as neuronal degeneration increases and affects larger areas of the brain. . In spite of the extensive work from several laboratories [73, 74], little is understood about factors that trigger the accumulation of misfolded proteins tau and β-amyloid (Aβ) and the resulting neuronal toxicity in AD. Researchers have generated transgenic *C. elegans* AD models by expressing the toxic human Aβ peptide (Aβ1–42) in body wall muscles [75-77] which can facilitate the identification of potential targets to understand the cause of AD [76, 78-80] (Table 2-1).

2.3.2.2 Huntington's Disease

HD is another age-dependent neurodegenerative disorder caused by abnormal expansion of glutamine repeats (polyglutamines or polyQ) in *huntingtin (htn)* [81]. Although *C. elegans* does not carry an *htn* counterpart, it has been shown that forced expression of human *htn-polyQ* in the worm causes neuro-degeneration similar to that seen in HD patients [82-85]. Therefore, advanced genetics and genomics technologies in *C. elegans* can be harnessed to understand disease mechanisms and discover candidate drugs. Researchers have also used the worm system to find drugs such as resveratrol, mithramycin (MTR), and trichostatin A (TSA) that reduce polyQ toxicity and promote neuronal survival [42, 86] (Table 2-1). These studies demonstrate the power of *C. elegans* in understanding the disease mechanism and drug discovery.

2.3.2.3 Parkinson's Disease

PD is one of the common neurodegenerative diseases of elderly people above the age of 65. One of the major causes of PD is the marked loss of dopaminergic (DA) neurons in substantia nigra, a region of the brain that controls balance and movement of the body. Its major symptoms are tremor, bradykinesis (slow movement), stiffness of the limbs and trunks or akinesia (inability to move), and postural instability (impaired balance and coordination). In order to understand the basis of α-synuclein (α-syn) accumulation (responsible for DA degeneration) and toxicity, researchers have generated transgenic *C. elegans*

strains over-expressing human α-syn that show protein accumulation similar to PD patients [9]. These animals serve as suitable models for molecular dissection of PD and screening of drug candidates. Thus, chemical and genetic screens have been carried out using α-syn-induced neuronal toxicity as an assay [87-91]. These screens have identified components of endocytosis, vesicular trafficking, and lipid metabolism (Table 2-1).

Besides mutations and other genetic modifications, several chemical compounds (e.g., 6-OHDA, MPTP and pesticides such as rotenone and paraquat) (Table 2-1) have been found to induce PD-like symptoms in humans and other animal models [92-97]. These chemicals cause degeneration of DA neurons by oxidative stress and/or inactivation of mitochondrial complex I [98]. The DA neurons in *C. elegans* are also susceptible to these neurotoxins and give rise to movement defects [99]. Such PD worm models have been valuable in exploring the mechanism of neuronal degeneration and the identification of potential neuroprotective compounds [10, 100-102] (Table 2-1).

2.4 High-Throughput and Automated Techniques to Manipulate *C. elegans*

Various features of *C. elegans*, particularly its small size, rapid growth and simple food requirements have made it a valuable model organism for high-throughput-based studies for addressing questions related to basic and applied biology. These include fundamental processes such as cell growth and differentiation as well as treatment of human diseases by understanding the molecular mechanisms underlying a disease and identifying and improving drug candidates and other therapeutic interventions as discussed in Section 2.3 [4, 5, 99, 102-105]. Therefore, introduction of HTS methods for *C. elegans* and their use at an early stage in the drug discovery process will significantly accelerate this process to create better candidates for clinical trials and ultimately better drugs to treat patients.

Over the years, several HTS methods have been developed to manipulate the worms in a rapid and efficient manner. All of them have shown promise and continue to evolve to meet new challenges and overcome shortcomings. Typically, these involve cultivating animals in multiwell format plates (either agar or liquid media-based) and screening for morphological and behavioural changes under a microscope. These methods could be semi-automated by the use of robotic and sorting devices. Methods have also been developed to rapidly screen for the viability of animals, using fluorescent dyes. In some cases, computer software tools have also been used to accelerate the analysis. In the remainder

of this section, major techniques available today will be discussed and highlight to their uniqueness, advantages and limitations will be provided.

2.4.1 Classical Approaches

Being a genetic model system, *C. elegans* is frequently used to screen for mutations that affect development and behaviour. The characterization of such mutations has been valuable in understanding how genes function and interact to control cellular activities. Typically, the mutant screening protocols involve growing worms on Petri dishes for about a week and observing animals under a microscope for desired phenotypes. Putative lines are grown and retested to confirm the presence of a mutation before initiating genetic experiments. Such an approach mostly involves working with a very small set of genes and often takes many years of hard work to obtain a reasonable understanding of biological processes. The discovery of RNA interference (RNAi) phenomenon has accelerated the pace of genetic analysis [106]. Depending on convenience, researchers can carry out RNAi experiments on traditional agar-based culture plates or in liquid media-containing microwell plates. The liquid medium has the advantage of scaling up the volume with less effort compared to the plate culture; and is, therefore, a method of choice for large-scale RNAi studies involving a large number of genes [107]. Several chemical screens have also successfully utilized the liquid media protocol to identify beneficial compounds and to assess the effect of toxic substances on animal health and viability [108, 109]. For example, as mentioned in Section 2.3, chemical screens in *C. elegans* disease models have identified several candidates that inhibit neuronal toxicity (Table 2-1). While the above plate and liquid culture-based protocols are well established, the process is slow, labour-intensive, and does not readily scale up. Furthermore, the phenotypic assays (such as movement and growth) are largely manual and therefore prone to systematic and random errors as well as subjectivity. This limits the use of *C. elegans* in large-scale studies that require rapid, sensitive, and quantitative assessment of phenotypes with very little or no variation in measurements. In order to overcome some of these limitations, a few high-throughput methods have been developed that utilize cutting edge engineering and computer technologies.

2.4.2 Engineering Approaches

To overcome the challenges encountered in classical approaches discussed in section 2.4.1, several techniques have been engineered. These include the use of robotic arms, the development of the Biosorter and the Complex Object Parametric Analyzer and Sorter (COPAS) systems, and finally the recent

advancements in the field of mirofluidics to assay worms. These are discussed in the remainder of this section.

2.4.2.1 Conventional Robotics

The conventional liquid handling robotic systems used in molecular biology experiments have been successfully adopted in worm screening protocols. These systems typically consist of a pipetter, a culture plate-handling unit, a microscope and a computer. The computer controls various operations, such as pipetter movement, volume adjustment and plate handling. The pipetter can dispense defined volumes of liquid media (containing bacteria and/or chemicals) into microwells of a culture plate (e.g., 96-well or 384-well plate). Worms are grown inside microwells for a desired period of time and their phenotypes are monitored by a microscope on a regular basis. In certain kinds of screens, such as those involving thermal avoidance behaviour [110], data collection and analysis could be automated by using a computer [111]. The speed, accuracy and automation afforded by robotic equipment have been valuable in carrying out many high-throughput screens in *C. elegans* (e.g., see [107, 112]). Although useful, a major drawback of conventional robotic systems is their high cost that limits their widespread use. Additionally, the instrumentation cannot be used for certain kinds of HTS-based *C. elegans* studies. For example, one key operation in screening worms is to obtain fluorescent and visual images of individual worms that have been fed with RNAi bacteria or treated with chemicals. This operation is difficult to perform in the microwell plate format due to the inherent motion of animals and fluorescent signal distraction. Although it is possible to analyze the speed and shape of moving worms using specialized software [52], the technology is not advanced enough; and therefore, it has not been widely adopted. The robotic systems are also not suitable for screens that require precise measurement of movement-related parameters (i.e. angle of body bends and frequency and amplitudes of sine waves), time course of phenotypic changes and single-cell observations.

2.4.2.2 Biosorter and COPAS

Two of the few automated HTS and sorting devices for *C. elegans* research available today are the BioSorter and the COPAS, both made by Union Biometrica (Figure 2-3). These are large particle flow cytometers capable of analyzing, sorting, and dispensing worms, cells and other micron-sized objects (up to 1500 μm). As the object passes through the flow cell, its optical density, length and fluorescence are measured with the help of lasers. This information is analyzed by computer software that in turn controls a pneumatic sorting mechanism to dispense the object in a predefined manner. Compared to COPAS, BioSorter is more flexible and has a few additional features that make it

suitable for a larger range of applications. Both systems can sort worms into multiwell microtiter plates in a rapid (more than 100 worms per second) and efficient manner. This has facilitated several high-throughput screens using phenotypes such as size, viability, and GFP fluorescence as screening criteria [107, 113-116]. These equipments have made significant contributions to *C. elegans* research by making large-scale animal-sorting and aliquoting a routine job, which was earlier not possible. However, similar to the robotic systems, COPAS and BioSorter have limited applications and cannot be used in screens requiring high-resolution single worm and movement-related analyses.

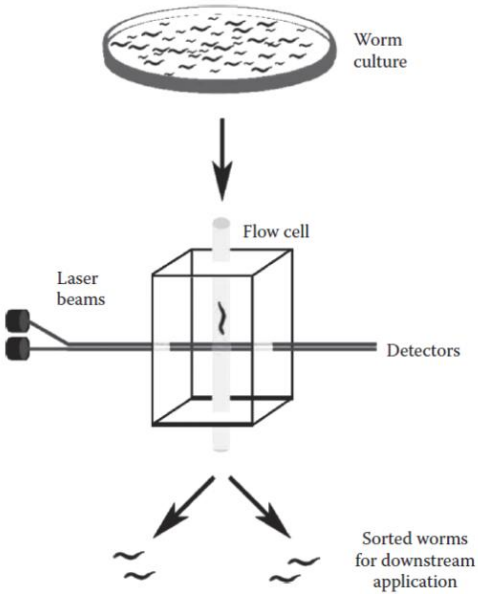

Figure 2-3 Principle of BioSorter and COPAS systems. As worms pass through the flow cell, various parameters, such as size and GFP fluorescence, are recorded. Depending on the experiment, animals can be sorted into different categories. [11] (Copyright ©, CRC Press 2011)

2.4.2.3 Microfluidic Devices

As reviewed earlier, many protocols are available to manipulate worms on agar plates and in liquid media, but there is virtually none that can efficiently analyze individual animals both at cellular and behavioural levels, at high resolution in a rapid, high-throughput, automated, and cost-effective manner. This has been a major impediment in the widespread use of *C. elegans* in drug discovery.

Recently, microfluidic techniques have been developed to overcome some of these limitations to facilitate more precise and quantitative studies in *C. elegans* [11-14, 117, 118]. Microfluidics is the science of understanding and controlling fluid flow at a microscale level. It offers numerous advantages over manual and robotic methods such as rapid analysis, reduced chemical consumption, lower

cost and automation. Due to their miniature size, microfluidic structures confer great precision in visualizing and quantifying biological processes in living systems. For example, microfluidics has been used in genetic and proteomic analyses [119, 120], cell cytometry [121], cellular biosensors [122], cell chemotaxis [123] and cell culture [124]. Drug discovery is one of the areas where microfluidics is expected to have enormous impact [125-129].

2.5 Microfluidic and other Miniaturized Approaches Applied to *C. elegans*

As discussed above, the microfluidic approach offers several advantages over traditional plate-based and macro-robotic methods in *C. elegans* HTS applications. Microfluidic environments are advantageous due to their low cost, high degree of control, accurate dosing, ability to analyze individual worms, and flexibility to integrate pre- and post-operational units for various applications. Microfluidic devices used in worm studies can be categorized into three streams. First, they have been employed to investigate animal's environmental interactive behaviours mostly focused on mechanical properties of worms [130-134] and their growth and chemical exposure interactions inside confined chambers [135-141]. Second category of worm-based microfluidic research is the studies investigating worms at the cellular and sub-cellular levels. Animals have to be immobilized in these assays for various applications such as neuro-behavioural studies [142-145], screening and sorting worms [146-151] and laser-assisted microsurgery [146, 149, 152-157]. In these cases the precision conferred by microfabrication helps capture worms at a certain location; thereby, facilitating a study of changes in cellular and molecular processes. Lastly, microfluidics has also been used to study animals' repulsive and attractive responses to external stimuli such as chemicals [158-161], light [47, 162, 163] or magnetic and electric signals [15, 16, 18, 21, 162, 164, 165]. Animals are allowed to freely move in these assays and the movement behaviour analysis is considered to be the most important phenotype to study. This section briefly summarizes the abovementioned microdevices and their applications in worm-based studies.

2.5.1 Miniaturized Force-Sensing Devices

Microdevices have been used recently to study physical parameters in live worms as they interact with the environment. Mechanical properties of worm cuticle and its body force exertion play important roles in biological processes such as mechano-sensation, locomotion, environmental adaptation and development. One of the setups incorporated a two-axis microstrain gauge-force sensor (at the base of micro-cantilever beams) to measure mechanical

interactive forces generated by moving worms (through body contact with SU8 pillars), as shown in Figure 2-4a and b [130]. The forces generated by *C. elegans* were found to be in a micro-Newton range (2.5 ± 2.5 µN) generated in hundreds of milliseconds of mechanical contact with pillars. Although brief, this interaction was sufficient to evoke a behavioural response demonstrating the efficiency of the neuronal circuit and applicability of micro-structured devices in studying worms' sensory ability. This technique is also promising in analyzing the genetics of locomotory neuronal system.

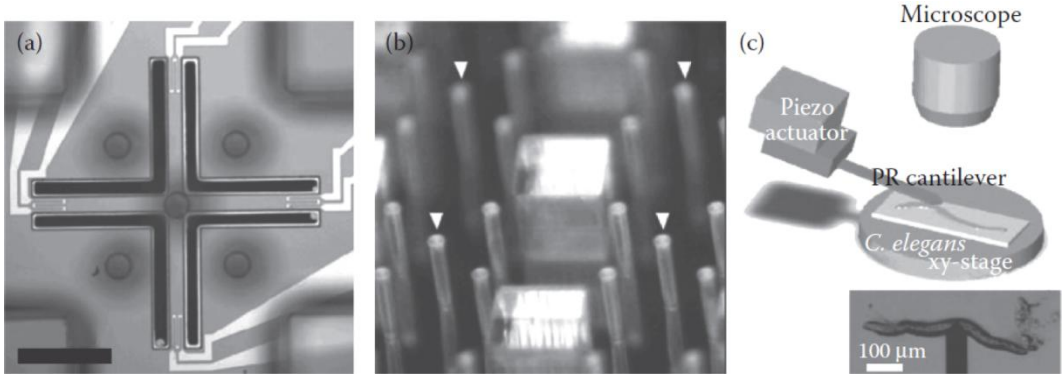

Figure 2-4 Force-sensing microdevices for C. elegans. (a, b) A MEMS device for measuring locomotion generated force [130]. (a) A cross-shaped bridge with a fabricated force sensing SU8 pillar at the center (shown by white arrows in (b) and four surrounding passive pillars. Each bridge is connected to a strain gauge at the other end forming a Wheatstone bridge configuration. (c) A piezoresistive cantilever-based sensor [131]. An actual image of a worm under compression beneath the cantilever actuator is shown on the bottom. (Reproduced by Permission of the Royal Society of Chemistry 2009 (a and b) and National Academy of Sciences USA 2007 (c))

Understanding the worm's body mechanics will help better identifying the underlying neuromuscular processes for various behavioural outputs. In another study, the mechanical property of the *C. elegans* cuticle was measured by a piezoresistive cantilever (Silicon-based) force-displacement sensor [131] (Figure 2-4c). Forces were applied through the cantilever tip on the worm cuticle, immobilized under the tip, and the stiffness was measured through the piezoresistive sensing mechanism. It was found that the force-displacement curve of the *C. elegans* body is linear showing that the body of the worm can be modeled as a cylindrical shell with an internal hydrostatic pressure. Using this model, it was estimated that the *C. elegans* cuticle has an effective elastic modulus on the order of 380 MPa. Reducing the internal hydrostatic pressure (by cuticle puncturing using a sharp tip or by hyperosmotic shock) had only a modest influence (~20% reduction) on the animals' stiffness. It suggests that the cuticle proteins may also contribute to stiffness of the body. Consistent with this, the mutants with altered body shape and cuticle structure had significant effect on stiffness. It was therefore concluded that the overall body stiffness is contributed by both cuticle stiffness and the internal hydrostatic pressure.

2.5.2 Devices Consisting of Microstructured Environments

Unlike in the laboratory where *C. elegans* is grown on a simple agar-based media, the natural habitat of the animal is far more complex consisting of soil, compost, and numerous microorganisms. Therefore, the worm has evolved a highly sophisticated nervous system to recognize external stimuli and generate an appropriate (attraction and repulsion) response as discussed in sections 2.2.2.2 and 2.2.2.3. In order to study such behaviours, researchers have fabricated microdevices that mimic soil-like environments. One of these consisted of agar-based microstructures in the form of an array of squared centered posts or grids [132]. The device was filled with a buffer solution and worms were allowed to swim and crawl in this microenvironment. It was observed that the wild-type worms moved faster in the grid whereas mutants such as *unc-29* (uncoordinated worms which exhibit abnormal sinusoidal movement) were severely compromised. Additional testing of two mechanosensory mutants (*mec-4* and *mec-10*) revealed defects in movement, thus revealing the role of the mechanosensory neurons in sensing obstacles in the environment and directing the movement of the animal. It is, therefore, possible to use this device in a genetic screen to identify genes involved in mechanosensation.

Two other microstructured devices were also described that consisted of cylindrical posts and sinusoidal channels [133]. The cylindrical post-containing device, called “artificial dirt,” had variable post diameters (100–500 μm) and interspacing (60–100 μm). This device was used to study the crawling behaviour of the worm. The movement of animals in the device was undulatory with dorsoventral bends, similar to the control model trajectory pattern on the agar surface, although the frequency of sinusoidal body posture was reduced compared to the agar gel. Topographic changes in the artificial dirt device were reported to have minimal effect on animals’ crawling behaviour (140±17 $\mu m.s^{-1}$ speed in the case of 100 μm post diameter and 100 μm interspacing compared to 200-250 $\mu m.s^{-1}$ speed on the agar surface). The sinusoidal channel device was used to study the waveform and trajectory of crawling worms, and the amplitude and wavelength of motion were quantified. Altogether, these devices are applicable in studies involving locomotion phenotypes analysis.

In addition to phenotypic assessment, categorizing worms based on their size/age is desired in biological experiments to lower the results variability due to sample non-uniformity. A microfluidic device containing a network of different microstructures inside a chamber with 3 input and 6 output channels was constructed for passive age- and size-based sorting of *C. elegans* [134]. Various microstructure configurations such as posts, pools and “smart filter and mazes” have been tested. These structures imposed flow resistances on worms of different sizes and acted similar to sieve-based cell sorters. The “smart filter and

maze" configuration had the optimal sorting with a throughput of 200 worms per minute with 94% adult recovery and 0.2% larvae contamination. Theoretically, this could provide a throughput of 2.9×10^5 to 1.73×10^6 worms per day which was significantly higher than the conventional manual methods and cheaper than the robotic ones described before.

2.5.3 Chamber-Based Devices for Study of Growth and Chemical Exposure

C. elegans has been used as a model organism for molecular and genetic studies of pathways involved in development, metabolism, stress responses and aging [166, 167]. In addition to genetic homology to human, the worm's life cycle is short with a high regeneration rate, which makes it an ideal model for HTS of developmental and aging processes. Hence, it is important to develop tools and techniques to study worms' physiology, development, regeneration and progeny in an automated manner. In this regard, a novel set of microfluidic designs incorporating growth chambers to culture and monitor worms for a longer duration have been investigated. One such system that was developed earlier had the shape of a compact disc (CD) with enclosed chambers in which worms could be kept alive and behaviourally assayed for more than a week [135]. Since this time period is enough to support growth for 2-3 generations, the device is useful to carry out a broad range of genetic, biochemical, and pharmacological experiments in a precise and controlled manner. The platform contained interconnected cultivation, nutrient and waste chambers, that were arranged in a row in an axial direction of a CD (Figure 2-5a).

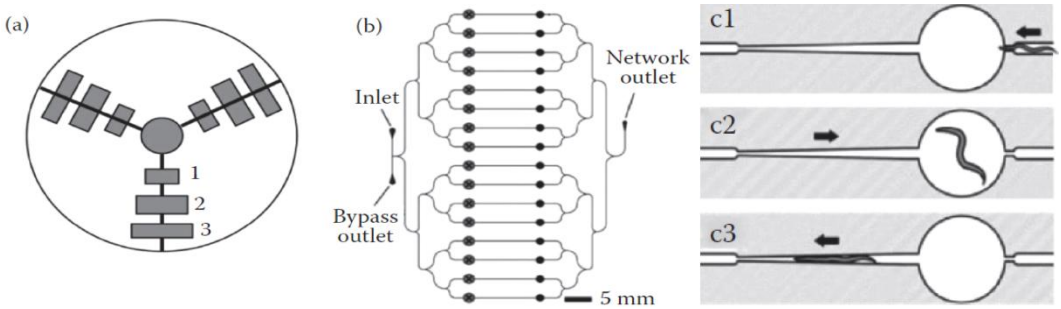

Figure 2-5 Microfluidic devices consisting of growth chambers. (a) A CD format device that has three interconnected chambers (1: nutrient, 2: cultivation and 3: waste) [135]. (b, c1–c3) An array format device [136]. (b) The left and right circles represent valves (to control liquid flow from the inlet to the outlets) and microchambers, respectively. (c1) The right end of the channel is just wide enough to allow entry of an early L4 stage animal. (c2) As the worm grows it is unable to escape the chamber. (c3) For observation purposes the worm can be immobilized into the narrow region of the middle channel. The arrows in c2 and c3 mark the direction of the liquid flow. (Copyright ©, CRC Press 2011 (a), Reproduced by the Permission of the Royal Society of Chemistry 2010 (b, c1–c3))

Upon rotation of the CD in Figure 2-5a, nutrients were pumped into the cultivation chamber while the waste was ejected to the outer chamber via centrifugal force-driven fluid mechanism. In the device shown in this figure, a single hermaphrodite placed in the cultivation chamber was able to reproduce after 3 days. The animals continued to reproduce till day 9 (1100 worms per chamber) indicating that the population was viable and fertile. After day 9, the chambers were saturated and many worms entered into the dauer stage due to the lack of nutrients and overcrowding. Accordingly, the effect of cultivation conditions on worms' health was determined by measuring the body bending frequency. Nonetheless, the compact and fully-automated (food introduction and waste removal with no human interventions) design of the device is highly suitable for studies requiring long-term observations of behaviour and reproduction with no human intervention. This is useful for instance in the *C. elegans*-based space project † where a low-weight, automatic and versatile tool is considered valuable in studying the biological effects of space travel on human.

Hulme et al. [136] recently reported a microfluidic device containing an array of tapered channels for long-term culturing and phenotypic analysis of worms (Figure 2-5b, c1–c3). In this device channels were connected to microchambers at one end to allow individual worms to be cultured over an extended period of time. By directing the worm into the tapered channel (via liquid flow), it could be immobilized for visualization. Reversing the liquid flow enforced the animal to return to the growth chamber. The survival and growth of the animal (which was similar to the plate-grown worms) were ensured by a continuous supply of bacterial solution and removal of the waste (performed once every day). And the effect of aging on reduction in locomotion behaviour was studied through the monitoring of the worms' swimming frequency inside the chambers. The parallel design of channels is suitable for HTS of chemicals to study changes in the growth and lifespan of the animals.

In a similar approach, Krajniak and Lu [137] developed a microchip that confined L1 stage animals in 8 chambers for long-term cultivation and high resolution developmental imaging. Worms were immobilized inside the chambers on-demand by injection of a biocompatible polymer (Pluronic F127) into the chamber which exhibited a thermo-sensitive sol-gel phase transition behaviour within 2ºC through external temperature control channels. This method was shown to have no effect on animals' development. Two days of culturing (L1 to YA stage) with continuous supply of nutrients and gas was achieved in this work. Worms were demonstrated to be viable by monitoring their locomotory behaviour and pharyngeal pumping rate inside the chambers.

† See BBC News, "Worms survived Columbia disaster", 2003-05-01.
URL: http://news.bbc.co.uk/2/hi/science/nature/2992123.stm

In another microfluidic device consisting of 48 microchambers (arrayed in a rectangular configuration), single animal loading into chambers, chemical delivery and body bend frequency characterization was demonstrated [138]. All chambers were connected to a single serpentine channel via narrowing microchannels. Worms inserted into the serpentine channel were loaded individually into the narrowing channels, until all channels were occupied. Afterwards, the worms were pushed into the chambers by a positive pressure flow. Chemicals were transferred into the chambers afterwards by injection into the serpentine channel. Reduction in animals' body bend frequency through exposure to the anesthetic Sodium Azide was demonstrated in the chambers. The fact that the worms remained in the chamber while wiggling in-place made extraction of body bend frequency data easier and applicable to tens of worms at a time.

In addition to fabricating microdevices of PDMS material, as described above, researchers have also used liquid microdroplets as isolation chambers for the worms. Due to their tiny size, the droplets provide unparalleled control and sensitivity in biochemical and molecular biological assays while reducing the cost of reagents. In a study focused on the viability and growth, *C. elegans* eggs were compartmentalized in small aqueous culture vessels (plugs) of 660 nL volume within a piece of tubing using perfluorocarbon oil as a carrier [139]. The eggs hatched into larvae in 2 days, and within 4 days adults were able to reproduce and survive inside plugs for up to 6 days. An application of droplet-based growth of worms could be used to study the effect of chemicals on neuronal development and behaviour. This was demonstrated by the use of MPP+ (1-methyl-4-phenylpyridinium), an active metabolite of neurotoxin MPTP (1-methyl-4-phenyl-1,2,3,6-tetrahydropyridine), in droplets (16–20 nL volume) that were generated by *n*-hexadecane oil as a shearing agent [140] in a T-shape droplet generation microchannel configuration. Droplets containing worms were arrayed in a rectangular configuration using a downstream droplet trapping chamber array. The effect of MPP+ in humans and other animal models, including *C. elegans*, has been described in details [98, 99, 168]. It causes degeneration of DA neurons leading to PD-like symptoms (see Section 2.3.2). The introduction of MPP+ in droplets affected the activity of animals, as measured by stroke frequency (2.6 Hz compared to 3.1 Hz in control animals). Additionally, exposed animals were frequently frozen in omega shape and exhibited reduced movement. Thus, the microdroplet system could be used for chemical screening in worms. Later on, Shi et al [141] integrated a tapering channel into the microdroplet based encapsulation array to immobilize and to image worms during the behavioural assay. Each droplet trap chamber was connected to a tapered channel at one side. They demonstrated the effect of neurotoxin 6-hydroxydopamine (6-OHDA) on DA neuron degeneration through immobilization

and fluorescent imaging as well as on animal mobility by stroke frequency measurement. Altogether, chamber-based microfluidic devices have been demonstrated to be highly efficient in manipulating worms at a single animal level, exposing them to chemicals with a high temporal resolution and assaying the worms at both cellular (imaging) and behavioural (developmental analysis of locomotion) levels.

2.5.4 Microfluidic Devices for Immobilization

One of the main challenges in observing worms in liquid environment is their continuous motion. This severely limits high-resolution imaging to analyze cellular processes, perform microsurgery, and characterize certain behavioural processes. The traditional methods of immobilization such as those involving chemicals to paralyze animals or glue to irreversibly bond them to a surface are slow and harmful, and hence not suitable in high-throughput experiments. In contrast, microfluidic systems employ several methods to immobilize worms in a rapid, efficient, and reversible manner to facilitate such experiments. Two of these, vacuum suction channels and the inflatable PDMS membrane layer inside the channel, can physically hold the worms. The other methods include temperature-based control to reduce swimming and body motion, and use of chemicals such as anesthetic (carbon dioxide (CO_2)) or biocompatible polymers (Pluronic F127) which exhibit thermo-sensitive sol-gel phase transition behaviour to immobilize worms. In the following sections various applications of the immobilization-based approaches, in carrying out genetic and cell biological studies, will be briefly discussed.

2.5.4.1 Neuro-Behavioural Studies

The optical transparency of *C. elegans* and its relatively simple nervous system have greatly aided the analysis of neuronal function in mediating behaviour. While the traditional plate-based approach is quite successful [36, 46], it is not suited for single worm and single neuron-based studies due to the small size of the animals and a lack of spatial and temporal control over stimulus delivery. The microfluidic approach can overcome these limitations. Two microfluidic devices, *olfactory* and *behaviour chips* [142], were developed to examine the activity of certain neurons that mediate movement and odor sensing (olfaction). The behaviour chip, consisting of a simple PDMS microchannel, had wide ends to allow worms to freely enter into the channel. The middle region was only slightly wider than young adults allowing them to squeeze inside but narrow down at one end to prevent them from escaping (Figure 2-6a). Thus, a trapped worm had little room to wiggle its body sideways, but the head could move freely. Because of this design, the sinusoidal body waves generated by the worm could

propagate along its body. This setup was used to measure the activity of a pair of neurons known as AVA that are major command neurons mediating backward locomotion. The findings not only confirmed the role of AVA neurons in reversal behaviour, but also revealed the precise duration of their activity by simultaneous imaging of the genetically encoded fluorescent calcium indicator G-CaMP in the AVA neuron.

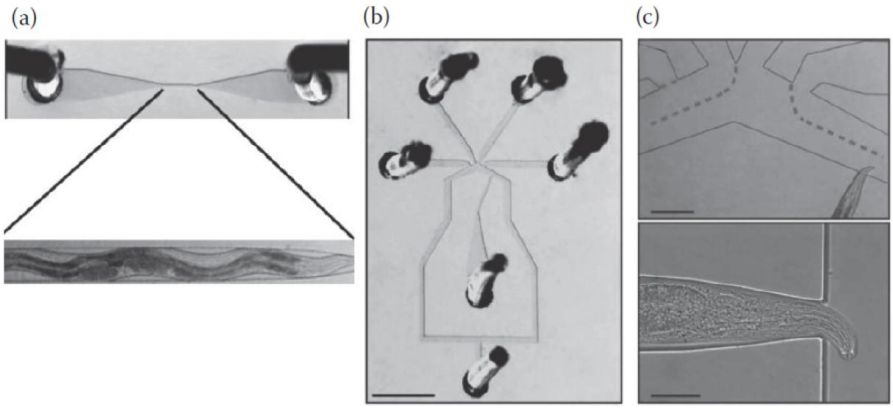

Figure 2-6 Microfluidic chips for analyzing behavioural and olfactory responses in C. elegans, modified from [142]. (a) The "behaviour" chip for studying neuronal activity in locomotion. The worm is trapped in the narrow region in the middle. (b) The "olfactory" chip design. Scale bar=2 mm (c) A close-up view of the olfactory chip showing the head region of an immobilized worm. The dotted lines mark the interfaces between the fluids. Scale bar 150 μm (top) and 30 μm (bottom). (Copyright ©, Nature Publishing Group 2007)

The olfactory chip, also made of PDMS, consisted of a tapered microchannel (wedge shaped) to trap the worm. One end of this trap was just wide enough to allow the worm's head to protrude out of the channel. This configuration allowed the nose of a worm to be exposed to chemicals that were supplied through a set of four channels (Figure 2-6b and c). This setup provided spatial and temporal control over chemical exposure that is not possible in a standard plate-based experiment. Additionally, the system allowed rapid and efficient recovery of the animals. The Ca^{+2} transient imaging of the ASH neurons (that respond to various stimuli such as mechanical, osmotic, and chemical) in such a setup revealed new roles when the animal was exposed to an osmotic stimulus. For instance, it was demonstrated that the ASH neuron chemosensation was strongly age-dependant with an increase in neuronal activity from day 1 to day 3 post-L4-stage aging and a sudden decline at day 5 [143]. A slight variation of this approach (immobilization with deflectable membrane and tapering channel simultaneously) was used to study the transient response of ASH and ASER neurons to dynamic changes in the chemical stimulus (sequences of glycerol, Sodium Dodecyl Sulfate (SDS) and copper in M13 buffer or ethanol exposure effect on sensing sodium chloride, NaCl) [144, 145]. Copper exposure produced the sharpest increase in the ASH intracellular Ca^{+2} followed by glycerol and SDS showing

different levels of activity of this neuron in chemosensation [144]. Results also showed that ethanol suppressed the ON-response of ASER neuron and interfered with this neuron's adaptation to NaCl [145]. These results demonstrate the power of microfluidic chips to understand the precise roles of neurons and how the neuronal activity modulates behaviour.

2.5.4.2 Screening and Sorting Worms

Over the years, the methods of phenotyping and mutant screening in *C. elegans* have matured from exclusively using morphological and behavioural criteria to combining them with fluorescent markers, such as GFP, to obtain detailed information on morphologies of cells and sub-cellular structures. While these approaches provide valuable information, the entire process of screening animals is manual and therefore slow, serial and subjective. Robotic systems such as Biosorter (see Section 2.4.2.2) provide a good alternative, but a number of factors limit their usage. In order to address this, several laboratories are developing microfluidic systems with varying degrees of automation and throughput. A majority of the microfluidic devices being described use a pressure-based immobilization approach. One of these consisted of suction ports (narrow channels with diameter less than an adult worm) located perpendicular to the main channel that carried worms (Figure 2-7) [146]. The application of suction through these ports physically immobilized the animal. The medium inside the main channel could be exchanged allowing new worms to be introduced into the channel. An advanced version of this setup consisted of multiple parallel microchambers, each of which was capable of immobilizing worms by suction to facilitate sub-cellular imaging and sorting.

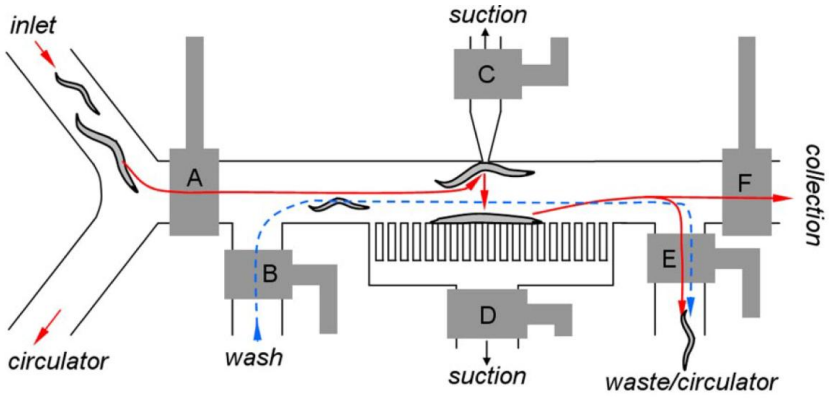

Figure 2-7 A microfluidic device to immobilize worms using side suction channels [146]. Worms enter the main channel from the left inlet. A–F mark different valves to direct the flow of worms. For high-resolution imaging, animals are briefly captured in the middle region by pneumatic valves applying suction pressure. The dotted blue line shows the direction through which worms are flushed during channel washing. (Copyright ©, National Academy of Sciences USA 2007)

In order to enable the screening of chemicals and RNAi libraries, the microchamber device could be connected to an interface chip consisting of an array of aspiration tips. When lowered in a microwell plate, the aspiration tips drew minute quantity of media from individual wells and delivered it to worms in microchambers. This integrated system promises to accelerate the screening of a large number of animals and chemicals in a high-throughput manner. Chung et al. [147] reported a modified version of the above-mentioned suction-based immobilization approach by incorporating a temperature control mechanism to allow better immobilization for high-resolution imaging and screening. The worms were first positioned in the detection zone by suction and then rapidly cooled to 4°C (within ~2 s). The two levels of control proved to be highly effective in complete immobilization of the animals, thus allowing detailed examination of neuronal processes. The entire procedure of worm handling and imaging was automated and shown to have a much higher resolution compared to other microfluidic-based screening devices.

The flexibility of the PDMS polymer offers possibilities to immobilize the worms in different ways. One such approach involves the use of compressible microchambers, in which worms are held in place by physical trapping. Such a microfluidic system typically consists of a bi-layered channel that contains pressurized air in the top layer and worms in liquid in the bottom layer. The layers are separated by a thin flexible PDMS membrane that deflects downward as the air pressure in the top layer is increased, thus confining the worm to a very small region and effectively trapping it (Figure 2-8). A microfluidic chip consisting of this control mechanism was recently used to screen for mutants in a high-throughput manner [148]. The device had three arms, one of which (main arm) was used to load, immobilize, and image worms. The other two arms were used to collect non-mutant (wild type) and mutant animals. The screening and sorting were aided by a computer to facilitate opening and closing of the channel valves to direct the worm flow. It was demonstrated that the device could screen worms at a sustained rate of 1500 per hour.

Another type of pressure-based device, developed by Hulme et al. [149], consisted of a tapered (wedge-shaped) channel that acted as a clamp. The flow of the liquid through the channel (toward the narrow end) forces a worm to move down the channel until it gets physically confined in the narrow region. A device consisting of 128 such parallel channels was shown to distribute and immobilize worms in less than 15 min [149]. The device allowed high-resolution imaging of cell morphology using GFP markers and was suitable for HTS of a large number of animals. It is often important to position and immobilize worms in a specific body orientation for enhanced imaging and sorting purposes. A microfluidic device was developed that could passively orient and screen worms in a lateral

orientation with 84% efficiency [150]. To achieve this, a curved narrow microchannel rather than a straight one was used to orient the worms in the dorso-ventral posture for fluorescent imaging and post-imaging sorting.

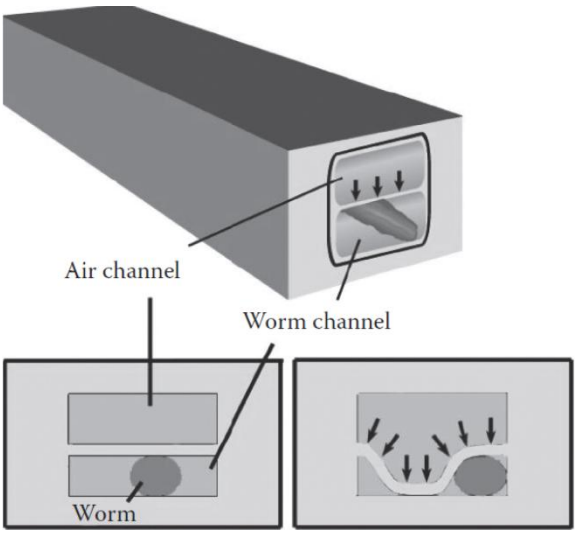

Figure 2-8 Schematic drawings of a three-layered microfluidic device for immobilization of C. elegans. The middle layer consists of a deflectable PDMS membrane that, in the presence of compressed air in the top channel, bends downward and physically wraps the worm in the bottom channel. [11] (Copyright ©, CRC Press 2011)

The final kind of immobilization approach involved the use of an anesthetic CO_2. Unlike the pressure-based approach, which is appropriate for only a short period (few minutes), CO_2 had the advantage of keeping animals immobile for a much longer duration (up to 2.5 hr) without any apparent defect in their behaviour [151]. Furthermore, it was relatively easy to introduce CO_2 in the PDMS-based channel as it diffused within 1-2 min and almost completely immobilized the animals. This makes it an attractive method that could facilitate high-throughput worm screening.

2.5.4.3 Laser-Assisted Microsurgery

As discussed before, laser ablation is one of the well-established methods used to knock out individual cells and neurons in animals for their functional analysis. Immobilization of *C. elegans* in a microfluidic channel provides a powerful means to perform surgical operations without the need for chemicals and agar gel pad mounting. Because it is possible to recover operated animals and image them in the channel over extended periods of time, the microfluidic approach offers unparalleled flexibility and control to explore sub-cellular structures and nerve regeneration processes *in vivo* [152]. Nearly all immobilization approaches discussed above have been used to perform laser-assisted ablations of neuronal processes. The suction pressure-based device

developed by Rohde et al. [146] was successfully used to sever the axon of a touch neuron and the process of regeneration was monitored subsequently. Guo et al. [153] and Zeng et al. [154] performed similar operations using a bi-layered microchannel design consisting of a flexible PDMS middle layer (Figure 2-8). Neuronal regeneration was shown to happen in ~70 minutes [153]. While both approaches appear to work efficiently, the bi-layered system may offer a better control as animals are completely surrounded by the membrane and have no room to wiggle. The tapered channel design, which was earlier developed by Hulme et al. [149] for phenotyping and screening, has also been adopted in surgical experiments. Allen et al. [155] used a variation of this design in a microfluidic chip consisting of several parallel two-stage tapering channels, each having a wide region to load worms and a shallow taper to immobilize animals. The worms were recovered after surgery and the process of nerve development was examined by time-lapse imaging. Effect of various chemicals on neuronal regeneration could be studied on worms using a combination of conventional well-based chemical exposure procedures and on-chip laser axonomy [157]. It has been demonstrated that kinase inhibitor staurosporine suppresses neuronal regeneration, while administration of a Protein Kinase C (PKC) activator enhances this process. These results were partially in agreement with other neuronal studies on different animal models showing the presence of some conserved biological processes between the worms and other animals. Advantageously, the worm-based studies are performed significantly faster and cheaper due to the advantages offered by microfluidic approaches discussed before.

While the above-mentioned pressure-based devices are quite successful, they can cause physical damage to worms due to excessive compression resulting in death of some of the animals. In order to overcome this limitation, Chung and Lu [156] developed a temperature-based microfluidic system. Their device consisted of two parallel channels that function independently to allow simultaneous worm-loading and exiting. The diameter and length of channels were comparable to the L1 worm (~14 μm and ~190 μm, respectively) to allow precise fit into the channel. A wide temperature control channel located perpendicular to worm channels rapidly cooled the animals such that they were completely immobilized. Specific neurons were ablated using a computer-based automated imaging and laser guiding system. Because of the automation, the setup could perform ablations in a high-throughput manner, something that was not possible with the traditional manual method.

2.5.5 Stimulus-Based Devices

As discussed in previous sections, typically, in order to visualize and manipulate worms within the surveyed microfluidic environments, their natural movement is suppressed by the use of hydraulic flows and mechanical confining forces. Although these methods are advantageous and bring automation and higher throughput to *C. elegans*-based assays, they are not suitable for performing behavioural studies on worms such as movement-based sorting and screening.

The flexibility of the design, operation, and integration of microfluidic devices has led to new applications in *C. elegans*-related behavioural research. One of these deals with the use of stimuli to manipulate the movement of the animals for behavioural and physiological studies. In spite of having a relatively simple nervous system [169], *C. elegans* responds to a diverse range of stimuli and exhibits both attractive and repulsive responses. The stimuli are detected by amphid sensory neurons in the head region (Figure 2-2) that are exposed to the outside at the base of the lips [46]. Although how environmental cues are processed by these neurons leading to altered movement is not fully understood, movement serves as an important readout to dissect the neuronal network and signaling. Hence, a stimulus-based microfluidic system could serve as a powerful tool to study movement-related neuronal disorders in *C. elegans* disease models.

Some behavioural assays, such as chemotaxis [158] and mechanosensation (discussed in sections 2.5.1 and 2.5.2) [130-133], have been performed using microfluidic and MEMS devices. The worms are not immobilized in such devices and are allowed to move freely, thereby allowing the study of their behavioural responses. Chemotaxis studies in worms have identified certain chemicals that elicit robust movement (attractive and repulsive) responses. A few other nonchemical agents such as light, temperature and electric field induce a similar behaviour. These methods are useful, yet there are limitations such as complexity in integration and control in a microscale device [130, 131], inability to switch on and off instantaneously [158] and in some cases, lethality [47], if used in microchannels. Nevertheless, one or more of these stimuli may be used to manipulate the movement of worms. In the following, the utility of these agents in a microfluidic environment will be first summarized and one of these, that is electric field, will be discussed in details as the focus of this thesis.

2.5.5.1 Chemical Stimulus

C. elegans can detect several types of volatile (e.g., alcohols, esters and aldehydes) and water-soluble (e.g., cations, anions, cyclic nucleotides, and amino acids) chemicals that are associated with food, danger or other animals

[46]. Compared to water insoluble chemicals that do not diffuse easily, and therefore are likely to be used for short-range chemotaxis, volatile odors rapidly diffuse through air due to their small size and can be detected at a very low concentration range (picomolar) making them suitable for long-range chemotaxis. In spite of the diversity of chemical compounds detected by *C. elegans*, several factors limit the application of the chemotaxis-based approach to manipulate worm movement in a microfluidic setup. These include a lack of control over chemical gradient, variability in chemosensory response of the animals, and sensory adaptation.

Qin et al. [158] studied *C. elegans* response to food and investigated their learning behaviour in microfluidic mazes. It was reported that *C. elegans* nematodes are capable of locating food in complex spatial environments and repeating the same behaviour after a few times of training in the absence of the food (learning). Individual worms were positioned on an agar surface and a T-shape microchannel was positioned on top of them in a way that the worm was located at one of the end reservoirs. Then, the food was placed in another reservoir and the worm was allowed to freely discover the food location. This process was repeated for 5 trials and the worm's approach time to the food was measured which was reduced from 15 min in trial 1 to 5 min in trial 5. After this, the worm was placed in the same reservoir with no food in the other (also repeated 5 times). The worms were observed to repeat the same migration direction each time towards the former food location but their approach time increased gradually. The results from this work demonstrate the applicability of maze-based microfluidic devices for elucidating the genetic and molecular basis of learning in the worms and investigating the conserved biological process.

Albrecht and Bargmann [159] developed a device which consisted of microchambers containing numerous microposts with spatiotemporal control over odor injection (e.g. isoamyl alcohol. Temporal pulses, spatial stripes and linear concentration gradients of odor stimulus patterns were used to study *C. elegans* chemotaxis response to an attractant, which was characterized as forward (straight or curve), pause, reverse, pirouette reverse (the reversal before an omega turn) and pirouette forward (the subsequent resolution of the omega turn) movements. In addition to statistical and quantitative analysis of chemotaxis, three new locomotion behaviours were discovered in this assay. The device operates robustly, repeatedly and independent of operator and time of experimentation. These characteristics are highly sought in advanced assays where versatile HTS is needed.

Spatial orientation of *C. elegans* body in response to varying concentrations of chemicals or two different chemicals simultaneously was studied in a microfluidic chip [160]. The device can be described as a microgripper that

restrains a worm by grabbing it at the middle and leaving the head and tail to move freely. The gripper is positioned at the center of a Y-shaped channel. Two different chemicals can be introduced inside the legs meeting each other in the center, where the gripper is located. The grabbed worm is therefore always oriented towards the axis of the Y-channel exit port along the chemicals interface axis and can orient its body into any of the side chemical streams. Spatiotemporal control over chemical gradients was achieved by this device. The chip also included a temperature control unit, and was used to study chemotaxis, osmotic avoidance, and thermotaxis of *C. elegans*. One interesting discovery showed that *C. elegans* can perform klinotaxis (head movement due to altering reactions of sensory neurons at either side of the body) in response to high concentration gradients of chemo-attractants and steep temperature gradients.

In addition to liquid chemicals, *C. elegans* can also sense gaseous substances. For instance, oxygen is necessary for the development and survival of *C. elegans* [170]. Under aerobic conditions, oxygen is typically required in mitochondria to carry out metabolic function. In the absence of oxygen (anoxia), worms cease movement and any development. This arrested state can last for several hours without any significant damage to tissues and physiological processes and, when supplied with oxygen, the animals resume normal function. The microfluidic approach has been used to study oxygen sensation and behavioural changes in worms. It has been found that the animals strongly avoid the lower (<2%) and the higher (>12%) oxygen levels and prefer to live within a range of 5–12% concentration [161]. Although potentially useful, oxygen is not suitable as a stimulus to control the movement of animals in a microfluidic setup because the response is variable and not fully penetrant.

2.5.5.2 Optical Stimulus

The response of *C. elegans* to light, known as phototaxis, has been studied in some detail [47, 163]. It was found that although *C. elegans* does not possess eyes, it senses light stimulus via ciliated amphid neurons and demonstrates repulsive or attractive reactions to it (dependent on the wavelength) in a dose-dependent manner. Although ultraviolet-A, violet and blue lights appeared to be most sensitive and induced reversals within few seconds, prolonged exposures (15 min) were detrimental, causing paralysis and death. In comparison, the repulsive response to green light was mild, low penetrant, and no paralysis was observed in 20 min exposure. Using a microfluidic device with microfabricated electrodes inside microchannels, Chuang et al. [162] were able to dielectrophoretically trap worms in the tail region while shining lights of various wavelengths on the freely moving head of the animal. Same avoidance behaviour to blue light and oblivious behaviour to green light was reported. While the

phototactic response is rapid, because of its lethal effect (in the case of UV-A, violet and blue lights) and low response (in the case of green light), it does not appear to be suitable to manipulate worm movement in a microfluidic setup.

2.5.5.3 Magnetic and Electric Field Stimuli

Magnetic field is another nonchemical agent whose effect has been studied in *C. elegans*. Exposure to both static magnetic fields (SMFs) and alternating current magnetic fields (ACMFs) induces a range of phenotypes. Bessho et al. [48] used ACMFs up to 1.7 Teslas (T) to intermittently expose growing worms and found that it caused a small but significant decrease in the growth and reproduction. The animals also showed reduced pharyngeal pumping and abnormal locomotion but these changes were transient and reversible. Similar to ACMFs, SMFs also have a range of effects on worms. Exposure of worms to 200 mT reduced their life-span and fertility [171]. SMFs were also shown to affect gene expression as determined by real-time Polymerase Chain Reaction (PCR) and microarray experiments [171, 172], thus linking developmental defects to molecular changes. While these studies highlight the effect of magnetic field on worms, there is no indication that it could serve as a stimulus to guide worms in a microfluidic channel and it is also difficult to be integrated into microchannels.

Electric field has long been reported to influence the movement of nematodes (electrotaxis) [173, 174]. In 1978, Sukul and Croll [49] for the first time showed that *C. elegans* exhibits electrotaxis behaviour. Subsequent studies showed that worms, exposed to a DC electric field on the open agar gel surface, swam toward the cathode electrode (negative pole) at an angle that was proportional to the field strength (15°–60° range) [60]. Genetic experiments have revealed that electrotaxis is mediated by certain amphid neurons (mainly ASJ and ASH, and to a lesser extent AWB, AWC, and ASK), since their removal abolishes this behaviour [60]. Although the mechanism of electric field response is unknown, the signal may mimic external stimuli that excite sensory neurons. This could lead to the generation of an electrical signal that propagates to other neurons and muscles, ultimately affecting movement of the animal. Although the genetic basis of electrotaxis is still unknown, this technique seems to hold promise as a stimulus for conducting movement-based behavioural assays on worms. This is because electric potentials (and hence electric fields) can be applied instantaneously, are easy to control, can be integrated well with devices and platforms used for worm-based researches, and more importantly can be multiplexed for parallelization of experiments for HTS.

2.6 An Ideal System for Behavioural Analysis

The main focus of this thesis is to develop technologies and methods for automating behavioural screening of nematodes especially the *C. elegans*. The emphasis is on technologies that are scalable so that HTS can be achieved. Control using electrical signals is among the most scalable technologies available; however, prior studies on effect of electrical signals on *C. elegans* behaviour and movement have tended to be on a culture plate which was not suited for such experimentation. For one, the format produced spatially varying electric fields which elicited a variable response from the worm. Therefore, despite the many neuronal studies made possible with these plate-based platforms [60], an accurate characterization of the electrotaxis movement behaviour has not been conducted.

In order to fully characterize the electrotaxis behaviour, it is important to experiment in an environment in which both the animal's spatial movement and the electric field distribution can be precisely controlled. Microfluidic environments as discussed in Section 2.5 offer these controls and are therefore highly suitable for the development of automated behavioural screening systems for nematodes. Another focus of this thesis is to develop the fundamental operational units required to perform these automated movement-based chemical/drug screening assays, in addition to the cellular- and neuronal-based ones on worms. A schematic diagram of such an envisioned system is shown in Figure 2-9.

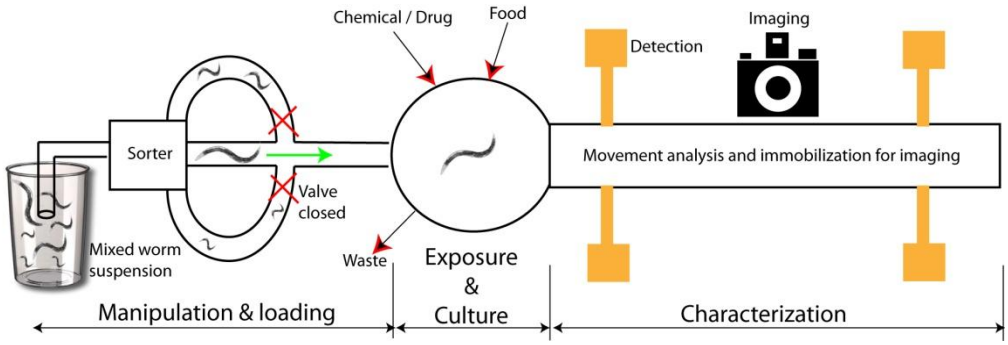

Figure 2-9 Schematic diagram of an envisioned movement analysis-based chemical/drug screening unit consisting of 3 main sections: (1) Manipulation and loading where worms are extracted from a mixed suspension, sorted based on size/behaviour and loaded individually into the next section; (2) Exposure and culture where the worm is maintained and exposed to the chemical/drug of interest with controlled dosage and exposure time while nutrients are supplied and waste is ejected; (3) Characterization where the effect of exposure is quantitatively measured at the behavioural (movement analysis) and cellular (immobilization and imaging) levels

In order for one to be able to develop such a system, various subcomponents are required to be separately designed and tested. As can be seen in Figure 2-9, the screening system consists of 3 main subunits: (1) manipulation and loading; (2) exposure and culturing; and (3) behavioural characterization. Technologies

for sorting of worms in a high throughput manner based on their behavioural differences to stimuli have to be developed. After the sorting, individual worms should be selected and transferred into the chemical/drug exposure unit shown in Figure 2-9. Technologies and methods for precise and automated manipulation of these millimetre-sized animals, and automatic arraying of them in microchannels have to be developed. After compartmentalizing individual worms inside the microchamber, an exposure unit should be capable of dispersing precise dosages of chemical candidates (and also nutrients and oxygen for long-term exposures) into the chamber while ejecting the waste material produced by the worm. Precise dosing technologies as well as suitable device design such that the worms are trapped in the chamber during exposure need to be developed.. After the drug exposure process, effect of the drug on each worm should be characterized both at cellular and behavioural levels. For the cellular-level studies, technologies and methods for immobilizing the worms in an automated manner inside microchannels and imaging them should be developed. For the behavioural analysis, the movement of the worm should be stimulated, monitored and automatically quantified.

2.7 Summary and Concluding Remarks

Understanding human biology has always been the important research endeavour and provides necessary understanding and tools to tackle human health issues and enhances the quality of life. Live organisms or systems, such as mammalian cells and whole-animals have been utilized to study conserved biological processes. Among several potential animal models, worms such as *C. elegans* [175] has attracted lots of attention in biological and neurological researches during the last decade due to their diverse assets. *C. elegans* reaches a relatively small size (~1 mm long and ~80 µm thick) at a fully-developed adulthood stage; while having a transparent body cuticle, allowing observation of the biological processes in the worm at cellular and neuronal levels under the microscope and during its physiological development. Combination of such benefits with the completely sequenced genome and simple mapped cellular system of *C. elegans* has made this animal a perfect model for performing biological assays, such as human diseases drug discovery [103, 104]. Behavioural analysis of worms can also provide valuable information in these assays. However, conventional methods of assaying worms are highly manual, time-consuming and labour-intensive while the robotic methods are expensive, inaccessible to researchers and more importantly, incapable of performing behavioural assays on worms.

MEMS and microfluidic devices and techniques permit better control of worm handling and its analysis with higher levels of automation and throughput [11, 12]. They enable study of body mechanics [131], screening and sorting [21, 146, 147], exploratory behaviour [158] as well as the ability to ablate certain cells, neurons or synapses using precise femtosecond lasers [152, 153]. Pneumatically generated liquid flows carry the worms inside such microdevices and techniques such as suction against the channel sidewall [146], deforming a thin PDMS membrane over the worm's body [154], temperature [147], and CO_2 exposure [151] has been used to immobilize worms. These methods are not completely applicable to behavioural studies since the mechanical forces utilized in their operation are always dominant to *C. elegans* inert ability to move. *C. elegans* movement response can be generated by exposure to external stimuli such as chemicals, light, mechanical stimulations and temperature; however, these stimuli are complicated to generate and control, lethal in some cases and slow in turning on and off. Alternatively, electrical stimulus generates a cathode-driven movement response in the worms, which is mediated by neuronal activities [49, 50, 60]. Electrical stimulus is easy to generate/modulate and can be applied on-demand. However, the movement response of worms on the agar plate is highly variable with variation in signal strength and waveform. Environmental conditions on open surface plates are also challenging to be precisely controlled. In an ideal behavioural screening system, electric field waveform and its distribution as the movement-inducing stimulus should be well controllable and uniform, the testing environment should be isolated and the movement behaviour of worms should be quantitatively measurable in a standardized method. This can lead to the development of automated screening devices that can eventually increase the throughput and accuracies associated with worm-based assays.

CHAPTER 3

3. Device Design, Methods and Experimental Procedures

As described in Chapter 2, the worms' movement behaviour cannot be studied in a quantitative manner by conventional and robotic methods, due to the lack of a robust, repeatable and rapid methodology. Microfluidic techniques have greatly facilitated the worm-based studies in the past decade (Section 2.5) but most of them have focused on animals' biological processes at cellular and neuronal levels. The focus of this thesis is to investigate the use microfluidics to design and develop devices and techniques that can first fully control and quantify nematodes' movement, and then use it to perform movement-based assays by developing novel microchips. Although many methods exist to assay the movement, as discussed in Section 2.5.5, electrical stimulation is desirable as it is easy to control and integrate into microfluidic chips and can be instantaneously turned on and off. In this research, electrical stimulation is investigated as a possible method to initiate movement behaviour in microenvironments. Characterization of the stimulated behaviour and the possibility of using electrical methods to sort, localize, immobilize and detect worms are investigated.

In order to design and develop all these techniques and devices, a wide variety of expertise in fluid mechanics, electronics and biology is required. This chapter mainly focuses on describing these fundamental aspects of the thesis

and the common experimental methodologies. This includes the fluidic- and electrical-based design criteria, biological sample preparations, microchips' fabrication, experimental setups and procedures and finally data post-processing techniques. Any device-specific experimental methodology will be more elaborately described in the next chapters where the relevant results are presented.

3.1 Design of Microfluidic Devices for the Study of Electrically-Initiated Movement Behaviour

A worm inside a microfluidic channel filled with liquid media, which is also electrically stimulated, can experience various forces. First, the worm may have surface charges on its body and hence possess a zeta potential that will induce an electrophoretic force on the worm propelling it towards the opposite charged electrode. The liquid surrounding the worm would experience an electroosmotic force that propels it and may induce a body force on the worm due to viscous drag. Finally, the worm may be stimulated by the electric field and can generate an internal propulsion force that may drive it towards the electrode of its preference. The balance of these forces will determine the overall motion of the worm in response to the electric field. The following subsections will analyze the theoretical basis of these phenomena to understand the significance of these effects on the worm's movement-based behaviour.

3.1.1 Fluid Flow in Microchannels

Liquid behaviour inside microfluidic environments is predominantly governed by the conventional laws of laminar-regime fluid mechanics. Reynolds number (*Re*) magnitude is used to determine the flow regime inside internal or external fluidic systems. The Reynolds number is defined as:

$$\mathrm{Re} = \frac{\rho V D_H}{\mu} \qquad 3\text{-}1,$$

where ρ (Kg.m^{-3}) is the density of the liquid media, V (m.s^{-1}) is the average velocity of the fluid, D_H (m) is the hydraulic diameter of the channel ($D_H=4A/P$) and μ (Pa.s) is the dynamic viscosity of the fluid. Hydraulic diameter is usually used for internal flows inside non-circular cross-sectional channels, which is the case for all of the microfluidic channels used in this research. It is defined as 4 times of the cross-sectional area (A [m^2]) divided by the wetted perimeter of the channel (P [m]).

Simple calculations will indicate that the *Re* number for microfluidic internal flows (channel sizes of 10s to 100s of micrometers in width and depth) would mostly fall under 100 in magnitude, which would confirm that these flows are in the laminar regime in such environments. For instance, for the electrotaxis microfluidic chip, commonly used in this thesis (Chapter 4), which was 0.3 mm wide and 0.1 mm deep, the hydraulic diameter is 0.15 mm. Using the fluid properties of water and a flow velocity of 5 $mm.s^{-1}$ (typically much lower in this thesis), *Reynolds* number can be calculated to be as low as 0.75. Therefore, laws for internal laminar flows are applicable to design the fluidic aspects of the devices utilized in this research. According to these laws, pressure-driven flows can easily be generated inside the microchannels by using positive displacement pumping (e.g. syringe pumps) or hydrostatic pressure actuation. Therefore, biological substances (i.e. worms) are transported inside the channels by a generated parabolic flow with no-slip conditions at channel walls. If the flow is not required in the channel, the pressure difference across the channel should be maintained at zero value. This has been applied in electrotaxis and sorting experiments where animals' inert movement analysis in response to electric fields in stationary media was sought.

3.1.2 Electric Fields Distribution in Microchannels and Induced Electrokinetic Flows

As discussed earlier, electrical signals inside microfluidic environments have been used extensively in this thesis to study animals' movement behaviour as well as to sort them, to detect their position, to localize and to immobilize them in the channels. From an electrical point of view, microfluidic channels can be modeled as simple electrical resistances, because there is an electrical resistivity associated with the media flowing in them. For instance, Figure 3-1 illustrates a network of 3 fluidic channels arranged in series. Assume that the channels have different lengths and widths, but have the same thickness. Each channel can be modeled as a resistor as demonstrated in the electrical analogous circuit. The electric field (*EF*) across a microchannel with uniform cross sectional area is defined as *EF=V/L*, where *V* (volts) is the voltage drop across that section and *L* (m) is the length of the channel segment. The voltage can be calculated from equation 3-2:

$$V = RI = \frac{\rho L}{A} I = \frac{\rho L I}{wt} \qquad 3\text{-}2,$$

where *R* (Ω) is the electrical resistance, *ρ* (Ω.m) is the electrical resistivity of the media in the channel, *I* (A) is the current, *A*(=*wt* [m^2]) is the cross sectional area

of the channel, and *w* and *t* are the width and the thickness of the channel (m), respectively.

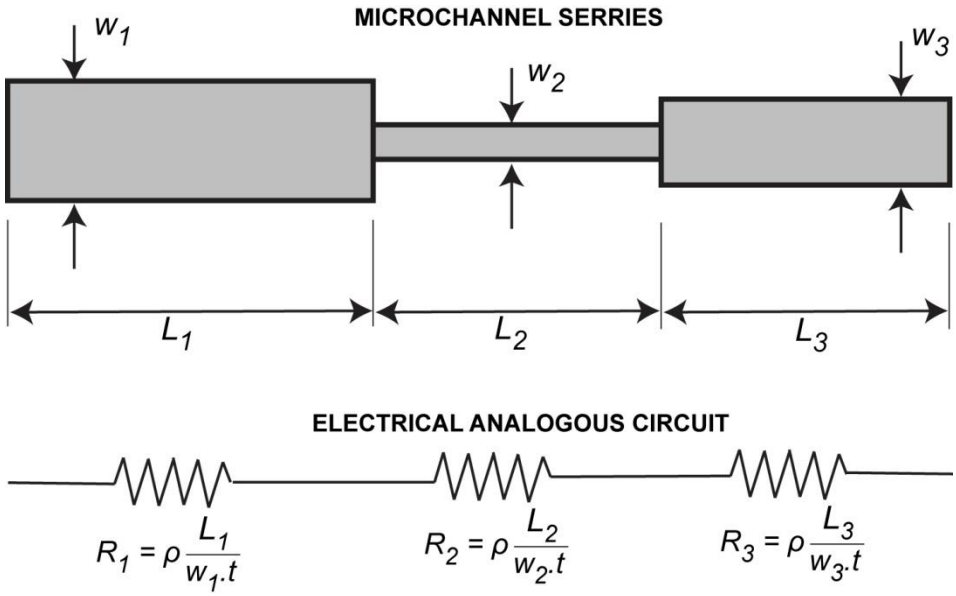

Figure 3-1 A three-channel microfluidic network and its electrical analog circuit [21]. (Reproduced by the Permission of the Royal Society of Chemistry 2012)

Using equation 3-2, the electric field across each microchannel section (wide-narrow-wide) in series in Figure 3-1 can be calculated from eq. 3-3.

$$EF = \frac{V}{L} = \frac{\rho I}{wt} \qquad 3\text{-}3$$

Equation 3-3 demonstrates that the ratio between electric fields of two microchannels (same thickness) arranged in series (same current passing through both) and different in width is inversely proportional to their width ratio (i.e. $EF_1/EF_2 = w_2/w_1$).

All the microfluidic channels and devices utilized in this research have been designed in accordance to these theoretical principles. To design the microfluidic devices which were more complicated in terms of their channel network, finite element-based multi-physical simulation tools, such as COMSOL Multiphysics, were employed. Models were drawn in 3 dimensional formats and a combination of fluidic and electric modules were used to model the electric field distributions inside the channels. This approach is more comprehensively discussed in Section 5.2.2 for the sorting device design.

When electric potential is applied across a microfluidic channel, the fluid contained in it will experience a body force that propels it towards an electrode. This kind of flow generated is known as electrokinetic flow. These flows are

caused by the spatial distribution of electrical charges in the floated objects or the media inside the channel itself. Briefly, a charged particle inside a channel (filled with liquid) will experience attractive forces towards the opposite-charge electrode if exposed to an electric field in the channel. Very soon the charged particle reaches a velocity where the electric attractive force is balanced by the drag forces and the particle moves at a constant velocity. This phenomenon is called an electrophoresis. Additionally, at the liquid-solid interfaces in the channel (such as walls), an electrical charge double layer will form due to the inherent surface charge of the channel and absorption of opposite charges in the liquid towards them. An electrical field across the channel would also exert a force on this double layer that causes it to move and drag the bulk of the liquid along. This phenomenon is called an electroosmotic flow. It was important to investigate the effect of electroosmotic flow and electrophoretic forces on worms exposed to electric fields inside microchannels. To do this, dead animals were prepared and put at rest inside the channels while being exposed to electric fields of various strengths. The use of dead animals was to exclude their inert response to the signal so the electrokinetic effects could have been studied. The range of applicable electric fields which did not induce significant electrokinetic flows to move the dead animals was determined and used throughout the experiments.

3.2 Nematode Sample Preparation

Nearly all experiments were done with synchronized stages of the worms. The worms were grown at room temperature (20 ºC) on standard nematode growth (NG) agar plates seeded with OP50 *Escherichia coli* (*E. coli*) bacteria. Gravid hermaphrodites were washed off culture plates using M9 buffer (3 gKH_2PO_4, 6g Na_2HPO_4, 5 g NaCl, and 1mL 1M $MgSO_4$ in 1 L). They were centrifuged and washed twice with M9 to remove excess bacteria and debris. A 2 mL of bleach solution (800 µL of 4 N NaOH and 1200 µL of commercial bleach) was added to 4 mL of the worms. The mixture was incubated at room temperature for 3 min and then centrifuged and washed with M9 (at least 3 times). The eggs were allowed to hatch in M9 for 24 hrs. They were subsequently transferred back to NG agar plates seeded with OP50 bacteria and were allowed to grow further. When required for testing, the worms were washed again with M9 and loaded in the microchannels. In some experiments (multi-trap sorting device discussed in Section 5.2.2), immediately prior to loading the worms into the device, M9 solution was replaced with DI water by centrifuging.

The strains used in this study were: (i) for *C. elegans*: N2, BC347 unc-54(s74), CB78 unc-6(e78), PS55 lon-2(e678), and PS250 dpy-5(e61). The PS55 strain also carries a him-5(e1490) mutation that increases frequency of males in

the progeny. The N2 strain was used as a wild-type reference in all assays; (ii) for *C. briggsae*, AF16 strain was used.

For investigating the effect of electrokinetic flows on the worms' movement (discussed in Section 3.1.2), dead animals were obtained. For this, wild-type *C. elegans* were synchronized using the above bleach protocol and kept in M9. The animals were left in the absence of food for one week at room temperature, resulting in their death. The dead animals appeared rod-shaped with no visible body bending or movement.

3.3 Microfabrication Techniques

All the devices used in this thesis were fabricated from PDMS polymer with embedded metal electrodes. These devices usually consisted of a single layer of PDMS, with the network of microfluidic channels imprinted in them, bonded to another flat layer of PDMS or glass (called single-layer devices). Devices consisting of more than two layers were also designed and developed (multilayer devices) with embedded polycarbonate (PC) or PDMS membranes. To develop these devices, master molds were made which consisted of microfluidic network design as protruded structures upon which PDMS was cast. Two major techniques were used, namely the conventional photolithography method with specialized thick photoresists to develop the master molds, and soft lithography [176, 177] to fabricate the devices as discussed below.

3.3.1 Fabrication of Master Molds

Development of PDMS devices required the fabrication of master molds (usually a silicon wafer) with the microchannels network defined on them as protruded features (usually photoresist). Development of the master molds was mostly done inside a cleanroom environment by using the conventional photolithography methods. The mask layouts, containing the 2-dimentional design of the microfluidic channel network, were designed in AutoCAD (Autodesk Inc., San Francisco, USA) and printed, using ultra high-resolution laser photo-plotting on transparency sheets. A range of various negative SU8 (15, 25, 100, 2015, 2025 and 2075) photoresists (MicroChem Corp., MA, USA) were used to obtain various layer thicknesses. The thickness of the photoresist governs the depth of the microchannels developed in next steps of fabrication. Photoresist thickness can be controlled by the spinning speed and the viscosity of the resist itself. Accordingly, a 3-in diameter silicon wafer was prepared by cleaning (15 s of acetone and methanol bath followed by a 5 min deionised water rinse and hotplate drying at 120^{o} C for 2 min) and plasma oxidization (50 W, 1 min) for SU8 resist adhesion enhancement. In a typical recipe, such as the one used for

fabrication of the electrotaxis device in Chapter 4, the SU8-100 was spun for 40 s at 1800 rpm. Spun photoresist was then prebaked on a hotplate at 65°C for 12 min and 95°C for 1 hr. After this, the prepared photoresist was exposed to UV light (~600 mJ.cm^{-2}) using the designed photomask under a mask aligner and UV exposure equipment. The exposed assembly was then post-baked on the hotplate at 65°C for 5 min and 95°C for 10 min and the non-exposed photoresist (for the case of negative resist) was removed by SU8 developer. This yielded a silicon wafer with the microchannel network protruding out of the surface dubbed the master mold (Figure 3-2a) (a step-by-step standard operation procedure to develop a SU8-100 based master mold is described in Appendix A-I). Fabrication process specifications such as pre- and post-bake steps are highly resist-dependent and provided by the manufacturers.

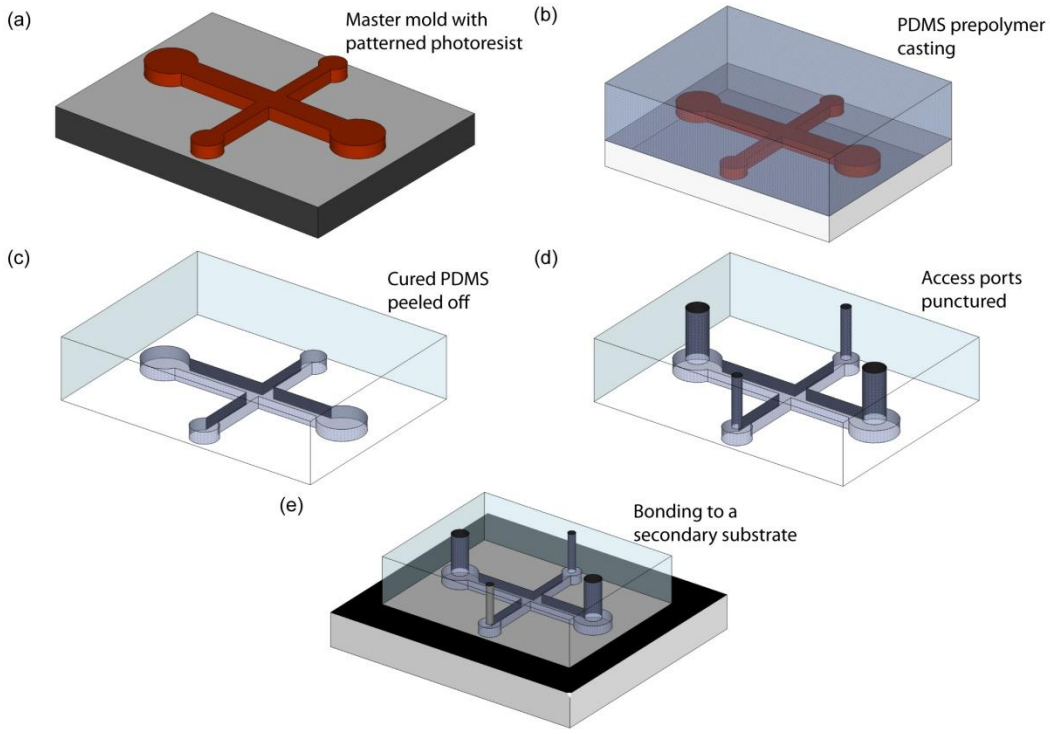

Figure 3-2 Soft Lithography technique; Schematic drawings of (a) master mold fabricated by photolithography, (b) PDMS prepolymer cast on the master mold, (c) Cured PDMS and peeled off, (d) Fluidic access holes punched into the PDMS and (e) Prepared PDMS slab bonded to a secondary substrate.[178]

3.3.2 Fabrication of Single-Layer Devices

These devices (e.g. electrotaxis (Chapter 4) or sorting (Section 5.2) devices) consisted of a single PDMS layer bonded directly to a glass slide or a secondary flat PDMS layer. PDMS pre-polymer mixture (Sylgard 184 kit, Dow Corning Corp., MI, USA; 10 to 1 ratio of the base to cross-linker) was cast on the master

mold (Figure 3-2b) and cured at room temperature for 24 hrs. The PDMS replica was then peeled off the master mold and cut into pieces containing individual microfluidic devices (Figure 3-2c). The inlet and outlet access ports were punched out at the reservoir areas (Figure 3-2d). The top surface of the PDMS replica and a bare PDMS piece of the same size were plasma oxidized (50 W for 30 s), micro-contact printed with PDMS pre-polymer (spun at 7000 pm, 40 s on a Si wafer), and bonded together, sealing the microchannel (Figure 3-2e). Inlet and outlet capillary glass tube tips (VWR International, USA, catalog number CA14672-380, 1.5 mm outer diameter, 20 mm long) were connected to the punched areas. Plastic tubes (Saint Gobain Performance Plastics, OH, USA, TYGON R-3603, 2.4 mm outer diameter and 10 cm long) were connected to the inlet and outlet glass tubes.

For devices requiring electrodes, copper wires (Arcor Electronics, USA, C24, 0.5 mm diameter) were inserted into the reservoir areas by punching through the PDMS elastomer from the side. Liquid PDMS prepolymer was then used to seal the surrounding areas of the electrodes and the device was placed on a hot plate (120 ºC) to cure. The device was then attached to a glass cover slip again using PDMS pre-polymer and cured. Some of the devices such as the sorter or the detection devices described in Section 5.2 and 5.3 required embedded wire electrodes inside a microchannel or chamber. A 100 µm diameter platinum (*Pt*) wire inserted inside and pass throughout the channel was used. To pass the electrode through the channel, a needle (BD, 22 G ×1 in, NJ, USA) was inserted into the PDMS layer after it was peeled off the master mold, and the Pt wire was passed through the needle into the channel at its back corner. The needle was then withdrawn out of the PDMS, leaving the *Pt* wire behind. This process was repeated at the other end of the channel to embed the electrodes inside the channels.

In some cases, a microchannel with variable height was required in this research. For instance, the immobilization chip used in Section 4.3.3 for FRET imaging of the worms required a trapping section with a thickness of 36 µm while the side access channels were 65 µm thick. In these cases, the master mold was prepared from multiple photolithography steps rather than just one step. Each photolithography step yielded a desired thickness for a specific region of the channel on the master mold. Design of appropriate alignment marks that enhanced the process of aligning subsequent layers was considered as the most important factor during the fabrication process of these devices. The photolithography processes for these molds started with the thinnest resist layer followed by the thicker ones.

3.3.3 Fabrication of Multilayer Devices

Some of the devices (immobilizer in Section 5.5 or integrated screening device in Chapter 6) required the integration of additional layers such as flexible PDMS or porous PC membranes to enhance the functionality of the device. Flexible PDMS membranes can act as actuatable valves, if integrated in between two microchannels that intersect each other, as discussed in Section 2.5.4. PC membranes provide media-exchangeable interfaces in between two microchannels over-crossing on the top and the bottom of the membrane [179]. These interfaces have been used as the worm pre-concentrators for the electric immobilization device in Section 5.5.

To fabricate multilayer devices, the first PDMS layer containing the designed network of channels was prepared as discussed in the previous section (Figure 3-2d). This layer was then plasma oxidized (50 W for 40 s) along with the PDMS and/or the PC membrane layer, microcontact printed on PDMS prepolymer (spun at 7000 rpm, 40 s on a Si wafer) and bonded to the PDMS/PC membrane. PDMS membranes were fabricated separately by preparing a 10 to 1 base to agent PDMS prepolymer, spinning 3mL of the prepolymer on a glass slide and curing it on the hotplate at 85 ºC for an hour. After being cured, the PDMS layer was cut with a scalpel across a line and the glass slide underneath it was broken. Figure 3-3 shows the thickness of PDMS membranes as a function of spinning speed all characterized by SEM imaging after membrane preparation (measured at 3 different locations and averaged).

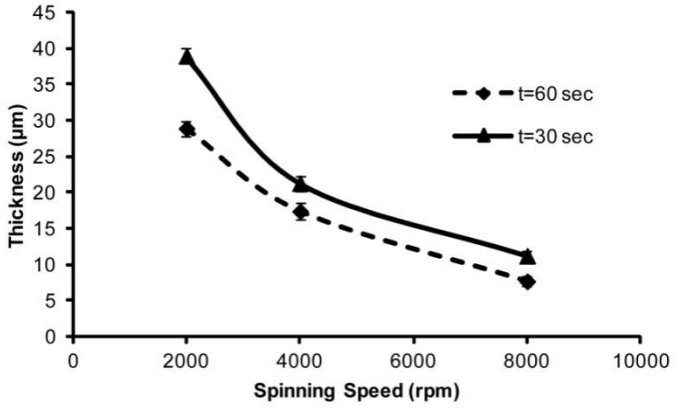

Figure 3-3 PDMS membrane thickness versus various spinning speeds for a total spinning time of 30 or 60 s

The prepared assembly of the first PDMS layer and the membrane was then plasma oxidized (50 W for 30 s) again with a second layer of PDMS containing additional channel networks, aligned under a microscope and bonded together. To have time for alignment, methanol can be sprayed on top of the layers after

plasma exposure. This allows the layers to be slid on top of each other for 1-2 minutes before the methanol is fully evaporated. After alignment, the assembly can be heated (85ºC for 10 min) to accelerate methanol evaporation. This process was sequentially repeated in case more layers were needed to be integrated. More device-specific fabrication discussions will be provided in the following chapters.

3.4 Experimental Setup and Common Operational Procedures

The experimental setup, to study nematodes' electrotaxis and its applications to sorting and drug screening in this thesis, is shown in Figure 3-4. It consisted of four major sub-units: (1) microfluidic chips (different chips will be discussed in subsequent chapters), (2) worm-handling unit (syringe pump, inlet and outlet tubes and connections), (3) electrical actuation (power supply, amplifier, function generator and electrodes) and (4) monitoring unit (fluorescent or stereo-microscope and camera). It should be stated that this setup was entirely or partially used in most of the experiments conducted in this research. A regular stereomicroscope would suffice to run the assays such as electrotactic movement analysis, sorting and drug screening. In some cases such as electrical immobilization and FRET-based neuronal imaging of the worms, fluorescent based imaging was required. These assays were then conducted under fluorescent microscopes as discussed in subsequent chapters.

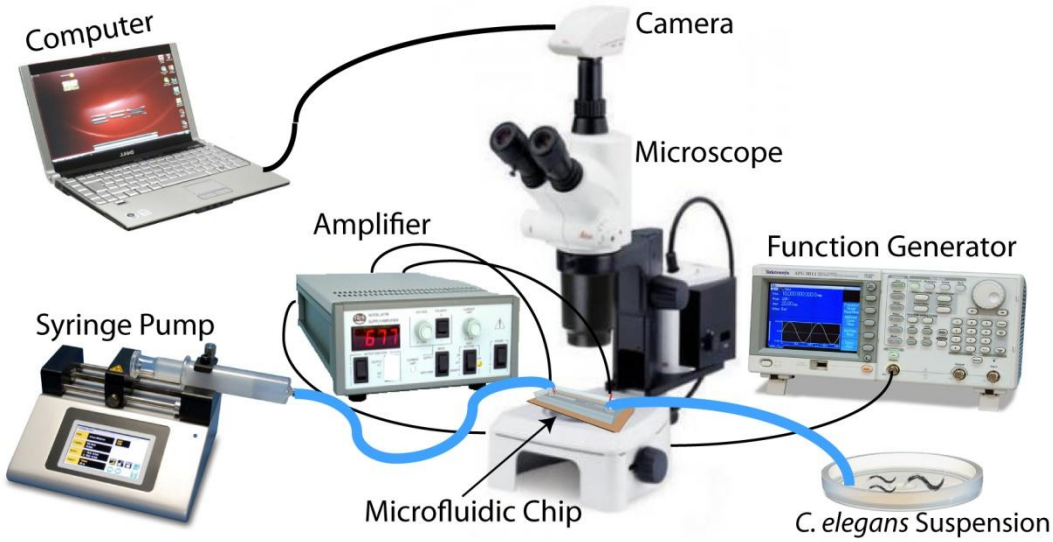

Figure 3-4 Experimental setup to study nematodes electroxis and its applications by using different microfluidic chips

3.4.1 Nematode Handling

All the experiments involved loading and unloading of the worms into and out of the microfluidic channels. The electrotactic behavioural characterization assays also required only a single worm to remain in the channel during experimentation. For this purpose, the worm suspension, illustrated in Figure 3-4, was diluted to contain approximately 1 worm in 20 mm^3 of M9. To load the animal inside the channel, the inlet tube of the microfluidic channel was dipped into the worm suspension and a negative pressure was applied at the outlet tube using the syringe pump (flow rate=200 $\mu L.min^{-1}$) while focusing on the inlet region of the device using the microscope. As soon as an animal was observed to enter the device, the pump was switched off and the syringe was disconnected from the outlet tube. The inlet and outlet tubes were then leveled at the same height to prevent any pressure-driven flows caused by the mismatch between the heights of the tubes (see Section 3.1.1). The experiment was then carried out by using the electrical actuation unit (Section 3.4.2) and also streamed and recorded by using the monitoring unit for further quantitative data post-processing (Section 3.5).

3.4.2 Types of Electric Signals

One of the most important focus areas of this research was to investigate nematodes' response to the electric fields at both behavioural and neuronal levels, as will be discussed in the subsequent chapters. Therefore, various electric field waveforms were generated, as shown in Figure 3-5, using the electrical actuation unit shown in Figure 3-4, and applied across the microfluidic devices utilized.

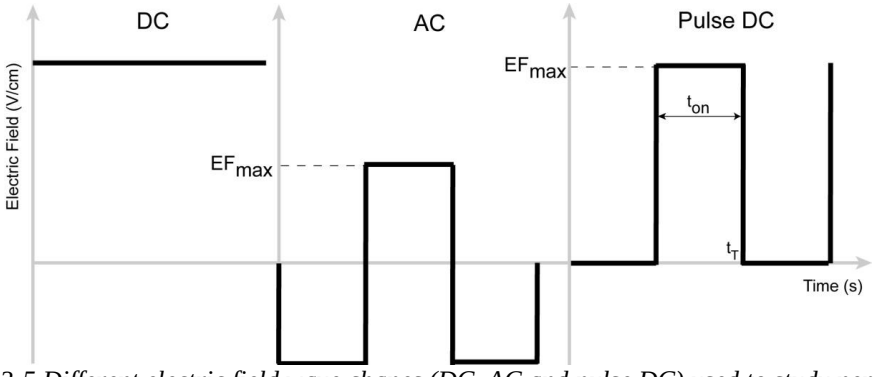

Figure 3-5 Different electric field wave-shapes (DC, AC and pulse DC) used to study nematodes electrotaxis at behavioural and neuronal levels. In addition to rectangular AC waves, triangular and sinusoidal waves were also utilized.

The function generator (AFG3022B, Tektronix Inc., OR, USA) shown in Figure 3-4 was used to generate the AC and pulse DC signals shown in Figure

3-5. It was set to output a desired electric field waveform with adjustable characteristics, such as the frequency ($f = 1/t_T$), maximum pulse electric field strength (EF_{max}), as well as the duty cycle calculated using Eq. 3-4. For a pulse DC field, the signal rises in a step-like manner from zero to a maximum set point for a controllable duration of time (duty cycle) and decays to zero for the rest of the signal cycle which is then repeated at a fixed frequency.

$$Duty\ Cycle\ (\%) = f \times t_{on} \times 100 \qquad \text{3-4,}$$

where t_{on} is the on-portion time of the pulse signal. Since the maximum pulse strength (V_{max}) output of the function generator did not exceed 5 V, the signal was subsequently amplified (677B, TREK Inc., NY, USA) and applied to microdevices, as shown in Figure 3-4. The rise and decay time of the pulse signal were 50 µs each in the function generator unit, which restricted the experimental frequency range to less than 1 kHz and the duty cycle to more than 10% in order to produce a rectangular-shape pulse waveform.

3.4.3 Electrotactic Behavioural Assay

It was mostly aimed to quantify worms` response to electric fields quantitatively in this thesis. Therefore, after loading an animal inside the microchannel as discussed in Section 3.4.1, various electric fields (Figure 3-5) were applied across the channel and animal's behaviour was investigated. For this purpose, the head orientation of the worm was determined in the microscope. The worms moved randomly in either direction (left or right) or remained stationary within the channel in the absence of any electric field. Various electric fields with a specific strength, duty cycle and frequency was then applied along the channel (parallel to the worm's body) in a direction opposite to its head orientation. The resulting electrotactic movement response was digitally recorded using a camera connected to the microscope for the entire duration of the experiment. The applied stimulus either induced the worm to turn inside the microchannel and move towards the cathode at its rear or did not generate such a response. For the responding worms, the time taken to reverse their direction, when field was reversed (response time, t_R), and the movement speed and body bend frequency (when field matched the worm motion direction) was measured through videos (see section 3.5.1). Since the turning response time was variable among individual worms (mostly within 40 s), the 40 s cut-off time was chosen to determine whether a worm was a responder or non-responder. Response times of t_R <15 s and t_R >40 s were dubbed "spontaneous response" and "no response", respectively. The 15 s cut-off value was selected according to the worms' response to DC electric fields which mostly happens within this time period (discussed later in Section 4.3.1). The aggregate population response time was then used for data analysis. Within 40 s time window, responders for 5

s, 10 s, and 20 s durations were also quantified. The responder worms were allowed to swim towards the cathode for a distance of 8 mm (used for measuring the swimming speed and body bend frequency) after which the polarity of the electrodes across the channel was reversed again and the worm's behaviour was continuously recorded. This process was repeated thrice for each animal to rule out a random electrotactic response. In the case of non-responding worms in the 40 s time window after signal reversal, the field was switched off, the worm was delivered to the center of the channel again pneumatically, and the same experiment was repeated for two more times. The signal characteristics (i.e electric field strength for DC and frequency or duty cycle for pulse DC) were then set to a different value and the experiment on the same worm was repeated for the desired spectrum of electric fields (1-13 $V.cm^{-1}$ in DC experiments) as well as frequencies (1-3000 Hz) and duty cycles (10%–90%) in the AC and pulse DC experiments. After this set of experiments, the worm was washed off the channel and new experiment was conducted on a newly loaded animal.

3.4.4 Chemotaxis, Lifespan and Reproducibility Assays

Chemotaxis and lifespan assays are among the most popular conventional methods used to screen the worms' behaviour and health state respectively. These assays were employed in the experiments conducted in this research to study the effect of electric field exposure (in electrotaxis, sorting and electric immobilization studies) on the worms. Chemotaxis assay was performed, as described earlier [51]. Agar plates contained 2% agar, 5 mM KPO_4 [pH6], 1 mM $CaCl_2$ and 1 mM $MgSO_4$. NaCl (100 mM) was used as a chemo-attractant. Each chemotaxis plate was divided into 4 quadrants with a marker. 10 µl of NaCl and 10 µl of water were spotted 2 cm apart from the centre of the plate on opposite sides. This was done 8 h before the assay. Electric-field-exposed worms were allowed to recover for 4 h on NG plates seeded with OP50 after experimentation. These worms were then washed with nanopure water twice and again with ice-chilled nanopure water. The worms were placed at the centre of the plate. After 1 hr, the worms within 2.5 cm from the water and NaCl spots were counted. The chemotaxis index (CI) was defined as

$$CI = \frac{N_{NaCl} - N_{Water}}{N_{Total}} \qquad 3\text{-}5$$

where N_{NaCl} and N_{water} are the number of worms inside the *NaCl* and water regions, respectively, and N_{Total} is the sum of N_{NaCl} and N_{water}.

For the lifespan assay [180, 181], exposed worms were placed on OP50 bacterial containing NG-agar plates. The animals were observed for 8 consecutive days and their survival rate was determined. To study the exposed-

worms' reproduction rate after the electrical immobilization assays in Section 5.5.4, the worms' were plated individually on NG-agar plates and their progeny (excluding small L1 and L2 worms) was counted after 72 hrs.

3.5 Experimental Data Post-Processing

Most of the experiments were recorded in a video format by the monitoring unit of the experimental setup demonstrated in Figure 3-4. These videos were either in a bright-field optical mode or a single (Green Fluorescent Protein, GFP) or double (CFP and YFP) channel fluorescent mode.

3.5.1 Movement Behaviour Quantification

Nematodes' movement behaviour was quantified in terms of their speed of swimming inside microchannels, body-bend frequencies, and rotation times during the change of swimming direction. Figure 3-6a demonstrates the movement of a L4 *C. elegans* inside a microchannel from right to left. A length measurement scale bar was microfabricated alongside the microchannels (Figure 3-6a) in all the devices where quantification of animal behaviour was required.

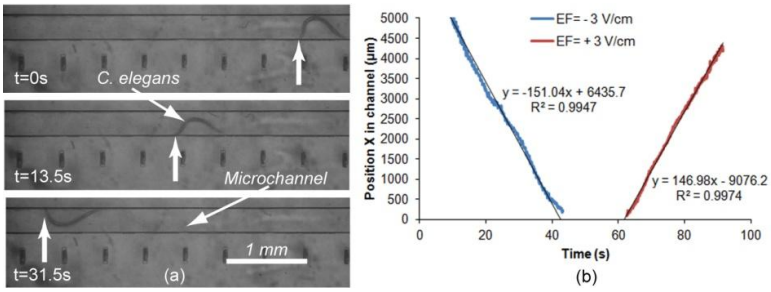

Figure 3-6 Movement analysis of worms, (a) L4-stage C. elegans movement inside a 300 µm-wide and 100 µm-deep microchannel, (b) backward (shown in (a)) and forward movement analyzed as position vs time using ImageJ and excel. Speeds are shown as the slopes of the fitted lines in (b) and rotation time is the time between the backward and forward (~20 s) movements.

The movement of worms was recorded by a camera (Nikon Coolpix P5100, NY, USA) and analyzed by ImageJ software (http://rsbweb.nih.gov/ij/, v1.43m, NIH, MD, USA) and AutoCAD (http:// www.autodesk.com). ImageJ was used to analyze videos and to obtain the snapshots (every 0.07 s) of recorded videos of the worm movements. The sequenced images were used to measure the distance traveled by the worm inside the channel. ImageJ software acquired the body centre X position of the worm in reference to X=0 (usually the bottom left corner of the snapshot) at different times, as illustrated in Figure 3-6b (drawn using Excel). Multiple plug-in codes (e.g. MTrack2 and Worms 4) have been developed by researchers that are accessible through the web for this purpose. A linear line, fit into the position datasets, was used to obtain the swimming speed

(the slope of the line) and rotational time between the forward and backward motion (the time between fitted lines base points).

The worms' lengths were also measured by linear approximation method using AutoCAD software. One image of each tested worm was imported to the software. A total of 15 lines were superimposed on the worms' body image. The lengths of the lines were added and the total length was compared to the reference value to determine each worm's length. This process was repeated three times for each worm and an accuracy of ~10 µm was obtained.

3.5.2 Neuronal-Level Response Quantification

To quantify the level of activities in *C. elegans*' neurons, FRET imaging technique was utilized, as discussed in Section 2.2.2.3. The worms were immobilized by being inserted and confined in a narrow channel. To compute the FRET efficiency, the time-lapse dual channel images of YFP and CFP fluorescence emission were collected under a laser scanning confocal microscope (TSC SP5 & DMI 6000 B, Leica, Wetzlar, Germany) with a 20X dry lens. An argon ion laser emitting at 458 nm was used for CFP excitation. To match the spectra of the donor and the acceptor, the detection channels were set as 465-500 nm for CFP and 515-570 nm for YFP emission respectively.

The worm was immobilized and a focus on the head region (approximately $1/4^{th}$ of the body length from the head) of the worm was obtained. A small image size was used (64 by 64 pixels) followed by line averaging and frame accumulation to enhance the photon counts and the signal to noise ratio while maintaining fast acquisition rate. All of the other acquisition parameters were kept consistent with the zoom factor of 3.1 and the scanning speed of 400 Hz. This yields the frame acquisition rate of 760 ms per frame for visualizing the trend of FRET changes corresponding to neuronal activities. FRET imaging was initiated while the responses of YFP and CFP fluorescence intensities were continuously recorded for 25 seconds.

FRET efficiencies were analyzed using the ImageJ processing software. The entire cell body of the immobilized worm was selected from a stack of time-lapse intensity images from YFP and CFP channels. Background subtraction was performed followed by photo-bleaching correction and the ratio analysis. Photo-bleaching effect was removed by subtracting the exponential decay component from the measured YFP intensity (Matlab, Mathworks, Natick, MA). The fractional changes of the intensity ratio through the electrical stimulation period were then analyzed. Further description of methods is provided in Section 4.3.3, where FRET assays to examine neuronal transient signalling is discussed.

CHAPTER 4

4. Electrotaxis of Nematodes in Microchannels - Behavioural and Neuronal Analysis

As discussed in previous chapters, nematodes (e.g. *C. elegans*) are among the most widely studied model organism in biomedical research. Generally, *C. elegans* assays are performed either on Petri dishes, multi-well plates or by using pneumatically controlled microfluidic devices as reviewed in Chapter 2. Although these assays provide invaluable information, most of them have been designed for cellular and sub-cellular studies (based on animal immobilization and fluorescent imaging) on the worm and are not well-suited to study its behaviour. Studying worms' behaviour is possible by precisely analyzing their movement in response to a stimulus. However, controlling the movement of worms and assessing it quantitatively is challenging as movement consists of complex set of voluntary responses such as forward/backward motions, stops, omega turns, etc that the worm unpredictably uses to navigate in environment. New microfluidic techniques are envisioned to be developed in this thesis (Section 2.7 and Figure 2-9) that can facilitate chemical screening assays on worms using the movement behaviour of animals. This chapter mainly focuses on developing a methodology, that unlike pressure-based microfluidic systems, uses an external cue to stimulate, control and characterize animal's movement in a quantitative and automated manner.

4.1 Stimuli-Based Movement Control of Nematodes

Worms respond to diverse external stimuli, such as food [158], light [47], temperature [160] and chemicals and exhibit either attractive (e.g., food) or repulsive (e.g., high temperature, light) movement responses [182]. Understanding a complex response such as worms' movement behaviour in response to these stimuli can enable us to better uncover the biological basis of animal-environment interactions. Since these interactions are mediated by neurons, it is ultimately possible to look for correlations between the behavioural responses and neuronal signalling pathways as well. Accordingly, a few standardized methods such as chemotaxis assay currently exist to stimulate and characterize the movement response in the worms. However, these methods are slow, not instantaneous, hard to control, difficult to implement in micro-devices and sometimes fatal to the animals. Electric signals on the other hand are well controlled, can be applied or removed instantaneously and easily integrate-able at low cost to specialized devices and setups.

The response of the worms to electric stimulus has been examined on open surfaces in some detail [49, 50, 60, 173]. *C. elegans* can sense DC electric fields (1-14 $V.cm^{-1}$) as revealed by its highly stereotypic movement behaviour towards the cathode pole of the field at an angle, if placed on an open agar gel surface (Figure 4-1) [49, 60]. This phenomenon is called electrotaxis. The analysis of the movement response on the gel surface revealed that it is mediated by some of the amphid neurons (Figure 2-2), such as ASJ and ASH, since loss of their activity severely compromises the electrotactic response [60]. Gabel et al [60] also studied worms' response to a sinusoidal AC electric field modulating between 0 and 10 $V.cm^{-1}$ fixed in direction but varying in frequency on an open surface agar gel. They monitored changes in turning angle (θ in Figure 4-1) of the forward movement (due to electric field strength modulation) of the worm at different frequencies by rotating the electrodes continuously around the Petri dish at various angular velocities. It was observed that for frequencies increasing from 0.1 Hz to 16 Hz, the angle of the forward motion (θ in Figure 4-1 towards the cathode) decreases from 25˚ to 17˚, respectively; and at f >16 Hz, the worms crawl in an almost straight line, just as they would when they are exposed to a fixed 5 $V.cm^{-1}$ (equivalent to the average of the modulating 0-10 $V.cm^{-1}$ AC signal) DC electric field.

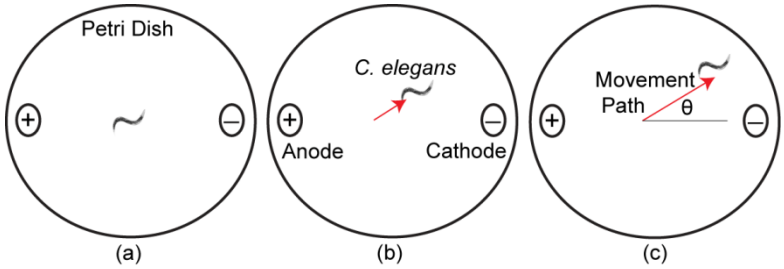

Figure 4-1 Schematic diagram of sequential (a-c) electrotactic movement of C. elegans exposed to a DC electric field on a Petri Dish, animal moves towards the cathode at an angle (θ) as described by Gabel et al. [60]

The biological relevance of electrotaxis is an interesting topic of research itself, which has been studied to some extent in the late-1950s, 60s and 70s [49, 183, 184]. It was suggested that in the case of plant parasitic nematodes, this behaviour might assist the worms in finding a host. It has also been argued that electrotaxis could play a role in the foraging behaviour of nematodes. Gabel et al. [60] suggested that the ability of *C. elegans* to respond to electrical stimulus may have evolved as a strategy for nematode parasites to exploit directional cues inside their hosts. The genetic analysis of electrotaxis in *C. elegans* could help researchers understand the basis of this behaviour and its evolutionary origin. By identifying genes and pathways that mediate this process, it should be possible to explain whether this is a conserved biological phenomenon or a process that evolved independently. However, an advanced method to assess the electrotactic behaviour more precisely both at behavioural and neuronal levels is needed to address these questions.

4.2 Microfluidic-Based Electrotaxis as the Optimal Method for Nematode Movement Assays

In the electrotaxis assay on open surface agar gel plates [60], discussed in section 4.1, the frequency of electric field modulation was introduced by the electrodes' rotation around the plate. It is hypothetically possible that on frequencies beyond 16 Hz, the worm was not provided with enough time to physiologically respond to the modulation and therefore a bimodal response to various frequencies was observed. Additionally, since these experiments were performed on open gel plates that are typically used to culture the organism, the electrical and environmental conditions were not tightly controlled leading to variation and complexity in the response. As shown in Figure 4-2, when a potential is applied between two electrodes inside a Petri dish, the electric field varies by as much as 40% along the central axis (cathode to anode) and by 60% in the direction perpendicular to it. Therefore, the response of the worms may not be clearly characterized in this setup. A simpler experimental setup, which

eliminates the complexity of rotational electric field of this experiment, can provide a more uniform electrical stimulation, and enable more accurate characterization of nematodes' electrotaxis.

In order to fully understand and characterize the electrotaxis behaviour of nematodes, it is very important to develop a platform on which the electrical stimulus, the environmental effects, and the movement of the animal can be precisely controlled and analyzed. This platform should also be easy to operate with minimal training of end users and be capable of analyzing movement in terms of quantitative parameters. Microfluidic technology was determined to be the best option that can address these issues as discussed in Section 2.5. In comparison to the Petri dish, the microchannel format (Figure 4-2) provides a very uniform electric field and also a uni-directional path for movement. The microchannel format simplifies the experimental setup and allows characterization of the innate electrotaxis response of the worms to electric field.

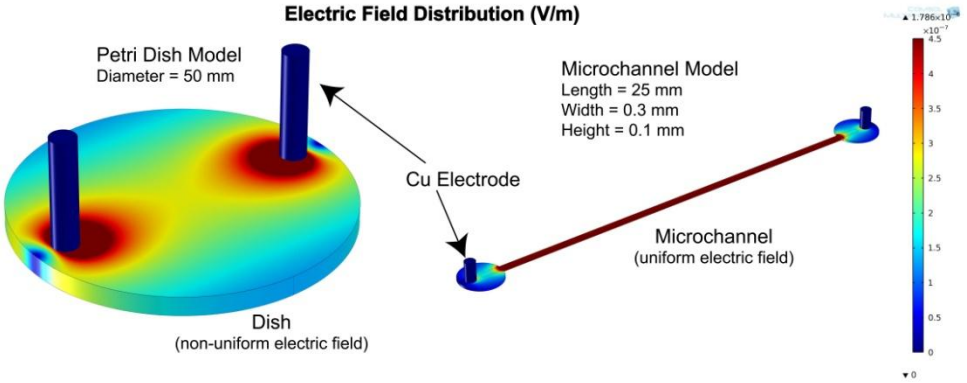

Figure 4-2 Electric field distribution (color contour) compared in a Petri dish and a microchannel both filled with water and instrumented with copper electrodes inserted at their end ports. A V=15 Volts potential was applied across the electrodes for both conditions.

In this chapter[‡], electrical signals inside microfluidic environments (using two microfluidic '*behavioural' and 'neuronal' analysis chips*) will be investigated as tools to precisely control and characterize the movement of nematodes.

[‡] Contents of this chapter have been collected from published articles (with permission):

1. Rezai, P., et al., *Electrotaxis of Caenorhabditis elegans in a microfluidic environment.* Lab Chip, 2010. **10**(2): p. 220-6.
2. Rezai, P., et al., *Effect of pulse direct current signals on electrotactic movement of nematodes Caenorhabditis elegans and Caenorhabditis briggsae.* Biomicrofluidics, 2011. **5**(044116): p. 1-9.
3. Rezai, P., et al., *In vivo Detection of Electric Field-induced Neuronal Activity in C. elegans* Under Preparation, 2012.

4.2.1 Design of the '*Behavioural Microchip*' for Precise Electrotactic Movement Assays

As illustrated in Figure 4-2, electric field distribution inside a microchannel is highly uniform and the internal environment of the channel can be perfectly isolated from any other external cues. However, in order to assess nematodes' electrotaxis inside microchannels, the dimensions of the channel had to be designed in a way that (1) worms could move freely in the channel but only along a single axis and (2) electrokinetic flows that affect the animals' movement could be avoided. The designs were all done in compliance with the criteria described in Chapter 3.

Schematic of the designed microfluidic *behavioural chip* is illustrated in Figure 4-3. It consisted of a simple microchannel (different dimensions tested according to the discussion above) instrumented with fluidic input and output tubes as well as copper electrodes at reservoirs at both ends of the channel. The fabrication process is fully described in Chapter 3, Section 3.3 and Appendix A.

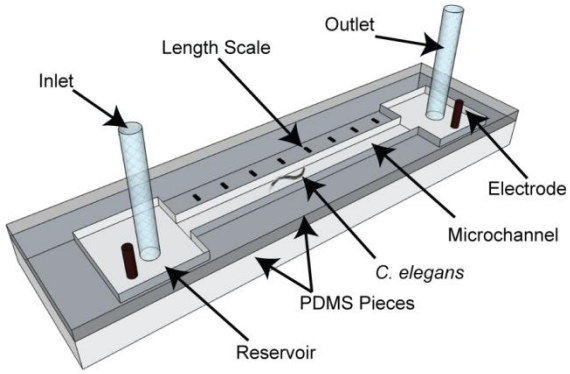

Figure 4-3 Schematic of the behavioural microchip (sealed PDMS microchannel with embedded electrodes in reservoir areas) for studying worms electrotaxis, [15] Reproduced by the Permission of the Royal Society of Chemistry 2010

The dimensional design of the microfluidic channel was done to suit the characteristic sizes of the animals used. The most important criteria in selecting the length of the microchannel were the ease of the animal loading and prevention of its escape from the channel during the experiments. Since the worms were loaded into the channel pneumatically (Section 3.4.1), it was important to have a long enough microchannel so that as soon as a worm was observed entering the channel, the flows could have been stopped before the animal exited the channel. Additionally, the swimming and crawling speeds of worms have been reported to be in the hundreds of micrometres per second range (250 $\mu m.s^{-1}$ considered averagely for designs). Therefore, in order to be able to keep the animal traveling in a single direction in the channel for 2-4

minutes (required for full movement assays), a length of 30-60 mm was required. A 50 mm channel (30, 50 and 70 mm tested) turned out to be optimally easy to load and assess animals in terms of their movement. Depth of the channels (100 µm) was designed to be slightly larger than the diameter of adult worms (~80 µm) to allow easy loading but which will restrain their movement along the depth of the channel. To design the width, straight microchannels (50 mm long and 100 µm deep) with varying widths of 2 mm, 1 mm, 500 µm, 300 µm, and 150 µm with electrodes instrumented in their reservoirs (Figure 4-3) were fabricated. Age-synchronized *C. elegans* worms (see Section 3.2 for details on growing same age/size animals) of various age and size, from L1 (~250 µm long) to young adult (~1 mm long), were loaded individually into the microchannels filled with M9 buffer and positioned in the central section (2.5 cm away from each electrode) using a syringe pump (see Section 3.4.1). In the absence of a stimulus, the animals had random movement in the microchannel (n=20). In some instances, it was observed that after traveling a certain distance in one direction, the animals turned and moved in the opposite direction. In two cases, the animals exited the channel after spending ~5 min inside the channel (from either side). The microdevice with 300 µm wide microchannel appeared to be the optimum in assays, because it guided movement along the channel axis without any obvious physical confinement and eliminated any perpendicular motion (observed in >500 µm wide channels) of the worms. The 150 µm wide microchannel was too narrow and appeared to interfere with the worms' normal swimming behaviour and hence was not used. Electrical resistance of the final designed channel (50 mm long, 0.3 mm wide and 0.1 mm deep) filled with the buffer M9 solution in all electrotaxis tests was ~700 KΩ.

The experimental setup to study nematodes' response to the electric fields (Figure 3-4) inside the designed *behavioural chip* consisted of 3 other major units in addition to the device: (1) a worm-handling unit (syringe pump, inlet and outlet connections), (2) an electrical actuation unit (power supply and electrodes), and (3) a monitoring unit (microscope and camera). Detailed experimental procedures, setups and information have been provided in Section 3.4 and Appendix A. As discussed in Chapter 3, electrokinetic flows (electrophoresis as well as electroosmosis) can occur more dominantly inside microscale channels upon application of electric fields. In order to determine the effect of these flows in the designed device, dead worms (see Section 3.1.2) were loaded individually into the *behavioural chip* (Figure 4-3) filled with M9 solution and positioned in the middle section (2.5 cm away from the electrodes) using the syringe pump (Section 3.4.1). Pneumatic flows were eliminated by balancing the hydrostatic pressure heads at the inlet and outlet of the microchannel. A wide range of electric field strengths (1–20 $V.cm^{-1}$) was applied across the channel. This range was chosen in accordance to the DC electrotaxis response range reported for

adult worms on open agar gel surfaces (4-14 $V.cm^{-1}$) [60]. This experiment showed that electrokinetic flows above 13 $V.cm^{-1}$ was able to move the dead worms towards the anode. No change in the morphology of dead worms was observed during this process. Furthermore, it was found that the electrokinetic effects (electrophoresis of the worm and electroosmosis of fluid) had no significant role in the movement of worms below 13 $V.cm^{-1}$ in these confined geometries.

4.3 Behavioural Assays Using Microfluidic-Based Electrotaxis

The microchannel format, as it is used here, provided a simple well-controlled platform to study and understand the electrotaxis behaviour of nematodes. To perform the electrotaxis assays, worms were loaded individually and positioned in the channel (described in details in Section 3.4.1). Their response to various electric field wave-shapes (Figure 3-5) was investigated. Effect of DC electric field strength (1-13 $V.cm^{-1}$) (section 4.3.1) as well as pulse DC electric field frequency (1-1000 Hz) and duty cycle (10-90%)(section 4.3.2) on percentage of responding worms, their rotation time (t_R), body bend frequency and swimming speed was investigated quantitatively as discussed in Section 3.5.1. Worm samples were prepared as described in details in Section 3.2. Nearly all experiments were done with synchronized stages of the animals as described before. Conservation of electrostatic behavioural response between *C. elegans* and another closely-related species *C. briggsae* were also studied.

In addition to behavioural movement responses of nematodes to DC and pulse DC signal, this phenomenon was also studied at a neuronal level in this chapter (Section 4.3.3) by using another microfluidic '*neuronal chip'*. As described in Section 2.2.2.3, neurons sense the presence of a diverse range of stimuli including the electric field and respond to it by generating an ionic signal transmitted between neurons to induce motor output. Genetically labelled worms with fluorescent protein sensors attached to specific target neurons for FRET imaging have assisted the study of transient signalling activities in individual neurons in response to external stimuli. Using the *neuronal chip* to immobilize worms for FRET assays in this chapter, live neuronal imaging has been used to correlate DC and pulse DC electrotaxis responses of *C. elegans* to Ca^{+2} transient activities in the ASH neuron as one of the majorly-involved neurons in electrotaxis.

4.3.1 DC Electrotaxis

Response of *C. elegans* and *C. briggsae* to DC electric field (Figure 3-5) in the *behavioural chip* is examined in this subsection with detailed investigations on the effect of age and size on electrotaxis, post-electric-field-exposure consequences, as well as cellular basis of this phenomenon.

4.3.1.1 DC Electrotaxis of C. elegans in the Behavioural Chip

The first task was to identify if the worm would respond to application of an electric stimulus inside a microchannel just as it would in a Petri dish [49, 50, 60, 173]. It should be emphasized that movement is in a crawling mode on a Petri dish and in a swimming mode inside a microchannel. Swimming was intended to be characterized as this thesis aimed to apply electrotaxis assays in chemical screening at later stages which are all done in liquid environments. The experimental setup discussed in Chapter 3 (Figure 3-4) allowed examining the response of the worms to an electric field. To identify the electrotactic behaviour in the microchannel in more detail, synchronized animals of different stages (from L1 to young adult, N>15 of each) were introduced into the microchannel individually. As discussed in section 4.2.1, the *behavioural chip* allowed the application of electric fields in the range of 1 to 13 $V.cm^{-1}$, that was examined in this experiment. After positioning the worm in the channel and eliminating all the pneumatic flows, various electric fields were applied across the channel (opposite to the worm orientation) and movement of the animals was monitored and recorded in a video format.

It was observed that the early stage animals (L1 and L2) displayed no obvious response in the 1-13 $V.cm^{-1}$ electric field range since they continued to swim randomly regardless of the direction and presence of the field. At later stages (L3 onwards), the animals responded robustly to the electric field but within a certain range, that was different for each stage and exhibited directed movement towards the negative pole (Figure 4-4). Reversing the direction of the applied electric field resulted in the reversal of the worm's movement which was quick (a sudden stop in the forward motion followed by attempts to perform the turn in <15s in most of the worms). It was also discovered that high-strength electric fields induced paralysis (i.e. 4 $V.cm^{-1}$ for young adults) which was also variable for different stages. Nonetheless, they resumed swimming upon the removal of the electric field, suggesting that this effect was reversible. A careful examination revealed that their swimming pattern in the non-paralyzed mode was typical of unexposed (not exposed to any electric field) animals in a liquid environment, except that the response was directional. This observation suggests that the electric field does not introduce a body force on the worm to make it move; rather it simply induces swimming behaviour. The finding that only

older worms responded to the electric field (in 1-13 V.cm^{-1} range) hypothetically suggests that this behaviour is developmentally regulated and is likely to be mediated by certain differentiated cell types that may be absent (or immature) at earlier L1 and L2 stages. Other hypothetical possibility could be that the early stage animals respond to electric fields above 13 V.cm^{-1}. But since electrokinetic flows were significant in this range, their response at these electric fields was not characterized in this experiment.

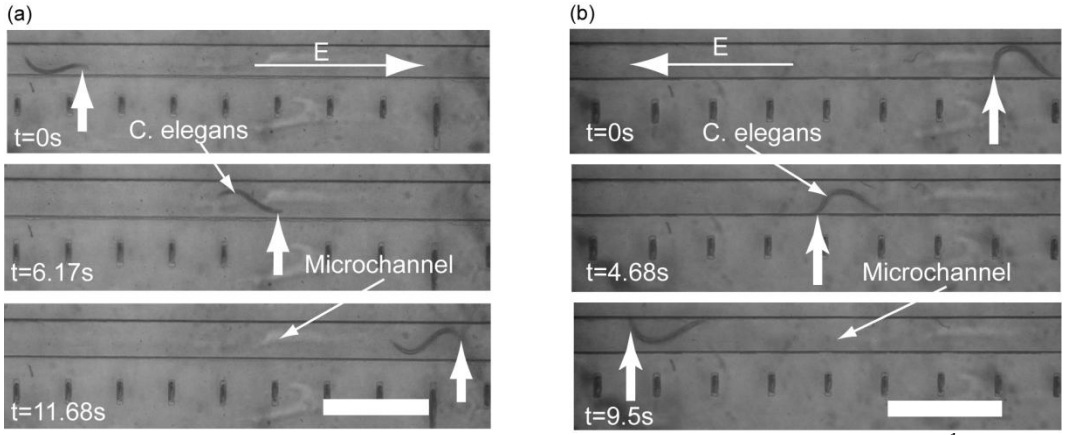

Figure 4-4 The movement of worms in an electric field. (a) The application of +8 V cm^{-1} electric field (E) caused an animal (724 µm long) to move with the speed of 308 µm s^{-1} to the right towards the cathode. (b) At a lower field strength in a reverse direction (-3 V cm^{-1}) another animal (847.5 µm long) moved with a speed of 342 µm s^{-1} to the left towards the cathode. Dark thick arrows illustrate the worm's position. Scale bars are 1 mm. [15] Reproduced by the Permission of the Royal Society of Chemistry 2010

In another attempt to delineate the effect of voltage and current on stimulating electrotaxis in the worms, synchronized young adult animals were suspended in a M9 media solution diluted with DI water. This dilution increased the electrical resistivity of the solution resulting in a higher electrical resistance (~20 MΩ compared to ~0.7 MΩ before) in the channel. It was observed that the young adult worms (n=5) responded similarly to electric fields regardless of the reduction in the current passed through the channel. Their body bends, speed of swimming towards the negative electrode and paralysis electric field limit was similar in both cases. This result suggests that the voltage difference (and hence the electric field) is a significant factor in inducing electrotaxis.

Altogether, the results demonstrated for the first time that older larvae and young adults of *C. elegans* respond to electric field in a liquid environment inside the microchannel and move towards the cathode. Contrary to earlier reports [60], where it was reported that the movement response of adult animals was at an angle to the anode-cathode axis [60], the microchannel-based electrotaxis response was uni-directional towards the cathode, in the direction of the anode-

cathode axis, for multiple developmental stages and hence better suited for characterization of this response in quantitative details.

4.3.1.2 Effect of Age on Electrotaxis

The developmental response of the worms to the electric field stimulus led to its characterization in further detail. Here, synchronized worms of L3, L4 and young adult stages (N>10 for each) were tested individually inside the channel for their electric filed response range as shown in Figure 4-5. Worms of a specific age were observed to respond robustly (100% responders) to electric fields higher than a minimum threshold limit (i.e. 2 $V.cm^{-1}$ for young adults) by moving towards the cathode. Below the minimum threshold limit, no directed response was observed and worms move randomly in the channel. Above the maximum threshold, the animals got momentarily paralyzed in the channel revealed from their curled tail and difficulty in swimming (reversible upon electric field removal). Using a length scale, fabricated alongside the microchannel (as shown in Figure 4-3), the speed of the worm at various electric fields in the response range was measured by image processing using the ImageJ software (Figure 4-5).

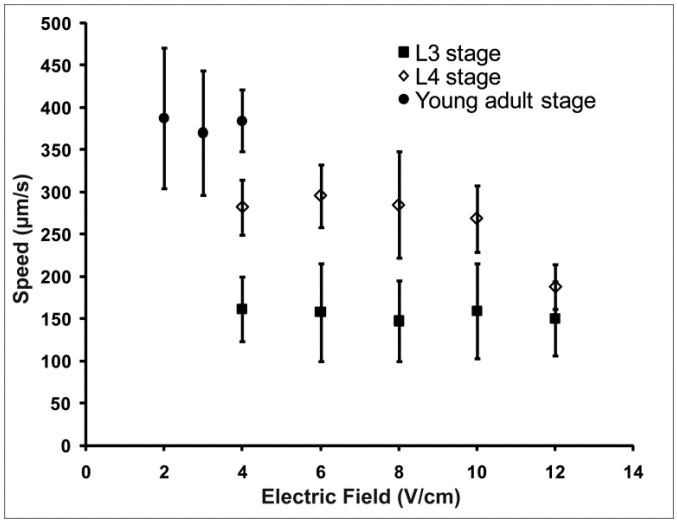

Figure 4-5 The effect of electric field strength on electrotaxis of different stages of C. elegans.only active range of response (movement with no paralysis) to electric field has been plotted for L3 and young adults. The 12 $V.cm^{-1}$ data point for the L4 stage is to show the paralysis effect and reduction in speed which has been eliminated from the plot for other 2 stages. The L3 stage worms (385–528 µm long, dark rectangles) responded to electric fields above 4 $V.cm^{-1}$ with a speed range of 100-216 $\mu m.s^{-1}$. The L4 stage worms (534–725 µm long, clear rhombuses) responded to electric fields between 4 and 10 $V.cm^{-1}$ with a speed range of 220-340 $\mu m.s^{-1}$. Due to the partial paralysis at 12 $V.cm^{-1}$, the speed of L4 stage worms was reduced. The young adults (920–1050 µm long, dark circles) had the lowest effective electric field range (2-4 $V.cm^{-1}$) since they were paralyzed above 4 $V.cm^{-1}$. Within the effective range, their speed ranged between 296 and 471 $\mu m.s^{-1}$. The upper threshold electric field was not observed for L3 stage worms due to the upper limit of allowable field without electrokinetic flow. [15] Reproduced by the Permission of the Royal Society of Chemistry 2010

The results in Figure 4-5 showed that the speed of individual worms at any one particular stage (age) does not change significantly with the applied electric field strength; however, older worms had a higher speed when compared with the younger ones (~80% increase between L3 and L4, and ~35% increase between L4 and young adults). Figure 4-6 demonstrates this difference in speed for L3 and young adult animal stages in an experiment with multistage animals loaded simultaneously in the *behavioural chip* and exposed to a 4 $V.cm^{-1}$ electric field (common response electric field for both L3 and young adult stages based on Figure 4-5).

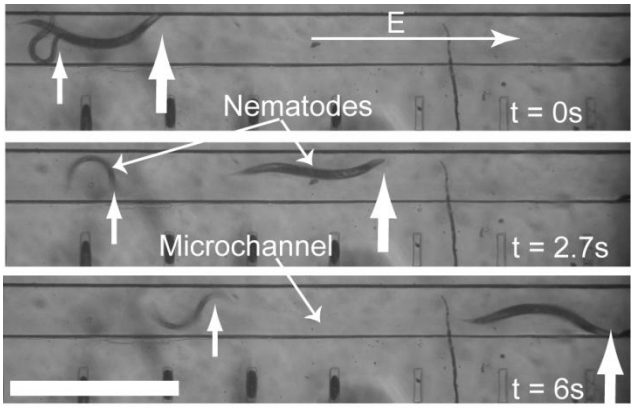

Figure 4-6 Separation of two animals (530 µm long L3 stage and 1000 µm long young adult) within 6 s upon application of 4 $V.cm^{-1}$ electric field due to their difference in electrotactic movement speed. The thin and thick white arrows mark the anterior ends of the L3 stage and young adult worms, respectively. The scale bar is 1 mm. [15] Reproduced by the Permission of the Royal Society of Chemistry 2010

The L3 stage animals responded to the electric field robustly (100% of worms responded) starting from 4 $V.cm^{-1}$ (minimum threshold). The maximum threshold (defined by the paralysis phenotype - revealed by occasional abnormal body bends and reduced speed) could not be observed, because animals continued to swim normally without a change in their speed even at the maximum field limit (13 $V.cm^{-1}$) in the channel. At later stages, animals appeared more sensitive to the electric field. Sensitivity to the electric field was defined as being responsive to lower electric fields and becoming paralyzed at lower threshold limits. Thus, while L4 stage animals were partially paralyzed at 10 $V.cm^{-1}$, the young adults exhibited this effect at 4 $V.cm^{-1}$. The minimum threshold responses at these two stages were 4 $V.cm^{-1}$ (L4) and 2 $V.cm^{-1}$ (young adult) respectively. These results demonstrate that the adult animals are more sensitive to the electric field and possess the shortest response range compared to L3 and L4 larvae.

The undulatory motion of the worms of different sizes was also studied to determine the frequency of body bending under various electric fields. Swimming behaviour without any electric field was used as the control. It was observed that

in the presence of electric field, the average bending frequency of the worms of different sizes (450–1000 mm long) (N = 15) ranged between 1.7 and 2.6 Hz. The bending frequency for each worm did not change significantly (<5% variation at maximum) with a change in the electric field strength or/and the direction; and it was in close approximation of the body bend frequency in electric field-free conditions (1.78–2.52 Hz for different size animals) demonstrating that the electric field did not have a significant effect on the worm's natural body motion. These measurements compare favorably with other studies on *C. elegans* in microstructured environments [132, 133] where the bending frequency increased from 1.5 Hz on a gel surface to 1.92 Hz in the microchambers filled with micropillars (see Section 2.5.2 for detailed review).

All in all, a low-voltage DC electric field could be used as an attractant to guide worms` movement without physiological and behavioural side effects. The cathode-driven electrotactic movement is robust, highly reproducible and sensitive. Within the optimum electric field response range of any given stage, the speed of movement of the animals remained unchanged, suggesting that the electrotaxis response in a microchannel is a binary phenomenon (all or none). Due to the high degree of precision and control offered by the *behavioural chip*, the electrotactic response could be characterized quantitatively in terms of speed of swimming towards the cathode, body bend frequency and rotation time upon stimulus reversal.

4.3.1.3 Cellular Basis of Electrotaxis in Microchannels

Mutant worms with defects in specific cell types have been used to explore the cellular basis of electrotaxis. Gabel et al. [60] had previously shown that the neuronal circuits of *C. elegans*, specifically the amphid sensory neurons, mediate electrosensory behaviour. Similar electrotactic experiments (1-13 $V.cm^{-1}$ electric fields in the *behavioural chip*) using young adult *unc-6(e78)* mutant animals that exhibit defects in neuronal differentiation were carried out. Studies on *unc-6* have shown that it encodes a netrin-like secreted protein that plays a crucial role in neuronal growth cone migrations [185]. The *unc-6* mutant animals are uncoordinated due to defects in dorsal and ventral nerve cords [186]. The analysis of *unc-6(e78)* young adults in the microchannel revealed no response to the electrical stimulus but in-place body shakes and bends while the stimulus was being applied. The animals showed no obvious sign of orientation and speed change following the application of electric fields for more than 2 minutes (Figure 4-7).

A muscle mutant *unc-54(s74)* was also tested in a similar setting to determine the contribution of muscles in electric field-driven swimming behaviour. The *unc-54* gene is necessary for the proper differentiation of the muscle myosin class II

heavy chain (MHC B) [187]. The *unc-54* mutant animals exhibit disorganized muscles and are severely uncoordinated (paralyzed) [188]. It was found that *unc-54(s74)* young adult worms respond to the electric field in a manner similar to that of wild-type worms (2–4 V cm^{-1} range), although their speed was significantly slower (*unc-54*: 88 $\mu m.s^{-1}$, wild type: 380 $\mu m.s^{-1}$, average speeds) (Figure 4-7). This is interesting considering that *unc-54(s74)* worms on standard culture plates (NG agar) exhibit almost complete paralysis. These results demonstrate that the electrosensory response in microchannels is primarily mediated by neuronal activity.

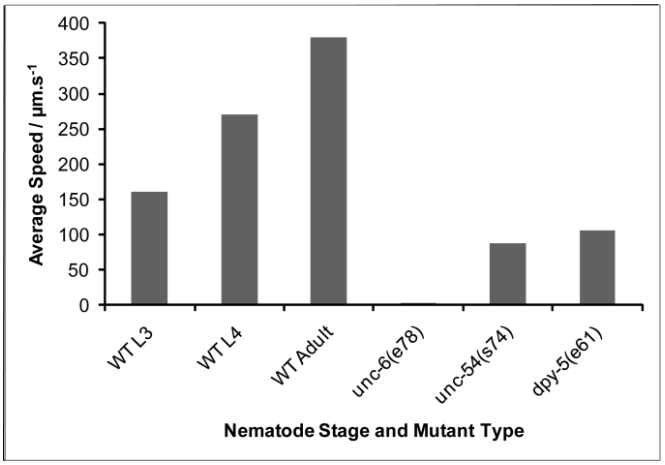

Figure 4-7 Average electrotactic speed of various wild type and mutant animals at their active response range (4-12 V.cm^{-1} for L3, 4-10 V.cm^{-1} for L4, 2-4 V.cm^{-1} for YA and all mutants) in a 5 cm-long, 300 µm-wide and 100 µm-deep microchannel. Unc-6(e78) had zero speed since it did not respond to the electric field. WT: Wild type. [15] Reproduced by the Permission of the Royal Society of Chemistry 2010

The results are consistent with the findings of Gabel et al. [60] and suggests that electrical cues are likely to be processed by the same set of neurons and genetic pathway regardless of the environment of animals. Furthermore, this work has uncovered the importance of muscles in mediating electrotaxis in a microfluidic environment. The differential speed of movement between mutant and wild type animals was later used to separate worms electrotactically on an agar surface by Manière et. al. [165].

4.3.1.4 Sensitivity of Electric Field Response: Size vs. Development

The experiments have revealed that adult worms respond to electrical fields much more robustly compared to the younger (L3 stage) animals (Figure 4-5). Considering that electrosensory behaviour is mediated by neurons (Figure 4-7), it is possible that adult worms have a mature nervous system and are therefore capable of processing neuronal signals more efficiently than the younger developing worms. Such a difference may also result from a change in the length

of worms since adult worms are significantly larger compared to L3 stage animals (~1000±100 µm and ~450±100 µm, respectively). To distinguish between these possibilities, two different mutant strains were tested that were shorter and longer (*dpy-5(e61)* and *lon-2(e678),* respectively) compared to the wild type. The *dpy-5* gene encodes a collagen that is necessary for the cuticle formation in developing larvae, whereas *lon-2* encodes a glypican family of heparan sulfate proteoglycans that negatively regulates DBL-1/BMP signaling to control body length [189, 190]. Mutations in these two genes give rise to opposite phenotypes. Thus while *dpy-5* mutant animals are approximately 60% shorter compared to the wild type (400±100 µm and 1000±100 µm at 62 h, respectively), the lon-2 mutant animals are roughly 30% longer (1300±100 µm at 62 h) than the wild type. Both these mutant animals are otherwise healthy and active.

The analysis of *dpy-5(e61)* animals in the microchannel (N=10, various electric fields) revealed that, unlike the wild type animals (effective response range of 2-4 $V.cm^{-1}$), these animals responded to the electric field robustly (100% responders in <15 s) starting from 4 $V.cm^{-1}$ and showed no sign of paralysis at the highest possible field tested (13 $V.cm^{-1}$). Their average speed (106 $\mu m.s^{-1}$) did not change in response to an alteration in the electric field strength and/or direction. In contrast, the *lon-2(e678)* animals did respond to the lowest threshold electric field as the wild type (2 $V.cm^{-1}$). However, these animals appeared extremely sensitive and were paralyzed under the influence of electric fields higher than 3 $V.cm^{-1}$. Due to their larger size, they were unable to move freely in the microchannel and exhibited abnormal movements. This precluded the measurement of their speed. These results demonstrate that longer worms are more sensitive to the electric field than shorter ones, suggesting that the size is a major determinant of the sensitivity of *C. elegans* to the electric field. This was most likely due to differences in the potential drop across the entire body that is greater in *lon* mutants compared to the wild type (~30%). This may also explain the variability in responses observed for different stages of wild type animals since they are not exactly alike.

4.3.1.5 Post-Exposure Effect of Electric Field

Considering that worms appeared paralyzed when exposed to the electric fields greater than their response range, experiments were conducted to study the effect of electric field on their behaviour, fertility and viability. In this experiment, 10 adult animals were aspired into the channel individually and a constant electric field (2-4 $V.cm^{-1}$) was applied across the channel for a duration of 10 min in each case. During this period, the polarity of the field was reversed every minute (while keeping the field strength constant) in order to keep the worm inside the channel and to prevent it from getting in direct contact with

electrodes. In one case, a young adult worm was also exposed to a 12 $V.cm^{-1}$ electric field (3X wild type young adults` maximum threshold electric field response limit) for duration of 10 min. Following the exposure, the worms were removed and grown on standard culture plates. It was found that in all cases (N = 11), the animals recovered successfully within few hours, exhibited normal sinusoidal pattern of movement (i.e., no uncoordinated movement), did not die prematurely (~18 days average age), and were fertile for 3-4 days (similar to the unexposed wild type worms). This demonstrates that the electric field stimulus causes no visible harm to *C. elegans* and that there are no apparent long-term developmental and behavioural changes following exposure. However, the possibility of certain cellular and molecular changes that could have occurred could not be ruled out. This will require more extensive analysis using molecular markers as well as cellular and sub-cellular studies.

4.3.1.6 DC Electrotaxis of C. briggsae and Comparison to C. elegans

C. briggsae is very similar to *C. elegans* in terms of morphology, development and genetic makeup [191]. The two species are likely to have been separated around 30 million years ago [192]. *C. briggsae* is frequently used in comparative studies to understand conserved mechanisms of gene function and biological processes [193].

The response of *C. briggsae* worms to constant DC field was also tested similar to what was done earlier for *C. elegans* [15]. Considering that the two species have a large number of conserved genes and appear morphologically similar [15], it was desired to compare their electrotactic responses to DC fields. For this, young adult *C. briggsae* animals (N=5, 845±40 µm length, 62 h post-L1 stage) were loaded individually into the *behavioural chip*; and DC electric fields (1-6 $V.cm^{-1}$) were applied across the length of the channel. All tested animals responded to the electric field and moved towards the cathode spontaneously after the application of the signal. The direction of the field was reversed twice for each worm, and every time, it was allowed to rotate and travel for a distance of 5 mm. The entire movement response was recorded and analyzed (Figure 4-8) as described in Section 3.5.1.

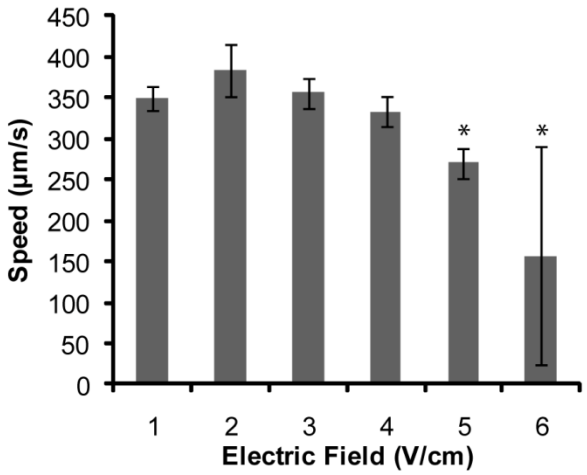

*Figure 4-8 C. briggsae (N = 5) DC electrotaxis speed at various electric field strengths. Based on the analysis of variance comparing the groups *: significant ($p<0.01$) reduction in speed at 5 and 6 V.cm^{-1} electric fields compared to 1–4 V.cm^{-1} (Reprinted with permission from [16]. Copyright © 2011, American Institute of Physics)*

It was observed (Figure 4-8) that *C. briggsae* responded to the electric fields in a range of 1-4 V.cm^{-1} and showed partial paralysis starting at 5 V.cm^{-1}. Consistent with this, the electrotactic movement speed at 5 and 6 V.cm^{-1} was significantly slower compared to the one at 1-4 V.cm^{-1} ($p<0.01$, ANOVA). The paralysis was initially observed in the tail region as animals appeared to gradually form coiled-shape configuration in the tail region. This gradually extended to the whole body, if the signal persisted, eventually leading to coiling. Although the higher threshold of response (4 V.cm^{-1}) of young adult *C. briggsae* was similar to that of *C. elegans* [15], It was observed that these animals, unlike *C. elegans* (which had 2 V.cm^{-1} lower threshold [15]), responded to DC electric fields as low as 1 V.cm^{-1} in a robust manner (100% responders, N = 5). However, similar to *C. elegans*, swimming speed of *C. briggsae* did not vary significantly with electric field strengths in the active range (1-4 V.cm^{-1}) ($p>0.01$, ANOVA) and had an average value of 356±20 µm.s^{-1}. For this particular assays, the DC electrotaxis experiment was also performed for *C. elegans* (N = 7, 719±37 µm length, 62 h post-L1 young adult) and observed an average speed of 296±43 µm.s^{-1} in the 2–4 V.cm^{-1} range. Since the forward movement of both species is a result of the motion of the body in a sinusoidal waveform propagating from head to tail, it was hypothesized that their speed is directly dependent on the body stroke frequency of motion and their sinusoidal wave's peak-to-peak value, which is primarily influenced by the channel width design in microfluidic devices rather than the electric signal characteristics. The body stroke frequency for both *C. briggsae* and *C. elegans* was on an average 2±0.1 Hz and resulted in slightly higher speed for *C. briggsae* (Figure 4-8).

An electric field with appropriate strength induces electrosensation and the locomotory behaviour in the animal. After this, it seems that the animal uses its mechanosensory system to optimally choose a constant body stroke frequency that depends strongly on environmental parameters (e. g. specific channel geometry) and, hence, demonstrate a constant speed in it. This hypothesis is supported by different speeds reported for *C. elegans* in experiments within various swimming or crawling environments [132, 133]. The findings in this section have the potential to use electric field-based microfluidic devices to study the worm movement and to understand the genetic basis of electrotaxis. Additionally, these techniques are designed and developed to facilitate HTS of chemicals using movement as an assay (Figure 2-9) that has historically not been possible with existing microfluidic formats. These will all be investigated in the remainder of the thesis especially in Chapter 6.

4.3.2 Pulse DC Electrotaxis

As discussed in section 4.3.1, under a constant DC field, both *C. elegans* and *C. briggsae* exhibit a steady-state, spontaneous, sensitive and fully penetrant movement response with a characteristic speed towards the cathode [15, 16]. When the field direction is reversed, a switch in the direction of the worm's movement in the microfluidic channel (turn) is very quick, typically happening in less than 15 s, irrespective of its age or size. Thus, constant DC electrotaxis is a good method to assay for the effect of a chemical or drug on the forward movement of the organism [194]. However, in order to understand the effect of the electric field on the neurophysical system of the worm and consequent changes in its movement, it is important to develop a method that could induce a proportionally variable and dynamic response in movement to a variation in the stimulus, either in an individual worm or in a population of them. Electric field is an ideal stimulus to modulate as it is easy to control at the microsecond timeframe. In this section, the use of pulsed electric field (pulse DC, See Figure 3-5) and its reversal on the speed and turning response time of *C. elegans* is investigated. Pulse DC waveform was chosen because it more closely resembled an on-off DC signal in comparison to a sinusoidal or triangular waveform. With a pulse DC signal, the duration of the electric field stimulation of the worm can be adjusted by changing the frequency and the duty cycle of the signal. Effects of frequency and duty cycle of the signal on movement phenotypes of interest (speed and turning time) are evaluated. In addition, the pulse DC electrotaxis behaviour of *C. elegans* is compared with that of *C. briggsae.* The results were compared to DC electrotaxis of these animals as well.

4.3.2.1 Pulse DC Electrotaxis of C. elegans in the Behavioural Chip

The same experimental setup (Figure 3-4) and microfluidic device (*behavioural chip*, Figure 4-3) used for DC electrotaxis studies was utilized in this assay. However, instead of a DC power supply, the device electrodes were connected to an electric signal generation unit for the application of pulse DC electric fields in the channel. This unit consisted of a function generator with a maximum voltage output of 5V, an amplifier with a 400 gain, a switch to reverse the polarity of electrodes, and copper wires to connect the setup to the device electrodes as discussed in Section 3.4. The function generator was set to produce a pulse DC potential waveform with adjustable characteristics, such as the frequency (*f*, Hz); maximum pulse voltage, as well as the duty cycle calculated using Eq. 3-4. As discussed in chapter 3, the pulse DC signal rises in a step-like manner from zero to a maximum set point for a controllable duration of time (duty cycle) and decays to zero for the rest of the signal cycle which is then repeated at a fixed frequency. Since the maximum pulse voltage output of the function generator did not exceed 5 V in the *behavioural chip* (leading to EF_{max}=1 $V.cm^{-1}$), the signal was subsequently amplified and applied to the microdevice. The rise and decay time of the pulse signal were measured to be 50 µs each, which restricted the experimental frequency range to less than 1 kHz and the duty cycle to more than 10% in order to produce a rectangular-shape pulse waveform.

Individual young adult *C. elegans* (62 h post-L1 stage) were loaded and positioned at the center of the microchannel. Upon exposure to a pulse DC electric field (EF_{max}=3 $V.cm^{-1}$ as measured previously in the DC electrotaxis experiments for a robust response in young adult animals [15], *f*=1000 Hz, Duty cycle=30%), worms were observed to swim towards the cathode (Figure 4-9i and ii) in a similar manner as previously reported for the DC electrotaxis (section 4.3.1.1) [15]. Reversal of the pulse DC field direction resulted in the animal turning its movement direction (Figure 4-9iii-vi) and moving towards the cathode again (Figure 4-9vii and viii). It was also observed that worms can be stimulated to move with pulse DC electric fields at other conditions such as *f*=1 Hz and 50% duty cycles. However, turning response time varied with changes in frequency and duty cycle. These findings led to investigation of the pulse DC electrotaxis response at other frequency and duty cycle levels.

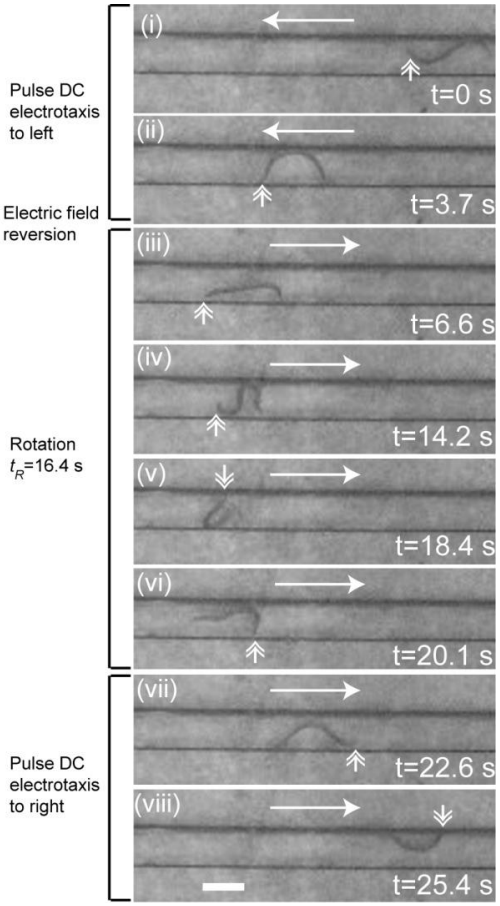

Figure 4-9 Pulse DC electrotaxis, sequential snapshots of a young adult C. elegans electrotaxis in response to a pulse DC electric field: EF_{max} = 3 V.cm^{-1}, f = 1000 Hz, Duty Cycle = 30%. Single-head arrows show the direction of the electric field and double-head ones point to the head of the worm. Scale bar = 0.3 mm. (Reprinted with permission from [16]. Copyright © 2011, American Institute of Physics)

4.3.2.2 Effect of Signal Duty Cycle on Electrotactic Swimming Speed and Turning Time

In order to examine the effect of the duty cycle on electrotactic response, *C. elegans* worms (N=14) were exposed to a range of duty cycles (from 10% to 90%) at a constant frequency of 1000 Hz (randomly chosen but comprehensively studied in the subsequent sections) and electric field of EF_{max}=3 V.cm^{-1}; and their forward motion speed (Figure 4-10) and turning response time (Figure 4-11) to the directional change of the signal were analyzed and compared to their DC counterparts. It was observed that there was no response among the worms to a 10% duty cycle signal. At 20%, a few responded, but the majority did not. The range from 30% to 90% duty cycle provided a more robust response. The speed of the worms remained constant with average values between a minimum of 290±37 μm/s and a maximum of 360±24 μm/s at different duty cycles in this

robust response range, as shown in Figure 4-10, which was also in close approximation of the DC electrotaxis speed. These speeds were statistically independent of duty cycle values ($p>0.1$, ANOVA) and were averaged at 315±37 μm/s. This result implies that even when the electrical stimulus is not continuous, it is sufficient to induce movement response in the worm beyond a certain threshold duty cycle.

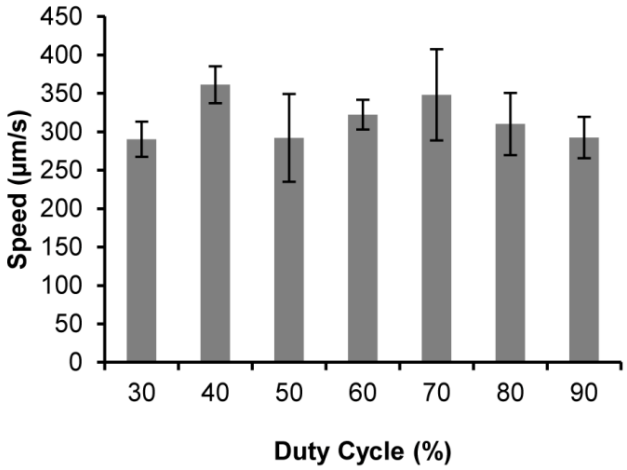

Figure 4-10 Effect of duty cycle on C. elegans (N=14) pulse DC electrotaxis forward motion speed. Frequency for all the experiments were 1000 Hz. (Reprinted with permission from [16]. Copyright © 2011, American Institute of Physics)

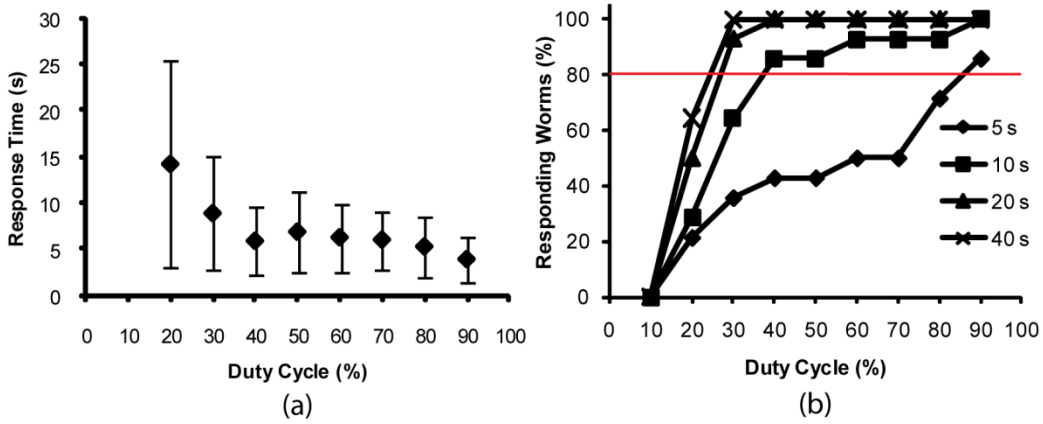

Figure 4-11 Effect of duty cycle on C. elegans (N=14) pulse DC electrotaxis: (a) average turning response time of solely the responder worms in 40 s (worms responding over 40 s excluded from the average, for instance at 20% duty cycle, only 9 out of 14 (64.3%) responded below 40 s and averaged in a), (no response at 10% duty cycle) and (b) percentage of responders at f=1000 Hz. Each curve in (b) shows the maximum time consumed by the worms to respond to the electric field reversal, turn, and initiate movement in the opposite direction. The red line in (b) corresponds to a cut-off value (80% responders) where any data above that for a population of worms was considered as a robust response. (Reprinted with permission from [16]. Copyright © 2011, American Institute of Physics)

Next, the turning response of the worms to DC and pulse DC signals, following a sudden change in field direction, was investigated. Here, the worms were exposed to a constant or pulsed DC signal (with a specific pre-set duty cycle at a fixed frequency of 1000 Hz) that was reversed suddenly. The turning response time of the worm was measured, as described in Sections 3.4.3 and 3.5.1. Since the turning response time was variable among individual worms (mostly within 40 s), the 40 s cut-off time was chosen to determine whether a worm was a responder or non-responder. Also, since the DC electrotaxis experiments demonstrated that worms perform a complete turn within 15 s of field reversal, this cut-off value was also selected to identify quick responders. Response times of t_R<15 s and t_R>40 s were therefore dubbed "spontaneous response" and "no response", respectively. The aggregate population response time was then used for data analysis. Within 40 s time window, responders for 5 s, 10 s, and 20 s durations were also quantified. The signal reversal was repeated three times to confirm that the turning response was genuine. The average turning response time for 3 $V.cm^{-1}$ DC electric field was 6.6±2.6 s for all responding young adult worms (100% response). However, it was found that the time for the worms to reverse their direction in response to pulse DC signals varied significantly (Figure 4-11a) for certain duty cycles, even though the experiments were done on a homogenous population of young adults. This variation in turning response time was greatest when the duty cycle was the smallest (large standard deviations at low duty cycles in Figure 4-11a) and reduced as the duty cycle increased and the signal approached constant DC. In addition to this, the number of worms showing turning response at lower duty cycles dramatically decreased such that none responded at 10% duty cycle in less than 40 s. In order to understand this phenomenon, population statistics was used as shown in Figure 4-11b, which plots the percentage of worms that responded to the pulse DC signal (at 1000 Hz frequency) of a certain duty cycle in a specific time window (i.e., 5, 10, 20, and 40 s). It was observed that at lower duty cycles, comparatively fewer worms responded quickly to the reversal of the pulse DC signal. For instance, only 20% of worms responded to 20% duty cycle signal with a turning response time of 5 s or less. However, 60% of them were able to respond to a change in the direction within 40 s. In another set of experiments (data shown later), young adults (N=10) were loaded into the channel individually and their response to 1 Hz frequency pulse DC electric fields with different duty cycles (10%-90% in 10% intervals) was investigated similarly. This signal was slower in terms of cyclic pulse application and the pulse durations were longer as compared to the f=1 kHz condition, therefore, it was chosen to resemble a DC signal which is turned on and off frequently. All the animals responded robustly to high duty cycle (>60%) pulses by moving towards the negative electrode. However, by lowering the duty cycle from 60% to 40%,

some worms did not respond to the stimulation anymore or the time of response initiation increased from few seconds to tens of seconds. Latency in response occurred in 40%-60% duty cycle range and the lack of response initiated at 40% duty cycle and below; where no oriented movement in the worms locomotion was observed at 1 Hz frequency in the 40 s experimental time window provided. At these conditions, they all either swam randomly in the channel or stayed at one location with in-place minimal body movements.

The results in Figure 4-11b show that at lower duty cycles, the worms in aggregate were unable to efficiently sense the direction of pulse DC signal and, unlike constant DC signal, take much longer time to respond. This could be due to an inherent limitation of amphid sensory neurons and/or other neurons involved in turning behaviour to respond to lower duty cycles of pulse DC signal. Figure 4-11b also shows that at higher duty cycles of the signal, greater number of worms showed turning response and in a faster manner (just as they would respond to a DC signal quickly in <15 s). For instance, the proportion of the worms responding to the reversal of signal within 5 s increased from 20% at 20% duty cycle to ~80% at 90% duty cycle. Hence, the turning time can be used as a measure of the dynamics of sensing by the worm. The variation of the duty cycle can provide a method to modulate the dynamic response in a population of worms. In summary, variation in the duty cycle of pulse DC signals and the turning response time to the field reversal together provide a unique method to elicit varying movement response to correspondingly varying electrical stimulus.

4.3.2.3 Effect of Signal Frequency on Electrotactic Swimming Speed

The effect of the frequency of pulse DC signal on the forward-motion electrotactic movement speed was also studied for *C. elegans* and *C. briggsae*. A duty cycle of 50% that induced robust response in the worms (more than 80% responders in less than 10 s in Figure 4-11b) was used for the pulse DC field with frequencies ranging between 1 and 1000 Hz. The speed of electrotactic forward movement is shown in Figure 4-12. Each data point corresponds to an average of 7 worms (tested one at a time, 62 h post L1 young adult, 719±37 μm long) examined. Average DC electrotactic speed is also depicted in the same figure for comparison. It can be clearly seen that the frequency does not have a significant effect on the pulse DC forward electrotactic movement speed ($p>0.1$, using ANOVA), which was also similar to their DC electrotactic movement speed. Such behaviour has been previously observed in *C. elegans* [60]. The *C. briggsae* worms (N=7) responded in a similar fashion (Figure 4-12), suggesting that the mechanism of electrotactic response is conserved between the two species.

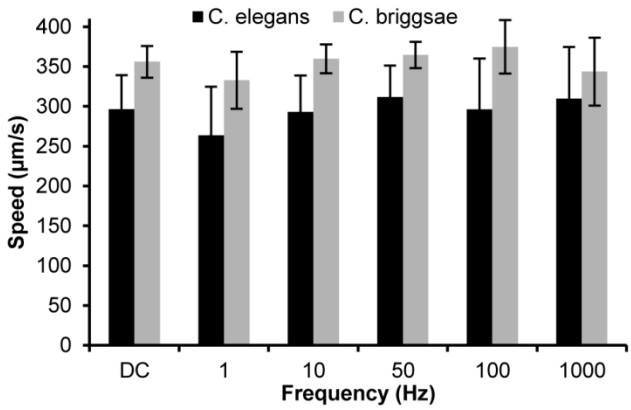

Figure 4-12 Effect of frequency on C. elegans (n=7) and C. briggsae (n=7) pulse DC forward electrotactic swimming speed at EF_{max} = 3V.cm^{-1} electric field and 50% duty cycle. Average DC electrotaxis speed is also plotted. (Reprinted with permission from [16]. Copyright © 2011, American Institute of Physics)

It was observed that both *C. briggsae* and *C. elegans* responded to pulse DC electric fields in a similar manner as to DC fields by moving towards the negative electrode inside the microchannel. The pulse DC-induced electrotactic speed of the animals did not vary significantly with changes in the frequency and the duty cycle of the signal; and it was similar to their DC electrotaxis speed.

4.3.2.4 Effect of Signal Frequency on Electrotactic Turning Time

In this section, the effect of the whole spectrum of pulse DC signal frequency (1-1000 Hz) and its directional changes on the turning behaviour of *C. elegans* worms has been studied all in the *behavioural chip*. Some of the duty cycle levels (<40% at 1 Hz or <30% at 1 KHz frequency) did not induce any electrotactic response inside the microchannel (Figure 4-11b), so a wider range of frequencies at all duty cycles were investigated to elucidate this behaviour thoroughly. Young adults (N>10 for each frequency level at *f* =1, 10, 100 and 1000 Hz) were assayed for pulse DC electrotactic movement response time as described in Section 3.4.3. The average response time of each worm (t_R, 3 trials) as well as the entire pool ($\bar{t_R}$) were determined at every responding frequency and duty cycle level. Figure 4-13 demonstrates the average response time, $\bar{t_R}$, variations based on duty cycle and frequency for pulse DC electrotaxis of young adult worms. Number of responding worms was also counted along with the response times at each frequency for the entire range of duty cycles.

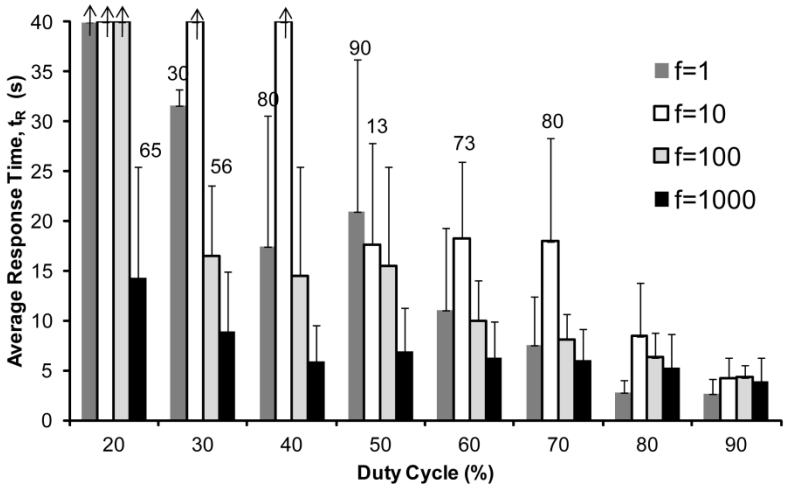

Figure 4-13 Average response time, $\bar{t}_R$, and percentage (from total of N>10 worms) of responding (t_R<40 s) worms to pulse DC electric fields with frequencies of 1, 10, 100, and 1000 Hz and varying duty cycles. The upward arrows on top of the columns at lower duty cycles indicate that the response was not observed in the beginning 40 s. The values on the standard deviation bars represent the percentage of responding worms to the specific field conditions. The columns with no value represent the assays with all the worms responding (100% response). The average turning response time for 3 V.cm^{-1} DC electric field was 6.6±2.6 s

As can be seen in Figure 4-13, increasing the duty cycle resulted in faster response among the worms at all frequency levels, as concluded in Section 4.3.2.2. However, not all the tested animals responded to the lower duty cycles, which was more exaggeratedly pronounced at 10 Hz frequency compared to the others. As seen in Figure 4-13, at each duty cycle, the average response time increased while increasing the frequency from 1 Hz to 10 Hz. However, at higher frequencies (100 Hz and 1000 Hz eventually), the average response time showed an overall decreasing trend towards (and even faster response than) the 1 Hz results at lower duty cycles. It is worth mentioning that *C. elegans* response to DC electric field reversion was robust (100% responding) and happened quickly in 6.6±2.6 s which was chosen as a comparison point. Therefore, worms demonstrated a DC-like response at 100 Hz and higher frequencies for duty cycles more than 20%. A similar response was also observed below 100 Hz but only above 50% duty cycles. Interestingly, the response time was observed to peak at around 10 Hz for most of the duty cycles tested (Figure 4-13) which prompted further investigation.

4.3.2.5 C. elegans Turning Response Weakens at Certain Frequencies

The initial experiments revealed that *C. elegans* has the slowest response to 10 Hz pulse DC signal compared to the other frequencies. To investigate this

further, the response of worms to 5, 15 and 50 Hz frequencies was also examined. Figure 4-14 and Figure 4-15 illustrate the percentage of the worms responding in such conditions and their average response time, respectively, in comparison with lower and higher frequency levels.

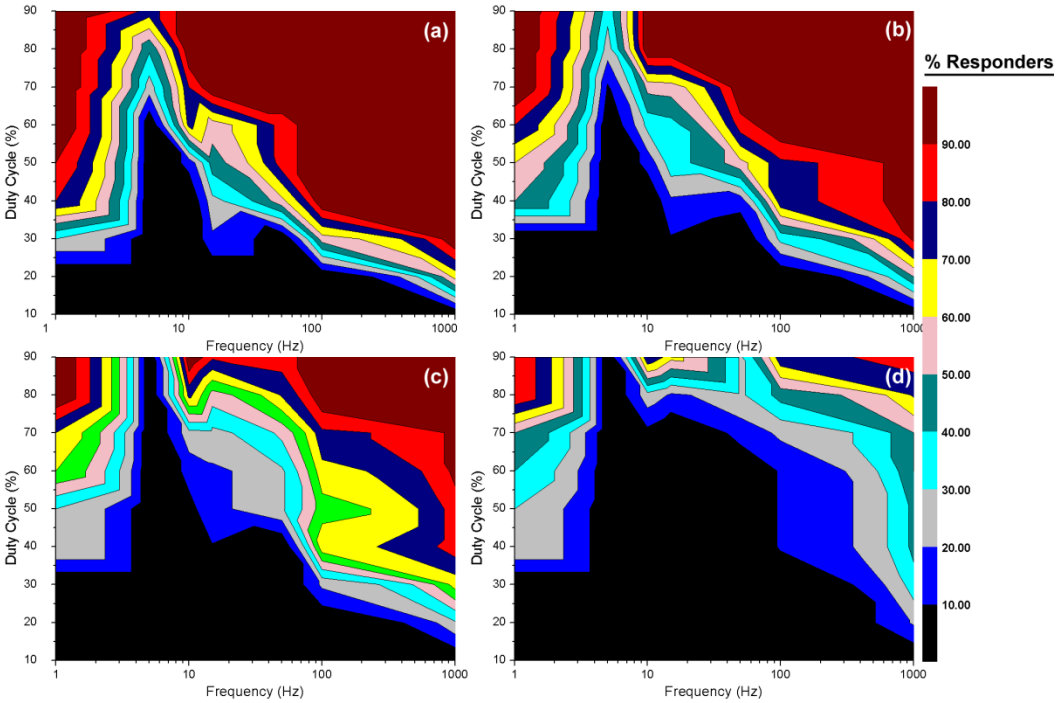

Figure 4-14 Percentage of responding worms in less than (a) 40 s, (b) 20 s, (c) 10s, and (d) 5 s, at different frequencies and duty cycles.

According to Figure 4-14, the percentage of the worms responding at each pulse DC frequency level increased again with the increase in the duty cycle from 10% to 90%. However, at a specific constant duty cycle, the highest number of worms' responded at 1 kHz frequency. The response at other frequencies was observed in the following order: 100 Hz > 50 Hz and 1 Hz (similar) > 15 Hz > 10 Hz > 5 Hz. Thus, at *f* =5 Hz, the lowest number of worms responded to the stimulus at each specific duty cycle. This means that electrotactic movement ability weakens from 1 Hz to 5 Hz frequency and then gradually strengthens when the frequency is increased from 5 Hz to 1 kHz. It can also be seen that the response becomes gradually similar to the DC electrotaxis as the frequency increases to 1 kHz (Figure 4-15). In addition, fast and robust response happens either at high frequencies with low to high duty cycles or at f ≤1 Hz but duty cycles of 50% and beyond.

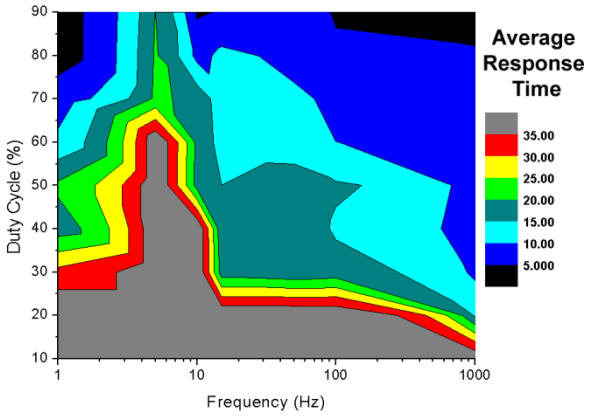

Figure 4-15 Average response time of adult worms to pulse DC electric fields at different frequencies and duty cycles

A spontaneous response was defined by response time (t_R) of less than 15s. Considering this, the pulse DC electrotaxis response was observed to be induced from duty cycles of even less than ~50% for all frequency levels except for the 5 Hz frequency and vicinities. Even at 90% duty cycle at *f*=5 Hz, less than 10% response in t_R<10 s was observed (Figure 4-14c and Figure 4-15). At *f* =5 Hz, only ~20% of the worms responded in between 10 to 20 s to 80% duty cycles (Figure 4-14b) and an additional 20% of them responded in 20-40 s (Figure 4-14a). This was at the condition that all other frequency levels at 80% duty cycle saturated to 100% worms responding (Figure 4-14) and an average response time of $\bar{t}_R$ £ 20s (Figure 4-15) to the field.

It was observed that at *f* =1 Hz and duty cycles lower than 40% most worms failed to respond to the signal and remained stationary in the channel (no response region). When the polarity of the electrodes was reversed, they were able to turn and orient their heads towards the cathode (mostly at 30% and 40% duty cycles) but did not initiate motion after that. This behaviour was also observed at *f* =10 Hz and 50% duty cycles. At *f* =1 Hz, for the worms regarded as non-responding, if the low duty cycle field was in their initial direction of motion, they continued moving towards that direction but when the field was reversed, they couldn't perform turn and move towards the opposite direction in the 40 s time window provided and were counted as non-responders. Other behaviours at 10 Hz and <50% duty cycles were frequent stops and premature turning in the channel.

Rotation response time of worms was dependent on the pulse DC signal duty cycle and frequency. The higher duty cycles resulted in a gradual increase in the proportion of the responding worms and an overall decrease over their response time and variability. It was demonstrated that the worms respond robustly to

pulse DC signals with low frequencies (f ≤1 Hz) at higher duty cycles (≥50%). Increasing the signal frequency to 5 Hz resulted in fewer worms responding to the field reversal. At this condition, increasing the duty cycle to 70% did not significantly affect the response and the average response time remained more than 20 s. However, higher frequencies resulted in an average response time reduction and higher number of the worms responding to the signal up to the point where at f =1 kHz and 30% duty cycle, more than 80% of the worms responded in less than 10 s to the field reversal. The electrosensory response time (forward-motion angle fluctuation due to electric signal modulation in frequency as mentioned before) of *C. elegans* was reported to be at a 60 ms (16 Hz) range [60]. However, this experiment was performed on an electrically non-uniform open surface (as shown in Figure 4-2), and therefore, it did not have sufficient control to measure the response time of the worm to uniform electric signals. Moreover, changes in the crawling direction (not complete reversal) of the worm, as the field rotated around it (with different frequencies), were studied in this assay. Crawling manoeuvring can be performed much more rapidly by the worm as opposed to complete reversals assayed in this thesis. However, complete reversals in a microchannel happen in binary modes (turn or no turn) as opposed to crawling direction changes on a Petri dish which can be fluctuating spatiotemporally. Behavioural pulse DC experiments in this section proved that the worms are much more sensitive (in turning) to 16 Hz frequency than a 5 Hz signal by demonstrating a faster and more robust turning towards the field direction upon its reversal.

4.3.2.6 Effect of Age on Pulse DC Electrotaxis

As described before, DC electrotaxis is mediated by amphid neuronal activity and varies with the age of animals. To investigate the effect of pulse DC on other stages, the response of L3 stage worms in the channel was tested. For this, a maximum electric field of EF_{max}=9 V/cm was used, since younger worms respond to higher electric fields (Figure 4-5) [15]. The behaviour of the worms was tested for the entire range of frequency (1-1000 Hz) at 50% duty cycle. Figure 4-16a illustrates how the L3 stage worms (N=17) responded to these electric signals. Figure 4-16b is the reproduced data at 50% duty cycle presented in Figure 4-14 for young adult worms for comparison purposes.

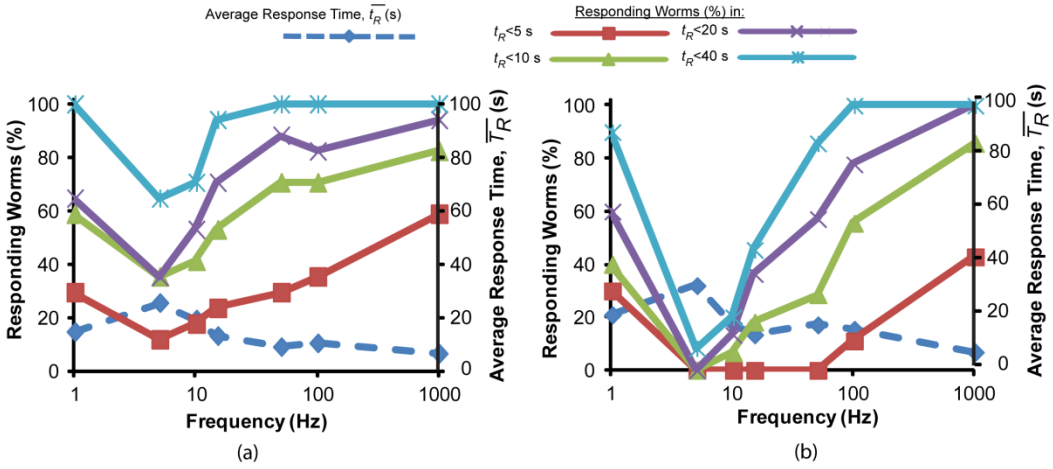

Figure 4-16 L3 (a) and young adult (b) stage C. elegans response to pulse DC electric fields (50% duty cycle) of various frequencies.

It was observed that L3 stage worms respond to pulse DC electric fields in a similar manner as young adult worms by moving towards the cathode. However, the response was more robust for L3 worms (higher number of responding worms compared to adults at all frequencies). Nevertheless, the same increase in response time and reduction in percentage of responding worms was observed at 5 Hz frequency for L3 stage worms. It has been well-established that amphid neurons are developed at the worm's L1 stage so this type of response was expected in the experiments. These results demonstrated that the worms' frequency-dependent response to pulse DC electric fields is not significantly age/stage-dependent as younger animals also showed latency in response in 5 Hz frequency vicinity.

4.3.2.7 Effect of Channel Dimensions on Pulse DC Electrotaxis

It was observed that the younger animals exhibited some electrotactic response at 5 Hz as opposed to a lack of response in the older animals (Figure 4-16). It was hypothesized that this phenomenon could have been due to the spatial constraints imposed on the older (larger) animals experimented inside the same microchannel as the younger ones. To test this possibility, the width of the channel was increased from 300 µm to 1 mm in a supplementary experiment. The response of the young adults (N=6) in this channel revealed that the worms oriented their body perpendicular to the channel axis for an extended period of time with some premature turning before reversing their direction of movement. However, the overall response of the animals was similar to what was observed previously. Thus, the response rate at 5 Hz frequency (50% duty cycle) was significantly lower and increased at lower and higher frequencies. Therefore, the channel width did not appear to be a factor in limiting the response of the worms at the 5 Hz frequency.

While the response for constant DC signal was found to be quick and similar for most worms, in the case of pulse DC signal, alterations in duty cycle and frequency affected the turning response time as well as the number of responding worms. These findings show that pulse DC method allows quantitative measurement of response behaviour of the worms. Therefore, this method has the potential to provide information about the transient response time of a population of worms to electrical signals. For instance, if the pulse duty cycle and frequency of the signal is less than that needed to evoke a neuronal response, then that signal will not be likely to affect movement even when applied for indefinite number of cycles. This suggests that the pulse DC method could be used as a tool to study the neuronal basis of such a behaviour that is not observed under constant DC conditions.

4.3.3 Correlation of Neuronal Signalling with Behavioural Response for DC and Pulse DC Signals

In section 4.3.2, it was argued that pulse DC signals can induce electrotaxis [16] in microchannels similar to DC electric fields (section 4.3.1). It was observed that the speed of movement in response to pulse DC fields is independent of frequency (1-1000 Hz) at a constant duty cycle (50%) and also independent of duty cycle (30-90%) at a constant frequency (1000 Hz). However, the same cannot be said about its turning response. It was observed that the higher duty cycles (at f=1000 Hz) resulted in faster turning time (t_R=6±2 s) and also greater number of the worms responding at a given experimental time (i.e. 5, 10, 20 and 40 s). Further experiments also demonstrated that the turning response time of *C. elegans* is highly dependent on the frequency of pulse DC signal (at fixed 50% duty cycle). This response was investigated for the adult worms and the optimized conditions were used to examine the younger stage worms (L3) to assess if the response was age-dependent. Latency in response was strongly dependent on the frequency with the worms being significantly irresponsive to pulses applied at f =5 Hz while higher and lower frequencies caused a more rapid electrotactic turning response. This phenomenon is needed to be investigated from a neuronal perspective.

The FRET-based calcium sensors (i.e. macromolecules expressing the cyan and yellow fluorescent protein at both ends), tagged to individual neurons in worms, became good candidates for probing neuronal signaling. In this section, FRET imaging technique [195] is used to demonstrate that this observation is closely correlated with neuronal Ca^{+2} transient levels and the manner they fire in response to electrical stimulations (see sections 2.2.2.3 and 3.5.2 for details). Briefly describing, FRET occurs through molecular dipole-dipole interactions, where the energy is transferred non-radiatively from one fluorescent protein, the

donor (CFP), with higher energy state to adjacent fluorescent molecule, the acceptor (YFP). Consequently, the quenched donor emission and increased acceptor fluorescent intensity can be observed [196]. The dipole interacting efficiency demonstrates strong distance dependency, thus FRET happens when the calcium binding (due to neuron signalling by Ca^{+2} release) leads to conformational changes in the sensor, which brings two proteins together.

Electrotaxis behaviour has been known to be governed by the amphid neurons (e.g. ASJ and ASH as the most dominant ones [60]) activities. FRET imaging for electrosensation studies was initially used to monitor ion transient signals in the ASH neuron in response to DC currents, as reported by Chokshi et al. [195]. Age-dependent response of the ASH neuron to DC currents has been investigated in this work. However, correlations between these neuronal activities and the actual behaviour of the animals have not been demonstrated. In this section, the FRET imaging technique has been adapted to understand the neuronal basis of the latency in turning response of the worms when stimulated with a pulse DC signal at 5 Hz. For this purpose, the animals must be immobilized and their neuronal activities measured using FRET while being exposed to the DC and pulse DC electric fields. A microfluidic '*neuronal chip*' was designed (based on the microchip reported earlier [195]) and developed to facilitate this process.

4.3.3.1 Neuronal Chip for FRET Imaging and the Experimental Setup

Experimental setup used in this assay was the same as the one discussed in DC and pulse DC experiments (section 4.3.2.1). The *neuronal chip* was developed and used for immobilization and FRET imaging of the ASH neuron upon exposing the worm to pulse DC electric fields of varying frequencies. The master mold for the *neuronal chip* was fabricated in two lithography steps using different SU8-2015 photoresist heights, as discussed in Section 3.3. The schematic of the *neuronal chip* is shown in Figure 4-17.

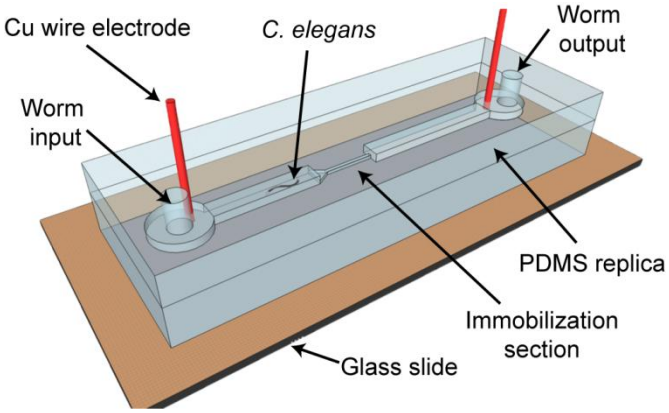

Figure 4-17 schematic of the neuronal chip used for worm immobilization and FRET imaging adapted from Chokshi et al. [195]. The main channels surrounding the immobilization section were 300 µm wide and 65 µm deep. The worm trap was 50 µm wide and 36 µm deep with the nose region narrowing down to 20 µm.

The main channels surrounding the worm trap (Figure 4-17, immobilization section) were 300 µm wide and 65 µm deep. The worm trap was 50 µm wide and 36 µm deep with the nose region narrowing down to 20 µm in order to make animal loading easier (nose region slows down the worm) and facilitate complete immobilization (channel thickness slightly thinner than the animals). Similar to the *behavioral chip*, two copper wires were inserted into the reservoirs for electric field application. The wires were connected to the amplifier and the function generator; and the FRET imaging was performed on a laser scanning confocal microscope (TSC SP5 & DMI 6000 B, Leica, Wetzlar, Germany).

4.3.3.2 Neuronal Imaging Assay

To quantify the FRET efficiency by using the *neuronal chip* (Figure 4-17), the time-lapse dual channel images of YFP and CFP fluorescence emission were collected under a laser scanning confocal microscope with a 20X dry lens. An argon ion laser emitting at 458 nm was used for CFP excitation. To match the spectra of the donor and the acceptor, the detection channels were set as 465-500 nm for CFP and 515-570 nm for YFP emission, respectively. The 62 hr synchronized worms expressing the calcium sensors were diluted and loaded into the input port of the imaging chip (Figure 4-17) manually, using a 10 ml syringe. Individual worms were immobilized inside the imaging section of the chip. A field of view (250 μm^2, 64 by 64 pixels) covering the head region (approximately $1/4^{th}$ of the body length from the head) of the worm was scanned with the laser. Electrical pulse DC signals (in the opposite head to tail direction) at fixed 50% duty cycle and various frequencies were applied after 5 seconds of illumination for another 25 seconds. All of the acquisition parameters were kept consistent throughout all repetitive measurements, which yielded simultaneous frame acquisitions of both CFP and YFP intensities every 760 ms to visualize the

trend of ratio (YFP/CFP) changes corresponding to neuronal activities. Moreover, control groups were also performed without electrical stimulation to obtain the base line of the intensity ratios without neuronal activities and to record the amount of photobleaching in YFP channel. The exponential decay component of the YFP intensity over time was then fitted using the curve fitting toolbox (Matlab, Mathworks, Natick, MA) [55].

Intensity ratios (YFP/CFP) over the 30 seconds of acquisition time were analyzed using the image processing software (Image J, v1.43m, NIH, MD). A region of interest (ROI) covering the neuronal ring of the immobilized worm was selected from a stack of time-lapse intensity images from both YFP and CFP channels. A sample image showing the field of view and the ROI is demonstrated in Figure 4-18. Background subtraction was performed for all images. Photobleaching correction was removed by subtracting the exponential decay component (control group) from the measured YFP intensity (with stimulation), followed by the ratio analysis. The fractional changes $((R_i - R_o)/R_o)$ of the intensity ratio through the electrical stimulation period were then analyzed and presented in percentage. R_i is the calculated ratio (YFP/CFP) at each time point, and R_o is the average of ratios obtained within the 5 second time period without electrical stimulation.

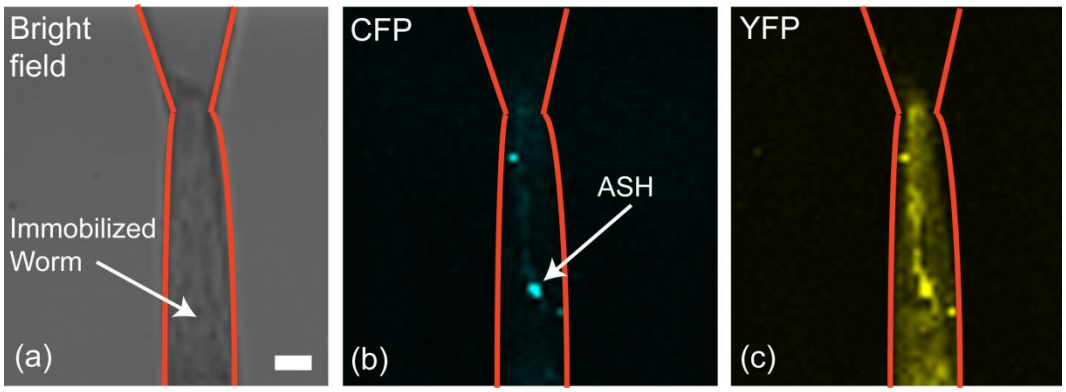

Figure 4-18 C. elegans immobilization for FRET imaging. Red lines demonstrate the boundaries of the microchannel for better visualization. (a) A brightfield image of an adult worm immobilized in the neuronal chip, Scale bar=25 µm. (b) A sample image from the CFP channel of the immobilized worm in (a). (c) Simultaneous sample image from the YFP channel. The images are 250 µm^2 in size that contain the head region and the ROI where the targeted genetically encoded ASH neuron was located.

4.3.3.3 Effect of Pulse DC Signal Frequency on ASH Neuron Activities and Its Correlation with the Behavioural Assay

The technique developed earlier by Chokshi et al [195] was employed to perform FRET imaging of the ASH neuron in immobilized worms in the *neuronal chip* shown in Figure 4-17. Three repetitive trials were done as described in the

experimental section 4.3.3.2. On each trial, N=~8 worms per frequency level were immobilized in the device (Figure 4-18) and exposed to a pulse DC electric field (voltage application at electrodes) at 50% duty cycle and various frequency levels (1, 5, 100 and 1000 Hz). After immobilizing the worm and following an initial rest (no electric field) for 5 s, a 25 s duration of pulse DC field was applied in the direction opposite to the worm's orientation (cathode being towards the tail), while continuously recording FRET images. The changes in CFP and YFP signals (at 1.43 Hz frame rate) were recorded and analyzed. FRET imaging experiments for N=8 control and N=8 DC-exposed worms were also conducted. Figure 4-19a shows FRET signals and standard errors in response to these stimulating electric signals.

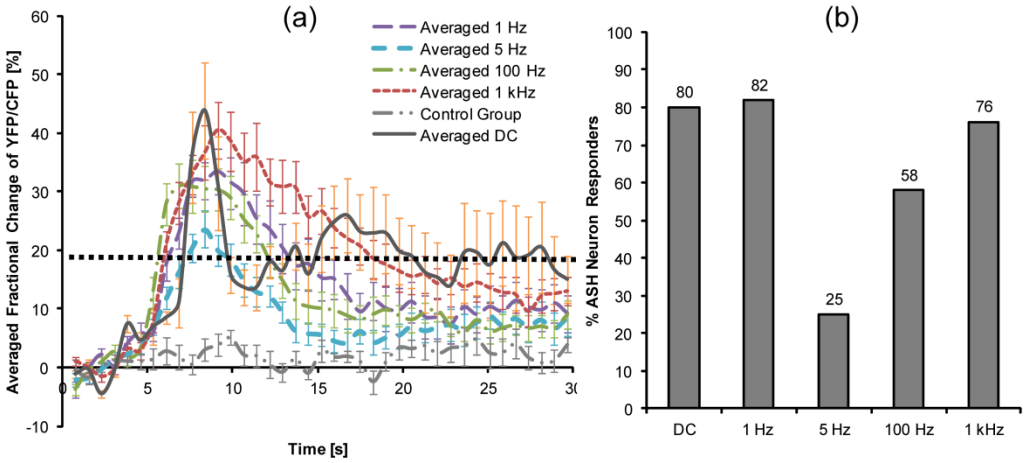

Figure 4-19 FRET imaging analysis of C. elegans ASH neuron response to DC and pulse DC electric fields of various frequencies at 50% duty cycle. (a) Fractional change of YFP/CFP intensities averaged for N=~24 worms per frequency level conducted in 3 trials. Worms were immobilized in the 'neuronal chip', FRET was initiated with no electric field applied. After 5 s, a pulse DC field with 50% duty cycle and various frequency levels (legend) was applied for another 25s. (b) Percentage of ASH neuron responders with FRET ratio higher than a cut-off value (3 times the standard deviation of the control group, dashed line in (a), which was chosen not based on any statistical principle). Values higher and lower than the cut-off were designated as ASH neuron responders and non-responders respectively.

As shown in Figure 4-19a, the worms exposed to 5 Hz frequency had the minimal YFP to CFP ratio change while the ratios were highest on other frequency levels in comparison to DC signal. This agrees well with the behavioral assays (Figure 4-14) where very few worms responded to 5 Hz frequency and had the slowest response time. In the imaging assay, it was also observed that not all the worms' neurons responded to the application of pulse DC signal. Figure 4-19b demonstrates the number of worms responding with the YFP/CFP ratio change above a certain cut-off value (3 times the standard deviation of the non-exposed control worms as depicted by a dashed line in Figure 4-19a). This

figure also demonstrates that neural response was triggered in a significantly less proportion of the worms at 5 Hz frequency as opposed to other frequencies.

In a DC condition, since the signal is continuous, the worms appear to be overly sensitive to the field with quick responses. The delayed pulse DC electrotaxis response at *f*=5 Hz suggested that this frequency of signal fails to stimulate the worms similar to other frequencies. At a neuronal level, the response of ASH amphid neuron to pulse DC signal (investigated using FRET) showed reduced neuronal activity at 5 Hz frequency signal as compared to other frequencies. This was in agreement with the behavioural assays suggesting that the electrotaxis response dependency on signal characteristics is governed and processed by neuronal activities. This method can also be used to study the role of other neurons in electrotaxis. In addition to this, the direction of electric field application (head to tail or reverse) can also be tested in the future experiments to better understand how the neurons respond to spatially variable stimulations.

4.4 Summary and Concluding Remarks

While most of the stimuli that induce movement in the worms are slow, complicated to integrate and control in microfluidic devices, and sometimes harmful to the animals, electric signals have demonstrated to be promising in overcoming such challenges and controlling the worms' movement on-demand inside microchannels. *C. elegans'* and *C. briggsae's* electrotaxis responses to DC and pulse DC electric field stimuli have been characterized comprehensively in this chapter at both behavioural and neuronal levels. Electrotactic locomotion stimulation incorporated inside the accurately controllable microfluidic environments potentially provides the necessary means for performing locomotion-based behavioural assays on a chip in a more accurate and automated manner. Additionally, since amphid neurons commonly sense electric signals, these 12 neurons can be particularly examined in terms of their response contributions by manipulating electric signals applied to the worm and monitoring the neurons activity, as demonstrated by the pulse DC behavioural experiments.

These findings demonstrate that the pulse DC signal provides a unique way to modulate the temporal exposure of the worm to electrical stimulus, resulting in a characteristic response that varies with the duty cycle and the frequency of the signal. The presented method provided the effective means to quantitatively assay the worms' electrosensory neurons activities and overall locomotory response times to various pulse DC electric field conditions by easily modulating the frequency and duty cycle of the signal and analyzing the reversal time of the worm. This was not possible with a pure DC signal, due to its continuous application manner and worms being over-sensitive to it. The pulse DC method

could also be more useful to study subtle changes in the responses of the worm to environmental and chemical influences as compared to constant DC electrotaxis. In addition, the use of pulse DC signals reduces the exposure time of the worms to electric signals by up to 70%, yet generating a response similar to constant DC fields. This should benefit the experiments where it is desirable to minimize the worms' exposure to the electric field. The methods and platforms introduced in this section can easily be used to examine the electrotaxis behaviour of various nematode species to a diverse range of electric signals such as sinusoidal and triangular waves with DC offsets.

Unlike previously described pneumatic microdevices that rely on forced liquid flow to move the worms, the use of electric field stimulus in assays appears to induce a precise and sensitive innate movement response. Therefore, it could be potentially used in the movement-based behavioural HTS assays for drugs/chemicals in a microfluidic format. For example, a combination of null mutations in dystrophin (*dys-1*) and MyoD (*hlh-1*) genes in *C. elegans* has been shown to cause progressive muscle degeneration similar to human DMD (Duchenne's muscular dystrophy) that impairs movement [4, 72, 197]. The electric field-based microfluidic channel may facilitate HTS of drugs that improve/restore movement, thereby, identifying potential candidates to test in human DMD patients.

CHAPTER 5

5. Micro-Electro-Fluidic Devices to Perform Unit Operations on *C. elegans*

5.1 Introduction[§]

Thus far, electrotaxis method has been developed and characterized as a tool for screening nematodes' movement behaviour and neuronal signaling quantitatively. There is a significant potential in utilizing electrotaxis- and electric-based microchips in the worm assays at both behavioural and neuronal screening levels. This includes assays involving screening for various neurotoxin chemicals, environmental pollutants and toxicology, drug discovery and genetic studies of electrotaxis. Many of these assays require high throughput suggesting that there is a need for the development of high-throughput microfluidic chemical screening system for nematodes' automated behavioural assays (using electrotactic movement phenotypic screening), such as the one discussed in chapter 2 (Figure 2-9). However, in order to realize this system, multiple components performing individual unit operations should be developed first. These components should be able to sort the animals based on their size/age, manipulate them inside microdevices, compartmentalize them inside chambers, expose them controllably to chemicals, immobilize them for imaging and

[§] Contents of this section have been collected from published article (with permission):

- Rezai, P., et al., *Electrical sorting of Caenorhabditis elegans.* Lab Chip, 2012. **12**: p. 1831-1840

automatically and quantitatively measure their movement behaviour electrotactically. Some of these components are developed in this chapter. Since electric-based actuation and sensing techniques can be multiplexed, parallelization of these techniques on a chip and eventual high throughput behavioural screening can be made possible through incorporation of the electric stimulus. In a similar vein, this chapter mostly focuses on the development of electric-based unit operation components, such as the sorter, position detector, movement inhibitor and finally the immobilizer unit.

Many of the worm-based assays as mentioned above require a large population of synchronized worms to be screened in a fast and quantitative manner. However, *C. elegans* worms are difficult to manipulate manually due to their small size as well as their inherent voluntary locomotion. Sorting the worms into synchronized stages is currently performed by manual or robotic methods, which are either slow, labour-intensive and time-consuming or expensive and inaccessible to the majority of researchers. They also lack the ability to sort the worms based on behavioural phenotype (locomotion). Additionally, they do not integrate well with microfluidic-based devices that automate the worm handling and analysis. Since electric fields were demonstrated to induce movement behaviour in a stage-specific manner, their application to sort animals behaviourally will be investigated in this chapter.

After acquiring a homogeneous (in size and behaviour) population of the worms by electrotactic sorting, it is required to manipulate and compartmentalize them for chemical exposure (exposure and culture module, Figure 2-9). Since these processes will be performed pneumatically (non-electrical) in this research, they will be discussed in Chapter 6, where the integrated drug-screening system is designed and developed. After exposure to chemicals, the worms should be screened both at the behavioural and cellular levels. This means that one should be able to analyze the worms' movement and also immobilize them for the purpose of cellular-resolution imaging. These processes are required at the characterization module of the integrated screening system (Figure 2-9).

To analyze the worm movement, electrotaxis method introduced in Chapter 4 is promising as compared to other stimulus-based movement screening methods. It is because, this method is very sensitive, distinct between developmental stages, quantitatively measurable, easy to control and apply and not harmful to the worms. Most of the movement quantification methods are however based on video recording and post-experimental image analysis. These methods are not suited for HTS of multiple worms in a multiplexed microchip with hundreds to thousands of screening units. There is a need for a method to analyze the movement on the chip in a high throughput manner. Various sensing techniques for detecting and quantifying cells and particles have been developed in the

literature. These methods will be investigated for sensing worms inside microchannels.

It is also important to localize and position the worm for certain operations such as for chemical exposure or for assays. Non-pneumatic methods for such positioning would be useful as they are scalable. Use of specialized electrical signals to localize and position the worm at appropriate locations will also be investigated in this chapter.

While the abovementioned advancements are required for on-chip movement behavioural assays, conventional fluorescent-based cellular/neuronal imaging is also needed to complement the information obtained from behavioural assays such as the chemical screening system in this thesis. While most of the immobilization methods (discussed in Section 2.5.4) are either irreversible (chemical) or complex to implement (micromechanical), there is a need for the development of an easy-to-operate, simple, reversible, touch-less and spatially not limited method to immobilize worms. Electrical signals again offer these advantages and will be investigated for on-chip non-mechanical animal immobilization.

In the rest of this chapter, the components introduced in this section (sorter, detector, localizer and immobilizer) will be designed, experimentally developed and tested on the worm models.

5.2 Sorting

C. elegans develops through 4 larval stages (L1–L4) in 2 to 3 days before becoming a young adult with a full length of ~1 mm and diameter of ~80 µm. As mentioned previously, biological screening assays involving *C. elegans* frequently require a large number of the animals. To attain an acceptable level of statistical accuracy in large-scale screening experiments, it is necessary that all the animals are of the same stage so that age-related variations can be minimized. The most commonly used manual method to age-sort the animals involves sacrificing gravid hermaphrodites by exposing them to a solution containing sodium hypochlorite (commercial bleach) while retaining the eggs intact. The isolated eggs are then grown to obtain a synchronized sample. Despite its abundant usage, this method is time-consuming, tedious and labour-intensive. The high-throughput robotic fluid handling systems, such as biosorter (Complex Object Parametric Analyzer and Sorter, COPAS, Union Biometrica; http://www.unionbiometrica.com), have also been used to obtain large populations of the synchronized worms [107]. But as discussed in Section 2.4.2, such systems are quite expensive, require active image-based feedback for sorting and are not useful in certain types of experiments. For example, they lack

the ability to sort the worms based on their locomotion behaviour. Additionally, they do not integrate well with microfluidic-based devices to automate the worm handling and analysis. More sophisticated microfluidic devices in terms of fabrication (multi-layers of PDMS microstructures aligned and bonded together) and operation (computer-controlled pneumatics) have also been developed which have revolutionized a diverse range of conventional assays on worms in terms of automation and throughput (see Section 2.5). However, most of these existing microfluidic pneumatic-based chips are also not ideal for behavioural studies involving locomotion induced by stimuli and subsequent characterization of that motion. Hence, sorting the worms based on their size or behavioural response to stimulated signals is not achievable with them. A method to synchronize the animals behaviourally, phenotypically and without sacrificing them can significantly enable the implementation of high throughput worm-based assays. Electrotaxis could potentially be used for this purpose.

While the precise mechanism of electrotaxis remains to be understood, the worms of specific ages respond to specific DC electric field ranges (Figure 4-5) and exhibit paralysis above a certain electric field (termed upper threshold) and are unable to move, as discussed in Chapter 4. The worms also fail to respond to the electric field below a certain limit (termed lower threshold) and continue to swim in random patterns in its presence. The range of response is lower for the older animals, as they are more sensitive to the electric field. This could be due to the fact that the bodies of the younger worms have higher electrical resistances compared to the older animals (when modelled as cylinders with characteristic length and diameter for age); therefore higher electrical potential gradient is needed to impose a comparable stimulus across their body to induce an electrotaxis response. This phenomenon has been used in this section to design and develop the first microfluidic behavioural sorter device that can sort the worms based on their age (YA from L3 or L4), sensitivity to electric field (YA from old adult) and phenotype (YA from muscular or neuronal mutants) in a passive manner and without a throughput limit.

Development, growth and synchronization of the animals have been described in details in Chapter 3. The strains used in this chapter are: N2, BC347 unc-54(s74), CB78 unc-6(e78), and VH17 (genotype: *ast-1(rh300) II, rhIs4 III*). The synchronized worms were used in all the experiments. The synchronized worms were transported in buffer M9 solution for all assays; however, immediately prior to loading the worms into the device, the M9 solution was replaced with deionised (DI) water by centrifuging.

5.2.1 Electric Field Traps for Manipulating Worms in Microchannels

As discussed earlier, electric fields above the maximum threshold limit for each developmental stage can paralyze the worms momentarily in a microchannel. This concept can be used to design electrical traps in a channel that have stronger electric fields than the rest of the channel, as discussed in section 3.1.2. Schematic of the device design is illustrated in Figure 5-1.

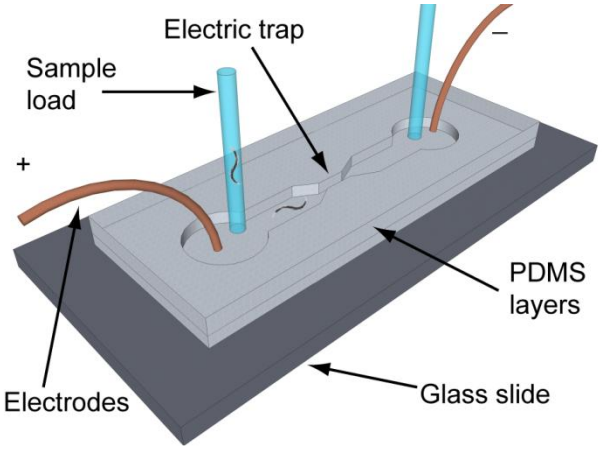

Figure 5-1 Microfluidic-based electric trap device for worm electrotactic manipulation main channel width: 300 µm, length: 30 mm, depth: 100 µm; narrow section width: 100 µm, length: 3 mm, depth: 100 µm; electrodes final distance 28 mm. [21] Reproduced by the Permission of the Royal Society of Chemistry 2012

The microfluidic channel shown in Figure 5-1 is electrically analogous to a network of resistances (see Figure 3-1). It consists of sections of different widths that can be represented by electric resistances connected in series. According to Eq. 3-2, for each section, the electric resistance is directly proportional to the length and inversely proportional to the cross-sectional area. A potential applied across the entire microchannel gets distributed in proportion to the sections' resistances. The higher the electrical resistance of the channel, the higher the potential drop (*V*), and the electric field (*EF*) is across that section. The ratio between the electric fields of two microchannels of the same height arranged in series is inversely proportional to their width (*w*) ratio, as calculated by using Eq. 3-3.

$$EF_{narrow}/EF_{wide} = w_{wide}/w_{narrow} \qquad 5\text{-}1$$

5.2.1.1 Fabrication of the Electric Trap Device

The electric trap device shown in Figure 5-1 was fabricated using soft lithography techniques [176] with two platinum electrodes (100 µm diameter, Sigma Aldrich, MO, USA) embedded at its reservoirs, as described in Chapter 3.

The electrodes were connected to a DC power supply to stimulate the required voltages and hence the electric fields across the channels (experimental setup previously described in Section 3.4).

The electric trap device consisted of a single main microchannel (300 µm wide and 30 mm long in total) which gradually narrowed down at the centre (called the electric trap, *ET*) to a 100 µm width and a length of 3 mm. The distance between the electrodes after fabrication was 28 mm. Using the design principle, described above and Eq. 5-1, the electric trap neck region in Figure 5-1 was 3 times narrower than the main channel; and therefore, the electric field in the trap was enhanced by 3 times as compared to the electric field in the wider sections for each applied voltage across the main microchannel.

5.2.1.2 Experiments using the Electric Trap Device

For experiments using the electric trap device (Figure 5-1), the possibility of electrotactic trapping of the worms of various stages at the narrowing entrance region of the channel at different electric fields was investigated. The synchronized wild-type N2 animals of various ages (N=10 each) were delivered from a sample suspension into the channel by applying suction at the outlet reservoir using a syringe pump and dipping the inlet tube into the worm suspension, as discussed in Section 3.4.1. The worms were positioned in the wide section of the channel and all pneumatic flows were eliminated before the electric stimulation. A constant electric field was applied across the axial direction of the channel and the electrotactic response of the worms towards the narrow section was recorded using a camera. The videos were analyzed using the ImageJ software to quantify the electrotactic movement as described earlier. Three different criteria were investigated: (i) the electric field required in the wide section to initiate electrotaxis, (ii) the electric field at which the worm started to demonstrate paralysis effects (tail coil and loss of control) in the wide section, but was still able to move towards the electric trap, and (iii) the electric field in the electric trap section, which inhibited the worm from entering this section.

5.2.1.3 Worm Response Characterization in the Electric Trap Device

The electric trap device, depicted in Figure 5-1, was designed to exploit the selectivity of the DC electrotactic response of different sizes (and ages) of animals in a batch format (Figure 5-2a). Applying a potential to the device (Figure 5-2a) causes different electric fields in the wide and narrow sections (electric trap) of the microchannel (see Sections 3.1.2 and 5.2.1 for detailed information). The local electric field is higher inside the electric trap and lower in the wide section; and their ratio can be set inversely by the ratio of their widths (1:3 in this device).

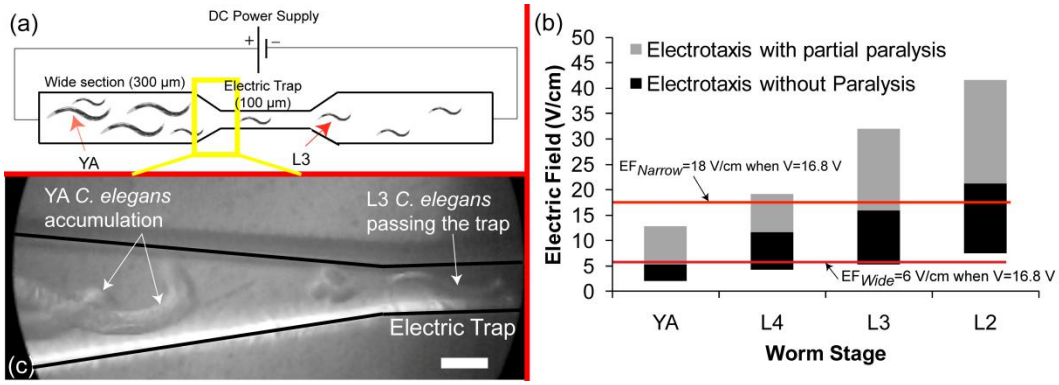

Figure 5-2 C. elegans single electric trap (ET) device, (a) single electric trap by narrowing the channel at the centre for local electric field enhancement (channel widths mentioned in the parentheses), (b) electric field ranges for electrotaxis with no paralysis in the wide section (black columns) and inhibitory trap electric fields (gray columns upper limit) preventing worms from entering the narrow section. The gray columns cover the region of partially paralyzed worms, still demonstrating electrotaxis in the wide section. Scale bar = 100 mm (c) L3 worms separated from YA worms using a 16.8 V potential across the channel generating electric fields demonstrated with red lines in (b). [21] Reproduced by the Permission of the Royal Society of Chemistry 2012

Experiments were conducted on the worms individually loaded in the device (N=10, ranging from L2 to YA) and behaviour of the animals was characterized in a complex electric field landscape. Potentials from 0 V to 40 V were applied. Based on the responses, a minimum voltage (required to initiate electrotaxis) and a maximum voltage (after which partial paralysis initiates) required for the electrotaxis of the worms in the wide section of the channel were identified. Voltages applied across the channel that inhibited each stage from swimming across the electric trap of the channel, were also identified. The electric field distribution inside different sections of the microchannel was simulated in COMSOL Multiphysics software for each of the critical voltage thresholds that were obtained experimentally. It was found that there is a range of electric fields in the wide section (black column in Figure 5-2b) that could induce electrotactic movement of the worms towards the narrow section. This range differed depending on the stage of the worm. The electric field inside the electric trap section was however always 3-fold higher than the wide section. When the electric field in the narrow section was in the range of the gray column region (Figure 5-2b), the worms were partially paralyzed while attempting to enter that section. However, it was observed that above the higher threshold of the gray column, the worms avoided entering the trap section - stopped their forward motion and turned back. This threshold electric field in the narrow region, which the worms instinctively avoided, also varied with their age. To test the age-based sorting in this device configuration, a 16.8 V potential was applied across the channel, which contained a mixed population of L3 and YA animals. The applied potential resulted in ~6 $V.cm^{-1}$ and ~18 $V.cm^{-1}$ electric fields in the wide and the narrow sections, respectively. The electric field in the wide section was sufficient

enough to induce electrotaxis for both L3 and YA animals (Figure 5-2b) towards the narrow section. However, the electric field in the trap was sufficiently high to induce full paralysis for YA, but not for the L3 stage, if they entered this section. The YAs that intended to enter the narrow section quickly appeared to sense the higher electric field, because they retreated back to the wider section while the L3 stage worms (less sensitive to electric field) continued to move inside the narrow section towards the cathode at the other end. This behaviour led to the separation of L3 worms (passed through the trap) from YAs (accumulated at the entrance region of the trap), as illustrated in Figure 5-2c. In a 2-4 min time duration of testing that included a mixed population of L3-YA (1:1 ratio, N=10 each), all L3 stage worms were observed to traverse the trap; whereas, YAs were electrically confined at the mouth of the trap. The population at the other side of the trap was 100% L3 and 0% YA. Simple calculations (power dissipation and heat generation) showed that heat generation was not significant to induce the avoidance behaviour in the narrow section (See Appendix B). Although this device enabled age-based sorting of worms and provided information about the threshold electric field for sorting, it could not be used in a continuous mode due to the accumulation of the trapped worms at the entrance region of the narrow section leading to eventual clogging and loss of control over time. Additionally, extracting the separated samples from the device was not convenient in this format. Therefore, the results obtained from these experiments were utilized to design a new continuous sorting device.

5.2.2 Continuous Behavioural Sorting Device

Based on the results obtained (Figure 5-2) from the single channel electric trap in Figure 5-1, the sorter device in Figure 5-3 was designed consisting of 20 parallel electric traps (100 µm wide, 500 µm long each) connecting two chambers (8 mm by 1.5 mm) at both ends. These dimensions were selected in order to fit the entire operational sections of the device (chambers and traps) under the microscope in a single field of view.

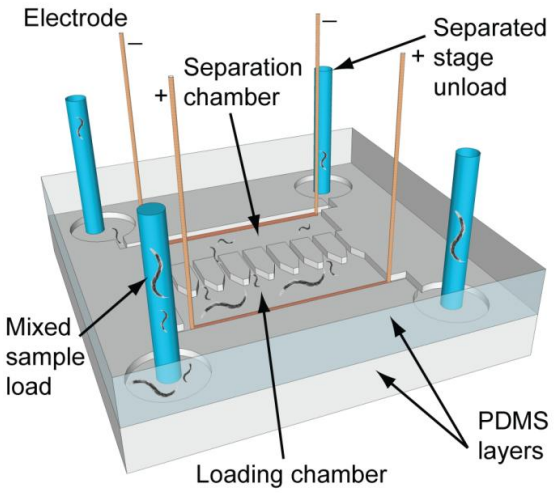

Figure 5-3 Continuous electrotactic sorter using the electric trap concept, Depth: 100 µm; Chambers: 8 mm×1.5 mm, Traps: 100 µm×500 µm, n = 20, pitch = 400 µm. [21] Reproduced by the Permission of the Royal Society of Chemistry 2012

As discussed in Chapter 3, the device can be modelled as a simplified electrical circuit of resistances arranged in series and parallel, as illustrated in Figure 5-4. The loading and separation chambers were modelled as R_1 resistors arranged in series with each electric trap (parallel together, R_2).

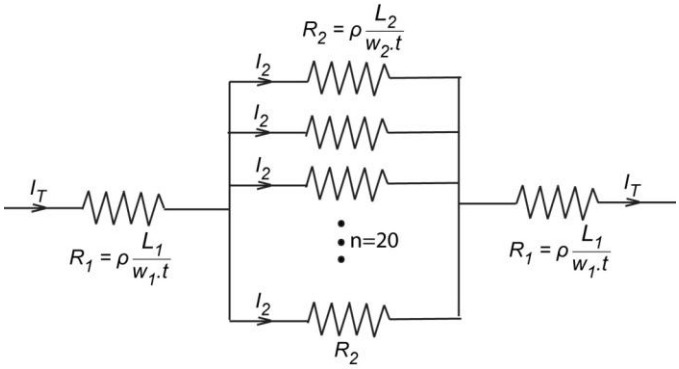

Figure 5-4 Electric analogous diagram of the continuous sorting device. R_1 and R_2 represent the chambers and individual traps electrical resistances respectively. $w_{chamber}=w_1=8$ mm, $w_{trap}=w_2=0.1$ mm [21]. Reproduced by the Permission of the Royal Society of Chemistry 2012

According to Eq. 3-3, the electric field for each chamber (EF_1) and trap (EF_2) is:

$$EF_1 = \frac{\rho I_T}{w_{chamber}.t} \qquad 5\text{-}2$$

$$EF_2 = \frac{\rho \frac{I_T}{n}}{w_{trap}.t}$$

Therefore, the ratio between the electric fields inside these two environments is:

$$\frac{EF_2}{EF_1} = \frac{w_{chamber}}{nw_{trap}} = \frac{8mm}{20 \times 0.1mm} = 4 \qquad 5\text{-}3$$

In the new design, as shown in Figure 5-3, parallel electric traps (n=20 with a pitch of 400 µm) of the same width (100 µm), but shorter in length (500 µm), were used to connect the loading and the separation chambers. Platinum wires (100 µm diameter) at the anterior region of the chambers, running across the device perpendicular to the axis of the electric traps (see Chapter 3 for fabrication method), were used to apply uniform electric fields inside all traps. In order to verify the electric fields acquired theoretically (Eq. 5-3) in the device at different applied voltages and assess its degree of uniformity, a 2D model of the device was simulated in COMSOL Multiphysics. The electric field distribution resulted from different potentials applied between the electrodes is shown in Figure 5-5. The electric field in each trap was 4 fold higher than the electric field in the chambers (as confirmed by theoretical design above). Simulation results confirmed that fairly uniform electric fields could be obtained across the device in the chambers with less than 1.5% field strength variation from the sidewalls of the chamber to the central region.

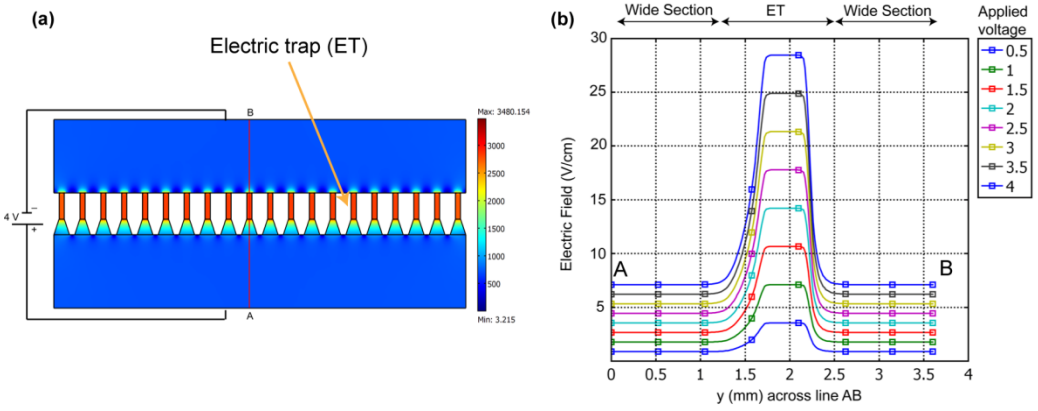

Figure 5-5 COMSOL Multiphysics simulation of the continuous sorting device. (a) Normal electric field distribution (V. m^{-1}) across the channel (colour contour) by applying a 4 V potential between the bottom and the top boundaries. (b) Electric fields across line AB in (a) by applying various voltages between the bottom and the top boundaries. All other surrounding and internal boundaries were set to electrical isolation and continuity, respectively. [21] Reproduced by the Permission of the Royal Society of Chemistry 2012

5.2.2.1 Experiments Using the Continuous Sorter

To prepare the sorting device for experimentation, it was placed under the microscope and filled with DI water, using a syringe pump connected to the

sample loading tube (Figure 5-3). After filling the chambers and all outlet tubes with DI water, the three other outlet tubes were sealed using cap interconnects and the flow rate in the pump was reduced to $0.1ml.h^{-1}$ in order to eject the trapped bubbles from the device through the porous gas permeable structure of PDMS. When all the bubbles were ejected, the syringe was disconnected and the caps were removed. All 4 tubes were then levelled at the same height in order to eliminate all the pressure-driven flows.

After completely filling the device with liquid media, two sets of loading methods were used - one for individual worm behavioural studies and one for sorting. Details of the loading methods are presented in Appendix CB. Briefly, in order to study the individual worms' behaviour in the chamber, the synchronized animals were prepared and diluted in a similar manner described in Chapter 3. The worms were loaded into the inlet tube of the device (n=5-10 at a time) and introduced into the loading chamber by using a manual hydraulic flow. A constant electric field ($\sim$1-7 $V.cm^{-1}$ in the chambers) was then applied from the loading chamber electrode towards the parallel electric traps and the separation chamber electrode, as illustrated in Figure 5-3. A video was recorded under the microscope and used later to analyze the worms' behaviour. The parameter studied here was the number of the worms attempting to move towards the separation chamber through the electric traps. An attempt was defined as an individual worm inserting one-third of its body length into the narrowing section of the electric trap.

A second loading method was used to characterize the sorting capability of the device. Populations of the wild type N2 worms (L3 or L4 stages) mixed with wild type N2 YAs; or OAs, the muscular and neuronal mutants mixed with YAs of GFP expressing the control animals (VH17) in a one-to-one ratio were introduced into the loading chamber of the device (see AppendixC). VH17 animals exhibit electrotactic movement and appear similar to the wild type in terms of growth, fecundity, and activity on NG agar plates. They were used in conditions where the mixed worms were not distinguishable from their size (e.g. YAs mixed with OAs or YA mutants mixed with YA wild types). When the loading chamber was filled with the worms, appropriate electric fields (based on the results (Figure 5-2) from the device in Figure 5-1) were applied across the device from the loading chamber towards the separation chamber and videos of the sorting process were recorded again. In this assay, the number of the worms attempting to pass (described earlier) and the number of them capable of passing through the electric traps was counted for each loaded worm stage at each applied electric field. After a few minutes, it was noticed that the rate at which the worms were crossing the trap reduced, indicating that sorting has occurred for this batch. At this stage, additional worms were loaded into the chamber while washing off the

sorted animals to the outlet tubes (semi-continuous operation). This was continued until all the loaded worms were sorted.

After sorting, the worms of different stages were counted based on their size and separation efficiency was calculated. In the case of OAs, neuronal or muscular mutants (mixed with VH17 animals), the sorted animals were collected from the separation chamber, transferred to a plate, and the number of GFP and non-GFP animals was counted under the fluorescent microscope.

5.2.2.2 Worms Behavioural Assay in the Continuous Sorter

The single microchannel with a narrowing trap (Figure 5-1) at the centre ensured that the worms could only move either along or against the electric field. However, the new design (Figure 5-3) allowed motion perpendicular to the field and hence the behaviour at the traps could potentially be different from that observed before. Therefore, a set of experiments were conducted to study individual worm's behaviour in the absence and presence of a desirable electric field in these chambers. Accordingly, in the first experiment, N=10 YA animals were introduced into the loading chamber with no electric field applied across the traps. After 10 minutes, only one of the worms was observed passing through the traps into the separation chamber. This demonstrated that, naturally, the worms have a preference to reside in the loading chamber in the absence of a stimulus. Next, the synchronized YA, L4, and L3 worms (N>100 each) at a low concentration were loaded into the chamber in a continuous manner (between 5 and 10 at a time, as described in the Section 5.2.2.1) and electric fields (in their DC electrotaxis range of response inside the chamber) were applied towards the separation chamber in order to study individual stages' response. Figure 5-6 shows the percentage of the worms (of the total present in the loading chamber) of different ages making an attempt to enter the electric traps when exposed to the electric field. The applied electric fields were in the electrotactic response ranges of those particular stages of the worms. Since the worms were not constrained to move in the direction of the electric field, not all of them attempted to move into the trap regions. Some moved laterally in the chamber; whereas, others (closer to the positive electrode) experienced minimal non-fatal movement difficulties (see Appendix D) during the electric field application. The percentage of the worms attempting an entry increased for the older animals as these are more sensitive to the electric field and respond more robustly [15].

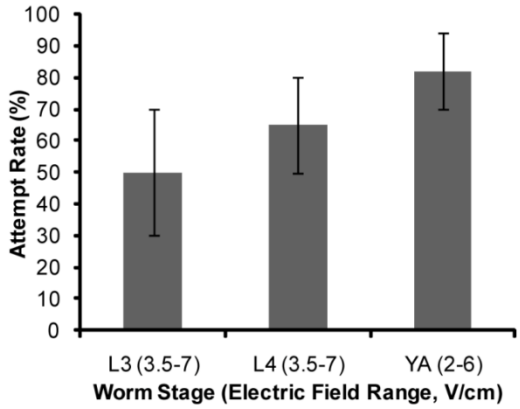

Figure 5-6 Attempt rate for different C. elegans stages to enter the electric traps under electric field exposure. Values inside the parentheses on the x axis are the electric field ranges used for this assay. [21] Reproduced by the Permission of the Royal Society of Chemistry 2012

5.2.2.3 Stage-Based Electrotactic Sorting

As described in the Section 5.2.2.1, the worms of two different developmental stages, readily distinguishable by size (i.e. YA and L3 or YA and L4), were mixed (1:1 ratio) in a highly populated concentration after synchronization and loaded into the device. Based on the results in Figure 5-2b, electric fields of ~3 $V.cm^{-1}$ and higher were needed to initiate electrotaxis in these worms. Therefore, the sorting device was tested in the 2-4 V potential range, which produced an electric field of 3.5-7 $V.cm^{-1}$ in the loading chamber (obtained through simulations in Figure 5-5). The number of attempts that the worms made for entering the electric traps as well as the number of successful passages through the traps towards the separation chamber was counted for each developmental stage of *C. elegans*. The percentage of the worms (out of the attempted ones) passing through the trap is shown in Figure 5-7a and b for YA-L4 and YA-L3 with the sorting experiments, each repeated 3 times. A throughput of 78 sorted worms per minute per load-run was observed in these experiments. The throughput is expected to be higher, if the device was run in a semi-continuous manner (i.e., loading the worms frequently without stopping the operation) or another sorting device was designed with higher loading capacity.

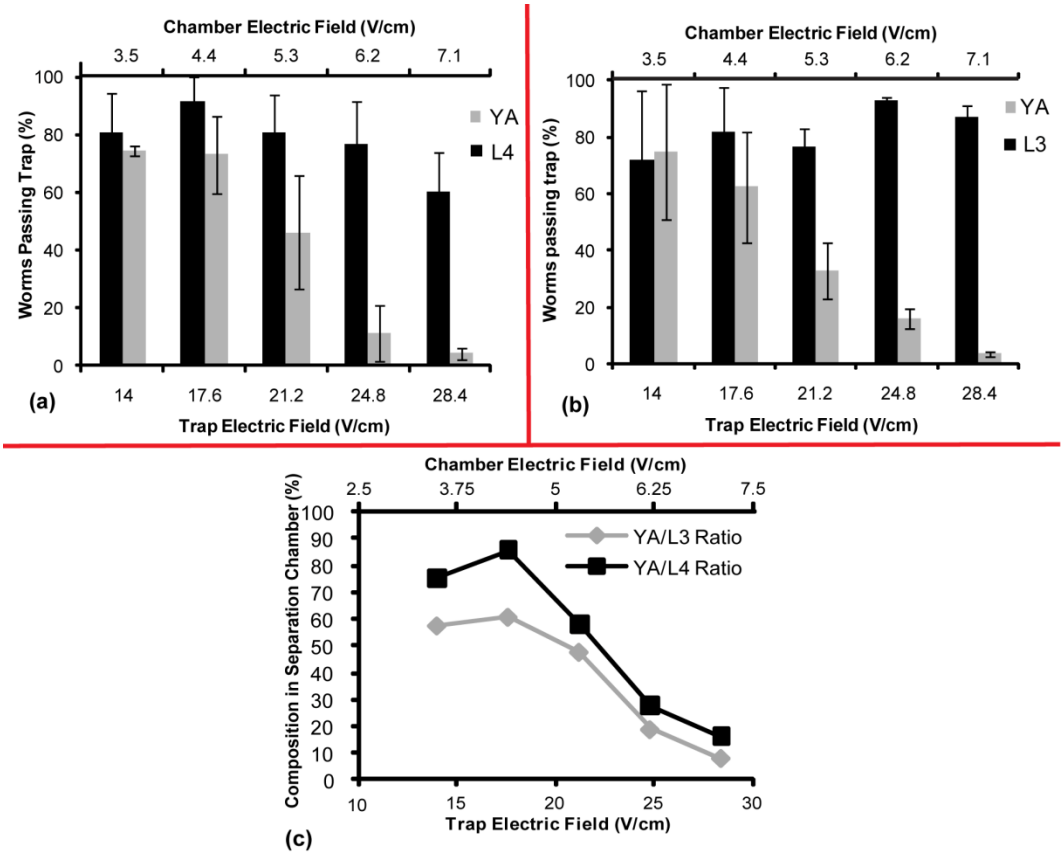

Figure 5-7 Electrotactic behaviour and sorting of mixed (1:1 ratio) samples of (a) YA-L4 and (b) YA-L3 in the sorting device. The x axis values show the applied electric field across the chamber (secondary x axis) as well as the induced electric field inside the electric traps (primary x axis). (c) Composition of YA-L4 and YA-L3 worms in the separation chamber after the sorting experiments. [21] Reproduced by the Permission of the Royal Society of Chemistry 2012

It can be seen in Figure 5-7 that more than 65% of the YA worms that attempted to enter, passed the electric field traps while the field in the trap region was 14 V.cm^{-1} or less. However, upon increasing the trap field strength, the percentage of the YA worms traversing through the trap dropped quite significantly to under 5% at 28.4 V.cm^{-1}. However, this increase in the electric field across the trap did not significantly affect the percentage of the L3 and L4 worms passing through; and they remained consistently above 70%. Between the L3 and L4 stages, the L3 had a higher percentage passing through (~90%) at 28.4 V.cm^{-1} trap electric field as compared to the L4 (~60%). The population composition of the worms that passed through the electric traps and arrived at the separation chamber at different electric fields for both these sets of experiments (i.e. YA-L4 and YA-L3) is shown in Figure 5-7c. As expected, at lower electric fields, the population in the separation chamber (output) is skewed towards the YA (80–90% YA), while at the high trap electric field, the population is skewed towards the L4 and L3 stages (less than 20% YA). This change in the

composition with electric field can be explained based on the results obtained in the earlier experiments with the single-trap channel (Figure 5-2b). The YA worms are the most sensitive and have a smaller electric field range (black column in Figure 5-2b) over which they move normally. They are followed by the L4 worms and the L3 worms move normally over a wider range of electric field and; therefore, are the least sensitive to high electric fields. Thus, higher electric fields in the trap region, that were imposed in the device, inhibited the YAs the most (<5% pass through) followed by the L4 stage (~60% pass through), and had virtually no effect on the L3 stage. Moreover, the L4 stages could be more effectively separated (80%) from the YAs at 24.8 $V.cm^{-1}$ trap electric field. Separating the L3s from the YAs was most optimally done at 28.4 $V.cm^{-1}$ trap electric field. It should be noted that the critical electric field needed to inhibit the worm movement for a particular stage was on average higher than the ones obtained in single-trap experiments (Figure 5-2b) for almost all the tested stages. This may be due to the shorter length (500 µm, 80% shorter) of the electric traps in the sorter device and less exposure time of the worm to this high strength field while attempting to pass.

5.2.2.4 Post-Sorting Chemotaxis and Lifespan Assays

It was shown in Chapter 4 that the electric field has no obvious detrimental effect on the movement and the reproduction of the worms [15]. In the current study, two additional experiments (lifespan and chemotaxis after sorting the worms in the device) were performed that further supported these observations.

Chemotaxis assay was performed, as described earlier [51] and also in Section 3.4.4. Chemotaxis assay plates were prepared accordingly. Each chemotaxis plate was divided into 4 quadrants with a marker. 10 µl of NaCl and 10 µl of water were spotted 2 cm apart from the centre of the plate on the opposite sides. Electrotaxis-based (EF = 8 $V.cm^{-1}$, I=80 µA, t=~2 min exposure) sorted worms (total of 166 young adults) were allowed to recover for 4 hrs on NGM plates, seeded with OP50. Control groups (N=176 young adults) were solely passed through the sorter with no electric field applied. These worms were then washed with nanopure water twice and again with ice-chilled nanopure water. The worms were placed at the centre of the chemotaxis plate. After 1 hr, the worms within 2.5 cm from the water and NaCl spots were counted. The chemotaxis index (CI) was calculated using Eq. 3-5.

For the lifespan assay [180, 181], sorted young adults (n=19) were placed on OP50 bacterial containing NG-agar plates. The animals were observed for 8 consecutive days and their survival rate was determined. A total of 15 unexposed worms were used as a control.

First, the chemotaxis response of the sorted animals to *NaCl* was tested. It was found that the sorted worms were comparable to the untreated control animals of a similar age (Figure 5-8a). Second, a lifespan assay [180, 181] was carried out and it was found to be similar to the lifespan of the control animals (Figure 5-8b). Together, these experiments demonstrated that the worms sorted by electric field in these devices could be used in a wide range of assays.

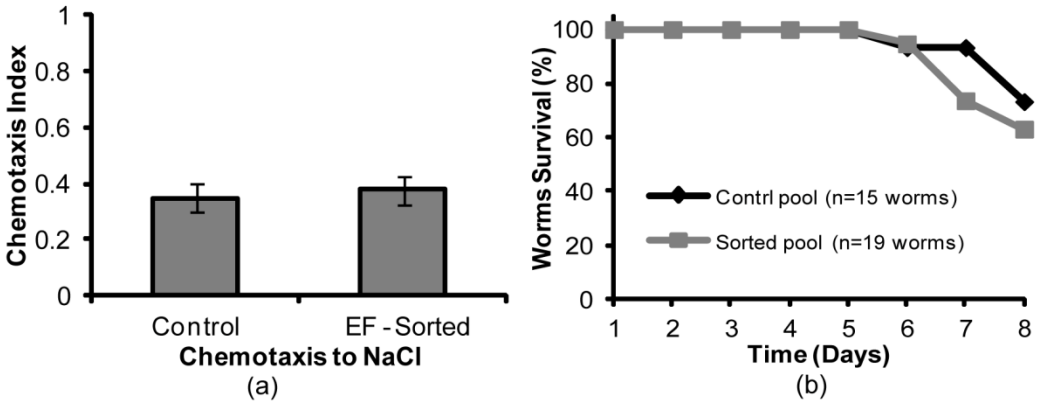

Figure 5-8 (a) Chemotaxis response of sorted and control worms for NaCl attractant and (b) lifespan analysis. Total number of worms was (a) n=166 sorted and n=176 control; (b) n=19 sorted and n=15 control animals. [21] Reproduced by the Permission of the Royal Society of Chemistry 2012

5.2.2.5 Electrotactic Sorting of Mutants

The method described in this subsection can also be used to sort the electrotaxis defective worms (e.g., neuronal or muscular mutants) from the healthy animals with potential application in mutant and genetic screening. It has been reported earlier that mutants of various types [15, 18, 60] show abnormal electrotactic responses. Two kinds of mutants, *unc-54(s74)* (muscle defective) and *unc-6(e78)* (abnormal neuronal differentiation), that were mixed with GFP expressing control animals (VH17, see Chapter 33 and Section 5.2.1 for details) in a 1:1 ratio, were used. The sorting process was conducted in two batches for more than 50 worms per batch at a certain electric field of response for the adult animals (3.4 $V.cm^{-1}$). The magnitude of the electric field in the trap was set such that the control animals, which respond to the electric field, will be able to pass through. The mutants would not be attracted to the trap due to the electric field; but, they are likely to cross the trap purely by chance. The worms that were able to cross the electric trap were collected from the separation chamber into a Petri dish and counted (Figure 5-9) under a fluorescent microscope. For the neuronal mutant, the pool of the sorted worms (n=64 and 55) contained 93% control animals and 7% mutants (Figure 5-9a) on average. For the muscle mutant, the distribution was 92% control and 8% mutant (n=52 and 65) (Figure 5-9b).

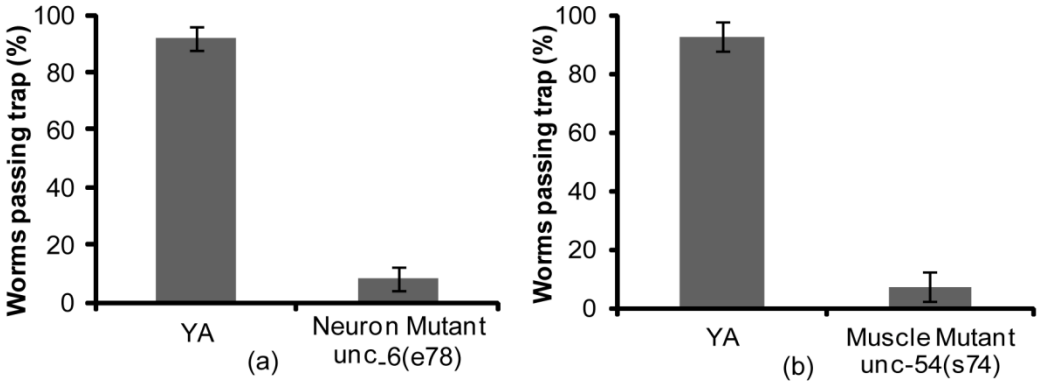

Figure 5-9 Sorting of young adults (YAs) from (a) neuronal mutants (unc-6(e78)) and (b) muscle mutants (unc-54(s74)). The total extracted number of worms in the separation chamber was (a) 64 and 55; (b) 52 and 65. Chamber electric field used was 3.4 V.cm^{-1} [21]. Reproduced by the Permission of the Royal Society of Chemistry 2012

The behaviour of individual muscle mutant worms in the loading chamber was further investigated while being exposed to the electric field. It should be mentioned that during the sorting experiments with desirable ranges of electric field in the trap, the healthy adult worms decreased the peak-to-peak amplitude of their body stroke while attempting to pass through the traps. For the muscle mutants, it was observed that although they were able to sense the electric field in the loading chamber and moved towards the traps with large body stroke peak-to-peak amplitudes, their control of the sinusoidal movement was not optimal; and therefore, they were not able to pass through the traps. In summary, the microfluidic sorting device presented here could be used to separate the electrotaxis mutants from the normal animals. This will be particularly useful in the genetic screening of the electrotactic mutants.

5.2.2.6 Electrotactic Sorting of the Young and the Old Adults

Sorting the young and the old adults from a mixed culture that were similar in size was also attempted. For this purpose, 62 hr adults of VH17 genotype (YA) were mixed with 86 hr old N2 adults (OA) in equal ratio. Since both stages are highly sensitive, a very low electric field (1.8 V.cm^{-1}) was utilized to perform the sorting experiment (Figure 5-10) in a manner similar to that used in the mutant sorting experiments.

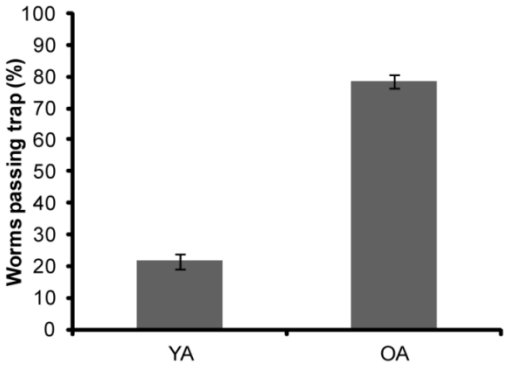

Figure 5-10 Sorting of young adults (YAs) and old adults (OAs) in the continuous sorting device. The total extracted number of worms in the separation chamber was 52 and 95. The chamber electric field used was 1.8 V.cm^{-1}. [21] Reproduced by the Permission of the Royal Society of Chemistry 2012

It has been reported that the electrotaxis swimming speed of the worms reduces by 70% as they age (for a week) after the YA stage [165]. However, interestingly, it was found that the older animals were more sensitive to the electric field compared to the younger ones. From two batches of the sorted worms, 79% were OA and the remaining the YAs. This assay could be used for assessing the electrotaxis sensitivity of the worms, if operated even at lower electric field signals.

The presented research in this subsection is the first demonstration of the electric field-based continuous sorting (behavioural) of *C. elegans* in microfluidic environments based on their age and mutation. DC electrotaxis has been applied in the continuous sorting of the worms in a parallel manner without load capacity restriction (with a minimum throughput of 78 worms sorted per minute per load-run) and without the need for a fluorescent marker in a micro-device containing electric field traps. The key aspect of this method is that it is passive and uses the inherent electrotactic response for sorting, leading to a simpler, more elegant and robust design. The wild-type worms of various developmental stages as well as the mutants can be efficiently separated from the young adults (~90% selectivity) in a continuous manner inside a lithographically made single-layer microfluidic device. This selectivity is somewhat low, but acceptable in some experiments (e.g., the mutant screening). For experiments requiring greater selectivity or throughput, one could perform multi-stage sorting, although this may increase the overall time. Throughput can also be increased easily by optimizing the design of the device that has higher loading capacity. Care should be taken as this would affect the electric field distribution in the device. This worm sorting device is easy to operate, amenable to automation and can be scaled up. Considering that the entire procedure takes only a few minutes to run and is cost-effective, it promises to simplify and accelerate experiments requiring

homogeneous cultures of the worms, to facilitate isolation of the mutants that have abnormal electrotaxis, to develop advanced microfluidic-based systems to study the neuronal basis of the movement-related defects in the worms and to facilitate high-throughput chemical screening and drug discovery.

5.3 Detection

As discussed before, after sorting the animals by a method such as the one discussed in Section 5.2, they should be isolated and exposed to chemicals in the integrated chemical screening system (Figure 2-9). The microfluidic-based electrotaxis screening technique, discussed in Chapter 4, can then be used at the characterization module of this system to assess the movement of worms. Swimming speed and body bend frequency of the worm are among the most important movement phenotypes of interest for these animals. Currently, majority of the movement phenotypic assays, i.e. the conventional agar plate- or the microfluidic-based ones, record the animals' movement in a video format and use various image post-processing tools to analyze the movement in terms of parameters, such as speed and body bend frequency. Therefore, these experiments require high resolution microscopes and image acquisition systems. In fact, this technique was initially incorporated in this thesis for analyzing the worms' electrotaxis in microchannels in Chapter 4. Although some of these software tools have been demonstrated to achieve medium throughput movement analysis of a number of the animals at a time, but they are not well-applicable to HTS of the movement for populations of the worms. Additionally, these tools are mostly custom-made at each laboratory and neither standardized nor accessible to all researchers. In the conventional plate-based assays, the worms can also exhibit more complicated movements to analyze; because, first, movement is a voluntary phenotype on the plate; and second, the surface conditions of the plate such as the concentration of chemicals or temperature may be highly variable.

As mentioned in the introduction section of this chapter, analyzing the worms' movement phenotypically and in a simple and perhaps on-chip manner would eventually lead to the development of higher throughput screening devices which are automated, fast in providing results without the need for microscopy and post-experimental analysis procedures as well as independent of all spatiotemporal factors such as environmental non-uniformities in chemical concentration, temperature, etc. Microfluidic devices are well-suited to meet these requirements; and hence, they have been incorporated recently to perform non-visual phenotypic assays on the worms. For instance, body volume size of *C. elegans* has recently been measured by a capacitive sensing method in a microfluidic channel [198]. The device consisted of a tapering microchannel with

microfabricated electrodes on the bottom of it that were used to measure the capacitance of the detection zone of the channel. The tapering design was important in increasing the sensitivity of the channel in detecting slight variations of capacitance upon passage of worms. This device measured the body volume of the worm by calibrating the capacitance change of the sensor upon the passage of the animal with its on-chip immobilization-based imaging and size measurement. The capacitance change was directly proportional with the animals' developmental stage. This chip is well-suited for body volume measurement of the worms without the need for microscopy after calibration, and with applications in detecting environmental toxicants that affect the animals' growth, as demonstrated in this research [198]. However, measurement of the movement phenotypes, such as speed and body bend frequency, is not possible with this microchip; as it immobilizes the animal inside the capacitive detection zone. For measuring the speed, the animal should be allowed to freely move in the channel.

Various electrical and optical methods have been developed to detect freely moving biological substances inside the microfluidic environments. For this, electrodes (electrical method) or fibres (optical method) are integrated into the microchannels to sense the electrical or the optical properties of a specific region (detection zone) of the channel. In both methods, a steady state condition in the detection zone is recognized and used comparatively to detect external objects that affect this steady-state condition. For instance, in the optical method, two aligned optical fibres along the cross section of a microchannel were used to excite and detect light in a cell counting application [199]. In a non-steady state condition, where a cell passes through the detection zone, the excitation light will get scattered and the intensity of the detected light will decrease. Although optical methods are widely used for serial sensing applications, they need a high degree of accuracy in fabrication (alignment of fibres) and integrating them to flexible PDMS-based devices would increase their chance of failure over time. Integration of the optical detectors into parallel microchannels assaying the worms is, therefore, more challenging. Electrical detection and sensing methods are easy to fabricate (microfabrication techniques) and amenable to multiplexing, using the present electronic technologies. Additionally, they would fit well with the other electrical components of the screening device presented in this thesis. In this method, the electrical properties such as the capacitance, resistance or impedance of the detection zone of the sensor will change upon the passage of biological objects (e.g. nematodes) through it. This is due to the differences between the electrical properties of the bio-organism versus that of the media in the detection zone. This method has already been used for sensing DNA molecules and small cells in the microfluidic devices [200].

In this section, a simple electric impedance-based detection method will be introduced that can sense the presence of the animal in a wide microchannel that the worm can freely move without immobilizing it. This component would automate the process of detecting the animal in a microchannel at a specific location. Speed of the worm inside the channel is defined as the distance travelled by the worm divided by the time of the travel. Two of such detectors positioned in a known distance along a channel would make it possible to measure the speed of the worm automatically with no need for imaging.

5.3.1 Impedance-Based Detection of Worms inside a Microchannel

Figure 5-11 illustrates a 2D schematic of a channel with two electrodes located at its walls in the middle (detection zone denoted by the gray circle) that are connected to an impedance analyzer equipment that can measure the cross-sectional impedance of the channel versus time. The working principle of this device is that the impedance of the detection zone will change from condition #1 with no worm to a different value in condition #2 where a worm is passing through the detection zone. The change in impedance can be measured and used as a detection of the worm at that location.

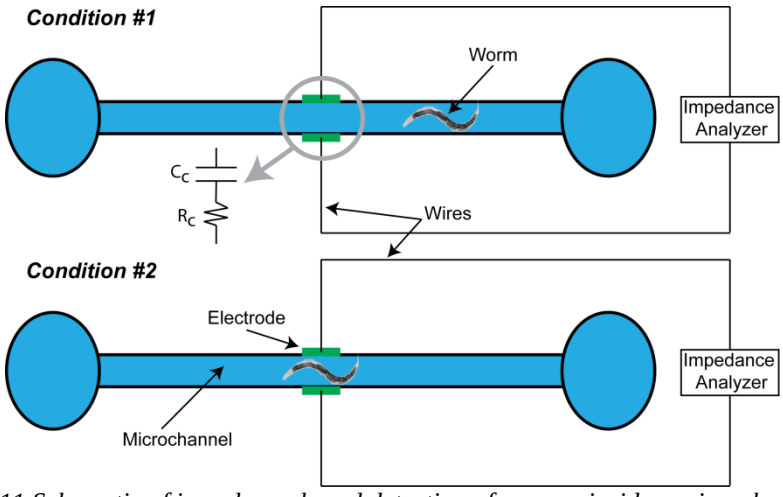

Figure 5-11 Schematic of impedance-based detection of a worm inside a microchannel upon passage through the detection electrodes region (detection zone) in condition #2. Simplified equivalent electrical circuit of the detection zone also illustrated in condition #1, R_c and C_c are the electrical resistance and capacitance (due to fluidic double layers formed on the electrode interfaces) of the detection zone.

Electrical impedance (denoted by Z in ohms (Ω)) is the resistance of an electric circuit to the passage of current, when an AC voltage (e.g. $V=V_0Sin(\omega t)$) is applied to it externally at a specific frequency ω (Hz). It is defined as the electrical voltage (V) divided by the current (I); and, it consists of a real (R, the

resistance of the circuit) and an imaginary part (*X,* the reactance of the circuit). Imaginary part of the impedance is a combination of capacitive *($Z_C=1/(j\omega C)$)* and inductive *($Z_L=j\omega L$)* impedances, where *j* is the imaginary unit vector, *C* is the capacitance (*F*) and *L* is the inductance (*H*) of the circuit.

Embedded electrodes inside microchannels (Figure 5-11) are usually modelled as an electrical resistance (R_c) arranged in series with capacitances (C_c) generated due to the formation of electric double layers on the electrode surfaces inside a liquid media (Figure 5-11, condition #1) [201, 202] with inductive effects being negligible. Electrical properties of a specific liquid media (M9 buffer solution in this thesis) will lead to the generation of specific impedance across a pair of electrodes inside a microchannel. Passage of any external object (e.g. micro-particles) or a bio-organism (pathogenic bacteria [201] or the worms in this research) across the electrodes (Figure 5-11, condition #2) would result in the change of the electrical properties of the sensing region such as the electrical resistivity or the permittivity. This would eventually result in a very small change in the impedance of the region, which can be sensed externally with an impedance analyzer system. These systems are, however, very bulky and expensive; and as mentioned before, alternative sensing methods are available that can enable the sensing of minimally changing signals, such as the ones encountered in impedance-based sensing of bio-organisms. Wheatstone bridge circuits are among these methods and have been used in this research.

A Wheatstone bridge is a rhombus-shape looped electrical circuit (Figure 5-13) with 4 legs. One of its leg consists of an unknown (to be measured) impedance, while the others consist of a variable and two other equal-size impedances. The loop is fed with a voltage across two diagonal ends of the rhombus loop and the resulting voltage is measured across the orthogonal diagonal ends. The bridge can be designed in a way (balanced mode by equalizing the variable and the unknown impedances) that the input voltage does not generate any output voltage. This is due to the induced electrical symmetry between the output measurement points. Any asymmetry in the electrical properties of the 4 legs can however result in the generation of an output signal that can be measured externally. The output signal can be amplified and filtered in some instances to increase the signal to noise ratio.

5.3.2 Design and Development of the Microfluidic Detector Device

The impedance detector device, illustrated schematically in Figure 5-11, was fabricated soft lithographically, as discussed in Section 3.3.2. The dimensions of the channel were mostly determined by the electrotactic experiments discussed

in Chapter 4. It was intended to sense the worms that are freely moving inside a microchannel, as opposed to the sensing mechanisms described in the literature, where the animals were immobilized and electrically sensed and characterized [198]. Accordingly, the device consisted of a straight main microchannel (same as the electrotaxis device: 0.3 mm wide, 0.1 mm deep and 50 mm long, Figure 5-12a) connected to 6 side microchannels aligned 2 by 2 at the sidewalls of the main microchannel (the electrode channels, Figure 5-12c). The electrodes (100 µm diameter Pt wires) were inserted from both sides into the electrode channels manually (see Section 3.3.2 for the fabrication method, Figure 5-12b). The electrode diameter was selected to be the same as the depth of the microchannel. This was expected to increase the sensitivity of the detector, as opposed to the lithographically-made 2D electrodes that lay solely at the bottom of the channel. Fabrication process for the wire electrodes was also easier and less expensive. After positioning the tip of the electrodes at the side of the main channel, a drop of PDMS prepolymer was placed into the reservoir of the corresponding electrode channel in order to embed the Pt wire inside an insulating layer. Channel surface tension dragged the liquid PDMS into the electrode channel. When the liquid PDMS interface reached approximately 4-5 mm away from the main channel sidewall, the device was positioned on the hotplate (170 °C) to quickly cure the PDMS prepolymer filler. Each pair of electrodes was then used to sense the impedance of the cross section of the channel at one location (‘*detection zone’*, Figure 5-12c), as discussed in section 5.3.1 and shown in Figure 5-11.

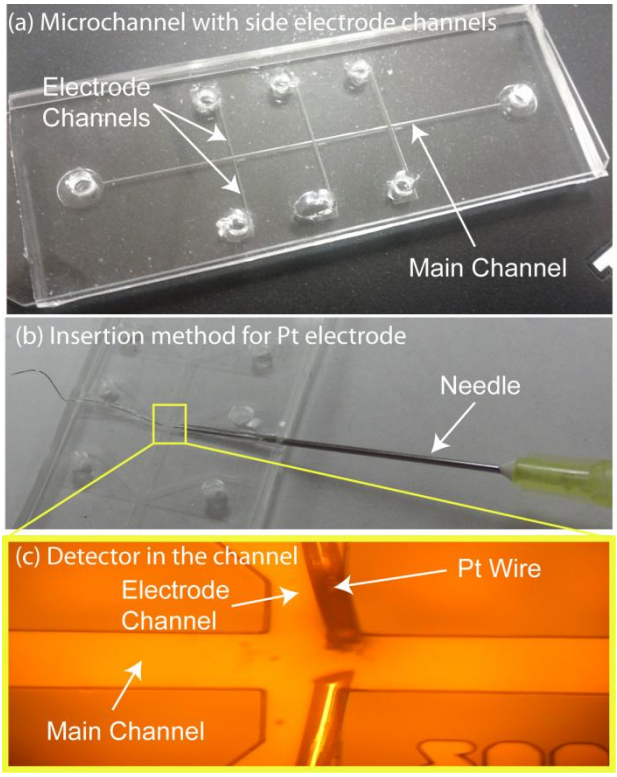

Figure 5-12 Microfluidic worm detector, (a) the fabricated PDMS microchannel with 3 sets of side channels for Pt electrode insertion, (b) method used for inserting Pt electrodes into the channel under the microscope, (c) finalized detection region of the device.

It is easy to fabricate this device, as it does not involve any metal deposition and patterning fabrication steps [198] that has to be done in a cleanroom environment. Sensitivity of the device is also expected to be higher because rather than only measuring the impedance of the channel at the bottom (usually done in microfabricated sensors), the entire cross section impedance is measured. This is because the diameter of the Pt wire used as the electrode was designed to be equal to the depth of the microchannel.

5.3.2.1 Sensing Experimental Setup

In order to measure the impedance of the detection zone, illustrated in Figure 5-12c, an AC voltage had to be applied to the electrodes and the current passed through had to be measured simultaneously (see Section 5.3.1). This was achieved automatically by using an Agilent Precision Impedance Analyzer 4294A system (Agilent Technologies, CA, USA). After measuring the impedance of the detector and finding an electrical equivalent circuit model for it by this method, the results were used to design an external Wheatstone bridge circuit that was utilized to sense the worms. Figure 5-13 shows the schematic diagram of this circuit.

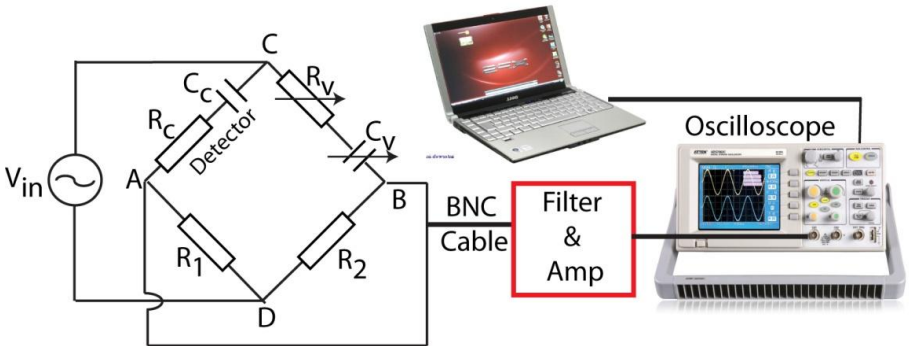

Figure 5-13 Schematic of the sensing experimental setup with detector device being modeled as a resistance (R_c) and a capacitance (C_c) and connected to the external circuit as a leg of a Wheatstone bridge. The Wheatstone bridge: detector channel is connected to the AC port in series with a potentiometer R_v and a variable capacitance C_v. R_1=R_2= 1 KΩ. AC sine wave signal is applied across CD (V_{in} by using a function generator). Output signal across AB is measured by the oscilloscope after being filtered and amplified and passed to the computer for recording.

The impedance detector device illustrated in Figure 5-11 (represented by a resistance, R_c, and a capacitance, C_c) was set as one of the Wheatstone bridge legs. It acted as the unknown variable leg of the bridge. R_v and C_v were the variable resistance and capacitance which were used to balance the Wheatstone bridge as discussed in Section 5.3.1. The Wheatstone bridge was assembled on the breadboard of a Virtual Instrumentation Suite ELVIS II+ (National Instruments, TX, USA) system. This instrument is an educational multifunctional unit that could also supply the sinusoidal input voltage (V_{in}, f =9 KHz) into the circuit by using its function generator module. Using this module, the loop was fed with a voltage across two points (C and D in Figure 5-13) and the resulting voltage was measured across two orthogonal ones (A and B in Figure 5-13). The 9 KHz frequency for the input signal was chosen to lower the effect of capacitance in the impedance ($Z_c=1/(j\omega C)$) of the detector as discussed below and later in section 5.3.3. The readout signal of the bridge was filtered (f >10 KHz) and amplified (1000x) using a custom-made amplifier and passed onto a DSO1012A Oscilloscope (Agilent Technologies, CA, USA) which was connected to a laptop for recording the output signal.

If the ratio of the two impedances in the known leg of the Wheatstone bridge ($|Z_2/Z_1|=R_2/R_1$, $R_2=R_1=1$ kΩ, Figure 5-13) is equal to the ratio of the two in the unknown leg ($|Z_v/Z_c|$, where $Z_v=R_v+(1/(j\omega C_v))$ and $Z_c=R_c+(1/(j\omega C_c))$, the Wheatstone bridge is assumed to be in a balanced condition and the voltage readout between the two midpoints (A and B) will be zero and no current will flow through. Therefore, the oscilloscope will ideally show zero signal readout. This is achieved by adjusting and setting the variable resistance and capacitance (Z_v) equal to the channel impedance (Z_c, measured initially by the impedance analyzer system as discussed in the result sections below) in order to set the

readout signal to zero in the absence of any worm ($Z_2/Z_1=Z_v/Z_c=1$). If the bridge becomes unbalanced by the passage of a worm across the detector ($Z_v/Z_c\neq1$), the signal readout across AB will be non-zero and amplified and sensed as a sinusoidal waveform by the oscilloscope with the same frequency of the input signal. It is worth mentioning that the amplitude of the detected signal is dependent on the significance of the change in the electrical properties of the detection zone due to the passage of the worm.

5.3.3 Detection Zone Electrical Characterization for Wheatstone Bridge Circuit Development

In order to develop a proper Wheatstone bridge, it was first required to measure the impedance of the detection zone (Figure 5-12c). For this purpose, the detection electrodes were connected directly to an Agilent Precision Impedance Analyzer system and M9 buffer was introduced into the channel. A sinusoidal waveform with a frequency sweep range of 40 Hz to 100 KHz and peak-to-peak voltage of $V_{p\text{-}p}=2V$ was applied across the detector wires and the amplitude and phase magnitudes of the passed signal was measured (solid lines in Figure 5-14a). The impedance magnitude was in the order of tens of kilo-ohms; and the phase of the signal appeared to reach a steady state of ~-12° at high frequencies. The impedance at low frequencies was highly influenced by the capacitive behaviour of the detector device as the phase angle was close to -90° and the signal amplitude declined as the frequency was increased to more than 5 kHz. The impedance analyzer also provides a best-fit electrical model to the signal. In this case, the electrical equivalent circuit of the signal was a serial RC model with $5k\Omega<R_c<70k\Omega$ and $4nF<C_c<20nF$ for three different detectors made with slight differences in the distance between the Pt wire electrodes in the detection zone. This provided the range of the variable resistance and capacitance (Z_v) needed for the development of the Wheatstone bridge (Figure 5-13).

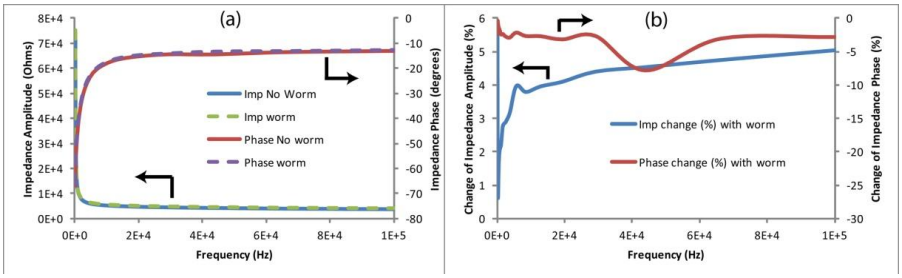

Figure 5-14 Impedance measurement of the detection zone with and without an adult worm, (a) Amplitude and phase of the signal in absence and presence of an adult worm between Pt electrode detectors at various excitation frequencies, (b) Percentage of amplitude and phase change upon passing the worm across the detector at various excitation frequencies

In order to measure the percentage of the signal change and to determine whether or not an amplification of the signal after the passage of an animal was needed, it was required to measure the impedance amplitude and the phase of the detection zone in the presence of worms as well. Adult worms (N>10) were therefore inserted individually into the channel (Section 3.4.1) and positioned in between the electrodes pneumatically and changes in the impedance amplitude and the phase were measured similarly (results for a single animal depicted as dashed lines in Figure 5-14a). Figure 5-14b illustrates the percentage of the impedance amplitude and the phase change, shown in Figure 5-14a, due to the presence of an adult worm across the detector electrodes. It was observed that the percentage of the impedance amplitude change reached 4-5% at high enough frequencies of the input signal (5-100 KHz). An experiment performed at 10 MHz frequency resulted in the same ~5% change in the signal amplitude (data not shown).

All in all, it was concluded that the detection channel should have been modeled electrically as an RC circuit in the design of the Wheatstone bridge. The magnitude of the variable resistance (R_v) and capacitance (C_v) in this bridge was also determined to be in the range of KΩ and nF, respectively. It was also concluded that in order to observe variations in output signal to the passage of the worms, high input signal frequencies (f >5 kHz) and filtration as well as amplification of readout signal was required.

5.3.4 Worm Detection Using the Wheatstone Bridge Configuration

Initial experiments using the impedance analyzer system helped in measuring the impedance magnitude of the detection zone and the expected percentage of the change in the signal due to the passage of a worm. The results were utilized to design the Wheatstone bridge and the rest of the experimental setup, as depicted in Figure 5-13. This setup was also more compact in size that could eventually be designed and fitted on a chip along with the microfluidic detection device. This is an important factor to be considered in the design of HTS devices for the worm movement analysis.

In order to perform the detection using the new setup, the main channel (Figure 5-12a) was filled with the M9 solution and the detection electrodes were connected to the Wheatstone bridge circuit, as configured in Figure 5-13. A sinusoidal input voltage with a peak-to-peak value of $V_{p\text{-}p}=40\ mV$ and a frequency of 9 KHz was then applied to the circuit, as shown in Figure 5-13; and the output signal was amplified by a 1000 gain and monitored using the oscilloscope. The variable resistance (R_v) and capacitance (C_v) on the Wheatstone bridge were

then adjusted manually to proper magnitudes (approximately equal to the detection channel resistance R_c and capacitance C_c), so that the output signal of the bridge was approximately zero, as depicted in Figure 5-15a. As discussed in section 5.3.2.1, the passage of a worm through the detection channel will result in the variation of R_c and C_c values; and subsequently, the Wheatstone bridge will become out of balance. This will lead to the generation of a potential difference across the points A and B in the Wheatstone bridge (Figure 5-13) and the passage of a signal with the same frequency of the input signal. This theory was tested by allowing the worms to pass through the detector while recording the output signal, as depicted in Figure 5-15b. It was observed that the worm presence could be detected by the observation of a sinusoidal output signal from the circuit, which had the same frequency of 9 KHz as well.

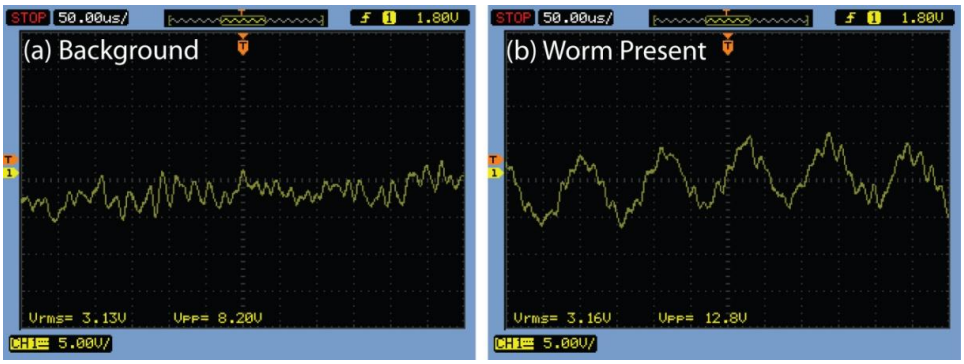

Figure 5-15 Worm detection using a Wheatstone bridge configuration, (a) Oscilloscope signal readout in absence of the worm when the Wheatstone bridge was in balance, (b) Adult worm passing between the Pt detector electrodes causing a change in the Wheatstone bridge balance state and generating a signal.

5.3.5 Integration of Detection into Electrotaxis Movement Screening

The detection system developed in this section was designed for measuring the worms' movement phenotypes, such as the speed and the body bend frequency on-chip without the need for experimental video recording and data post processing. In order to use the detection technique to measure the worm electrotactic speed in the channel, some adjustments were made to the system.

The movement of the worm along the length of the main microchannel (Figure 5-12a) should have been controllably stimulated, simultaneously with the sensing mechanism. This has been achieved through the incorporation of electrotaxis electrodes into the reservoirs of the main microchannel (figure not shown) as developed and discussed in Chapter 4. However, during the preliminary experiments, it was observed that the application of a DC voltage across the main microchannel, in order to induce electrotaxis, will interfere with

the detection circuit and brings the Wheatstone bridge out of balance. This outbalance was not fixable by further adjusting the variable impedance of the bridge due to being out of the range of the setup. Therefore, it was decided to separate and isolate the electrotaxis circuit from the detection one. This meant that when the worm was electrotactically stimulated to move in the main channel, the detection circuit had to be off and vice versa when the sensing was being performed. This was assumed to guarantee a minimum crosstalk between the circuits.

Isolation of the electrotaxis and the detection circuits was achieved by taking advantage of the pulse DC electrotaxis phenomena (Section 4.3.2) and a custom-made LabVIEW program to control the two circuits sequentially. It was shown that the worms exhibit electrotaxis even in a pulse DC signal which is on and off with specific frequency levels. The worms' movement across the main channel of the detection device was stimulated with a pulse DC signal of 0.25 Hz frequency and 75% duty cycle, and the detection was performed during the off half-cycle of the signal (1 s), where no voltage was being applied across the main channel. In order to even further reduce the crosstalk, some adjustments to the main circuit had to be made, such as an addition of two relay switches to isolate the electrotaxis circuit from the detection one, while one was on and the other was off. Worms' electrotactic stimulation and simultaneous sensing was achieved using this method (Figure 5-16); however, a gradual bubble generation problem at the detector electrode region prevented completing the double-stage sensing of the worm across the length of the channel for speed data acquisition. The generated bubble expanded in size with time, leading to the blockage of the main channel. This caused a discontinuity in the electric field required for electrotaxis of the worm. Therefore, simultaneous electrotaxis stimulation and sensing was only achieved at one detector.

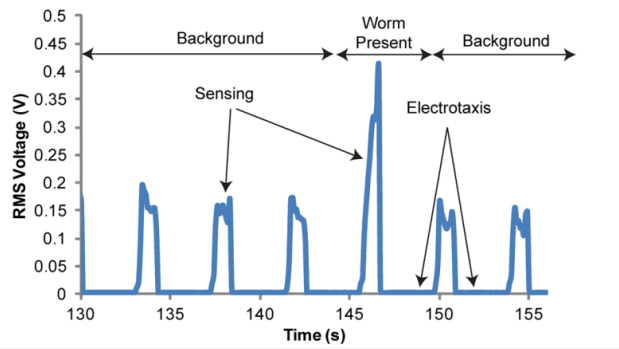

Figure 5-16 Simultaneous electrotaxis and sensing of a young adult worm inside the detection device. A pulse DC signal of f=0.25 Hz, 75% duty cycle (3 s electrotaxis and 1 s sensing) and EF_{max}*=3* $V.cm^{-1}$ *was used. The presence of the worm was detected as an increase in the RMS voltage output of the Wheatstone bridge after filtering and amplification*

The bubble generation problem at the detector wire discussed above was further investigated by performing a simple experiment. The sensing electrodes were disconnected from the Wheatstone bridge and allowed to be electrically floated. A DC electric field of 15 volts was applied across the main microchannel (Figure 5-12a) for electrotaxis stimulation. It was observed that the bubble got generated similar to the previous experiment meaning that the bridge configuration was not leading to this phenomenon. When the potential difference across the floating detection electrodes was measured, it was discovered that application of the electrotaxis voltage across the main channel leads to the generation of a ~>1V potential difference between the two detector electrodes. This would eventually provide the necessary energy for the initiation of an electrolysis reaction and the release of hydrogen gas that led to the generation of bubbles over time. Hypothetically, this phenomenon had occurred solely due to the asymmetric configuration of the detector electrodes and the resulting difference in their potential state. This phenomenon was prevented by properly aligning and fully embedding the Pt electrodes in PDMS all the way towards the tip of the electrodes at the sidewalls of the main microchannel. This was achieved by controlled injection of PDMS prepolymer (preferably half-cured) into the electrode channels with a syringe pump and under a microscope during the fabrication steps. In order to reduce the generated voltage amplitude across the detector electrodes, an electrical circuit was added to the system. So, whenever the electrotaxis circuit was running, the detector electrodes were connected to each other externally in order to zero their potential difference. These attempts resolved the bubble generation problem and a double-detector electrotactic speed measurement assay is currently under investigation.

Most of the worm movement screening methods use video recording of the locomotion and software-based post-experimental analysis, which are time-consuming and not suitable for high throughput assays. Development of on-chip sensors to analyze the worms' movement can greatly facilitate these assays. One of the first-of-its-kind sensors that have been developed in this section was a simple position detector for sensing the worms inside microchannels when they moved through certain locations in the channel. Presence of the worms was sensed as variations in the electrical impedances in this method. A Wheatstone bridge configuration was used to sensitively detect these slight variations. In contrast to few other worm detection techniques, this method senses a freely moving worm in the channel and is easy to fabricate. This can eventually lead to the development of devices that can measure the speed of the worms on chip, which is necessary for HTS of the populations of the worms individually in parallelized screening channels. Further characterization of the impedance signal variations, while a single worm passes through the detection zone of the device, can hypothetically lead to the acquisition of other movement-specific parameters.

The detector device would facilitate analysis of the forward motion speed; however, the worms' movement in a channel can be categorized into forward/backward motions, turns and sudden stops. For full movement control and analysis, the stop phase should also be stimulated and characterized externally.

5.4 Localization

The worms' locomotion can be categorized into forward and backward locomotion, turns and stops inside the microchannels as detailed in Chapter 2. Forward motion and turns were characterized in terms of electrotactic swimming speed and rotation times inside the channel using DC and pulse DC electrotaxis, as discussed in Chapter 4. Localization of the worms (stop) is also an important control mechanism [203] in their full-movement screening and potentially chemical exposure. Additionally, localization can be applied in on-chip high speed imaging applications, where the worm should be localized on the imaging sensor momentarily. Localization can also be applied in investigation of neuronal pathways involved in this mechanism. It is also an important control mechanism for high throughput automated handling and screening of the worms' behaviour in a microfluidic channel.

Researchers have reported the use of microchannels containing mechanical valves [142, 146, 154] and agar-filled channels with local electrodes alongside the channel wall [164] to localize the worms at desired locations. In the latter case, high-strength DC electric fields opposing the initial crawling direction of the L4-stage worms were used to reject the worms from entering a certain region of a channel and to localize them in a similar manner as the one discussed in this section. However, this technique was found to be ineffective in controlling the older (adults) or the younger (L3) stages of *C. elegans*. It has also been recently demonstrated that the wild-type worms move faster compared to the mutants in the presence of a DC electric field [15]; and hence, they could be pre-concentrated in an open surface agar gel plate [165]. However, the variability of the method was considerable, probably due to the distribution of the electric field was not uniform over the entire gel surface. In this section, use of AC electric fields for on-demand localization of the worms inside microchannels at any desired location for extended period of time without any physical confinement will be investigated in details.

5.4.1 Use of Electrotaxis to Localize *C. elegans*

In Chapter 4, it was demonstrated that the worms prefer to move towards the cathode pole of an applied electric field in a microchannel. Reversal of the field

resulted in a turning response that happened within 15 s in case of a DC electric field and was found to depend on frequency in the case of a pulse DC electric field. Based on this behavioural response, it can be hypothesized that application of an AC signal that switches the location of the cathode pole from one side of the worm to the other at every cycle can potentially hold the worm at one location if applied at a faster rate than the animal's response time itself. Upon exposure of the worms to AC electric fields at specific frequency levels, their locomotion can potentially be confined to shorter distances, until the animal becomes localized at one spot. One important factor in the design of the experiment is that the worms are irresponsive to pulse DC signals at frequencies in the range of 5 Hz as discussed in Sections 4.3.2 and 4.3.3. Therefore, an AC signal in the same frequency level might cause complications in the response that should be taken into account. Localizing worms by AC electric fields was investigated and the response of the worms of various ages and mutations was characterized for various signal frequencies.

5.4.2 Localization of *C. elegans* using an AC Electric Field

The experimental setup used to study the effect of AC electric field on the worms' electrotaxis behaviour was illustrated in Figure 3-4. As discussed before, it consists of a microchannel (Figure 4-3, 5 cm long, 300 µm wide and 100 µm deep) with electrodes embedded at both reservoirs that are connected to an electrical setup that could apply different AC waveform electric fields (Figure 3-5). The microdevice was constructed of PDMS prepolymer, using soft lithography and microcontact printing methods, as described in Section 3.3.2. Other methods to load the worms inside the channel, to apply electric fields and to record and analyze the animals movement behaviour were all described in Chapter 3. Development, growth and synchronization of the animals have been described in details in Chapter 3. The strains used in this section were the N2 and BC347 unc-54(s74). Synchronized worms were used in all the experiments.

The worms were loaded individually into the microchannel using a syringe pump and placed in the middle of the channel (2.5 cm away from each electrode). To illustrate the localization behaviour inside the microfluidic channel, a constant DC electric field (with proper strength based on Figure 4-5) was applied across the channel to stimulate the animals to initiate swimming toward the cathode for a 3 mm short distance (Figure 5-17a). Afterwards, an AC electric field with square waveform (1 Hz frequency) was applied for specific duration of time (20 s) and the response of the animal was recorded (using the camera) (Figure 5-17b). It was observed that during the application of the AC field, the worm remains localized at one spot with minor movements and turns. Application

of a DC field afterwards would stimulate the electrotaxis movement again (Figure 5-17c).

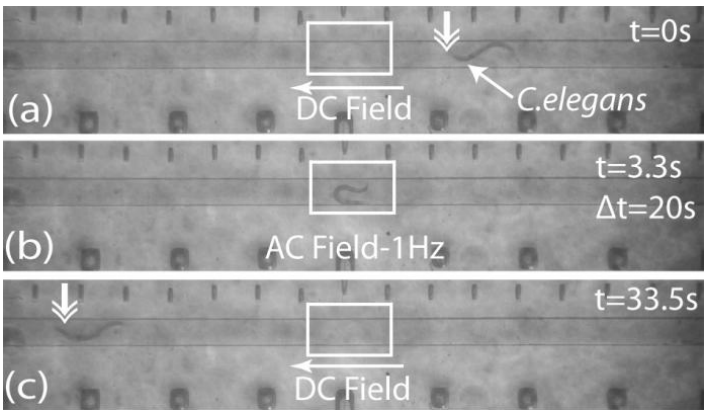

Figure 5-17 AC electrotaxis response of a worm; the worm's swimming is initiated by DC electric field in (a) and (c). AC electric field is used to localize the animal in the middle of the channel in (b) for 20 s. [18] Reproduced by the Permission of the American Institute of Physics 2010

These results demonstrated that a combination of DC and AC electric fields could be used to efficiently guide and localize the worms in a microfluidic channel without the use of physical constraints (such as the vacuum suction or a deformable PDMS membrane) or additional side-channel electrodes [164]. It should be mentioned that this technique is not as suitable as mechanical-based methods for immobilizing the worms but essential and useful for the pulse-based electric immobilization method which will be addressed in section 5.5 of this chapter.

5.4.2.1 Effect of Signal Frequency, Animal Age and Mutation on Localization

The observations discussed above warranted further investigation of the behaviour of various stages of the worms under AC field exposures at various frequencies (rectangular waveform with *f* between 20 mHz and 3 KHz). Results are shown in Figure 5-18 for various stages of the animal in comparison to the muscle mutated worms.

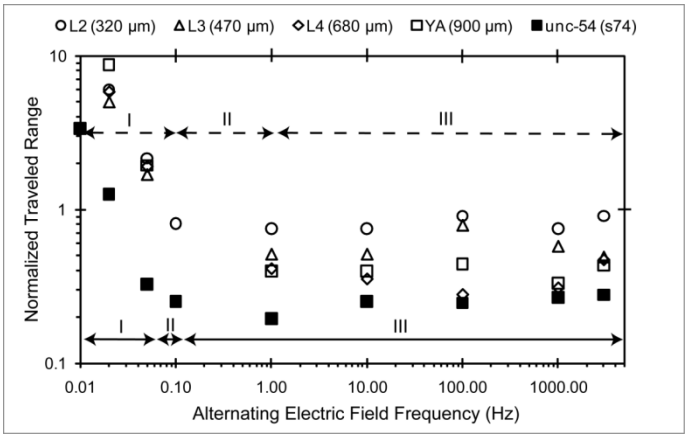

Figure 5-18 The AC electrotaxis response at various stages. Normalized traveled range (traveled range (µm)/average stage length (µm)) decreased with frequency increase for all stages. Regions I, II, and III correspond to DC-like electrotaxis, one-directional movement, and localization frequency range, respectively, illustrated for wild type (dashed double side arrowed lines) and muscle mutant nematodes (solid double side arrowed lines). Applied electric field was 10, 8, 6, and 3 V.cm^{-1} for L2, L3, L4, and young adult stages, respectively, Average length for each developmental stage is stated in the legend parentheses. [18] Reproduced by the Permission of the American Institute of Physics 2010

It was found that at low frequencies (between 20 and ~100 mHz), the L2 and the older stage animals moved in one direction (towards cathode) in the positive half of the cycle and reversed their direction (by turning towards cathode) in the negative half of the cycle (portion I in Figure 5-18). The distance traveled (as measured by the displacement of the head) during each AC field half-cycle before direction reversal was measured and called as “traveled range”. The traveled range data (shown in Figure 5-18) was normalized using the average length of the nematodes tested at each developmental stage (N=10 for each stage). At frequency ranges between ~100 mHz and ~1 Hz, the nematodes swam in the following pattern (termed “stop and go”). When the polarity of the AC electric field coincided with the direction in which they were initially traveling, the animals continued to move in that direction. Interestingly, field reversal (during the other half cycle) did not alter their direction of travel. The animals were either momentarily localized or their speed was severely reduced. Subsequently, in the next cycle, they continued their forward motion. This demonstrates that although nematodes are able to sense the field reversal, they are unable to reverse their movement direction (one-directional movement shown as portion II in Figure 5-18). At higher frequency ranges (~1 Hz to 3 KHz), we found that young adults were almost completely localized in the channel, with movement being restricted to an average distance of 0.41 of their body length (See portion III of Figure 5-18). It appears that the frequency of signal switching is just enough for the worms to sense the direction, but before they could initiate movement the direction of the field had reversed. Consequently, the animals were unable to

move at all. The nematodes stayed localized in the channel for the entire duration of the AC electric field, with no or a few rotations. Frequencies of 5 Hz and vicinity (worms not responding to them) were avoided due to the observations reported in the pulse DC experiments (Sections 4.3.2 and 4.3.3). Subsequent application of the DC electric field induced them to move towards the cathode (Figure 5-17c).

Synchronized worms of various ages (the L1 to young adult stage) were also tested using the same AC square waveform and frequency ranges. The results are shown in Figure 5-18. All developmental stages (except for the L1 stage) responded to the AC electric field in the same manner as the young adults, but with a slight variation in their range of localization. All stages demonstrated decreased traveled range with increase in frequency. Frequencies above ~1 Hz appeared to localize the worms; but, as shown in Figure 5-18, the older animals responded more robustly to the AC electric field (the average normalized traveled range of 0.41 for the young adults and 0.91 for the L2 stage for $f \geq 1$ Hz). For the older animals, more instantaneous responses to the AC electric field were also observed, in comparison to the younger ones. For example, it was observed that some L2 and L3 stages (N=4 out of 20 total), being exposed to the frequencies above 1 KHz, failed to respond instantaneously and traveled for a short distance (<1 mm), before being localized. This phenomenon was not observed in the L4 and the young adult stages that were localized immediately upon AC electric field application. All stages that showed a response exhibited a few or no rotations at the point of localization, although the shorter worms (the L2 stage) preferred to orient their body perpendicular to the axis of the microchannel.

In addition to the wild-type, the young adult worms with defective body wall muscles (*unc-54(s74)* mutant [187]) were also tested for their response to square AC electric field (Figure 5-18). The animals showed AC and DC electrotaxis; but since they had considerably lower mobility compared to the wild-type animals (Figure 4-7) [15], even less average normalized traveled range (0.25) and reduced localization frequency range (100 mHz–3 KHz) were observed.

5.4.2.2 Effect of AC Signal Waveform and Duty Cycle on Localization

The effect of sinusoidal and triangular AC signals on the young adult stage worms in frequency ranges above 1 Hz (localization range) were also tested. The response of the animals was found to be the same as square waveforms. Square waveforms with varying duty cycles (1% up to 80%) were also tested on the young adults to minimize the electric field exposure time while preserving the localization effect (data not shown). Even 1% duty cycle signals localized the worms in the same manner as square waveforms reducing the exposure time by 99%.

In addition to the forward motion of the worm characterized through body stroke frequency and speed of locomotion, stops are also dominantly observed inside microchannels. The work described in this subsection demonstrated the applicability of AC electric fields to inhibit movement of *C. elegans* in a microfluidic environment for an extended period of time. The AC localization technique is applicable to various worm stages and highly controllable due to being incorporated in a microfluidic device. Localization of the worms at any desired location in the channel is also possible with the AC localization technique. Since movement is controlled by neurons and muscles, this discovery holds promise in the development of microfluidic-based high-throughput assays to study and manipulate these two cell types in the worms that are responsible for a diverse range of locomotion behaviours.

5.5 Immobilization and Imaging

One of the advantages of the worm model is its transparency that allows imaging of the animal at the cellular level and its correlation with behaviour. High content imaging is complementary to behavioral analysis and both are increasingly coupled in screening with worms. Genetically-encoded fluorescent tagging and imaging of cells and neurons is one of the most widely used methods for screening the worms. For this purpose, the animals should be immobilized completely to be able to obtain the highest resolutions in the image and hence the most accurate results. Fluorescence imaging of the worms has been extensively used in conventional and advanced microfluidic devices for phenotypic analysis [146, 147] as well as cellular and neuronal studies [153, 154]. Since movement behaviour is governed by neuronal activities, it is also crucial to be able to image such activities, as demonstrated in Section 4.3.3, in order to correlate the animals' behaviour with these neuronal signalling actions.

Conventional methods utilize anesthetic chemicals, such as sodium azide or specialized glues to immobilize the worms on a glass cover slip [11] (discussed in Chapter 2). These methods are slow, low throughput, labour-intensive, fatal to the animal and non-reversible as well as not characterized for the effect of the chemicals on the worms' cellular activities. In addition to conventional immobilization methods, different micromechanical techniques, such as tapering microchannels or deformable PDMS membranes, have also been recently investigated (reviewed in Section 2.5.4). These platforms have greatly facilitated the immobilization of the worms at higher throughputs for phenotypic assays. However, they are complicated to fabricate and operate, can only immobilize the worms at designated locations, are serial and perhaps limited by the number of the cycles of operation before failure.

In this section, application of high voltage but brief electrical pulses (based on previous studies of the worm electrotaxis [15, 16, 18, 20, 21]) will be investigated as a way to induce reversible paralysis that will immobilize the worm for imaging purposes. Unlike conventional or other microfluidic-based methods, the electrical signals can immobilize the worms without any external mechanical or chemical actuation units.

5.5.1 Application of High-Strength Electric Fields to Immobilize Worms

In Chapter 4, it was demonstrated that the worms respond to a specific range of electric field which is associated with their age. Above an upper limit of this field range, they got reversibly paralyzed in the channel. In fact, this phenomenon was utilized to sort the worms in section 5.2. Here, it was hypothesized that higher strength electric fields can be used to immobilize the worms inside the channel on-demand and at any location in the chip. However, strength, duration and number of the possible exposures as well as post-exposure effects are to be characterized. In contrast to other methods, this technique can be easily developed and operated, is applicable at any location in the chip, can potentially immobilize multiple worms at a time and finally is highly robust and versatile (due to advantages of being electrically actuated rather than mechanically or chemically).

5.5.2 Experimental Setup and Methods Used for Electric Immobilization of Worms inside Microchannels

The experimental setup used in this study was described and shown in Section 3.4 and Figure 3-4, respectively. Instead of an optical microscope, a fluorescent microscope (Zeiss Axioimager, Germany) for GFP imaging of the immobilized worms was utilized. Fluorescent images were used to assess the quality of images obtained by electrical immobilization in comparison to anesthetically-immobilized worms. A 3-layer microfluidic device (see Figure 5-19 and fabrication method in section 3.3.3) was used for immobilizing and imaging the worms. The microfluidic device was fabricated by the conventional soft lithography method [176]. The device consisted of polycarbonate membranes (5µm-pore diameter, ~10×2 mm^2) sandwiched between a main microchannel (50 mm×0.5 mm×0.1 mm) at the bottom and 3 positioning channels (3 parallel channels, each 15 mm×0.5 mm×0.1 mm, 17 mm apart) on the top.

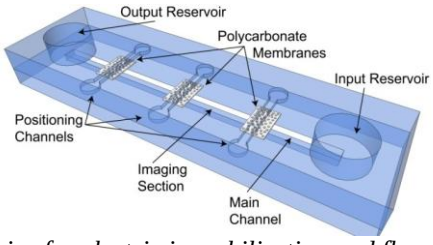

Figure 5-19 Microfluidic device for electric immobilization and fluorescent imaging of C. elegans, Main channel: 50mm×0.5mm×0.1mm, Positioning channels: 15 mm×0.5 mm×0.1 mm, Reservoirs: 5mm diameter, Polycarbonate membrane: 5µm pore diameter

Immobilization was done electrically through the application of various electric field pulses across the 2 electrodes inserted at the two ends of the main microchannel (input/output reservoirs). The device was positioned under the microscope. The electrodes of the microfluidic device were connected to the power supply unit. This unit contained an AFG3022B Tektronix function generator with a maximum voltage signal output of 5 V. The function generator was used to produce various pulses with the controlled strengths (EF_{max}), exposure duration times (on-time of the signal) and number of pulses. Function generator output signal was connected to a 677B TREK amplifier with a maximum gain of 400 that was used to magnify the signal strength up to the desired values (300-500 V potentials resulting in 60-80 $V.cm^{-1}$ electric fields in the channel) right before applying it to the microfluidic device electrodes.

5.5.2.1 Loading Methodology

Development, growth and synchronization of the animals have been described in details in Chapter 3. The strains used in this chapter were N2, VH17 (genotype: *ast-1(rh300) II, rhIs4 III*) and DY127 (genotype: *unc-119(ed4);bhEx37[unc-119(+)+lin-11::gfp]*). The synchronized worms were used in all the experiments.

For loading the worms into the main channel of the device, this layer was initially filled with M9 solution through the inlet and outlet of the main channel. Synchronized worms were washed off the NG plate into a M9 suspension solution. A pipette was used to pick up a single worm from the suspension and transfer it into the inlet reservoir of the main channel (for imaging experiments). For viability studies larger number of the animals was loaded into the reservoir. The worm(s) were transferred into the main microchannel by applying a suction force via a 10 ml syringe at the positioning channel (Figure 5-19) adjacent to the worm-loaded reservoir. This operation aspirated the worm(s) into the main channel positioning it (them) at the overlapped intersection of the channels. The suction force was then released and a second suction at the central positioning channel was used to transfer the worm(s) more towards the center of the channel. All suction forces were then released leaving the animal(s) in the

channel. It was observed that a suction force applied only at the central positioning channel was not strong enough to load the worms from the reservoir into the channel. Hence, 3 channels in the positioning layer were incorporated for a more convenient worm-loading process.

5.5.3 Electric Immobilization and Fluorescent Imaging

After loading the worm in the channel and positioning it at the desired location under the fluorescent microscope lens, rectangular pulse DC electric fields [16] of various characteristics were utilized to immobilize the worms. These electric signals were applied through the insertion of the electrodes (by using adjustable probe station electrodes connected to the power supply unit) into the reservoirs of the main channel.

Effect of three different pulse parameters on immobilization and subsequent GFP imaging of the worms inside the microfluidic device were studied: (i) maximum electric field strength of the pulse (EF_{max}), (ii) exposure time (T_{on}) and (iii) number of pulses. A proper pulse with adequate strength (EF_{max} between 60 and 100 V.cm^{-1} tested) and exposure time (T_{on} between 0.1 and 1 s tested) was investigated for proper immobilization of the animal while preventing its death and minimizing the adverse effect on post-exposure progeny counts. While the aim was to immobilize worms with only one pulse, the effect of multiple pulses (1 to 10 pulses, 5 min apart in application to the worm) was also investigated for long term (~1 hr of continuous immobilization) imaging applications. All the GFP images were acquired immediately after the immobilization of the worms by manual focusing, as described in previous section. It was desired to obtain fluorescent images from electrically immobilized worms which were quantitatively comparable to that obtained by conventional anesthetic-based immobilization methods. The GFP strains used here helped in assessing whether or not individual neurons (that are fluorescing) were observable by electrical immobilization and imaging. Table 5-1 lists the set of experiments conducted for imaging the worms. Images acquired with the electrical technique were compared to the ones obtained by conventional anesthetic-based immobilization (sodium azide exposure) method.

Table 5-1 Experimental electrical conditions used to immobilize worms

Exp.	Pulse strength (V/cm)	Number of pulses	Pulse Duration (s)
1	60	1	0.5
2	80	1	0.1
3			0.5
4			1
5		5	0.5
6		10	0.5
7	100	1	0.5

First, in order to investigate the feasibility of the method, individual animals were loaded into the channel, as described in section 5.5.2.1, and immobilized by using two different electrical pulse conditions (single 0.5 s duration pulses of 80 or 100 $V.cm^{-1}$ strength). This was done for two different fluorescent worm strains (VH17 and DY127) and was compared to the images acquired from the worms immobilized anesthetically (sodium azide protocol) and loaded into the channel. Figure 5-20 shows a comparison between the fluorescent images of the immobilized animals using the conventional anesthetic (Figure 5-20a) and electric pulse methods for VH17 (Figure 5-20b) and DY127 strain worms (Figure 5-20c). The images were qualitatively similar (with visible individual neurons), showing that the electric method for immobilization is promising but comparatively simpler.

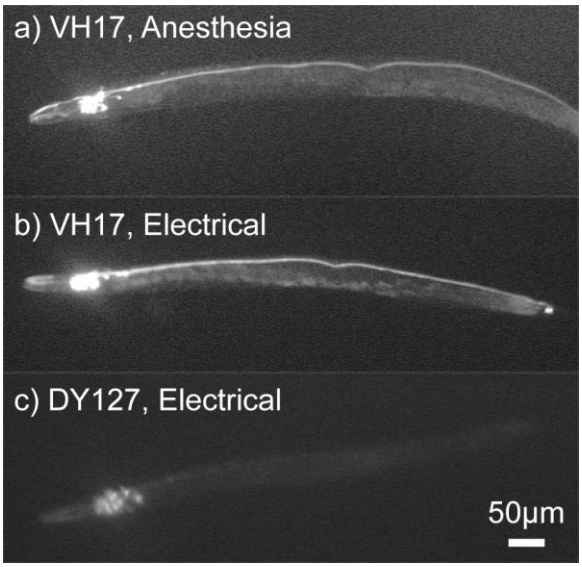

Figure 5-20 Fluorescent images of VH17 and DY127 strains immobilized with (a) anesthesia or one electrical pulse in the microdevice with specifications of (b) 80 V/cm, 0.5s duration and (c) 100 V/cm, 0.5s duration. Images from electrically immobilized worms are qualitatively satisfactory and individual neurons could be observed.

5.5.3.1 Effect of Pulse Characteristics on Immobilization

The effect of pulse strength and duration as well as the number of pulses (for long-term immobilization) on the worms immobilization was studied (Table 5-1), as discussed in section 5.5.3. The results are shown in Figure 5-21.

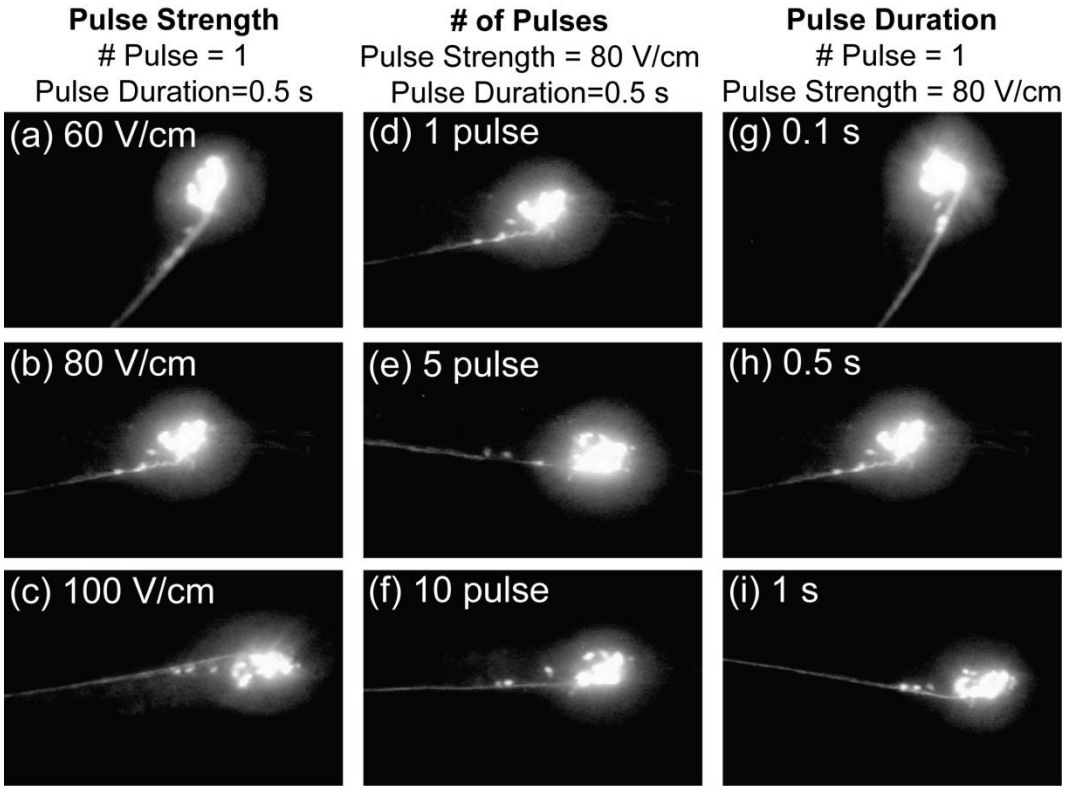

Figure 5-21 Effect of pulse strength (a-c), number of pulses (d-f) and pulse duration (g-i) on immobilization of VH17 strain worms through the quantitative analysis of the GFP images obtained immediately after immobilization. Good images were defined as the ones that individual neurons on the head were distinguishable (c, f, h and i being the best followed by b, d and e being satisfactory) and the worm was positioned horizontally in the field of view (a and g not satisfactory in this regard)

As shown in Figure 5-21, all three parameters were important in completely immobilizing the worms electrically. Higher pulse strengths resulted in better immobilization, as depicted in Figure 5-21a-c. The animals were observed to be immobile during the pulse (complete straight body shape), but moved (wiggling at the same location or translating with complete strokes) immediately after exposure to a single 0.5 s duration pulse of 60 $V.cm^{-1}$ (Figure 5-21a). Therefore imaging the worm under these conditions by manually focusing on the fluorescent neurons was difficult and less successful (1 out of 10 images were acceptable). Most of the worms exposed to this condition were swimming naturally as before within 2 min of the first pulse exposure. Higher single pulse strengths were able to completely immobilize the worms for longer durations and imaging was easily performed (Figure 5-21b-c). The worm's body after the first 80 $V.cm^{-1}$ electric pulse was not entirely straight as compared to the 100 $V.cm^{-1}$ pulse, but image qualities were acceptable as individual neurons were distinguishable.

The number of pulses was significantly important in immobilization at lower pulse strengths such as 60 $V.cm^{-1}$ conditions (data not shown). With the same condition, a second pulse after 5 minutes immobilized the worms for the pulse duration and the worms did not move anymore after removal of the pulse for the next 5 minutes until the next pulse was applied. Only a few instances of hesitant motion were observed in them during this period of time. This characteristics was not observed in higher pulse numbers (>1) in 80 and 100 $V.cm^{-1}$ conditions or after 4 pulses of 60 $V.cm^{-1}$ was applied.

Pulse duration was also significant in completely immobilizing the worms (Figure 5-21g-i). It was found that at 80 $V.cm^{-1}$, a 0.5 s duration pulse and higher was required to obtain a complete immobilization. This could be reduced to 0.2 s at 100 $V.cm^{-1}$, but had to be increased to a second or beyond at 60 $V.cm^{-1}$.

5.5.4 Viability, Reproduction and Long Term Immobilization Assay

In order to study the effect of high-strength electric field pulses and the long-term electrical immobilizations (multiple pulse exposures in 5 min intervals) on the viability and reproduction rate of the worms, a set of 9 experiments were conducted, as listed in Table 5-2.

Table 5-2 Experiments conducted for viability, reproduction and long-term immobilization assessment. Exposure time set to 0.5 s for all experiments

Exp.	Pulse strength (V/cm)	Number of pulses
1	60	1
2		5
3		10
4	80	1
5		5
6		10
7	100	1
8		5
9		10

Populations of 7-10 wild-type animals (62 hr young adults) were loaded into the channel simultaneously by using the method described in section 5.5.2.1. For each loaded batch, one set of experimental parameters (Table 5-2) was used to immobilize the worms. The time lag between the pulses for multi-pulse experiments was kept constant at 5 min. The worms were then recovered from the device and plated individually on agar plates with bacteria *E. Coli* OP50 (one worm per plate). The worms were then monitored after 48 hrs for general health assessment. The number of progenies on the plate after 72 hrs was also counted for each plate for comparison to control animals (not immobilized at all). For this, the worms on each plate were washed off with 500 µl of M9 solution. This

solution was agitated to uniformly distribute the worms and 20 µl of the suspension was picked and placed under the microscope (repeated 3 times for each plate). The number of the worms other than the L1 and L2 stages was counted and averaged in order to avoid considering the worms of the second generation (the L3 and the higher stages progeny of the exposed mother counted only).

N=7 worms per experimental condition (9 experiments in Table 5-2) were exposed and re-plated (OP50 seeded agar plates) individually as discussed above. The animals' survival, behaviour and reproduction rate were screened over 72 hrs after plating, as shown in Figure 5-22.

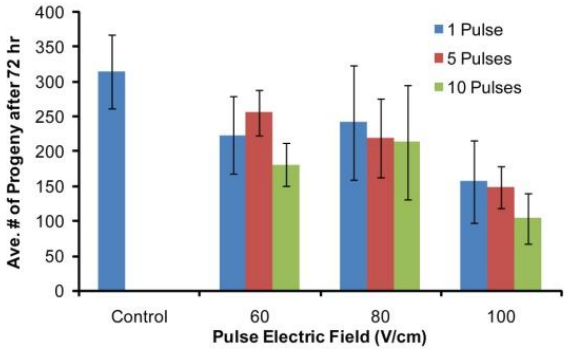

Figure 5-22 Worms (N=7 for each condition) reproduction rate 72 hrs after immobilization with different number of electrical pulse of 0.5s (condition on x axis) compared to unexposed control animals

The results demonstrated that although the worms appeared to be paralyzed after pulse application, they were able to recover after being transferred to *E. coli*-bacteria (OP50) seeded agar plates (100% viable after 72 hrs). They moved normally and were indistinguishable from the control animals in their movement behaviour. However, their reproduction was affected, presumably due to the stress caused by the high voltage electric field. On average, the worms that were exposed to electric pulses showed a reduction in the reproduction, regardless of the field strength and the number of pulses, when compared to the control group. However, when compared with each other, high electric field strengths (i.e. 100 $V.cm^{-1}$) had a slight reduction effect on the animals' reproduction rate. At the lower electric field strength, such as 60 and 80 $V.cm^{-1}$, it was possible to expose the worms to higher number of pulses (up to 10) with no significant effect on their reproduction. This could potentially lead to applications where repetitive immobilization and long-term imaging is required. However, at higher electric field strengths (100 $V.cm^{-1}$), higher number of pulses led to reduction in their reproduction rate significantly.

DC and AC electrotaxis methods, described in the previous sections, make it possible to perform full movement-based assays on a chip. However, it is mostly

desired to assay the worms at the cellular and sub-cellular levels as well. This requires the animals' full immobilization and imaging capability. While most of the methods developed thus far for immobilization are either chemical-based and fatal to the worms, or mechanical-based and serial, limited in space and prone to failure, an electrical method was developed in this section that can immobilize the worms on-demand and at any location in the channel by using high-strength electrical pulses with very short adjustable durations. The method also integrated well with other components needed for electrotaxis assays, as no further fabrication steps were required. Although the method was viable to the worms, it influenced the reproducibility of the animals. Therefore currently it is better suited for assays which the off-spring generations are not required to be studied. Further biological assays are needed to assess the effect of electrical immobilization method at cellular and genetic levels. Electrical immobilization technique, if further characterized and perfected, can enhance the throughput and robustness of the existing screening microfluidic platforms. The technique can also be easily programmed by an external power supply and a computerized controller.

5.6 Summary and Concluding Remarks

Behavioural studies on the worms require full control of movement with the ability to characterize this phenotype in an automatic manner. The capability of inducing movement in a desired direction (DC electrotaxis) and to localize the animals at a specific location (AC electrotaxis) inside microfluidic environments can be very useful in such applications. Incorporating the electrotaxis screening method in movement-based microfluidic assays could help study diseases, screen for chemicals/drugs and examine their mechanism of action in the worms.

Development of microfluidic-based chemical screening platforms for nematode behavioural assays can only be achieved by the design and the automation of novel engineered devices that can perform unit operation procedures needed in such assays. These include the capability of sorting and manipulating the worms at a single-animal resolution, exposing them to chemicals controllably, and screening their post-exposure effects (cellular and behavioural) quantitatively. In this chapter, electrical signals were utilized to develop multiple microfluidic-based devices and techniques in order to sort the animals based on age and phenotype, sense them inside channels, inhibit their locomotion for behavioural studies and finally immobilize them for neuronal fluorescent imaging. Usage of electrical stimulus throughout these devices is advantageous as these signals are fast, accessible, controllable, amenable to multiplexing and HTS as well as viable to the worms.

Altogether, the devices and methods designed and developed in this chapter are well applicable to the development of microfluidic devices that can automatically study the worms' movement behaviour in an on-chip high throughput manner. The devices can be integrated in combinations to perform more complicated operations on the worms. For instance, the age-synchronized worms can be obtained by using the sorter device connected to an electrotactic screening chip equipped with position detector and immobilization modules. The worms can then be screened for their forward motion (DC electrotaxis), turning (pulse DC electrotaxis) and stop (AC electrotaxis) behaviours, and finally immobilized and imaged for their cellular level assay in a single chip. Although this was not the main goal of this thesis, but advancement of these devices, as done in this chapter, will pave the way for the development of automated systems for multifunctional worm-based assays in the future.

CHAPTER 6

6. Integrated Microfluidic Device for Nematode Chemical Screening by Electrotactic Movement Assay

Worms have been widely utilized in high throughput toxicology, pharmacology, and crop protection studies as discussed in Chapter 2. All these nematode-based chemical screening assays are conventionally done manually in multi-well plates. These assays are low in throughput and qualitative in characterization and analysis. Apparently, all these assays can benefit from the automation of various processes, such as worm manipulation and encapsulation, controlled chemical exposure and phenotypic screening afterwards.

Robotic screening systems have significantly increased the throughput of these assays as compared to manual methods. These systems can quickly pick and place nematodes with single-animal resolution into the well-plates, disperse chemicals automatically in a high-throughput manner and perform high content fluorescence based imaging of the worms. Movement screening has also been achieved in these studies through incorporation of the animals' locomotion monitoring by using software- and computer-based recording and analysis, as addressed before. However, this method is expensive as it uses large volumes of chemicals and need for robotic equipments making it in-accessible to the majority of researchers. Additionally, nematodes' movement in the liquid wells or on agar

plate is voluntary and uncontrollable as well as subjected to environmental effects such as chemical and temperature gradients. Therefore it is not suited for automated analysis. These challenges are addressable by microfluidic devices that are developed with lower cost, consume less chemical agents, are amenable to parallelization and provide controllable environments for the study of nematodes, as discussed in Section 2.5. For instance, Chung et al. [138] developed (Section 2.5.3) a multi-chamber microfluidic device that could capture individual worms, expose each to anesthetics and screen the effect on its body-bend frequency automatically inside the chamber. However, in this case, due to the compartmentalization of the worms inside the chambers for the entire duration of the assay, it was not possible to study other movement phenotypes, such as speed and turning time with this platform. These movement-based phenotypes provide valuable information about the physiological state of the animals, as discussed in Chapters 3 and 4. Therefore, development of automated worm assays that test and quantify these phenotypes is highly desired. Several electric-based microfluidic techniques and devices were developed in Chapters 4 and 5 of this thesis that are well-suited for the automation of the behavioural chemical screening assays on the worms.

6.1 A Microfluidic Device for Behavioural Chemical Screening on Worms

In this chapter, an integrated proof of principle microfluidic device is developed that is capable of manipulating the worms and compartmentalizing individual animals inside microchambers, where they can be controllably exposed to chemicals without the need for robotic automation. After exposure, electrotaxis method was used to screen the worms' movement on-demand and in terms of quantitative parameters, such as swimming speed, body bend frequency and turning time. The microfluidic platform also provided an isolated environment that was uniformly controllable in terms of external stimuli (chemical, temperature, fluid flow and electric field). This single channel device is easily scalable to thousands of channels, where movement-based chemical screening on nematodes can be done in a high-throughput manner. This platform can greatly facilitate toxicology, pharmacology and other chemical screening assays on the worms.

6.1.1 Device Design and Experimental Setup,

Schematic of the device design for the worm movement-based chemical screening is shown in Figure 6-1. As seen in Figure 6-1a, the device consisted of three modules: (i) animal manipulation (*worm suspension* and *collector* channels

as well as the *PDMS membrane valve and actuation channel*); (ii) chemical exposure module (*exposure chamber,* shallow *drug transfer channels* and the main *drug channel*); and (iii) movement screening module (*main channel* for electrotactic assay and side *electrodes*). The worms will be loaded into the device from the suspension channel. As shown in Figure 6-1b, the *collector channel* is shallower than the *suspension* and the *main channel*. This is to facilitate the loading of a single animal inside the *collector channel* at a time. Therefore, its dimensions have to be designed accurately. The worm will be exposed to the chemicals in the *exposure chamber* (Figure 6-1c). These chemicals are introduced into the device from the *drug channel,* infusing into the chamber from the side *drug transfer channels*. *Drug transfer channels* are designed with a depth that does not allow the passage of the encapsulated worm from the *exposure chamber* into the main *drug channel*.

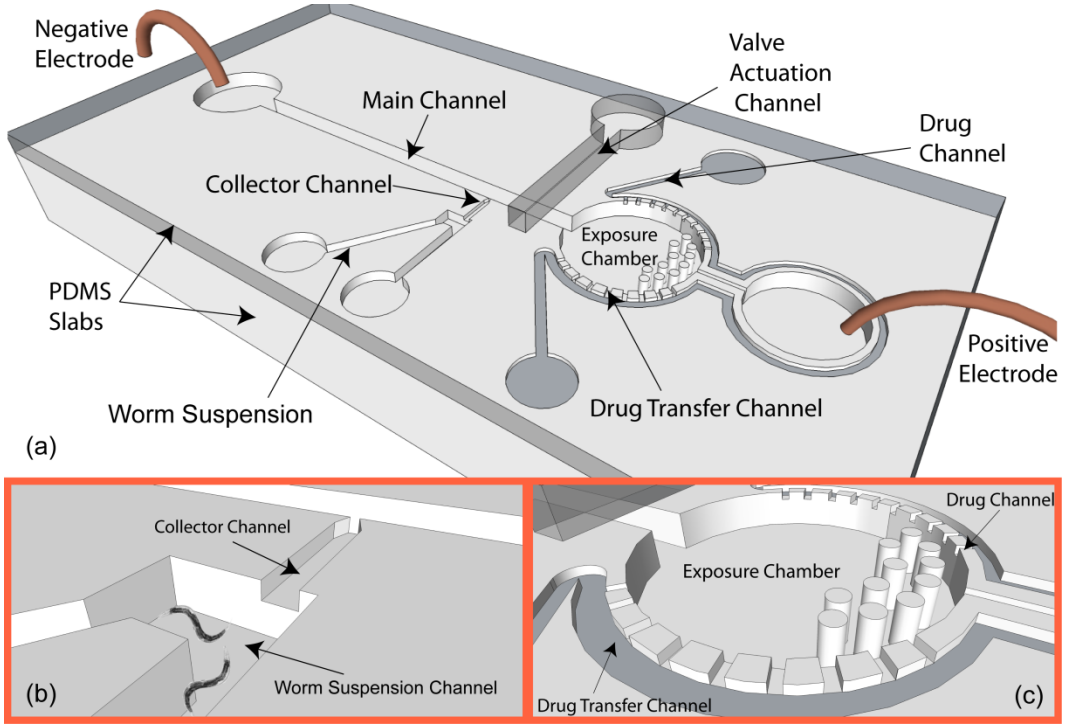

Figure 6-1 Schematic of the integrated chemical screening device, (a) the entire 3-layer device with the manipulation (PDMS valve, worm suspension and collector channels), drug exposure (exposure chamber, drug transfer and the main drug channels) and movement screening (main electrotaxis channel and side electrodes) modules, (b) close-up look at the collector channel interfacing the main and the suspension channels with reduced height for facilitating single animal loading, (c) the exposure chamber, side drug transfer channels (shallow) and surrounding drug channel for introducing the chemical into the device.

As shown in Figure 6-1b and c, the bottom layer of the device consisted of microchannels and chambers with three variable depths, one for the collector channel; one for the main channel, exposure chamber and reservoirs; and the

last for the drug transfer channels. As discussed in Section 3.3.2, multilayer photolithography with various photoresist thicknesses was used to develop the master molds (one for the bottom main layer with all modules and the other one for the top *valve actuation channel,* shown in Figure 6-1a) for this device. The side drug transfer and the worm collector channels were 25 µm and 40 µm deep, respectively (fabricated in 2 consecutive SU8-25 based photolithography steps). The *main* electrotaxis *channel* (0.3 mm wide), the worm *suspension channel*, and the *exposure chamber* (2 mm diameter) were all ~0.1 mm deep (fabricated altogether in a third SU8-100 based photolithography step). The thicknesses mentioned above were designed in order to fit a single worm in the *collector channel*, to freely let the worm swim in the *main electrotaxis channel* and the *exposure chamber*, and to prevent the worm to escape to the main *drug channel* through the side *drug transfer channels*. PDMS prepolymer (10:1 ratio of base to agent volumes of the Sylgard 184 kit, Dow Corning) was cast over the two molds and peeled off, as described in Section 3.3.2. In the fabrication of the valve membrane, PDMS prepolymer was spun at 4000 rpm on a transparency sheet (20 µm thickness achieved, as shown in Figure 3-3) and bonded to the valve actuation layer by plasma oxidation and, then, to the main layer . Details of the fabrication are described in Section 3.3.3. Input and output fluidic tubes were then installed and electrodes were inserted into the end reservoirs of the device and connected to a 2636 model Keithley DC power supply. The chemical exposure and animal manipulation modules of the fabricated device are shown in Figure 6-2a. Figure 6-2b shows the 2D side-view schematic of the device (dashed black line illustrated in Figure 6-2a). The experimental setup used in this study was described and shown in Section 3.4 and Figure 3-4. Similar to all other experiments, the tests were all performed under a stereo-microscope connected to a digital camera (Figure 3-4) used to record the experiments in a video format for post-experimental image analysis to extract the movement phenotypes of the worms.

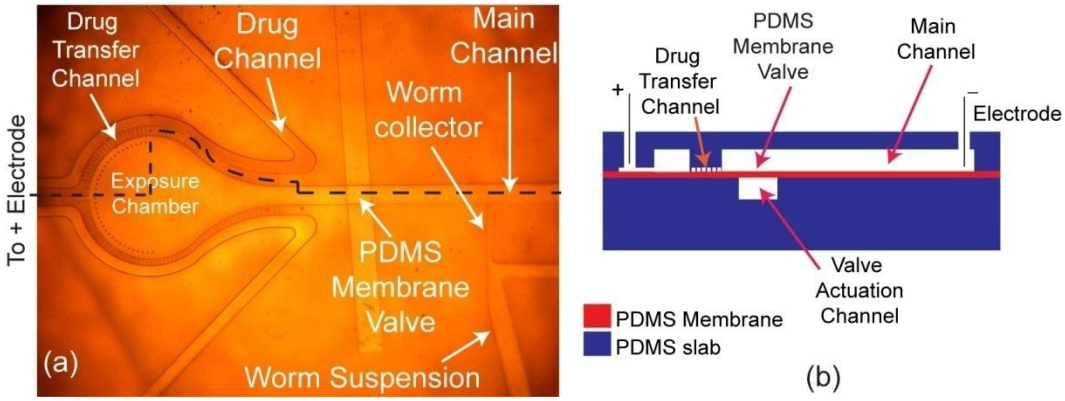

Figure 6-2 Fabricated integrated chemical screening device: (a) Optical image from the device showing (b) Schematic of side view of the black dashed line in (a)

6.1.2 Integrated Microfluidic Chemical Screening Device – Module Characterization

In this section, operation of the device at each of the three modules, described above, is discussed in details.

6.1.2.1 Animal Manipulation Module

Behavioural studies on worms at a single animal resolution are of great interest to biologists. For this, individual worms have to be isolated from a population automatically in an integrated chemical screening device. Therefore, the worm manipulation module, shown in Figure 6-1a and b, was designed and used to select one worm from a suspension of the synchronized animals and to load it into the exposure chamber pneumatically. The worm strain used in this study was *C. elegans* N2 young adults (62 hr post-L1), grown and synchronized, as discussed earlier in Section 3.2.

The operation of this module was straightforward, as it only required insertion of the worms into worm suspension channel using a syringe at a fixed flow rate (0.5 $ml.min^{-1}$, Figure 6-3a) in order to trap an individual worm in worm collector channel (Figure 6-3b). The collector channel was designed with such a depth (36 µm) and length (0.9 mm) that it would trap only one worm. The collector channel was wider (~70 µm) at the inlet (connected to worm suspension channel) and narrower (~30 µm) at the outlet (connected to the main channel) (Figure 6-1b). The flow rate used to load the worms was sufficient to introduce one worm into the collector channel, but was not high enough to push the worm out from the other side, thereby trapping a single worm (Figure 6-3c). Once the worm was trapped, the resistance to flow in the collector channel increases, redirecting the rest of the flow to the outlet of the suspension channel. The remaining worms in the suspension channel was flushed out and collected for use in the next round of loading. Subsequently, a short pneumatic pulse in the cleared suspension channel inlet resulted in the ejection of the trapped worm from the worm collector channel and into the main channel (Figure 6-3d). At this stage, a continuous flow in the main channel towards the exposure chamber transferred the worm to the chamber. The pillars in the chambers were used to prevent the worm escape from the chemical exposure chamber into the side electrode channel. The PDMS membrane valve was then closed (by pressurizing the valve actuation channel to 20 psi using an external solenoid valve) to prevent the worm escape from the exposure chamber (Figure 6-3e).

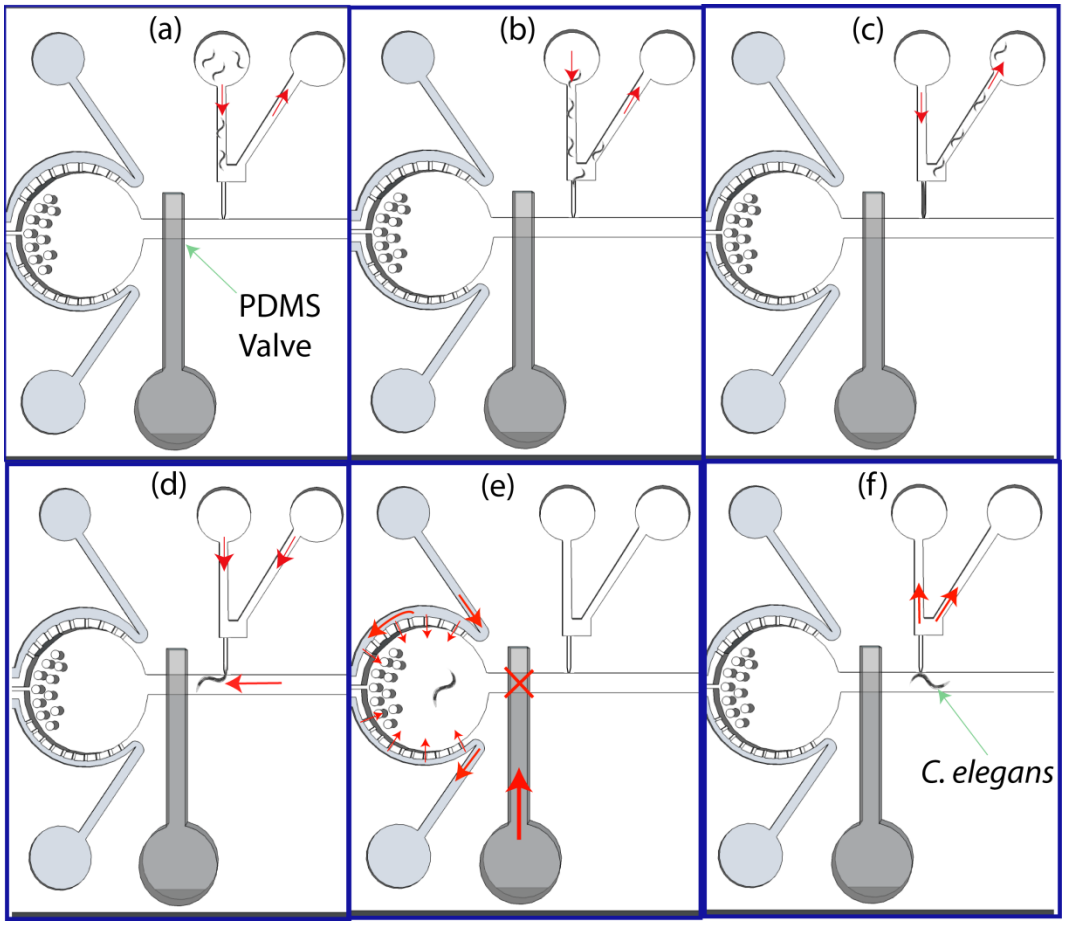

Figure 6-3 Sequential schematic images of loading an animal from the suspension channel into the exposure chamber, red arrows show the direction of flows. (a) Population of worms introduced inside the suspension channel; (b) One worm getting trapped in the collector channel; (c) Trapped worm being inserted into the collector channel by continuous flow in the suspension channel; (d) Washing extra worms out of the suspension channel; (e) Pressure pulse in the suspension channel ejecting the trapped worm into the main channel; (f) Transferring the worm into the exposure chamber and closing off the valve for introducing the drug inside; (g) Suction at the suspension channel after worm exposure to bring the animal back to the main channel for electrotactic assay.

The system was investigated for integrated and continuous functionality. For this purpose, a group of worms were loaded in a 10 ml syringe and introduced into the worm suspension channel using a syringe pump. The worm collector channel (narrower and thinner than the main and the suspension channels) only accommodated one worm at a time as shown in Figure 6-4a and b. As soon as one worm was trapped (Figure 6-4b), the rest of the animals were guided to the output of the suspension channel, until there were no worms left (as discussed above) and the collected animal was completely trapped (Figure 6-4c). The suspension channel was then pressurized further to push and load the animal to the main channel (Figure 6-4d) and position it into the exposure chamber by a

flow in the main channel (Figure 6-4e). The PDMS membrane valve was then closed to prevent the worm from escaping the exposure chamber, as discussed before.

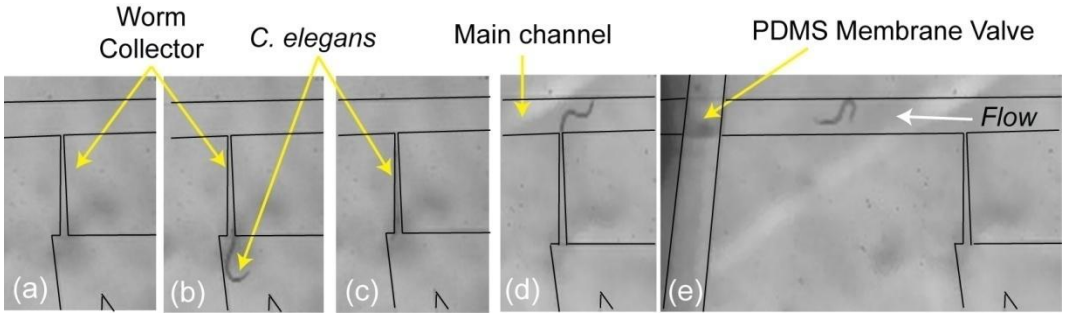

Figure 6-4 Collection (a and b) and loading (c-e) of one worm into the exposure chamber of Figure 6-2a. Channel walls were highlighted with black lines for enhanced visualization.

The device was capable of successfully collecting single animals from a population and encapsulating them inside the designated chamber for chemical exposure (success rate of 100% by test-loading 10 YA animals). In addition to individual animals, a controlled number of worms could also be isolated one by one from the suspension and into the chamber. Since the operation was performed semi-automatically (manually activating and deactivating operational solenoid valves by switches), the rate of loading for a single animal was approximately one minutes, from the animals' introduction into the suspension channel to one being encapsulated in the exposure chamber. This rate can be accelerated to a few seconds, if the operation of the solenoid valves were to be computerized.

As one of the main advantages of the presented device, the entire operation is also easily expandable to higher number of manipulation modules all connected to the same suspension channel to encapsulate multiple worms in an array of screening modules. This would facilitate performing chemical screening in a higher throughput manner. This was avoided as only a proof of principle device was aimed to be demonstrated in this chapter.

6.1.2.2 Chemical Exposure Module

Chemicals can be administered to the worms through ingestion, injection or body exposure. The technique envisioned to be used in this thesis for chemical delivery was aimed to be amenable to multiplexing and parallelization for HTS in the future. Injection of the worms in the laboratory is mostly done by immobilization of the animals on cover slip glasses and using micro-needles, controlled spatially by precise XYZ microcontrollers, to inject the animals. This process is labour-intensive and time-consuming. Although microfluidic devices can be used to inject the worms; but, this requires high level of automation and

design of actuators on a chip, which is more complicated to perform and integrate at a high-throughput level. Therefore, body exposure and absorption as well as possible ingestion of the chemical by the worm were identified to be the most suitable options for chemical administration in the design of the integrated device in this chapter. This method is easy to develop, can be integrated with the existing high-throughput chemical preparation systems by using proper fluidic interfaces and can also be potentially multiplexed from a single unit to hundreds for HTS.

In chemical screening assays on the worms, it is important to control the dose exposure of the animals. Precise dosing was performed by accurately controlling the exposure time of the worm to a chemical solution at a fixed concentration in the drug exposure module. This exposure module consisted of an *exposure chamber* to hold the collected worm and the *drug channel* surrounding the *exposure chamber* to introduce the chemicals into the chip (Figure 6-1c). The *drug channel* was connected to the *exposure chamber* through an array of thinner *drug transfer channels*. These channels were thinner than the *drug channel* and the *exposure chamber* to prevent the worms from escaping out of the chamber, but, allow the introduction of chemicals from the *drug channel* into the *exposure chamber* pneumatically. After loading individual worms into the exposure chamber (Figure 6-4), the chemicals could be introduced into the *drug channel* (and eventually to the *exposure chamber* through side *drug transfer channels*) as shown schematically in Figure 6-3e.

To test the efficiency of this design to transfer chemicals into the *exposure chamber* and its spatiotemporal concentration uniformity, the entire device was initially filled with M9 solution (Figure 6-5a), while time-lapse images from the *exposure chamber* were continuously acquired. Blue color dye (0.15 g of Methylene blue powder, SIGMA ALDRICH, MO, USA) was dissolved in 10 mL of M9 buffer (with its concentration used as the reference concentration) in a separate syringe and introduced into the *drug channel* at a flow rate of 1 $mL.min^{-1}$ using a syringe pump. Figure 6-5b-d illustrates the transition of drug concentration from 100% M9 to 100% methylene blue over 6 s. After this, pure M9 solution was introduced again into the *drug channel* similarly to exchange the solution inside the chamber to its initial M9 state (data not shown due to similarity).

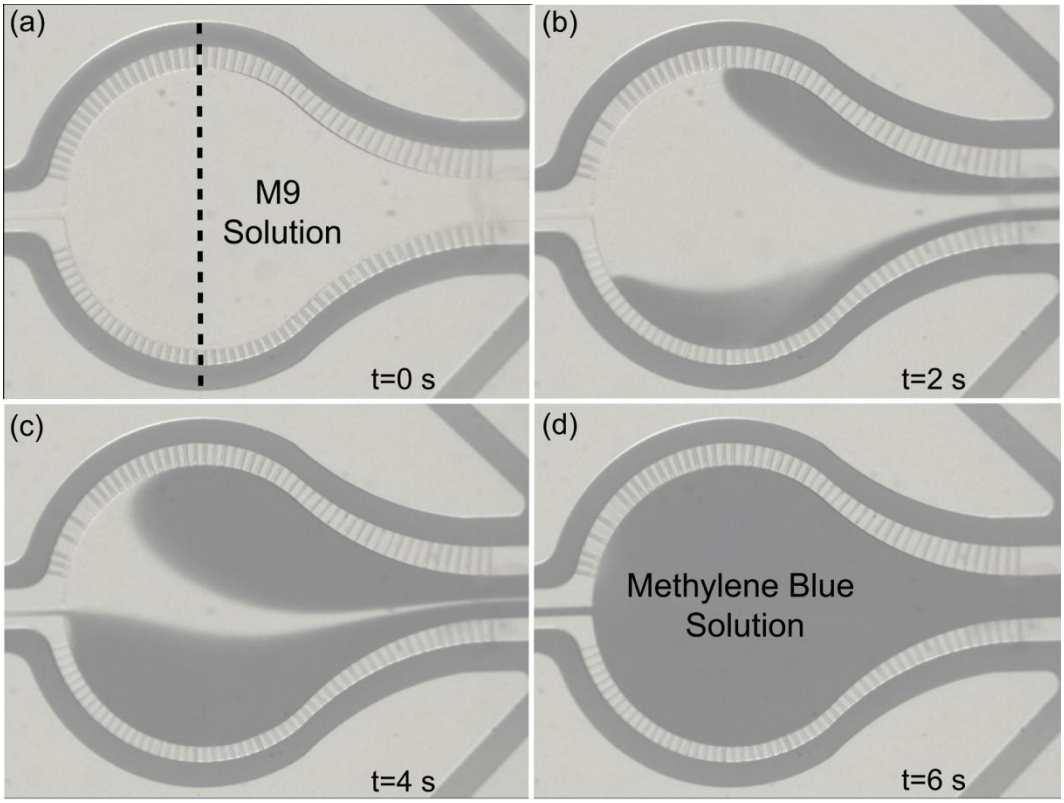

Figure 6-5 Spatiotemporal chemical concentration uniformity in the exposure chamber using methylene blue dye in M9 as the drug model; (a) pure M9 (no flow in drug channel), (b-c) 1 mL.min^{-1} methylene blue flow in the drug channel and concentration transition from pure M9 to methylene blue in the chamber, (d) pure methylene blue solution reached within 6 s. Dashed line in (a) was used to measure the intensity of light across the diameter of the exposure chamber.

ImageJ software was used to analyze the images obtained in Figure 6-5 for assessing the concentration of the transferred chemical into the chamber, as shown in Figure 6-6. Intensity of gray light across the dashed line in Figure 6-5a (diameter of the *exposure chamber*) was measured for this purpose.

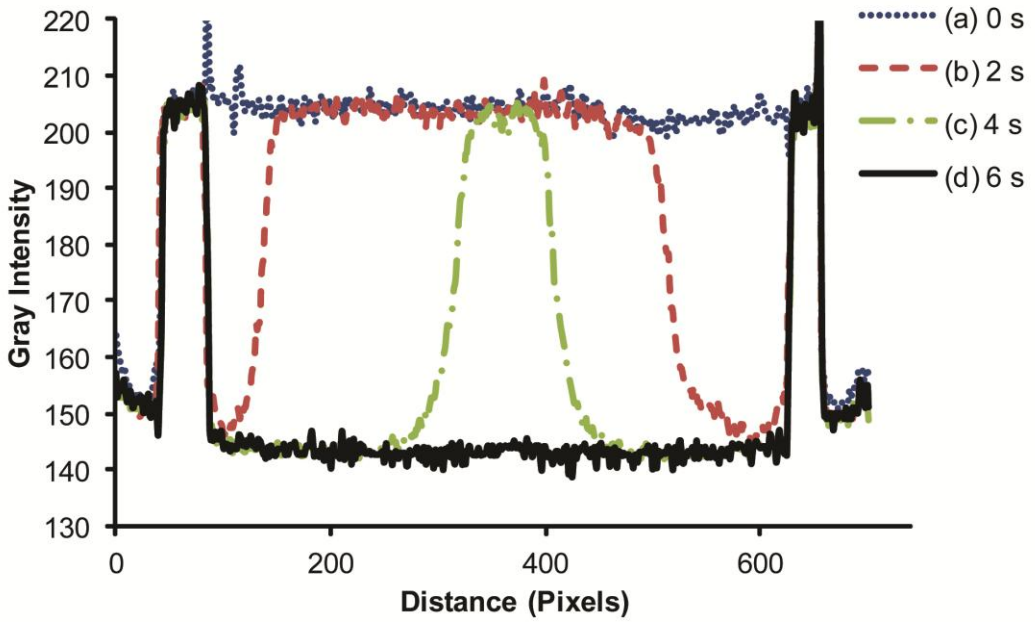

Figure 6-6 Chemical concentration uniformity curves across the exposure chamber diameter (interpreted as gray color intensity analyzed by ImageJ across the dashed line illustrated in Figure 6-5a)

As can be seen in Figure 6-6, the intensity of the light in the *drug channel* (beginning and end of each curve) remained constant at all times as expected. By introducing the methylene blue solution, the intensity of the light inside the exposure chamber and at its peripheral (2 s and 4 s curves) started to drop to that of the drug channel. Finally, at 6 s, the intensity of the light inside the chamber was constant and uniform across the diameter and equal to that of the drug channel. These results demonstrated that the device is capable of transferring chemicals into the exposure chamber in a well spatiotemporal-controlled manner. The concentration of the *exposure chamber* content could be exchanged completely within 6 s from M9 to the target chemical and vice versa (data not shown).

6.1.2.3 Movement Screening Module

The movement screening module was used to quantitatively study the worms swimming behaviour after exposure to the chemical. First, the PDMS valve, between the exposure chamber and the main channel was opened and suction was applied at the worm suspension channel. This process transferred the exposed worm from the chamber to the main screening channel (schematically shown in Figure 6-3f). After this, any external flow in the main channel was

minimized by levelling all the input and output tubes such that there was no hydrostatic pressure difference between them. Then, a 3 $V.cm^{-1}$ electric field (selected based on the age of the animal and the previous electrotaxis results in Figure 4-5) was applied across the channel to induce electrotaxis. The animal was allowed to swim for 8 mm after which the direction of the electric field was switched and the rotation time of the worm was examined (similar to electrotaxis assays in Chapter 4). This was repeated two more times to obtain the average movement characteristic values. The entire assay was recorded in a video format. Animals' response was then analyzed, as discussed in Section 3.5.1, for the extraction of swimming speed, body bend frequency and turning times.

Using the procedure discussed above, more than 20 young adult *C. elegans* worms were recollected from the chamber as shown in Figure 6-7(a1-a2) in less than a second after opening the PDMS membrane valve. The applied electric field discussed above induced electrotaxis in the worm (Figure 6-7(b1-b6)) similarly to the experiments done by the simple *behavioural chip* examined in Chapter 4.

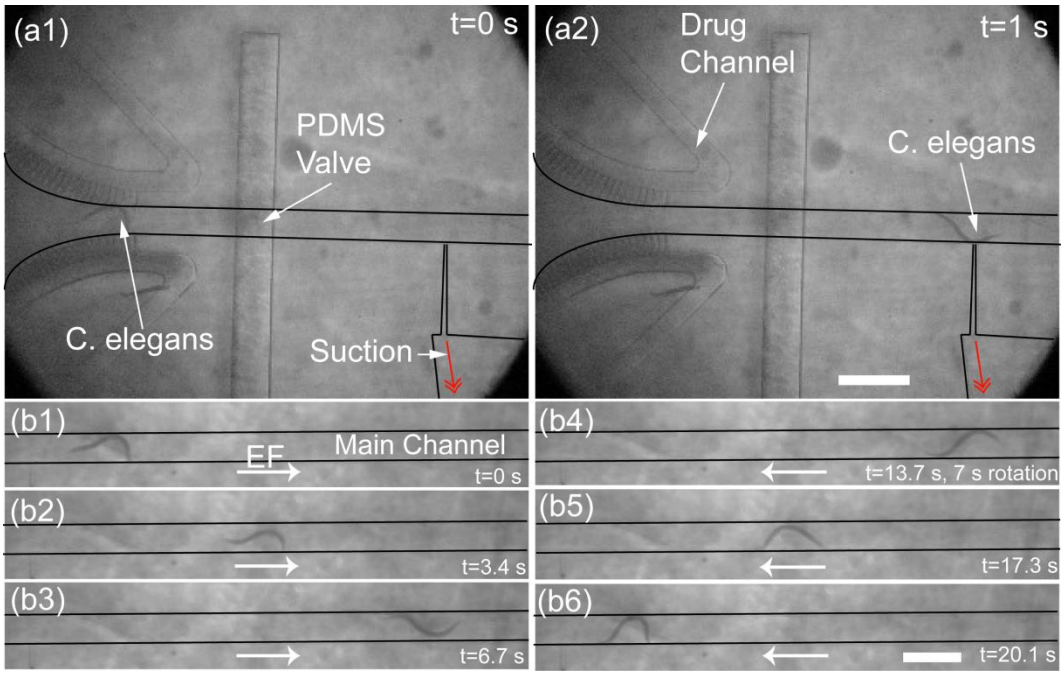

Figure 6-7 Experimental results for characterization of the movement screening module; (a1-a2) Applying a suction at the worm suspension channel transfers the worm in 1 s from the exposure chamber to the main channel for (b1-b6) the electrotaxis assay. Electric field (EF) of 3 $V.cm^{-1}$ was used from left to right (b1-b3) and from right to left (b4-b6). Average speed of 490 $\mu m.s^{-1}$ and rotation time of 7 s was measured after video analysis. Scale bars are 0.6 mm.

The results from these experiments concluded that the worm manipulation module described in Section 6.1.2.1 could successfully encapsulate worms without affecting their electrotaxis behaviour after being passed through the

narrow collector channel. This was because their speed and rotation times were similar to the ones obtained in Figure 4-5. Therefore, the device could have been used to perform the actual chemical exposure and electrotactic screening in the next step.

6.2 Exposure to Sodium Azide and Electrotactic Movement Screening

As a proof of principle test to demonstrate the operation of the integrated device, individual young adults (N=5) were collected and compartmentalized inside the chamber individually, as illustrated in Figure 6-4. A 1 mM sodium azide solution was prepared and introduced into the drug channel at a 1 $mL.min^{-1}$ flow rate. As shown in Figure 6-5, this process resulted in the immediate transportation of the chemical into the exposure chamber through the side *drug transfer channels* (Figure 6-1c) with a uniform concentration achieved rapidly in the chamber. The worm was exposed for 1 minute after which the contents of the exposure chamber were exchanged again with M9 buffer solution. This was continued for 30 s (although it only took 6 s to empty the chamber, washing was continued for 30 s to ensure a complete ejection of the chemical) to ensure ejection of the sodium azide completely from the device. According to Figure 6-6, it only took a few seconds to entirely change the content of the chamber, so the 30 s washing procedure was sufficient to make sure the device was cleared of the injected chemical. Then, as discussed in section 6.1.2.3, the exposed worm was transferred to the main screening channel and its electrotaxis behaviour was assayed under a 3 $V.cm^{-1}$ electric field condition. Figure 6-8 illustrates the results for N=5 young adults exposed to 1 mM of sodium azide solution for 1 min in comparison to the control young adults (N=5), which were only introduced into the chamber, kept for 1 min and electrotactically assayed with no chemical exposure. Videos obtained from the experiments were analyzed as discussed in Section 3.5.1.

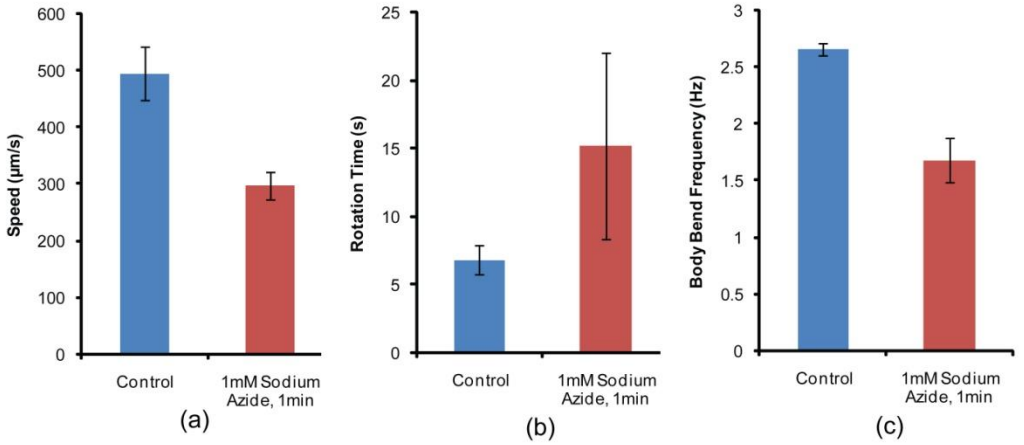

Figure 6-8 Exposure of young adults (N=5) to sodium azide (1 min) and its effect on (a) swimming speed, (b) rotation time and (c) body bend frequency in comparison to control young adults (N=5) which were not exposed to chemicals and only passed into the device

As shown in Figure 6-8, swimming speed, body bend frequency and turning time of the control group (passed through collector channel) were all comparable to those obtained for the animals tested in Chapter 4 for electrotaxis. These results demonstrate the successful operation of the integrated device for loading, chemical exposure and electrotacic screening of the worms. The swimming speed of the exposed animals was reduced on an average by 40% upon exposure to 1 mM sodium azide for 1 min (Figure 6-8a). Similar reduction was also observed in the body bend frequency of the animals while swimming (Figure 6-8c). The turning time of the worms in response to a switch in the electric field direction approximately doubled, as shown in Figure 6-8b.

6.3 Summary and Concluding Remarks

The results demonstrated that the integrated screening device has the capability of manipulating the worms, exposing them to chemicals at a single animal resolution with perfect spatiotemporal control and finally screening their movement quantitatively and on-demand. Sodium azide is used in the laboratory for immobilizing the worms at sufficiently high concentrations. In this work, it was demonstrated that the effect of a 1 min exposure to a low concentration 1 mM sodium azide solution can be measured electrotactically in terms of the reductions in speed and body bend frequency as well as an increase in the turning time of the young adult animals in the channel. Although this work has been done as a proof of principle study, this device can be used in any study where the effect of chemical compounds on worms is sought at a behavioural level. This includes applications from assessing toxic substances to screening drug libraries against the worm disease models. As one of the main advantages,

when compared to other behavioural microdevices where the worms are screened inside confined microchambers, this device provides additional parametric information such as speed and rotation time of the worm. The worm can also be extracted from the chip after exposure and movement screening for other biological assays or re-screened in the device at later developmental stages which is usually sought in the age-based studies.

The device can be improved significantly in the future for more enhanced functionality, robustness and automation. The subcomponents and methods developed in Chapter 4 are generic and were designed to be used as the building blocks of the microfluidic drug screening device in the future (Figure 2-9). Some of the components that can be integrated into the microchip investigated in this chapter are the electrical position detectors (Section 5.3) and an immobilizer (Section 5.5). Both of these components can be added to the movement screening module of the chip inside the main channel (Figure 6-2a). As discussed before, two position detectors in the beginning and at the end of the electrotactic runway can be used to measure the speed of the worm automatically without the need for video recording. Design and development of advanced detectors, as discussed before, can also lead to the measurement of additional movement parameters, such as the body bend frequency. Electrical immobilization method can also be used to image the animals in the main channel, after the movement screening, for cellular level phenotypic studies.

With the techniques and components developed in this thesis, it is not far from reality to envision the development of platform device illustrated in Chapter 2 (Figure 2-9) in near future. All the pneumatic (this chapter) and electrical (Chapters 3 and 4) components of this device have been developed as stand-alone units. Interfacing these devices in a few different combinations can lead to the development of semi- and fully-automated microfluidic chips for behavioural and cellular based chemical screening on nematodes.

CHAPTER 7

7. Summary and Recommendations for the Future Work

7.1 Summary of the Thesis Work

Although *in vitro* studies on different biological cell lines have provided us with valuable information about the functionality of chemical compounds in the process of drug discovery, they ignore the complexity of biological processes in the context of multi-cellular organisms that involve interactions between different types of cells and tissues. Therefore, they often fail to produce desired results in subsequent animal and human trials. Consequently, animal models that can better mimic the human biological processes are sought to perform various steps of the drug discovery and development process, such as administration, distribution, metabolism, and toxicity. Although large mammals such as monkeys and mice are closer to humans evolutionarily and therefore are better models biologically, they are difficult and expensive to breed and maintain in the laboratory. In addition, they grow slowly and are not conducive to high throughput experimentation. Therefore, other animal models that are less expensive to cultivate and are more suitable for high throughput experimentation are sought in these studies.

Nematodes (i.e. *C. elegans*, *C. briggsae*) are among the most widely studied small organisms for high throughput biomedical researches. They grow fast on

Petri dishes in the laboratory, are small and well amenable to high throughput assays, survive in liquid media and can be exposed and screened against chemicals and most importantly, have been researched extensively and modeled for various human diseases as well as used in other applications such as toxicology and crop protection. Given that the worm's genome containing many human disease gene orthologs, and several of these mediate conserved biological processes, it could accelerate identification of potential drug targets, thereby facilitating testing in mammal animal models, and eventually in humans. Furthermore, *C. elegans* offers advanced genetic and genomic tools to identify drug action and potential side effects that could be utilized to accelerate the process of drug discovery. Despite being widely used, nematodes are difficult to handle due to their small size and to assay due to their inherent movement which is challenging to control.

Manual methods for handling these animals on Petri dishes, treating them with biochemical compounds and screening them are only suitable for lower throughput studies. The lack of a robust automated high throughput method to quantify behavioural and cellular changes has hampered the widespread use of nematodes in these kinds of assays. Over the years, many protocols and tools have been developed to handle worms in a higher throughput fashion inside multi-well plates or as standalone platforms. All of them have shown promise and continue to evolve to meet new challenges and overcome shortcomings. Among these are the robotic and the microfluidic methods. They offer many advantages to address instrumentation issues and bottlenecks in high throughput fundamental and applied biology.

The robotic methods utilize animal immobilization and laser-based excitation and detection for phenotypic studies on nematodes. Although they can reach very high throughput levels in experiments, they are expensive and are not suited for performing behavioural assays on worms. In recent years, several new applications of microfluidics in *C. elegans* have emerged that include phenotypic sorting, cell ablations, drug exposure, and behavioural studies [11-14, 117, 118, 204]. Because of their focus on imaging cells and/or certain regions of the worm, they mostly rely on pneumatics to immobilize animals. These devices have been successful in automating some steps and providing an increased throughput that is not possible with traditional manual approaches. While advantageous in many applications, most of them are not suitable to study movement behaviours of worms. In cognisance of this situation, instrumentation required for performing behavioural chemical screening on worms using post-exposure assaying of their movement was developed in this thesis.

To perform assays at a behavioural level, a stimulus-based microfluidic approach that can control movement was found suitable. Among various stimuli

that nematodes respond to, electric field was found to be the most promising one due to a number of factors such as easy and inexpensive setup, instantaneous on/off control, no gradient or decay over time, compatibility with liquid culture media, viability, scalability, and the ability to induce movement in a desired direction without sensory adaptation.

Electric field was demonstrated as a powerful stimulus to control movement of worms (*C. elegans* and *C. briggsae*) in a microfluidic environment. First, the response of the worms to DC electric field was fully characterized. A low-voltage DC electric field (2-13 $V.cm^{-1}$) in the axial direction of a buffer-filled microchannel was shown to stimulate animals to move toward the negative pole (electrotaxis) [15]. This response was quantified in terms of speed of swimming, body bend frequency and turning time in response to electric field direction reversal. While the speed of movement increases, as animals grow older, for a given stage it is independent of the electric field strength. Changing the direction of the electric field causes the animals to immediately turn back and resume motion in the reverse orientation with an average turning time of less than 15 s. This behaviour appears to be primarily mediated by neurons, and to some extent muscles, since mutations affecting these cell types failed to show a normal response. Any such defect can be quickly revealed in the microfluidic assay in the form of reduced speed, altered body bends, and sporadic pauses. Most importantly, the electrotactic response was fully penetrant, immediate, and highly sensitive. Additionally, evidence was provided that the exposure to the electric field has no discernible effect on the ability of animals to survive and reproduce.

Second, the response of the worms to pulse DC electric field was also characterized. It was found that worms responded to pulse DC signals with as low as 30% duty cycle (f =1 KHz) by moving towards the negative electrode at the same speed as constant DC fields. The speed was independent from both duty cycle and frequency for the responding worms. *C. briggsae* was found to be more sensitive to electric signals compared to *C. elegans*. Time taken by the worm to turn in response to a turning electric field was also measured as a behavioural response. The turning response was spontaneous for a DC electric field and similar for most of the worms, however, a pulse DC signal resulted in variable turning response in them [16]. The electrotactic reversal response of worms to pulse DC signals of various frequencies (1-1000 Hz) and duty cycles (10%-90%) inside a microfluidic channel device was investigated. Moreover, alterations in duty cycle and frequency affected the turning response time as well as the number of responding worms. Worms appeared to respond faster to higher duty cycles at all frequency levels. However, it was interestingly observed that the turning response to frequencies close to 5 Hz significantly hinders while

lower and higher frequencies resulted in faster and more robust responses. This behavioural observation encouraged further investigations at a neuronal level.

Third, the behavioural response to electrical stimulus was correlated to the molecular functioning of its neurons and investigated in significant detail. The firing of the ASH neuron (a polymodal amphid neuron that responds to multiple sensory cues including electric field activity) and its activity was measured using the FRET assay as previously reported by Chokshi et al. [195]. It was found that the ASH response was slower at frequencies near 5 Hz range which corresponds with the results obtained in the behavioural screening assay. This finding suggests that neuronal activities can be correlated with animal's behaviour and can be used as an important tool to probe the functions of genes and pathways that mediate such behaviour. The fundamental techniques developed here are amenable to parallelization and hence can be applied to HTS applications. These findings also suggest that the microfluidic electrotaxis approach could serve as a powerful tool to facilitate high-throughput study of *C. elegans* disease models, identify molecular changes and genetic pathways, and screen for chemicals/drugs as candidates for potential treatment options.

Therefore, the next part of this thesis explored the development of various components for high throughput experimentation using worms and put them together in an integrated screening system for automated chemical exposure and assaying of these worms. Such a system has a wide application in drug discovery, toxicology, neurobiology, crop protection, etc.

First, with the use of the recent understanding of differential response of worms of various ages, mutations, and sizes to electric field, an automated sorting device was designed and tested. Using local electric field traps in a microfluidic device, worms have been efficiently sorted from a mixed culture in a semi-continuous flow manner (with a minimum throughput of 78 worms per minute per load-run) and synchronized populations of animals were obtained. In addition to sorting larvae, the device could also distinguish between young and old adults efficiently. Unlike fluorescent based sorting systems that use active imaging based feedback, this method is passive and automatic and uses the innate behaviour of the worm. Considering that the entire procedure takes only a few minutes to run and is cost-effective, it promises to simplify and accelerate experiments requiring homogeneous cultures of worms as well as to facilitate isolation of mutants that have abnormal electrotaxis. More importantly, this method of isolating and separating worms using locomotion as a defining characteristic promises development of advanced microfluidics-based systems to study the neuronal basis of movement-related defects in worms and facilitate high-throughput chemical screening and drug discovery assays.

Second, the electrotaxis movement described above was mostly analyzed by video recording and image post-processing methods. However, in order to develop this method further into a stage that it can be applied to HTS assays, it was required to analyze worms movement on the chip. To facilitate this, an on-chip position detection sensor was designed and developed. Electrical impedance sensors were chosen as the most suitable to sense the presence of freely moving worms at designated locations as they are easier to fabricate and amenable to multiplexing. A Wheatstone bridge was incorporated to increase the sensitivity of the sensor. The electrical sensing mechanism was synchronized with the electrotaxis driving field in the main channel by taking advantage of the pulse DC electrotaxis technique. While the pulse DC signal drove the electrotactic movement, the sensing was done during the off-time cycle of the signal. This can eventually lead to electrotactic screening channels with two on-chip detectors for measuring the movement properties such as the speed and body bend frequency of the worm.

Third, AC electric fields were used to localize and position the worm in a specified region inside the microchannel. Symmetric square-wave AC fields of 1 Hz frequency and higher were found to effectively localize worms in the channel.

While AC electric field is ideal for localizing the worms, it is not perfectly suited for imaging as the worms still wiggle at the same location. Imaging the worms is frequently needed in most of the assays and it demands for a robust immobilization of the animal. For this purpose, application of a high strength but very short electrical pulse was investigated as a method to immobilize the worms for fluorescent-based neuronal imaging. Effect of various pulse strengths, durations and numbers on immobilization was studied. More interestingly, it was demonstrated that although these pulses completely immobilize the worms for a period of time, the animals are able to recover on an agar plate afterwards and survive for a few days. However, their rate of reproduction was increasingly affected with increase in the pulse strength or the number of pulses.

Finally, the components described above and discussed in the thesis chapters are essential to the development of an integrated microfluidic system that can automatically screen the effect of chemical compounds on worms in a high throughput manner and also at a behavioral level. To show a proof of principle of a simplified version of this system, a single channel chemical screening device was developed. The device was capable of selecting an individual worm out of a populated suspension, manipulating and compartmentalizing it in an exposure chamber, exposing it to a controlled amount of a chemical compound, and finally screening the effect of that compound quantitatively on animal’s swimming behaviour using the on-demand electrotaxis assay. This system is precise, automated and most importantly can be scaled up

to hundreds of units on a single chip for HTS. Other components developed in the thesis (i.e. electrical sorter, detector and immobilizers) can be integrated with this device in order to develop an envisioned fully automated chemical screening platform. A schematic of such a system is illustrated in Figure 7-1. The device is highly similar to the single channel screening device discussed in Chapter 6, however, instead of a single animal; it can compartmentalise and expose several worms simultaneously. After the exposure, the animals can be arrayed pneumatically inside the parallel assay channels and electrotactically screened in a medium to high throughput manner (dependent on the level of multiplexing). A worm sorter can be added before the assay loading port in Figure 7-1 and position detectors, localizers and immobilizers can be added to individual assay channels for automation.

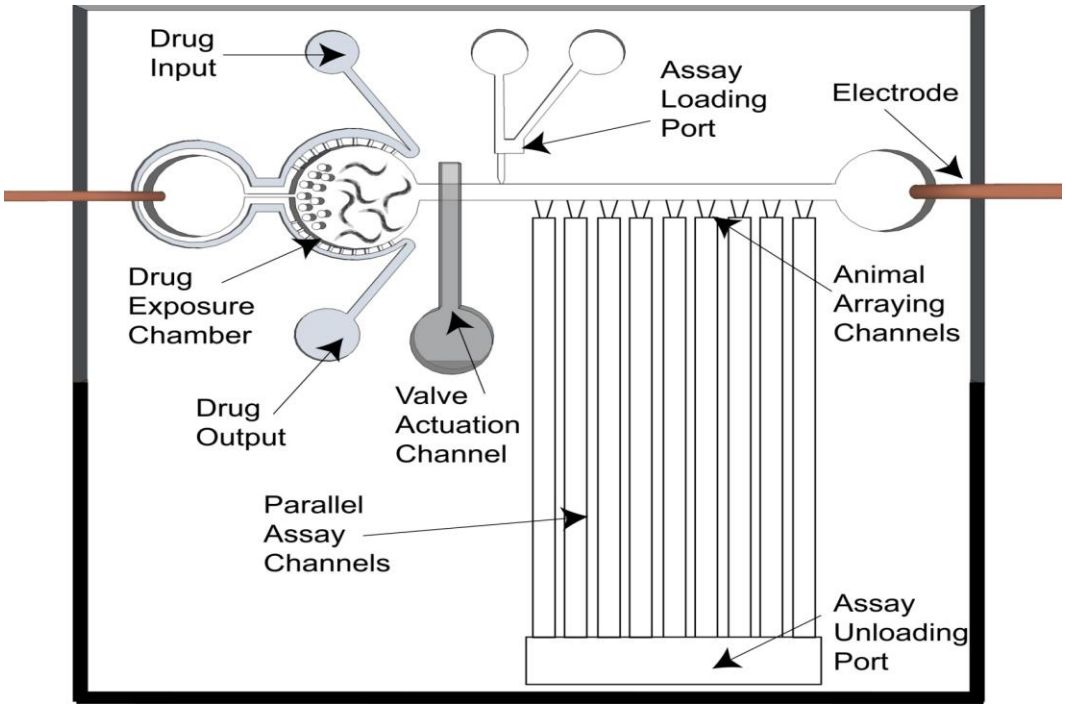

Figure 7-1 Schematic of an envisioned integrated medium throughput microfluidic chemical screening system

7.2 Research Contributions

Research contributions to the body of the existing knowledge are both at fundamental and applied levels as discussed below.

7.2.1 Nematodes Electrotaxis for Full Movement Control and Quantitative Analysis

Electrotaxis was demonstrated for the first time inside microchannels and was found to be a robust, repeatable and reliable for behavioural characterization of the worm. This behaviour was fully characterized for various DC, pulsed DC and AC signals. A new electrotaxis-based assay for behavioural screening has been developed. Since the microchannel format provides a unidirectional path for movement with uniform electric fields in an isolated environment, it could be used extensively to study different movement phenotypes of worms. Not only these phenotypes could be observed qualitatively, they could also be quantified in terms of swimming speed, body bend frequency and turning time at a single animal level. DC electric fields were used to assess forward motion while pulse DC signals were more useful in examining worms turning behaviour and their sensitivity to electric fields. Some key findings were that the speed of the worm undergoing electrotaxis was independent of the electric field but their turning response was highly dependent on the frequency of the signal being applied.

7.2.2 Development of a Correlative Neuro-Behavioural Assay

Turning response time of worms to a full reversion of a pulse DC electric field in the microchannel was found to be highly dependent on the duty cycle and the frequency of the signal. While a 5 Hz frequency pulse DC signal (50% duty cycle) resulted in a very late or even no electrotaxis response in the channel, higher or lower frequencies resulted in faster and more robust electrotactic responses. This phenomenon was demonstrated to be correlated with the ion transient signals in the ASH neuron (an amphid neuron that is responsible for electrosensation) in worms using a FRET-based assay. Therefore, the pulse DC behavioural assay could now be used to assess neuronal functioning in worms where individual neurons can be knocked out and examined for electrotaxis. This can facilitate assays studying neuronal activities and pathways in electrotaxis.

7.2.3 Age-Based and Phenotypic Sorting of Worms

DC electrotaxis assays showed that this behaviour is variable among different stages of worms. This fundamental discovery was used for the first time in electrically sorting the worms. Younger nematodes are less sensitive to electric fields and respond to stronger fields as compared to older animals. Microfluidic devices were constructed that contained regions of high electric fields that acted as valves to which worms of different stage responded differently. Using this method, worms of varying ages and mutations were sorted and separated. This

is useful in assays where synchronized-age animals are required (almost all assays) which can save significant amount of time and resources when compared to conventional methods. Additionally, this technique has the potential of being applied in mutagenesis assays where extraction of electrotactic-defective mutants is sought.

7.2.4 Micro-Electro-Fluidic Techniques for Immobilizing Worms

A new electrical technique for worm immobilization was developed to facilitate imaging assays. Most of the conventional immobilization methods (using anesthetics or glue) are non-reversible, uncharacterized chemically, and time-consuming for the users. Microfluidic methods developed in the literature operate on the basis of dynamic micromechanical parts or by confining the channel geometries. These devices are more difficult to fabricate and are complicated to operate as they require automation by computer. They are also more prone to failure or clogging over extended cycles of operation. The electric immobilization method utilizes short-term but strong electrical pulses to immobilize the worms in the channel. Therefore, it does not require any mechanical parts, can immobilize worms at any location in the channel, and operates on individual or group of animals in parallel. Integrated with the electrotaxis assay, the device does not require any additional fabrication steps as the electrical pulses are applicable through the same electrodes used for electrotaxis.

7.2.5 Electrotaxis-Based Microfluidic Technique for Mutant Assessment and Chemical Screening

Since electrotaxis behaviour reveals clues about the state of worms' neurological and muscular systems (demonstrated by testing multiple mutant strains), it can be used by biologists, toxicologists and drug researchers to study the influence of chemicals, drugs and other environmental parameters on worm models. As a proof of principle, the first integrated microfluidic chip that could collect individual animals from a population, expose them to controlled dosage of drugs and finally screen them quantitatively at a behavioural level by using the electrotaxis screening technique was developed.

Electrotaxis screening has been demonstrated to be applicable in chemical screening assays by testing a *C. elegans* Parkinson's disease model induced by feeding neurotoxins 6-OHDA, MPTP and Rotenone (off chip exposure). The technique has been shown promising by being far more sensitive in detecting behavioural changes compared to standard plate-based assays (S. Salam et al.,

Unpublished manuscript). The integrated microfluidic chip is expected to fully automate such assays for higher throughputs and more precise controls.

7.3 Applications of Nematodes' Electrotaxis in the Literature

Electrotaxis of *C. elegans* in microchannels is one of the main contributions of this thesis [15]. After its publication, a few research groups around the world have adapted this technology to perform various application-based operations on nematodes. Carr et al. [194] studied the effect of the levamisole drug on parasitic and non-parasitic nematodes using a microfluidic chip equipped with the electrotactic screening technique. Sensitive, real-time and high resolution screening and reduction in the experimentation time has been achieved in this work. The same group also used a sinusoidal microchannel with varying amplitude and electrotactic-driven movement to study the locomotion adaptation of *C. elegans* in a simple way [205]. Difference in the adaptation of the mutant and the wild type worms to channel amplitude modulation has been demonstrated. In a different approach, the application of local electric valves inside microchannels to localize the worms spatially has been demonstrated [164]. This was reviewed more thoroughly at Section 5.2. Chuang et al. developed a technique to trap and manipulate the worms electrically inside microchannels [162]. Dielectrophoretic technique is a well established method to manipulate cells and microparticles [206], and it was shown that this phenomenon is also applicable to trapping and manipulating the worms. A range of electric field intensities and frequencies to viably trap the worms have been explored in this work with demonstration of repulsive phototaxis to blue light under dielectrophoretic trapping conditions. This suggested that neuronal activities remain unimpaired under the influence of intense electric signals. Selectivity of electrotaxis response between different stages of the worms and also various mutants has led to the application of this method for size-based sorting of the animals in this thesis [19, 21-23] as well as other research works [165, 207], which were reviewed in section 5.2. Last but not least, Chokshi et al. have investigated the transient response of neurons to DC electric currents by using a microchip that can immobilize the animals, apply DC electric currents and perform FRET imaging of the neuronal activities in response [195], as described and used in section 4.3.3. Age-dependent variation in the electrotactically-induced response of ASH neuron has been demonstrated.

7.4 Concluding Remarks and Recommendation for the Future Work

In recent years, several microfluidic and miniaturized devices have been designed to assay *C. elegans*. All of these have demonstrated the potential to probe worms in a manner that is not feasible by traditional manual protocols. Using these devices, the phenotypes of animals could be precisely and quantitatively characterized. Additionally, they provide a suitable format to handle a large number of animals individually and in parallel, thus accelerating the study of biological processes. These advantages make microfluidic devices ideal for high-throughput applications to identify drugs and gene targets in *C. elegans* disease models. The work in this thesis has shown that the electric field-based microfluidic systems could serve as powerful tools to manipulate, control and quantify the movement of worms to facilitate the study of movement-related disorders; to correlate behavioural observations with corresponding neuronal activities; to sort animals based on their age or phenotype for accelerating sample synchronization and identification of movement- and electrotactic-defective mutants; to detect movement-related parameters of the animals on the chip for automating screening assays; and to immobilize worms at any location in the channel without the need for micromechanically-operated parts to facilitate imaging of these animals. While this is promising, there are certain challenges that need to be addressed to perfect these techniques more efficiently. In this respect, it is satisfying to note that several laboratories are making an effort to overcome some of these limitations as discussed in Sections 2.5 and 7.3, and if the progress in the past one decade is of any indication, then there is every hope that microfluidic devices will soon be used in *C. elegans*-based assays.

As stated, more work is needed to develop and test these new systems and make them available to end users for routine applications. The devices need to be robust and working efficiently over hundreds of thousands of cycles without breaking down. Most of the device breakdowns in this thesis have been observed due to the failure of the fluidic interconnects (bond problems and leakage) and the electric ports (copper electrodes degradation over 6 months or failure due to the user misusage). To resolve these issues, next generation of the devices should be fabricated by deposition of patterned electrodes (preferably microfabricated noble metals) that can be embedded on a chip and restrained from user access as well as preserved from electrochemical reactions. Fluidic access ports should also be improved by fixing the input/output tubes onto the chip and providing better external input ports that are fixed and not movable by the user. One of the other problems that needed more attention was stabilizing the pneumatic flows inside the channel during electrotactic assays. This can later

on be resolved by the design and incorporation of microvalves on the main channel to enclose it during the assay to make sure that there is no external flow causing variations in results.

In order for the electric field-based microfluidic devices to facilitate HTS, it will be necessary to automate the analysis of *C. elegans* movement. Based on the work in this thesis, two solutions exist: (1) automating the post-processing image analysis procedure and/or (2) development of detectors and position sensors for on-chip movement assessment. Currently, movement analysis is done by manual examination of captured images which is suitable for low throughput experimentations. This process is data intensive, time consuming, and a key bottleneck in increasing the throughput of the experiment. For automating the image processing procedure, specialized software (MATLAB-based being the best option) is to be developed that can easily analyze videos and extract worm movement phenotypes efficiently in an automated, user-independent and quick manner. This can suit medium to high throughput assays on multi-channel devices in the future. In a totally separate automation attempt which is more suitable for later-stage very high throughput microfluidic screening devices, the electrical detection technique developed to sense the position and quantify the speed of the worm needs to be further improved so that multiplexing technology that is already in existence could be used to parallelize the measurement process. Having two sets of position detectors, at the beginning and end of each screening microchannel, will reveal the presence of the worm at detector locations as it moves in response to an electric field. This information, when fed to a computer, could easily allow determination of the speed of each worm independently. Obviously, design of software is also required for automation of these processes. The detection method, when developed to its full capacity, can also be used to screen for other phenotypes of worms. An array of microscopic detectors in a certain region of the channel (Figure 7-2) (that covers the entire body of the worm) can be used to acquire complete spatial information of the body shape of the worm in the form of electrical output signals at each time in the channel. These signals can be post-processed for extraction of parameters such as body length and volume of the worm as well as the frequency of the bends.

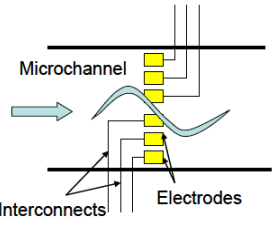

Figure 7-2 Schematic of the envisioned multi-electrode detector

The sorter device described in Chapter 5 demonstrated the separation of worms of two different ages in a semi-continuous manner. This was achieved by inducing a local high electric field between two chambers which repelled the older stage animals while allowing the younger ones to pass through towards the other chamber and become separated. Ideally, separation of all 4 larval stages from the adult one is demanded in assays. To expand the sorter device to accommodate this need, five chambers arranged in series with four adjustable local electric field traps (with embedded microelectrodes across each trap) between them is needed to be developed. The local fields can be adjusted to gradually increase from the first trap towards the last one. This design can hypothetically sort animals of all ages into the five chambers according to their sensitivity to the electric field as discussed in Chapter 4. Results obtained in Section 5.2 should be used to better design this multi-stage worm sorter device.

Any plan involving development of HTS microfluidic systems cannot afford to ignore the importance of imaging and data processing components. Automated high-resolution image capture and robust analysis is crucial for the success of high-throughput experiments. Although visual analysis could be done in some cases, the power of the system will only be fully utilized if most decisions were performed in an automated manner. This means that the imaging software must be integrated with the electrical immobilization and imaging technique developed in Section 5.5 and be highly trainable to distinguish between broad ranges of phenotypes to be screened and should be capable of performing such operations in real time, mostly in a user-independent manner. Depending on the type of experiments, both bright-field and fluorescent images will require processing. Typically, such images are acquired by a differential interference contrast (DIC) fluorescence microscope connected to a digital or video camera. While currently there is no real substitute of it, CMOS lensless imaging technology may hold promise in some future microfluidic systems. The main advantages of CMOS sensors are high-speed image acquisition (that lowers the effect of inherent motion in worms), small size, and low cost of design and operation compared to standard microscopes. This has led to the development of a few prototypes in recent years [208-213]. The optofluidic microscopy technique incorporated a microchannel to deliver worms over a series of micro-apertures fabricated on a metal-coated CMOS sensor to generate direct projection images. Yet another device was described that captures both monochrome and colored images of worms over a field-of-view of more than 24 mm^2 [214]. This was done by recording animals using incoherent in-line holography and digitally reconstructing diffraction holograms to create the entire image. In summary, the CMOS sensor approach appears to work for *C. elegans*, raising the possibility that it could become a viable imaging option in future microfluidic applications and integrated

with the techniques developed in this thesis such as the electric immobilization module.

In addition, certain types of experiments require following worms over a period of time (e.g., after feeding a chemical), and therefore the devices must be capable of keeping them alive, capture images at defined time points, and transfer data to a computer for analysis. The integrated microfluidic chip developed in this thesis is capable of culturing and exposing worms for up to 1-2 h, however, for longer encapsulations, the device should be equipped by feeding and waste removal modules. One of the other challenges observed in this device was the possibility of the worm ejection from the exposure chamber (pneumatically) while the chemical was being introduced inside. This can be addressed by incorporating a holder channel at the corner of the exposure chamber to hold the worm against the wall of the chamber (by a suction force) and to release it after the exposure chamber content was replaced by the drug.

APPENDICES

A. Standard Operation Procedures for Electrotactic Screening

I. Photolithography for Master Mold Fabrication

This process should be done in a cleanroom environment.

1) Use 30 ml acetone, 30 ml methanol and deionized (DI) water to clean a 3-inch silicon wafer. Silicon wafer is kept sequentially in the acetone and methanol baths each for 30 sec, and then rinsed with DI water for 5 min.
2) Use a nitrogen (N_2) blow gun to dry the surface of the wafer. Then heat up the wafer on a hotplate at 140 º C for 4 min for dehydration.
3) Plasma oxidize the surface of the silicon wafer at 50 W for 60 sec to increase the adhesion of photoresist to silicon in the next step.
4) Spin-coat 3 mL of SU8-100 photoresist on top of the wafer at 1750 rpm for 40 sec (results in a thickness of ~100µm).
5) Prebake the resist-coated wafer on the hotplate at 65 º C for 10 min and ramp the temperature to 95 º C (slowly in 2 minutes) and keep at this setting for an additional hour.
6) Use a photomask (containing channel structure design) to expose the resist to 550-600 $mJ.cm^{-2}$ dosage of the near UV light (350-400 nm).
7) Post-bake the resist on the hotplate at 65 º C for 1 min and 95 º C for 10 minutes.
8) Develop the resist (SU8 developer solution) for 10-15 min. After development, rinse the surface of the wafer with isopropanol alcohol (IPA) and check for the formation of white color residuals on the surface. In case of observing white residuals, continue developing for some additional time and IPA check until the resist is entirely developed.

Note: At this stage, another layer of photoresist can be spun on the wafer for the purpose of multi-height master mold fabrication. Repeat processes 1.4 to 1.8 as many time as needed

II. Soft Lithography for Microchannel Fabrication

1) vigorously mix 35 ml of PDMS elastomer base with 3.5 mL of the curing agent in a disposable container to make PDMS prepolymer.
2) Cover the insides of two large (9 cm diameter) Petri dishes with aluminum foil. Make the fit as flush as possible; the bottom especially must be flat.

Place the fabricated master mold (patterns facing up) and a blank silicon wafer into each of the dishes.

3) Pour 20 mL of PDMS mix onto the master mold dish and 15 mL of the mix into the other one. Eliminate air pockets underneath the mold by gently pressing on it with a disposable wooden applicator.
4) Cover both dishes and set aside for a day to cure. Alternatively, for faster curing, remove air bubbles from the PDMS using a vacuum degasifier for 30 min. Leave the dishes on a hot plate for two hours at 80°C to cure.
5) After the PDMS has cured, remove the foil and peel off the PDMS from its mold. Keep the channel and the blank PDMS faced down on an aluminum foil when not handling them.
6) Use the Harris Uni-Core (2.5 mm) to punch indentations (inlet/outlet) at both ends of the channel. Cut the channel and the blank PDMS into similar sizes (or slightly larger) with a scalpel.
7) Take the channel, the blank PDMS strip and a glass slide (75×25 mm^2) to a plasma oxidizer, likely located in a cleanroom. Load all three components into the plasma oxidizer and apply plasma for 40sec at 50W forward power.
8) After plasma oxidation, align and stick the channel piece (up side down) to the blank strip, then stick the assembly to the glass slide from the back side of the blank strip. Set aside for a day to complete the bonding.
9) Attach two lengths of plastic tubing (inner diameter 1/32”, outer diameter 3/32”), each at least six inches long, to the punched reservoirs using PDMS prepolymer glue. These will serve as inlet/outlet tubes. Use fluidic plastic connectors at the other end of these tubes for attaching them to syringes.
10) Use 22 gauge insulated copper wiring for electrodes (2 wires of 3”). They should be inserted into the channel reservoir and secured (using PDMS prepolymer glue) beside the inlet tube on the side closer to the channel. This process should be done on the hotplate (120 ºC) so that PDMS prepolymer glue does not flow into the channel while sealing off the inserted wires.

III. Electrotaxis Experiment

1) 3.1) Place and fix the fabricated PDMS microchannel in the center of microscope stage (preferably XY-movable) and turn on microscope with a camera mounted on the eyepiece or the C-mount port and connected to a monitor. Focus on the microchannel entrance region with a field of view of 5-8 mm^2.
2) In order to apply a DC, pulse DC or AC electric signal, use a function generator connected to an amplifier. If only a DC signal is desired, a

simpler system like a DC power supplier can be used. Connect the power supply or amplifier's output wires to the microchannel's electrodes.

3) Fill a small (35 mm diameter) Petri dish with M9 physiological buffer. Attach microchannel's output tube to a disposable syringe. Submerge the mouth of the inlet tube in the M9 and gently pull back on the syringe's plunger (or use a syringe pump in the withdrawal mode) to aspire liquid into the channel. When the inlet and the outlet tubes were filled in with M9, disconnect the syringe from the tube. Level both tubes at the same height to prevent any hydrostatically driven flow.
4) Apply a DC voltage to the channel and read out the current using the power supply and ensure that resistance (R=V/I) is around 0.6MΩ for the specific electrotaxis device (50 mm length, 0.3 mm width and 0.1mm height).
5) If satisfied with the channel's integrity, fill the Petri dish with diluted sample worm suspension and follow the above steps to load worms into the channel. Focus on the entrance region of the microchannel and keep applying suction while dipping in the inlet tube into the worm suspension.
6) As soon as a worm is observed in the microscope, the syringe can be disconnected and the flow can be manipulated hydrostatically by raising one of the tubes to a few centimeters of height. Place the worm at the center of the channel by using this method and then lay both inlet tubes flat at the same elevation.
7) Before applying the electric signal, set the power supply to the appropriate voltage: L3s respond to electric fields of >4 $V.cm^{-1}$, L4s respond to 4-10 $V.cm^{-1}$, and young adults respond to 2-4 $V.cm^{-1}$. Turn on the electric voltage and allow a minute of pre-exposure for the worm to acclimatize to the field. The worm should respond to the signal and start moving towards the cathode. When the minute has passed, use the camera to begin recording.
8) If doing AC or pulse DC electrotaxis, the maximum responsive electric field can be adopted from above and frequency and duty cycle of the signal can be modulated as desired.
9) When experiment is finished, remove all liquid (and worms) from the channel, rinse it with de-ionized water, and leave it to dry on a hot plate at 125°C for two hours.

B. Heat Generation in the Single Trap Sorting Device

Resistance of the single trap device was approximately 400 KΩ. Adult worms avoided the trap at a voltage of 12 V with a current of 30 µA. This resulted in a power dissipation of $P=RI^2$=360 µW. Applying this for a minute theoretically gave an energy of Q=Pt=21.6 mJ to the system. Weight of the M9 in the channel and reservoirs was 16.6 µKg. So the temperature difference generated was DeltaT=Q/(mc)=21.6mJ/(16.6µKg×4190J/KgK)=0.31 K. So temperature increase was not that significant in the device. Also in the main sorter device, DI water was used instead of M9 with currents in the nA range which further reduced the heat generation issue. And corresponding worm behaviors and avoidances from the traps were observed in this device.

C. Sample Loading Methodology for the Sorting Device

To load individual worms of various stages (n=10) in the single electric trap channel (Figure 5-1), a syringe was connected to the outlet of the channel and the inlet was dipped into the worm suspension. A suction force was applied to introduce flow into the tubes and the channel. As soon as a worm was visualized in the channel (through the microscope zoomed at the entrance region), the syringe was disconnected and the tubes were leveled to kill the flow. The worm was positioned in the side wide sections.

For the continuous sorting device (Figure 5-3), two sets of loading methods were used (one for individual worm behavior studies and one for separation) since the conditions in this device could be highly different from the single channel device due to the two-dimensional movement possibility provided in the chambers. In order to study individual worm's behavior in the chamber, synchronized stage samples were prepared and diluted in a similar manner described before. A few worms were picked up from the sample suspension using a pipette and loaded into the inlet tube of the device. The outlet tube of the loading chamber was opened to atmospheric pressure and the inlet and outlet tubes of the separation chamber were both closed to prevent flows from the loading chamber to the separation one. Manual pressure heads (by raising the tube for a few centimeters) in the inlet was used to load the worms from the tube into the loading chamber. As soon as a few worms were observed in the chamber (n=5-10), the inlet tube was descended at the same height of the other tubes and the flow was eliminated. The number of loaded worms was counted and a constant electric field (~1-7 V/cm in the chambers) was then applied from

the loading chamber electrode towards the parallel electric traps and the separation chamber electrode as illustrated in Figure 5-3. A video was recorded under the microscope and used later to analyze the worms' behavior. The parameter studied here was the number of worms attempting (by inserting 1/3rd of their body into the narrowing section of the electric traps) to move towards the separation chamber through the electric trap.

To characterize the sorting capability of the device, mixed populations (L3, L4, OA, muscle mutant, and neuronal mutant each mixed with YA in a 1:1 ratio) of worms (highly concentrated) were introduced into the loading chamber of the device. In order to achieve the populated loading, the inlet and outlet tubes of the loading chamber were both elevated at the same height in a vertical situation. Both interconnects to the separation chamber were closed. This prevented any hydraulic flow from happening. A fixed volume (60 µl) of the mixed sample was then transferred to the loading chamber inlet tube by using a pipette. The setup was then left for approximately 5 min so the worms were gravitationally forced to descend in the tube and enter the reservoir region of the loading chamber. After this time period, a pressure head between the inlet and outlet tubes of the loading chamber was used to bring the highly populated worm sample from the reservoir into the loading chamber. When the chamber was filled with worms, the inlet tube was lowered to the same height as all other tubes and any additional flow was eliminated. Proper electric fields (based on the results from the device in Figure 5-2) were applied across the device from the loading chamber towards the separation chamber and videos of the sorting were recorded again. In this assay, we counted the number of worms attempting to pass (described before) and the portion of them capable of passing through the electric traps for each loaded worm stage at each applied electric field. After a few minutes that the sorting process was saturated (reduction in rate of passing), additional worms were loaded into the chamber similarly as described above while washing off the sorted animals to the outlet tubes. This was continued until all the loaded worms were experimented and exposed in the device. After sorting, different worms were recognized from their size differences in the age-based sorting experiments. For the case of mutated/wild type sorting, the wild type animals were GFP activated (VH17 strain) before mixing with the mutants. The separated population was collected from the separation chamber, transferred to a plate, and the number of GFP and non-GFP animals was counted under a microscope.

D. Effect of Worms' Proximity to the Positive Electrode in the Sorter Device

One of the main problems encountered in this device was due to the proximity of the Pt electrodes to the electric traps inside the chambers. Even though the worms did not demonstrate viability issues on the range of electric fields tested (0-7 V/cm in the chambers), we observed that at areas neighboring the Pt wire electrodes, some worms lose their control of motion on higher electric fields (specially above ~5 V/cm) and start being attracted towards the positive electrode. We hypothesis that since the electric field streamlines are converging towards the electrodes at this region, a non-uniform electric field is generated near the electrodes causing dielectrophoresis forces to be exerted on the worms body [162]. This phenomenon could have caused reduction in the attempt rate especially for younger worms (since higher fields are required for their electrotaxis) which has to be considered for more efficient responses and hence better sorting efficiency in the future designs. However, to achieve a satisfactory rate of sorting (enough number of worms entering the chamber and hence enough number of attempts), further studies were conducted using a more populated sample loaded into the device as described in the experimental section. These assays showed promising results in sorting using electric fields in a 0-7 V/cm range as discussed later.

GLOSSARY OF TERMS

1-methyl-4-phenyl-1,2,3,6-tetrahydropyridine (MPTP)

A neurotoxin, $C_{12}H_{15}N$, that destroys dopamine-producing neurons of the substantia nigra and causes symptoms (as tremors and rigidity) similar to those of Parkinson's disease.

6-hydroxydopamine (6-OHDA)

A neurotoxin that is closely related to dopamine and is readily taken into dopaminergic and noradrenergic neurons via their normal reuptake mechanism, whereupon it destroys the neuron terminals, causing the organism to lose the ability to perform simple actions to obtain rewards [215].

α-synuclein (α-syn)

Synuclein: A family of structurally related proteins (α, β, and γ-synuclein) that are abundant in neurons and form aggregates in various neurodegenerative diseases. α-Synuclein (140 aa) is a component of plaque amyloid in Alzheimer's disease and accumulates in Lewy bodies, and an α-synuclein allele is linked to various familial cases of Parkinson's disease, interacts with synphilin, and is degraded by neurosin [216].

β-amyloid (Aβ)

A fragment of amyloid precursor protein (amyloid B, 39–43 aa) produced by the action of secretases and the main component of plaques in the brain in Alzheimer's disease [216].

Akinesia

Loss or impairment of the power of voluntary movement [217].

Aldehyde

An organic compound containing the group CHO, formed by the oxidation of alcohols. Typical aldehydes include methanal (formaldehyde) and ethanal (acetaldehyde) [217].

Alzheimer's disease (AD)

A neurological disease characterized by progressive loss of intellectual ability. The disease, which is named after German physician Alois Alzheimer (1864–1915), is associated with general shrinkage of the brain tissue, with deposits of β-amyloid protein and abnormal filaments composed of tau protein in the brain, and changes in the neurotransmitter systems within the brain that include a loss in the activity of cholinergic neurons. Some inherited forms are associated with a genetic locus on chromosome 21 [218].

Amino acid

Any of a group of water-soluble organic compounds that possess both a carboxyl (–COOH) and an amino ($–NH_2$) group attached to the same carbon atom, called the α-carbon atom. Amino acids can be represented by the general formula $R\text{-}CH(NH_2)COOH$. R may be hydrogen or an organic group, which may be nonpolar, basic, acidic, or polar; the nature of the R group determines the properties of any particular amino acid. Through the formation of peptide bonds, amino acids join together to form short chains (peptides) or much longer chains (polypeptides). Proteins are composed of various proportions of about 20 commonly occurring amino acids. The sequence of these amino acids in the protein polypeptides determines the shape, properties, and hence biological role of the protein [218].

Bradykinesa

Abnormal slowing of bodily movements, notably as a feature of Parkinson's disease and of parkinsonism [215].

Collagen

An insoluble fibrous protein found extensively in the connective tissue of skin, tendons, and bone. The polypeptide chains of collagen (containing the amino acids glycine and proline predominantly) form triple-stranded helical coils that are bound together to form fibrils, which have great strength and limited elasticity. Collagen accounts for over 30% of the total body protein of mammals [218].

Diapause

A period of suspended development or growth occurring in many insects and other invertebrates during which metabolism is greatly decreased. Some long-lived species may undergo diapause as adults, but for many others the egg is the diapausal stage. Diapause is often triggered by seasonal changes and regulated by an inborn rhythm; it enables the animal to survive unfavourable environmental conditions so that its offspring may be produced in more favourable ones [218].

Dopaminergic neuron (DA)

One type of a class of neurons all of which use biogenic amines as neurotransmitters.

Dorsoventral bends

Of, denoting, or extending along an axis joining the dorsal and ventral surfaces [217].

Duchenne’s Muscular Dystrophy (DMD)

A severe form of muscular dystrophy caused by a genetic defect and usually affecting boys [217].

Dystrophin

A protein found in skeletal muscle, which is absent in sufferers from muscular dystrophy [217].

Elastic modulus

The ratio of the force exerted upon a substance or body to the resultant deformation [217].

Electroosmosis

Osmosis under the influence of an electric field [217].

Electrophoresis

The movement of charged particles in a fluid or gel under the influence of an electric field [217].

Electrophysiology

The branch of physiology that deals with the electrical phenomena associated with nervous and other bodily activity [217].

Endocytosis

The process by which materials enter a cell without passing through the plasma membrane. The membrane folds around material outside the cell, resulting in the formation of a saclike vesicle into which the material is incorporated. This vesicle is then pinched off from the cell surface so that it lies within the cell. Both phagocytosis and pinocytosis are forms of endocytosis. In *receptor-mediated endocytosis*, cells selectively take in substances (e.g. hormones, low-density lipoproteins) that bind to receptors on the cell surface [218].

Escherichia coli

A species of Gram-negative aerobic bacteria that is found in the intestine and is also widely used in microbiological and genetics research. The motile rod-shaped cells ferment lactose and are usually harmless commensals, although certain strains are pathogenic and can cause a severe form of food poisoning. Studies of *E. coli* laboratory cultures have revealed much about the genetics of prokaryotes; the species is also frequently used in genetic engineering, particularly as a host for gene cloning and the expression of recombinant foreign genes in culture [218].

Eukaryote

An organism consisting of a cell or cells in which the genetic material is DNA in the form of chromosomes contained within a distinct nucleus. Eukaryotes include all living organisms other than the eubacteria and archaea [217].

Fluorescent protein

Members of a structurally homologous class of proteins that share the unique property of being self-sufficient to form a visible wavelength chromophore from a sequence of 3 amino acids within their own polypeptide sequence. It is common research practice for biologists to introduce a gene (or a gene chimera) encoding an engineered fluorescent protein into living cells and subsequently visualize the location and dynamics of the gene product using fluorescence microscopy [219].

Forward genetics

The traditional approach to genetic investigation, in which the aim is to identify the gene that governs a particular function. Mutant phenotypes provide clues about genetically controlled functions, and co-inherited genetic markers indicate the region of the genome containing the responsible gene. This information enables the gene to be isolated and cloned [218].

Gene

A unit of heredity composed of DNA. In classical genetics, a gene is visualized as a discrete particle, forming part of a chromosome that determines a particular characteristic. It can exist in different forms called alleles, which determine which aspect of the characteristic is shown (e.g. tallness or shortness for the characteristic of height).

A gene occupies a specific position on a chromosome. In view of the discoveries of molecular genetics, it may be defined as the sequence of nucleotides of DNA (or RNA) concerned with a specific function, such as the synthesis of a single polypeptide chain or of a messenger RNA molecule, corresponding to a particular sequence of the genetic code [218].

Genomic

The haploid set of chromosomes in a gamete or microorganism, or in each cell of a multicellular organism. The complete set of genes or genetic material present in a cell or organism [217].

Genotype

The genetic composition of an organism, i.e. the combination of alleles (see Gene) it possesses [218].

Glutamine

One of the 20 types of amino acids

Hermaphrodite

An animal, such as the earthworm, that has both male and female reproductive organs [218].

Homologue

In evolution, homologues are characteristics that are similar in different species because they have been inherited from a common ancestor [220].

Hox gene family

Hox genes are the architects of embryonic development. Their discovery in 1984 fundamentally altered the courses of evolutionary and developmental biology, and led to a molecular reunion of these two fields in the form of evolutionary developmental biology [221].

Huntingtin (htn)

The protein (3144 aa) encoded by the *IT15* gene that has variable numbers of polyglutamine repeats in Huntington's disease. The *IT15* gene is widely expressed and required for normal development [216].

Huntington's disease (HD)

A hereditary disease marked by degeneration of the brain cells and causing chorea and progressive dementia [217].

In silico

Describing biological processes or experiments that are simulated by a computer program (from Latin, literally 'in silicon') [218].

In vitro

Describing biological processes that are made to occur outside the living body, in laboratory apparatus (literally 'in glass', i.e. in a test tube) [218].

In vivo

Describing biological processes as they are observed to occur in their natural environment, i.e. within living organisms [218].

Mitochondria

A structure within the cytoplasm of eukaryotic cells that carries out aerobic respiration: it is the site of the Krebs cycle and electron transport chain, and therefore the cell's energy production. Mitochondria vary greatly in shape, size, and number but are typically oval or sausage-shaped and bounded by two membranes, the inner one being folded into finger-like projections (*cristae*); they contain their own DNA. Components of the electron transport chain and, in plants, the alternative respiratory pathway are located in the inner mitochondrial membrane. They are most numerous in cells with a high level of metabolic activity [218].

Mutation

A sudden random change in the genetic material of a cell that potentially can cause it and all cells derived from it to differ in appearance or behaviour (i.e. in phenotype) from the normal type. An organism affected by a mutation (especially one with visible effects) is described as a *mutant*. *Somatic mutations* affect the nonreproductive cells and are therefore restricted to the tissues of a single organism but *germ-line mutations*, which occur in the reproductive cells or their precursors, may be transmitted to the organism's descendants and cause abnormal development.

Mutations occur naturally at a low rate but this may be increased by radiation and by some chemicals (mutagen). Most are point mutations, which consist of invisible changes in the DNA of the chromosomes, but some (the chromosome mutations) affect the appearance or the number of the chromosomes. An example of a chromosome mutation is that giving rise to Down's syndrome.

According to the neutral theory of molecular evolution, the majority of point mutations in DNA are neither useful nor harmful and can spread throughout a population by genetic drift. Mutations that alter phenotypes are generally harmful, but a very small proportion may increase an organism's fitness; these spread through the population over successive generations by natural selection. Mutation is therefore essential for evolution, being the ultimate source of genetic variation [218].

Nucleotide

An organic compound consisting of a nitrogen-containing purine or pyrimidine base linked to a sugar (ribose or deoxyribose) and a phosphate group. DNA and RNA are made up of long chains of nucleotides (i.e. *polynucleotides*) [218].

Oocyte

A cell in an ovary which may undergo meiotic division to form an ovum [217].

Orthologs

Genes or proteins found in different species that are so similar in their nucleotide or amino acid sequences that they are assumed to have originated from a single ancestral gene. If one compares the genome of Saccaromyces cerevisiae and Caenorhabditis elegans, most orthologs have “core functions.” That is, they generate the proteins used in intermediary metabolism, DNA-, RNA-, and protein-metabolism, transport, secretion, and cytoskeletal structures. In contrast, the genes from ***C. elegans*** that function in intercellular signaling and gene regulation are not found in the yeast genome [220].

Paraquat

Trade name for an organic herbicide used to control broadleaved weeds and grasses. It is poisonous to humans, having toxic effects on the liver, lungs, and kidneys if ingested. Paraquat is not easily broken down and can persist in the environment adsorbed to soil particles. [218].

Parkinson's disease (PD)

A progressive disease of the nervous system marked by tremor, muscular rigidity, and slow, imprecise movement, chiefly affecting middle-aged and elderly people. It is associated with degeneration of the basal ganglia of the brain and a deficiency of the neurotransmitter dopamine [217].

Pharynx

The membrane-lined cavity behind the nose and mouth, connecting them to the oesophagus. *(Zoology)* the part of the alimentary canal immediately behind the mouth in invertebrates [217].

Phenotype

The observable characteristics of an organism. These are determined by its genes (see genotype), the dominance relationships between the alleles, and by the interaction of the genes with the environment [218].

Piezoresistive

A piezoresistive material exhibits electrical resistance change in response to mechanical stress.

Polymerase Chain Reaction (PCR)

A technique used to replicate a fragment of DNA so as to produce many copies of a particular DNA sequence. PCR is commonly employed as an alternative to gene cloning as a means of amplifying genetic material for DNA sequencing. The two strands of the DNA are separated by heating and short sequences of a single DNA strand (*primers*) are added, together with a supply of free nucleotides and DNA polymerase obtained from a bacterium that can withstand extreme heat. DNA polymerase uses single-stranded DNA as its template but requires a short section of double-stranded DNA to initiate the replication reaction. Hence, oligonucleotide primers are chosen so that their sequences are complementary to short regions flanking the region of DNA that is to be amplified; the oligonucleotides hybridize with the flanking sequences, forming the necessary double-stranded primers. In a series of heating and cooling cycles, the DNA sequence flanked by the primers doubles with each cycle and is thus rapidly amplified [218].

Protein Kinase

An enzyme that catalyses the transfer of a phosphate group from ATP to an intracellular protein, thereby affecting the biological activity of the protein (see kinase). Protein kinases phosphorylate specific amino-acid residues of their target proteins, usually either serine, threonine, or tyrosine. They play an important role in increasing or decreasing enzyme activity and in transmitting signals from receptors on the cell surface. The activity of the protein kinases is itself controlled by cyclic AMP, calcium ions, or other intracellular chemicals. It can be reversed by the action of phosphatase enzymes in the cell [218].

Ras Gene family

A family of oncogenes, first identified as transforming genes of Harvey and Kirsten murine sarcoma viruses. ('ras' from rat sarcoma because the murine Harvey virus obtained its transforming gene during passage in a rat). The ras superfamily is usually divided into three families, ras, rab, and rho [216].

Resveratrol

A polyphenol compound found in certain plants and in red wine, which has antioxidant properties and has been investigated for possible anti-carcinogenic effects [217].

RNA interference (RNAi)

The ability of double-stranded RNA to interfere with, or suppress, the expression of a gene with a corresponding base sequence. The phenomenon occurs in many types of organisms, including plants, fungi, and animals. Double-stranded RNA, which is normally a rarity in cells, is cut into fragments by a ribonuclease enzyme called Dicer. Processing by Dicer results in a short (typically 21-nucleotide) single strand of RNA being incorporated into an assemblage of proteins called the *RNA-induced silencing complex* (*RISC*). The RISC binds to the target RNA and either blocks translation or triggers cleavage and degradation of the mRNA. RNA interference is now used as a powerful and versatile experimental tool to suppress particular genes, as a form of knockout [218].

Rotenone

A toxic crystalline substance ($C_{23}H_{22}O_6$) obtained from the roots of derris and related plants, widely used as an insecticide [217].

Saccharomyces

An industrially important genus of yeasts. S. cerevisiae, of which there are at least 1000 strains, is used in baking, brewing, and wine making; it is also used in the production of various proteins and other compounds in biotechnology,

including industrial alcohol, and for experimental studies in cell biology and genetics [218].

Somatic

Relating to all the cells of an animal or plant other than the reproductive cells. Thus a somatic mutation is one that is not heritable [218].

Staurosporine

An inhibitor of a range of PKC-like protein kinases, derived from *Streptomyces* sp [216].

Substantia nigra

One of the basal ganglia, implicated in motor control. It is a dark, pigmented area in the midbrain, just below the thalamus, containing neurons that synthesize and release dopamine and project primarily to the striatum. Lesions in this area are associated with Parkinson's disease [222].

Tau

A protein (352 aa with multiple isoforms) that co-purifies with tubulin and co-assembles into microtubules. It has tandem repeats of a tubulin binding domain. Tau isoforms are found in all cells and are highly expressed in neurons where they associate with axonal microtubules. *Tau tubulin kinase* (1244 aa) is a casein kinase type enzyme that will phosphorylate both tau and tubulin [216].

Transgenic

Describing an organism whose genome incorporates and expresses genes from another species. Transgenic individuals are created by genetic engineering, using suitable vectors to insert the desired foreign gene into the fertilized egg or early embryo of the host. For example, the gene for rat growth hormone can be inserted into fertilized mouse eggs to produce mice with cells that produce rat growth hormone. Transgenic organisms offer considerable commercial potential [218].

Tremor

An involuntary quivering movement: *a disorder that causes tremors and muscle rigidity* [217].

Trichostatin A (TSA)

An antifungal antibiotic isolated from *Streptomyces platensis*. It is a potent inhibitor of histone deacetylase (HDAC) and will activate the transcription of genes that have been silenced by methylation [216].

Yeast

A microscopic fungus consisting of single oval cells that reproduce by budding, and capable of converting sugar into alcohol and carbon dioxide [217].

Zeta potential

The potential difference existing between the surfaces of a solid particle immersed in a conducting liquid (e.g. water) and the bulk of the liquid [223].

REFERENCES

1. Kaletta, T. and M.O. Hengartner, *Finding function in novel targets: C. elegans as a model organism.* Nat Rev Drug Discov, 2006. **5**(5): p. 387-98.
2. Ashrafi, K., et al., *Genome-wide RNAi analysis of Caenorhabditis elegans fat regulatory genes.* Nature, 2003. **421**(6920): p. 268-72.
3. Kwok, T.C., et al., *A small-molecule screen in C. elegans yields a new calcium channel antagonist.* Nature, 2006. **441**(7089): p. 91-5.
4. Segalat, L., *Invertebrate animal models of diseases as screening tools in drug discovery.* ACS Chem Biol, 2007. **2**(4): p. 231-6.
5. Johnson, J.R., et al., *Caenorhabditis elegans: a useful tool to decipher neurodegenerative pathways.* Biochem Soc Trans, 2010. **38**(2): p. 559-63.
6. Kirienko, N.V., K. Mani, and D.S. Fay, *Cancer models in Caenorhabditis elegans.* Dev Dyn, 2010. **239**(5): p. 1413-48.
7. Irazoqui, J.E., J.M. Urbach, and F.M. Ausubel, *Evolution of host innate defence: insights from Caenorhabditis elegans and primitive invertebrates.* Nat Rev Immunol, 2010. **10**(1): p. 47-58.
8. Voisine, C. and A.C. Hart, *Caenorhabditis elegans as a model system for triplet repeat diseases.* Methods Mol Biol, 2004. **277**: p. 141-60.
9. Lakso, M., et al., *Dopaminergic neuronal loss and motor deficits in Caenorhabditis elegans overexpressing human alpha-synuclein.* J Neurochem, 2003. **86**(1): p. 165-72.
10. Nass, R., et al., *Neurotoxin-induced degeneration of dopamine neurons in Caenorhabditis elegans.* Proc Natl Acad Sci U S A, 2002. **99**(5): p. 3264-9.
11. Rezai, P., et al., *Microfluidic systems to study the biology of human diseases and identify potential therapeutic targets in C. elegans*, in *Integrated Microsystems*, K. Iniewski, Editor. 2011, CRC Press. p. 581-608.
12. Hulme, S.E. and G.M. Whitesides, *Chemistry and the worm: Caenorhabditis elegans as a platform for integrating chemical and biological research.* Angew Chem Int Ed Engl, 2011. **50**(21): p. 4774-807.
13. Ben-Yakar, A., N. Chronis, and H. Lu, *Microfluidics for the analysis of behavior, nerve regeneration, and neural cell biology in C. elegans.* Curr Opin Neurobiol, 2009. **19**(5): p. 561-7.
14. Chronis, N., *Worm chips: microtools for C. elegans biology.* Lab Chip, 2010. **10**(4): p. 432-7.
15. Rezai, P., et al., *Electrotaxis of Caenorhabditis elegans in a microfluidic environment.* Lab Chip, 2010. **10**(2): p. 220-6.
16. Rezai, P., et al., *Effect of pulse direct current signals on electrotactic movement of nematodes Caenorhabditis elegans and Caenorhabditis briggsae.* Biomicrofluidics, 2011. **5**(044116): p. 1-9.
17. Rezai, P., et al. *Electric Field Control of C. elegans Movement in Microfluidic Channels*. in *13th International Conference on Miniaturized*

Systems for Chemistry and Life Sciences (MicroTAS 09) 2009. Jeju, Korea.
18. Rezai, P., et al., *Behavior of Caenorhabditis elegans in alternating electric field and its application to their localization and control.* Appl Phys Lett, 2010. **96**(15): p. 153702.
19. Rezai, P., et al., *Transport, Localization and Separation OF Caenorhabditis Elegans using Electrotaxis for Movement Based Behavioral Assays in Drug Discovery*, in *14th International Conference on Miniaturized Systems for Chemistry and Life Sciences (MicroTAS 10)* 2010: Groningen, The Netherlands. p. 160-162.
20. Rezai, P., et al., *In vivo Detection of Electric Field-induced Neuronal Activity in C. elegans* Under Preparation, 2012.
21. Rezai, P., et al., *Electrical sorting of Caenorhabditis elegans.* Lab Chip, 2012. **12**: p. 1831-1840
22. Rezai, P., et al., *Electrical Sorting of Caenorhabditis elegans*, in *15th International Conference on Miniaturized Systems for Chemistry and Life Sciences (μTAS2011)*. 2011: Seattle, USA. p. 723-725.
23. Rezai, P., et al., *Separation of caenorhabditis elegans by electrotaxis in a microdevice*, in *Solid-State Sensors, Actuators and Microsystems Conference (TRANSDUCERS), 2011 16th International*. 2011: Beijing, China. p. 2766-2769.
24. Rezai, P., et al., *Electrical Immobilization and Fluorescent Imaging of C. elegans.* Under Preparation, 2012.
25. Drews, I.I., *Drug discovery today - and tomorrow.* Drug Discov Today, 2000. **5**(1): p. 2-4.
26. Walhout, M., et al., *A model of elegance.* Am J Hum Genet, 1998. **63**(4): p. 955-61.
27. Attia, G.R., et al., *Transforming growth factor beta inhibits steroidogenic acute regulatory (StAR) protein expression in human ovarian thecal cells.* Mol Cell Endocrinol, 2000. **170**(1-2): p. 123-9.
28. Wolfe, J.H., *Gene therapy in large animal models of human genetic diseases. Introduction.* ILAR J, 2009. **50**(2): p. 107-11.
29. Mather, J.P. and P.E. Roberts, *Introduction to Cell and Tissue Culture: Theory and Technique*. 1998, Springer: PLENUM PRESS.
30. Gulati, R. and R.D. Simari, *Defining the potential for cell therapy for vascular disease using animal models.* Dis Model Mech, 2009. **2**(3-4): p. 130-7.
31. Meyer, M. and J. Vilardell, *The quest for a message: budding yeast, a model organism to study the control of pre-mRNA splicing.* Brief Funct Genomic Proteomic, 2009. **8**(1): p. 60-7.
32. Morgan, D.O., *Cyclin-dependent kinases: engines, clocks, and microprocessors.* Annu Rev Cell Dev Biol, 1997. **13**: p. 261-91.
33. Walberg, M.W., *Applicability of yeast genetics to neurologic disease.* Arch Neurol, 2000. **57**(8): p. 1129-34.
34. Khurana, V. and S. Lindquist, *Modelling neurodegeneration in Saccharomyces cerevisiae: why cook with baker's yeast?* Nat Rev Neurosci, 2010. **11**(6): p. 436-49.

35. Antoshechkin, I. and P.W. Sternberg, *The versatile worm: genetic and genomic resources for Caenorhabditis elegans research.* Nat Rev Genet, 2007. **8**(7): p. 518-32.
36. Hobert, O., *Specification of the nervous system.* WormBook, 2005: p. 1-19.
37. Denayer, E., T. de Ravel, and E. Legius, *Clinical and molecular aspects of RAS related disorders.* J Med Genet, 2008. **45**(11): p. 695-703.
38. Moghal, N. and P.W. Sternberg, *The epidermal growth factor system in Caenorhabditis elegans.* Exp Cell Res, 2003. **284**(1): p. 150-9.
39. Baumeister, R. and L. Ge, *The worm in us - Caenorhabditis elegans as a model of human disease.* Trends Biotechnol, 2002. **20**(4): p. 147-8.
40. Siddiqui, S.S., et al., *C. elegans as a model organism for in vivo screening in cancer: effects of human c-Met in lung cancer affect C. elegans vulva phenotypes.* Cancer Biol Ther, 2008. **7**(6): p. 856-63.
41. Powell, J.R. and F.M. Ausubel, *Models of Caenorhabditis elegans infection by bacterial and fungal pathogens.* Methods Mol Biol, 2008. **415**: p. 403-27.
42. Voisine, C., et al., *Identification of potential therapeutic drugs for huntington's disease using Caenorhabditis elegans.* PLoS One, 2007. **2**(6): p. e504.
43. O'Hagan, R. and M. Chalfie, *Mechanosensation in Caenorhabditis elegans.* Int Rev Neurobiol, 2006. **69**: p. 169-203.
44. Goodman, M.B., *Mechanosensation.* WormBook, 2006: p. 1-14.
45. Mori, I., H. Sasakura, and A. Kuhara, *Worm thermotaxis: a model system for analyzing thermosensation and neural plasticity.* Curr Opin Neurobiol, 2007. **17**(6): p. 712-9.
46. Bargmann, C.I., *Chemosensation in C. elegans.* WormBook, 2006: p. 1-29.
47. Ward, A., et al., *Light-sensitive neurons and channels mediate phototaxis in C. elegans.* Nat Neurosci, 2008. **11**(8): p. 916-22.
48. Bessho, K., et al., *Biological responses in Caenorhabditis elegans to high magnetic fields.* Experientia, 1995. **51**(3): p. 284-8.
49. Sukul, N.C. and N.A. Croll, *Influence of Potential Difference and Current on the Electrotaxis of Caenorhaditis elegans.* J Nematol, 1978. **10**(4): p. 314-7.
50. Viglierchio, D.R. and P.K. Yu, *On nematode behavior in an electric field.* Rev. Nematol., 1983. **6**: p. 171-178.
51. Hart, A.C., *Behavior.* WormBook, 2006: p. 1-67.
52. Buckingham, S.D. and D.B. Sattelle, *Strategies for automated analysis of C. elegans locomotion.* Invert Neurosci, 2008. **8**(3): p. 121-31.
53. Shingai, R., *Durations and frequencies of free locomotion in wild type and GABAergic mutants of Caenorhabditis elegans.* Neurosci Res, 2000. **38**(1): p. 71-83.
54. Goodman, M.B., et al., *Active currents regulate sensitivity and dynamic range in C. elegans neurons.* Neuron, 1998. **20**(4): p. 763-72.
55. Kerr, R., et al., *Optical imaging of calcium transients in neurons and pharyngeal muscle of C. elegans.* Neuron, 2000. **26**(3): p. 583-94.

56. Hilliard, M.A., et al., *In vivo imaging of C. elegans ASH neurons: cellular response and adaptation to chemical repellents.* EMBO J, 2005. **24**(1): p. 63-72.
57. Kimura, K.D., et al., *The C. elegans thermosensory neuron AFD responds to warming.* Curr Biol, 2004. **14**(14): p. 1291-5.
58. Suzuki, H., et al., *In vivo imaging of C. elegans mechanosensory neurons demonstrates a specific role for the MEC-4 channel in the process of gentle touch sensation.* Neuron, 2003. **39**(6): p. 1005-17.
59. Faumont, S. and S.R. Lockery, *The awake behaving worm: simultaneous imaging of neuronal activity and behavior in intact animals at millimeter scale.* J Neurophysiol, 2006. **95**(3): p. 1976-81.
60. Gabel, C.V., et al., *Neural circuits mediate electrosensory behavior in Caenorhabditis elegans.* J Neurosci, 2007. **27**(28): p. 7586-96.
61. O'Hagan, R., M. Chalfie, and M.B. Goodman, *The MEC-4 DEG/ENaC channel of Caenorhabditis elegans touch receptor neurons transduces mechanical signals.* Nat Neurosci, 2005. **8**(1): p. 43-50.
62. Luo, L., et al., *Olfactory behavior of swimming C. elegans analyzed by measuring motile responses to temporal variations of odorants.* J Neurophysiol, 2008. **99**(5): p. 2617-25.
63. Clark, D.A., et al., *Short-term adaptation and temporal processing in the cryophilic response of Caenorhabditis elegans.* J Neurophysiol, 2007. **97**(3): p. 1903-10.
64. Jones, A.K., S.D. Buckingham, and D.B. Sattelle, *Chemistry-to-gene screens in Caenorhabditis elegans.* Nat Rev Drug Discov, 2005. **4**(4): p. 321-30.
65. van Ham, T.J., et al., *Neurodegenerative diseases: Lessons from genome-wide screens in small model organisms.* EMBO Mol Med, 2009. **1**(8-9): p. 360-70.
66. Hoffman, E.P., R.H. Brown, Jr., and L.M. Kunkel, *Dystrophin: the protein product of the Duchenne muscular dystrophy locus.* Cell, 1987. **51**(6): p. 919-28.
67. Campbell, K.P., *Three muscular dystrophies: loss of cytoskeleton-extracellular matrix linkage.* Cell, 1995. **80**(5): p. 675-9.
68. Mariol, M.C. and L. Segalat, *Muscular degeneration in the absence of dystrophin is a calcium-dependent process.* Curr Biol, 2001. **11**(21): p. 1691-4.
69. Mariol, M.C., et al., *Dystrophin-dependent muscle degeneration requires a fully functional contractile machinery to occur in C. elegans.* Neuromuscul Disord, 2007. **17**(1): p. 56-60.
70. Carre-Pierrat, M., et al., *The SLO-1 BK channel of Caenorhabditis elegans is critical for muscle function and is involved in dystrophin-dependent muscle dystrophy.* J Mol Biol, 2006. **358**(2): p. 387-95.
71. Carre-Pierrat, M., et al., *Blocking of striated muscle degeneration by serotonin in C. elegans.* J Muscle Res Cell Motil, 2006. **27**(3-4): p. 253-8.
72. Gaud, A., et al., *Prednisone reduces muscle degeneration in dystrophin-deficient Caenorhabditis elegans.* Neuromuscul Disord, 2004. **14**(6): p. 365-70.

73. Glenner, G.G. and C.W. Wong, *Alzheimer's disease: initial report of the purification and characterization of a novel cerebrovascular amyloid protein.* Biochem Biophys Res Commun, 1984. **120**(3): p. 885-90.
74. Kosik, K.S., C.L. Joachim, and D.J. Selkoe, *Microtubule-associated protein tau (tau) is a major antigenic component of paired helical filaments in Alzheimer disease.* Proc Natl Acad Sci U S A, 1986. **83**(11): p. 4044-8.
75. Link, C.D., *Expression of human beta-amyloid peptide in transgenic Caenorhabditis elegans.* Proc Natl Acad Sci U S A, 1995. **92**(20): p. 9368-72.
76. Link, C.D., et al., *Gene expression analysis in a transgenic Caenorhabditis elegans Alzheimer's disease model.* Neurobiol Aging, 2003. **24**(3): p. 397-413.
77. Fay, D.S., et al., *In vivo aggregation of beta-amyloid peptide variants.* J Neurochem, 1998. **71**(4): p. 1616-25.
78. Kraemer, B.C., et al., *Molecular pathways that influence human tau-induced pathology in Caenorhabditis elegans.* Hum Mol Genet, 2006. **15**(9): p. 1483-96.
79. Hassan, W.M., et al., *AIP-1 ameliorates beta-amyloid peptide toxicity in a Caenorhabditis elegans Alzheimer's disease model.* Hum Mol Genet, 2009. **18**(15): p. 2739-47.
80. Fonte, V., et al., *Interaction of intracellular beta amyloid peptide with chaperone proteins.* Proc Natl Acad Sci U S A, 2002. **99**(14): p. 9439-44.
81. Gil, J.M. and A.C. Rego, *Mechanisms of neurodegeneration in Huntington's disease.* Eur J Neurosci, 2008. **27**(11): p. 2803-20.
82. Faber, P.W., et al., *Polyglutamine-mediated dysfunction and apoptotic death of a Caenorhabditis elegans sensory neuron.* Proc Natl Acad Sci U S A, 1999. **96**(1): p. 179-84.
83. Morley, J.F., et al., *The threshold for polyglutamine-expansion protein aggregation and cellular toxicity is dynamic and influenced by aging in Caenorhabditis elegans.* Proc Natl Acad Sci U S A, 2002. **99**(16): p. 10417-22.
84. Satyal, S.H., et al., *Polyglutamine aggregates alter protein folding homeostasis in Caenorhabditis elegans.* Proc Natl Acad Sci U S A, 2000. **97**(11): p. 5750-5.
85. Parker, J.A., et al., *Expanded polyglutamines in Caenorhabditis elegans cause axonal abnormalities and severe dysfunction of PLM mechanosensory neurons without cell death.* Proc Natl Acad Sci U S A, 2001. **98**(23): p. 13318-23.
86. Parker, J.A., et al., *Resveratrol rescues mutant polyglutamine cytotoxicity in nematode and mammalian neurons.* Nat Genet, 2005. **37**(4): p. 349-50.
87. Kritzer, J.A., et al., *Rapid selection of cyclic peptides that reduce alpha-synuclein toxicity in yeast and animal models.* Nat Chem Biol, 2009. **5**(9): p. 655-63.
88. Kuwahara, T., et al., *A systematic RNAi screen reveals involvement of endocytic pathway in neuronal dysfunction in alpha-synuclein transgenic C. elegans.* Hum Mol Genet, 2008. **17**(19): p. 2997-3009.

89. Su, L.J., et al., *Compounds from an unbiased chemical screen reverse both ER-to-Golgi trafficking defects and mitochondrial dysfunction in Parkinson's disease models.* Dis Model Mech, 2010. **3**(3-4): p. 194-208.
90. Hamamichi, S., et al., *Hypothesis-based RNAi screening identifies neuroprotective genes in a Parkinson's disease model.* Proc Natl Acad Sci U S A, 2008. **105**(2): p. 728-33.
91. van Ham, T.J., et al., *C. elegans model identifies genetic modifiers of alpha-synuclein inclusion formation during aging.* PLoS Genet, 2008. **4**(3): p. e1000027.
92. Menegon, A., et al., *Parkinson's disease, pesticides, and glutathione transferase polymorphisms.* Lancet, 1998. **352**(9137): p. 1344-6.
93. Betarbet, R., et al., *Chronic systemic pesticide exposure reproduces features of Parkinson's disease.* Nat Neurosci, 2000. **3**(12): p. 1301-6.
94. Langston, J.W. and P.A. Ballard, Jr., *Parkinson's disease in a chemist working with 1-methyl-4-phenyl-1,2,5,6-tetrahydropyridine.* N Engl J Med, 1983. **309**(5): p. 310.
95. Langston, J.W., et al., *Chronic Parkinsonism in humans due to a product of meperidine-analog synthesis.* Science, 1983. **219**(4587): p. 979-80.
96. Onofrj, M. and M.F. Ghilardi, *MPTP induced parkinsonian syndrome: long term follow-up and neurophysiological study.* Ital J Neurol Sci, 1990. **11**(5): p. 445-58.
97. Bocchetta, A. and G.U. Corsini, *Parkinson's disease and pesticides.* Lancet, 1986. **2**(8516): p. 1163.
98. Blum, D., et al., *Molecular pathways involved in the neurotoxicity of 6-OHDA, dopamine and MPTP: contribution to the apoptotic theory in Parkinson's disease.* Prog Neurobiol, 2001. **65**(2): p. 135-72.
99. Harrington, A.J., et al., *C. elegans as a model organism to investigate molecular pathways involved with Parkinson's disease.* Dev Dyn, 2010. **239**(5): p. 1282-95.
100. Nass, R., et al., *A genetic screen in Caenorhabditis elegans for dopamine neuron insensitivity to 6-hydroxydopamine identifies dopamine transporter mutants impacting transporter biosynthesis and trafficking.* J Neurochem, 2005. **94**(3): p. 774-85.
101. Marvanova, M. and C.D. Nichols, *Identification of neuroprotective compounds of caenorhabditis elegans dopaminergic neurons against 6-OHDA.* J Mol Neurosci, 2007. **31**(2): p. 127-37.
102. Locke, C.J., et al., *Acetaminophen attenuates dopamine neuron degeneration in animal models of Parkinson's disease.* Neurosci Lett, 2008. **439**(2): p. 129-33.
103. Segalat, L., *Drug discovery: here comes the worm.* ACS Chem Biol, 2006. **1**(5): p. 277-8.
104. Artal-Sanz, M., L. de Jong, and N. Tavernarakis, *Caenorhabditis elegans: a versatile platform for drug discovery.* Biotechnol J, 2006. **1**(12): p. 1405-18.
105. Silverman, G.A., et al., *Modeling molecular and cellular aspects of human disease using the nematode Caenorhabditis elegans.* Pediatr Res, 2009. **65**(1): p. 10-8.

106. Fire, A., et al., *Potent and specific genetic interference by double-stranded RNA in Caenorhabditis elegans.* Nature, 1998. **391**(6669): p. 806-11.
107. O'Rourke, E.J., A.L. Conery, and T.I. Moy, *Whole-animal high-throughput screens: the C. elegans model.* Methods Mol Biol, 2009. **486**: p. 57-75.
108. Moy, T.I., et al., *Identification of novel antimicrobials using a live-animal infection model.* Proc Natl Acad Sci U S A, 2006. **103**(27): p. 10414-9.
109. Bischof, L.J., D.L. Huffman, and R.V. Aroian, *Assays for toxicity studies in C. elegans with Bt crystal proteins.* Methods Mol Biol, 2006. **351**: p. 139-54.
110. Wittenburg, N. and R. Baumeister, *Thermal avoidance in Caenorhabditis elegans: an approach to the study of nociception.* Proc Natl Acad Sci U S A, 1999. **96**(18): p. 10477-82.
111. Hertweck, M. and R. Baumeister, *Automated assays to study longevity in C. elegans.* Mech Ageing Dev, 2005. **126**(1): p. 139-45.
112. Breger, J., et al., *Antifungal chemical compounds identified using a C. elegans pathogenicity assay.* PLoS Pathog, 2007. **3**(2): p. e18.
113. Doitsidou, M., et al., *Automated screening for mutants affecting dopaminergic-neuron specification in C. elegans.* Nat Methods, 2008. **5**(10): p. 869-72.
114. Boyd, W.A., S.J. McBride, and J.H. Freedman, *Effects of genetic mutations and chemical exposures on Caenorhabditis elegans feeding: evaluation of a novel, high-throughput screening assay.* PLoS One, 2007. **2**(12): p. e1259.
115. Byrne, A.B., et al., *A global analysis of genetic interactions in Caenorhabditis elegans.* J Biol, 2007. **6**(3): p. 8.
116. Dupuy, D., et al., *Genome-scale analysis of in vivo spatiotemporal promoter activity in Caenorhabditis elegans.* Nat Biotechnol, 2007. **25**(6): p. 663-8.
117. Lockery, S., *Channeling the worm: microfluidic devices for nematode neurobiology.* Nat Methods, 2007. **4**(9): p. 691-2.
118. Hulme, S.E., S.S. Shevkoplyas, and A. Samuel, *Microfluidics: streamlining discovery in worm biology.* Nat Methods, 2008. **5**(7): p. 589-90.
119. Easley, C.J., et al., *A fully integrated microfluidic genetic analysis system with sample-in-answer-out capability.* Proc Natl Acad Sci U S A, 2006. **103**(51): p. 19272-7.
120. Navratil, M., C.E. Whiting, and E.A. Arriaga, *Microfluidic devices for the analysis of single cells: leaving no protein uncounted.* Sci STKE, 2007. **2007**(388): p. pe29.
121. Fu, A.Y., et al., *A microfabricated fluorescence-activated cell sorter.* Nat Biotechnol, 1999. **17**(11): p. 1109-11.
122. Bousse, L., *Whole cell biosensors.* Sensors and Actuators B: Chemical, 1996. **34**(1-3): p. 270–275.
123. Sinclair, J., et al., *A cell-based bar code reader for high-throughput screening of ion channel-ligand interactions.* Anal Chem, 2002. **74**(24): p. 6133-8.

124. Park, T.H. and M.L. Shuler, *Integration of cell culture and microfabrication technology.* Biotechnol Prog, 2003. **19**(2): p. 243-53.
125. Dittrich, P.S. and A. Manz, *Lab-on-a-chip: microfluidics in drug discovery.* Nat Rev Drug Discov, 2006. **5**(3): p. 210-8.
126. Kang, L., et al., *Microfluidics for drug discovery and development: from target selection to product lifecycle management.* Drug Discov Today, 2008. **13**(1-2): p. 1-13.
127. Wen, Y. and S.T. Yang, *The future of microfluidic assays in drug development.* Expert Opin Drug Discovery, 2008. **3**: p. 1237–1253.
128. Fernandes, T.G., et al., *High-throughput cellular microarray platforms: applications in drug discovery, toxicology and stem cell research.* Trends Biotechnol, 2009. **27**(6): p. 342-9.
129. Carstens, C., et al., *Opportunities and limits of cell-based assay miniaturization in drug discovery.* Expert Opin Drug Discovery, 2010. **5**: p. 673–679.
130. Doll, J.C., et al., *SU-8 force sensing pillar arrays for biological measurements.* Lab Chip, 2009. **9**(10): p. 1449-54.
131. Park, S.J., M.B. Goodman, and B.L. Pruitt, *Analysis of nematode mechanics by piezoresistive displacement clamp.* Proc Natl Acad Sci U S A, 2007. **104**(44): p. 17376-81.
132. Park, S., et al., *Enhanced Caenorhabditis elegans locomotion in a structured microfluidic environment.* PLoS One, 2008. **3**(6): p. e2550.
133. Lockery, S.R., et al., *Artificial dirt: microfluidic substrates for nematode neurobiology and behavior.* J Neurophysiol, 2008. **99**(6): p. 3136-43.
134. Solvas, X.C., et al., *High-throughput age synchronisation of Caenorhabditis elegans.* chem Commun (Camb), 2011. **47**: p. 9801–9803.
135. Kima, N., et al., *Automated microfluidic compact disc (CD) cultivation system of Caenorhabditis elegans.* Sensors and Actuators B: Chemical, 2007. **122**(2): p. 511-8
136. Hulme, S.E., et al., *Lifespan-on-a-chip: microfluidic chambers for performing lifelong observation of C. elegans.* Lab Chip, 2010. **10**(5): p. 589-97.
137. Krajniak, J. and H. Lu, *Long-term high-resolution imaging and culture of C. elegans in chip-gel hybrid microfluidic device for developmental studies.* Lab Chip, 2010. **10**(14): p. 1862-8.
138. Chung, K., et al., *Microfluidic chamber arrays for whole-organism behavior-based chemical screening.* Lab Chip, 2011. **11**(21): p. 3689-97.
139. Clausell-Tormos, J., et al., *Droplet-based microfluidic platforms for the encapsulation and screening of Mammalian cells and multicellular organisms.* Chem Biol, 2008. **15**(5): p. 427-37.
140. Shi, W., et al., *Droplet-based microfluidic system for individual Caenorhabditis elegans assay.* Lab Chip, 2008. **8**(9): p. 1432-5.
141. Shi, W., et al., *Droplet microfluidics for characterizing the neurotoxin-induced responses in individual Caenorhabditis elegans.* Lab Chip, 2010. **10**(21): p. 2855-63.

142. Chronis, N., M. Zimmer, and C.I. Bargmann, *Microfluidics for in vivo imaging of neuronal and behavioral activity in Caenorhabditis elegans.* Nat Methods, 2007. **4**(9): p. 727-31.
143. Chokshi, T.V., D. Bazopoulou, and N. Chronis, *An automated microfluidic platform for calcium imaging of chemosensory neurons in Caenorhabditis elegans.* Lab Chip, 2010. **10**(20): p. 2758-63.
144. Wang, J., et al., *Microfluidic worm-chip for in vivo analysis of neuronal activity upon dynamic chemical stimulations.* Anal Chim Acta, 2011. **701**(1): p. 23-8.
145. Wang, Y., et al., *Identification of the neuronal effects of ethanol on C. elegans by in vivo fluorescence imaging on a microfluidic chip.* Anal Bioanal Chem, 2011. **399**(10): p. 3475-81.
146. Rohde, C.B., et al., *Microfluidic system for on-chip high-throughput whole-animal sorting and screening at subcellular resolution.* Proc Natl Acad Sci U S A, 2007. **104**(35): p. 13891-5.
147. Chung, K., M.M. Crane, and H. Lu, *Automated on-chip rapid microscopy, phenotyping and sorting of C. elegans.* Nat Methods, 2008. **5**(7): p. 637-43.
148. Crane, M.M., K. Chung, and H. Lu, *Computer-enhanced high-throughput genetic screens of C. elegans in a microfluidic system.* Lab Chip, 2009. **9**(1): p. 38-40.
149. Hulme, S.E., et al., *A microfabricated array of clamps for immobilizing and imaging C. elegans.* Lab Chip, 2007. **7**(11): p. 1515-23.
150. Caceres Ide, C., et al., *Laterally orienting C. elegans using geometry at microscale for high-throughput visual screens in neurodegeneration and neuronal development studies.* PLoS One, 2012. **7**(4): p. e35037.
151. Chokshi, T.V., A. Ben-Yakar, and N. Chronis, *CO2 and compressive immobilization of C. elegans on-chip.* Lab Chip, 2009. **9**(1): p. 151-7.
152. Ben-Yakar, A. and F. Bourgeois, *Ultrafast laser nanosurgery in microfluidics for genome-wide screenings.* Curr Opin Biotechnol, 2009. **20**(1): p. 100-5.
153. Guo, S.X., et al., *Femtosecond laser nanoaxotomy lab-on-a-chip for in vivo nerve regeneration studies.* Nat Methods, 2008. **5**(6): p. 531-3.
154. Zeng, F., C.B. Rohde, and M.F. Yanik, *Sub-cellular precision on-chip small-animal immobilization, multi-photon imaging and femtosecond-laser manipulation.* Lab Chip, 2008. **8**(5): p. 653-6.
155. Allen, P.B., et al., *Single-synapse ablation and long-term imaging in live C. elegans.* J Neurosci Methods, 2008. **173**(1): p. 20-6.
156. Chung, K. and H. Lu, *Automated high-throughput cell microsurgery on-chip.* Lab Chip, 2009. **9**(19): p. 2764-6.
157. Samara, C., et al., *Large-scale in vivo femtosecond laser neurosurgery screen reveals small-molecule enhancer of regeneration.* Proc Natl Acad Sci U S A, 2010. **107**(43): p. 18342-7.
158. Qin, J. and A.R. Wheeler, *Maze exploration and learning in C. elegans.* Lab Chip, 2007. **7**(2): p. 186-92.

159. Albrecht, D.R. and C.I. Bargmann, *High-content behavioral analysis of Caenorhabditis elegans in precise spatiotemporal chemical environments.* Nat Methods, 2011. **8**(7): p. 599-605.
160. McCormick, K.E., et al., *Microfluidic devices for analysis of spatial orientation behaviors in semi-restrained Caenorhabditis elegans.* PLoS One, 2011. **6**(10): p. e25710.
161. Gray, J.M., et al., *Oxygen sensation and social feeding mediated by a C. elegans guanylate cyclase homologue.* Nature, 2004. **430**(6997): p. 317-22.
162. Chuang, H.S., et al., *Dielectrophoresis of Caenorhabditis elegans.* Lab on a Chip, 2011. **11**(4): p. 599-604.
163. Burr, A.H., *The photomovement of Caenorhabditis elegans, a nematode which lacks ocelli. Proof that the response is to light not radiant heating.* Photochem Photobiol, 1985. **41**(5): p. 577-82.
164. Carr, J.A., et al., *Unidirectional, electrotactic-response valve for Caenorhabditis elegans in microfluidic devices.* Appl Phys Lett, 2011. **98**(14): p. 143701.
165. Manière, X., et al., *Running Worms: C. elegans Self-Sorting by Electrotaxis.* PLoS One, 2011. **6**(2): p. e16637.
166. Hekimi, S. and L. Guarente, *Genetics and the specificity of the aging process.* Science, 2003. **299**(5611): p. 1351-4.
167. Tatar, M., A. Bartke, and A. Antebi, *The endocrine regulation of aging by insulin-like signals.* Science, 2003. **299**(5611): p. 1346-51.
168. Przedborski, S., et al., *MPTP as a mitochondrial neurotoxic model of Parkinson's disease.* J Bioenerg Biomembr, 2004. **36**(4): p. 375-9.
169. White, J.G., et al., *The structure of the nervous system of the nematode Caenorhabditis elegans.* Philos Trans R Soc Lond B Biol Sci, 1986. **314**(1165): p. 1-340.
170. Van Voorhies, W.A. and S. Ward, *Broad oxygen tolerance in the nematode Caenorhabditis elegans.* J Exp Biol, 2000. **203**(Pt 16): p. 2467-78.
171. Hung, Y.C., et al., *Effects of static magnetic fields on the development and aging of Caenorhabditis elegans.* J Exp Biol, 2010. **213**(Pt 12): p. 2079-85.
172. Kimura, T., et al., *The effect of high strength static magnetic fields and ionizing radiation on gene expression and DNA damage in Caenorhabditis elegans.* Bioelectromagnetics, 2008. **29**(8): p. 605-14.
173. Caveness, F.E. and J.D. Panzer. *Nemic galvanotaxis*. in *Proceedings of the Helminthological Society*. 1960. Washington, USA.
174. Gupta, S.P., *Galvanotactic reaction of infective larvae of Trichostrongylus retortaeformis.* Exp Parasitol, 1962. **12**: p. 118-9.
175. Brenner, S., *The genetics of Caenorhabditis elegans.* Genetics, 1974. **77**(1): p. 71-94.
176. Xia, Y. and G.M. Whitesides, *Soft Lithography.* Annu. Rev. Mater. Sci., 1998. **28**: p. 153-184.
177. McDonald, J.C., et al., *Fabrication of microfluidic systems in poly(dimethylsiloxane).* Electrophoresis, 2000. **21**(1): p. 27-40.

178. Rezai, P., W. Wu, and P. Selvaganapathy, *Microfabrication of Polymers for bioMEMS*, in *MEMS for Biomedical Applications*, S. Bhansali and A. Vasudev, Editors. 2012, Woodhead Publishing Limited: Cambridge, UK. p. In Press.
179. Ismagilov, R.F., et al., *Microfluidic arrays of fluid-fluid diffusional contacts as detection elements and combinatorial tools.* Anal Chem, 2001. **73**(21): p. 5207-13.
180. Dorman, J.B., et al., *The age-1 and daf-2 genes function in a common pathway to control the lifespan of Caenorhabditis elegans.* Genetics, 1995. **141**(4): p. 1399-406.
181. Klass, M.R., *Aging in the nematode Caenorhabditis elegans: major biological and environmental factors influencing life span.* Mech Ageing Dev, 1977. **6**(6): p. 413-29.
182. Gaugler, R. and A.L. Bilgrami, *Nematode behaviour*. 2004, Wallingford, Oxfordshire ; Cambridge, MA: CABI Pub. xxiv, 419 p.
183. Bird, A.F., *The attractiveness of roots to the plant parasitic nematode Meloidogyne javanica and M. hapla.* Nematologica, 1959. **4**: p. 322-335.
184. Caveness, F.E. and J.D. Panzer, *Nemic galvanotaxis*, in *Proceedings of the Helminthological Society*. 1960: Washington. p. 73-74.
185. Ishii, N., et al., *UNC-6, a laminin-related protein, guides cell and pioneer axon migrations in C. elegans.* Neuron, 1992. **9**(5): p. 873-81.
186. Hedgecock, E.M., J.G. Culotti, and D.H. Hall, *The unc-5, unc-6, and unc-40 genes guide circumferential migrations of pioneer axons and mesodermal cells on the epidermis in C. elegans.* Neuron, 1990. **4**(1): p. 61-85.
187. MacLeod, A.R., J. Karn, and S. Brenner, *Molecular analysis of the unc-54 myosin heavy-chain gene of Caenorhabditis elegans.* Nature, 1981. **291**(5814): p. 386-90.
188. Moerman, D.G., et al., *Mutations in the unc-54 myosin heavy chain gene of Caenorhabditis elegans that alter contractility but not muscle structure.* Cell, 1982. **29**(3): p. 773-81.
189. Gumienny, T.L., et al., *Glypican LON-2 is a conserved negative regulator of BMP-like signaling in Caenorhabditis elegans.* Curr Biol, 2007. **17**(2): p. 159-64.
190. Thacker, C., J.A. Sheps, and A.M. Rose, *Caenorhabditis elegans dpy-5 is a cuticle procollagen processed by a proprotein convertase.* Cell Mol Life Sci, 2006. **63**(10): p. 1193-204.
191. Gupta, B.P., R. Johnsen, and N. Chen, *Genomics and biology of the nematode Caenorhabditis briggsae.* WormBook, 2007: p. 1-16.
192. Cutter, A.D., *Divergence times in Caenorhabditis and Drosophila inferred from direct estimates of the neutral mutation rate.* Mol Biol Evol, 2008. **25**(4): p. 778-86.
193. Baird, S.E. and H.M. Chamberlin, *Caenorhabditis briggsae methods.* WormBook, 2006: p. 1-9.
194. Carr, J.A., et al., *A microfluidic platform for high-sensitivity, real-time drug screening on C. elegans and parasitic nematodes.* Lab Chip, 2011. **11**(14): p. 2385-96.

195. Chokshi, T.V., D. Bazopoulou, and N. Chronis, *Probing the physiology of ASH neuron in Caenorhabditis elegans using electric current stimulation.* Appl Phys Lett, 2011. **99**(5): p. 53702-537023.
196. Jares-Erijman, E.A. and T.M. Jovin, *Imaging molecular interactions in living cells by FRET microscopy.* Curr Opin Chem Biol, 2006. **10**(5): p. 409-16.
197. Chamberlain, J.S. and G.M. Benian, *Muscular dystrophy: the worm turns to genetic disease.* Curr Biol, 2000. **10**(21): p. R795-7.
198. Jung, J., et al., *Microchip device for measurement of body volume of C. elegans as bioindicator application.* J. Micro-Nano Mech., 2011.
199. Schafer, D., et al., *Microfluidic cell counter with embedded optical fibers fabricated by femtosecond laser ablation and anodic bonding.* Opt Express, 2009. **17**(8): p. 6068-73.
200. Sun, T. and H. Morgan, *Single-cell microfluidic impedance cytometry: a review.* Microfluid Nanofluid, 2010. **8**: p. 423–443.
201. Yang, L. and R. Bashir, *Electrical/electrochemical impedance for rapid detection of foodborne pathogenic bacteria.* Biotechnol Adv, 2008. **26**(2): p. 135-50.
202. Sabounchi, P., et al., *Sample concentration and impedance detection on a microfluidic polymer chip.* Biomed Microdevices, 2008. **10**(5): p. 661-70.
203. Shingai, R., *Durations and frequencies of free locomotion in wild type and GABAergic mutants of Caenorhabditis elegans.* Neurosci Res, 2000. **38**: p. 71-83.
204. Shi, W., et al., *Microfluidic platform for the study of Caenorhabditis elegans.* Top Curr Chem, 2011. **304**: p. 323-38.
205. Parashar, A., et al., *Amplitude-modulated sinusoidal microchannels for observing adaptability in C. elegans locomotion.* Biomicrofluidics, 2011. **5**: p. 024112.
206. Pethig, R., *Review Article-Dielectrophoresis: Status of the theory, technology, and applications.* Biomicrofluidics, 2010. **4**(2).
207. Han, B., et al., *A sorting strategy for C. elegans based on size-dependent motility and electrotaxis in a micro-structured channel.* Lab Chip, 2012. **Accepted Article**.
208. Heng, X., et al., *Optofluidic microscopy--a method for implementing a high resolution optical microscope on a chip.* Lab Chip, 2006. **6**(10): p. 1274-6.
209. Bishara, W., H. Zhu, and A. Ozcan, *Holographic opto-fluidic microscopy.* Opt Express, 2010. **18**(26): p. 27499-510.
210. Pang, S., et al., *Implementation of a color-capable optofluidic microscope on a RGB CMOS color sensor chip substrate.* Lab Chip, 2010. **10**(4): p. 411-4.
211. Zheng, G., et al., *Sub-pixel resolving optofluidic microscope for on-chip cell imaging.* Lab Chip, 2010. **10**(22): p. 3125-9.
212. Isikman, S.O., et al., *Optofluidic on-chip tomography.* Conf Proc IEEE Eng Med Biol Soc, 2011. **2011**: p. 8463-6.
213. Isikman, S.O., et al., *Optofluidic Tomography on a Chip.* Appl Phys Lett, 2011. **98**(16): p. 161109.

214. Isikman, S.O., et al., *Color and monochrome lensless on-chip imaging of Caenorhabditis elegans over a wide field-of-view.* Lab Chip, 2010. **10**(9): p. 1109-12.
215. *A Dictionary of Psychology. Edited by Andrew M. Colman. Oxford University Press 2009. Oxford Reference Online. Oxford University Press. McMaster University. 7 September 2012 <http://www.oxfordreference.com/views/ENTRY.html?subview=Main&entry=t87.e1147>*.
216. *A Dictionary of Biomedicine. Oxford University Press Inc. Oxford Reference Online. Oxford University Press. McMaster University. 7 September 2012 <http://www.oxfordreference.com/views/ENTRY.html?subview=Main&entry=t312.e9419>*.
217. *Oxford Dictionary of English. Edited by Angus Stevenson. Oxford University Press, 2010. Oxford Reference Online. Oxford University Press. McMaster University. 7 September 2012 <http://www.oxfordreference.com/views/ENTRY.html?subview=Main&entry=t140.e0880140>*.
218. *A Dictionary of Biology. Elizabeth Martin and Robert Hine. Oxford University Press, 2008. Oxford Reference Online. Oxford University Press. McMaster University. 7 September 2012 <http://www.oxfordreference.com/views/ENTRY.html?subview=Main&entry=t6.e174>*.
219. Campbell, R.E., *Fluorescent proteins.* Scholarpedia, 2008. **3**(7): p. 5410.
220. *A Dictionary of Genetics. Robert C. King, William D. Stansfield and Pamela K. Mulligan. Oxford University Press, 2007. Oxford Reference Online. Oxford University Press. McMaster University. 7 September 2012 <http://www.oxfordreference.com/views/ENTRY.html?subview=Main&entry=t224.e4534>*.
221. *Martin J. Cohn "Hox Genes" Encyclopedia of Evolution. Ed. Mark Pagel. Oxford University Press 2003. McMaster University. 7 September 2012 <http://www.oxfordreference.com/views/ENTRY.html?subview=Main&entry=t169.e205>*.
222. *A Dictionary of Psychology. Edited by Andrew M. Colman. Oxford University Press 2009. Oxford Reference Online. Oxford University Press. McMaster University. 7 September 2012 <http://www.oxfordreference.com/views/ENTRY.html?subview=Main&entry=t87.e8115>*.
223. *Oxford Dictionary of English. Edited by Angus Stevenson. Oxford University Press, 2010. Oxford Reference Online. Oxford University Press. McMaster University. 7 September 2012 <http://www.oxfordreference.com/views/ENTRY.html?subview=Main&entry=t140.e0970000>*.